



**MONASH** University

DOCTORAL THESIS

---

**Evolutionary consequences of sex-specific  
selection in external fertilizers and  
hermaphrodites**

---

*Author:*  
Colin OLITO

*Supervisor:*  
Dr. Tim CONNALLON

*A thesis submitted in fulfillment of the requirements  
for the degree of Doctor of Philosophy at  
Monash University in 2017*

*in the*

School of Biological Sciences  
Centre for Geometric Biology

December 5, 2017



## Copyright Notice

© The author (2017)

I certify that I have made all reasonable efforts to secure copyright permissions for third party content included in this thesis and have not knowingly added copyright content to my work without the owner's permission.



## *Abstract*

### **Evolutionary consequences of sex-specific selection in external fertilizers and hermaphrodites**

by Colin OLITO

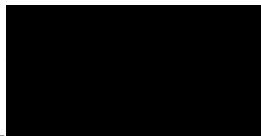
Understanding how genetic diversity is generated and maintained over time is the great goal of evolutionary biology. Owing to fundamental differences in female and male reproductive biology, selection is expected to favour the evolution of different phenotypes in each sex. When phenotypic optima differ between the sexes, pleiotropic effects among genes expressed by both sexes can give rise to sexually antagonistic selection (abbreviated SA hereafter), where beneficial alleles for one sex are deleterious for the other. Because selection acting on one sex can counterbalance opposing selection on the other, SA selection can place a significant genetic constraint on adaptation, and under some conditions, maintain genetic variation that would otherwise be lost if selection were limited to one sex. Despite intensive study over recent decades, previous theoretical and empirical research on sex-specific and SA selection has focused on a relatively narrow range of reproductive contexts – species with physically separated sexes (dioecious species), with internal fertilization. In this thesis, I explore the consequences of sexual conflict and SA selection for the maintenance of genetic variation, and the evolution of reproductive and life-history traits in two non-traditional, but very common, taxonomic groups: external fertilizers and simultaneous hermaphrodites. My work on external fertilizers addresses the underlying biology of selection on reproductive timing (phenology). Using a combination of theoretical models and a laboratory flume experiment, I demonstrate how SA selection and the maintenance of variation in phenological traits commonly arises from biologically realistic conditions. My work on hermaphrodites focuses on extending recent SA theory in hermaphrodites to a multi-locus context to show how the parameter conditions permitting SA polymorphism are expanded by linkage between SA loci. I then explore the consequences of SA polymorphism for evolutionary transitions from hermaphroditism to separate sexes.



## Declaration

This thesis contains no material which has been accepted for the award of any other degree or diploma at any university or equivalent institution and that, to the best of my knowledge and belief, this thesis contains no material previously published or written by another person, except where due reference is made in the text of the thesis.

Signature:



Print Name: Colin Olito

Date: December 5, 2017



## Publications during enrolment

- Olito, C., M. Bode, D. J. Marshall. 2015. Evolutionary consequences of fertilization mode for reproductive phenology and asynchrony. *Marine Ecology Progress Series* 537:23–38.
- Olito, C., D. J. Marshall, and T. Connallon. 2017. The evolution of reproductive phenology in broadcast spawners, and the maintenance of sexually antagonistic polymorphism. *American Naturalist* 189:153–169.
- Olito, C. 2016. Consequences of genetic linkage for the maintenance of sexually antagonistic polymorphism in hermaphrodites. *Evolution* 71:458–464.
- Olito, C., C. W. White, D. J. Marshall, and D. M. Barneche. 2017. Estimating monotonic biological rates using local linear regression. *J. Exp. Biol.* 220:759–764.

### Thesis including published works declaration

I hereby declare that this thesis contains no material which has been accepted for the award of any other degree or diploma at any university or equivalent institution and that, to the best of my knowledge and belief, this thesis contains no material previously published or written by another person, except where due reference is made in the text of the thesis.

This thesis includes four original papers published in peer reviewed journals and no submitted publications. The core theme of the thesis is the evolutionary consequences of sexually antagonistic selection in external fertilizers and hermaphrodites. The ideas, development and writing up of all the papers in the thesis were the principal responsibility of myself, the student, working within the School of Biological Sciences under the supervision of Dr. Tim Connallon.

The inclusion of co-authors reflects the fact that the work came from active collaboration between researchers and acknowledges input into team-based research.

For chapter 2, my contribution to the work involved the following:

I conceived the study jointly with my co-authors, performed the analyses with assistance from Dr. Michael Bode, and wrote the manuscript with assistance from my co-authors.

For chapter 3, my contribution to the work involved the following:

I conceived the study, performed the analyses with assistance from Dr. Tim Connallon, and wrote the manuscript with assistance from my co-authors.

For chapter 5, my contribution to the work involved the following:

I performed the analyses, and wrote the manuscript with minor editorial feedback from Dr. Tim Connallon.

For Appendix A, my contribution to the work involved the following:

I conceived the study, designed the methodology, and wrote the software jointly with Dr. Diego Barneche, and wrote the manuscript with assistance from my co-authors.

Student Signature: 

Date: December 5, 2017



The undersigned hereby certify that the above declaration correctly reflects the nature and extent of the student's and co-authors' contributions to this work. In instances where I am not the responsible author I have consulted with the responsible author to agree on the respective contributions of the authors.

Main Supervisor Signature: 

Date: December 5, 2017

TABLE 1: Publications included in this thesis.

Thesis Chapter	Publication Title	Status	Nature and % of student contribution	Co-author name(s), Nature, and % of co-author's contribution*	Co-author(s), Monash student Y/N*
2	Evolutionary consequences of fertilization mode for reproductive phenology and asynchrony	Published	33% Conception, 80% Analysis, 80% Writing	Michael Bode: 33% Conception, 33% Conception, 20% Analysis, 10% Writing Dustin J. Marshall: 33% Conception, 10% Writing	No
3	The evolution of reproductive phenology in broadcast spawners, and the maintenance of sexually antagonistic polymorphism	Published	80% Conception, 75% Analysis, 80% Writing	Dustin J. Marshall: 10% Conception, 10% Writing Tim Connallon: 10% Conception, 25% Analysis, 10% Writing	No
5	Consequences of genetic linkage for the maintenance of sexually antagonistic polymorphism in hermaphrodites	Published	100% Analysis, 100% Writing	N/A	N/A
App. A	Estimating monotonic biological rates using local linear regression	Published	75% Conception, 50% Design, 50% Software Dev., 70% Writing	Craig R. White: 10% Writing Dustin J. Marshall: 10% Writing Diego R. Barneche: 25% Conception, 50% Design, 50% Software Dev., 10% Writing	No



*“Anyone can have a great idea if they never read anything!”*

– Anonymous



## *Acknowledgements*

I am indebted to many friends and colleagues, whose unwavering support, encouragement, and patience made this thesis possible. I am especially grateful to my advisor, Dr. Tim Connallon. I have relished every minute of our many stimulating discussions, chalkboard sessions, and friendly talks. I am proud to be the first graduate of the Connallon Lab. I am also most grateful to my co-advisor, Dr. Dustin Marshall, for helping me find the confidence to follow my passion, and begin viewing academics as my career rather than just school. Thanks also for finding my spirit animal(s). Toowit-toowoo. Many thanks also to my other committee members, Dr. Damian Dowling, and Dr. Bob Wong for their support and encouragement along the way.

Special thanks are in order for two of my good friends and lab-mates, Dr. Ted Y. Chang, and Dr. Diego Barneche. Our informal and passionate discussions and sounding-board sessions were, to me, the essence of what graduate school should be. I am also grateful to Dr. Crispin Jordan for many stimulating discussions. Many thanks also to Clementine Lasne, and the MEEG lab: Amanda, Amy, Belinda, Evatt, Giulia, Hayley, Henry, Karin, Keyne, Lucy, Lukas, Marcelo, Martino, Matt, and Rolanda for their friendship, patience, and willingness to help at the drop of a hat.

Thanks to the many others who helped me along the way, whether in an official capacity, or as friends, including Fiona Hibbert, Ric San Martin, Justin Cally, Dr. Craig White, and Dr. Matthew Hall. I am also grateful for the financial support provided by the School of Biological Sciences, as well as a Deans International Postgraduate Student Scholarship, and Deans Postgraduate Student Scholarship.

Thanks also to Dr. Hamish Spencer and Dr. Manus Patten for their thorough review, and insightful (and humorous) comments on an earlier version of this thesis.

Finally, my deepest love and gratitude to my family. My wife, Chandra, for having the courage to set out on this adventure, and the strength, fortitude, and humour to get through each day with the girl and me. You made this possible. My mother, Carmen, for her unyielding optimism, support, and positive energy. And my daughter, Elena, for being the most singular, perfect, effervescent, wonderful little human I will ever know. You are the brightest light in my life, and my greatest teacher. Insofar as a pursuit as inherently selfish as science and theory can be done *for* someone else, this has all been for you.



# Contents

<b>Copyright Notice</b>	<b>iii</b>
<b>Abstract</b>	<b>v</b>
<b>Declaration</b>	<b>vii</b>
<b>Publications during enrolment</b>	<b>ix</b>
<b>Acknowledgements</b>	<b>xv</b>
<b>1 Introduction</b>	<b>1</b>
1.1 External fertilizers . . . . .	2
1.2 Hermaphrodites . . . . .	3
1.3 Estimating monotonic biological rates . . . . .	5
<b>2 Evolutionary consequences of fertilization mode for reproductive phenology and asynchrony</b>	<b>7</b>
2.1 Abstract . . . . .	7
2.2 Introduction . . . . .	8
2.3 Materials and methods . . . . .	9
2.3.1 Fertilization modes . . . . .	10
2.4 Analytic solutions . . . . .	12
2.4.1 Case 1: Constant fertilization success . . . . .	12
2.4.2 Case 2: Internal fertilizers . . . . .	13
2.4.3 Case 3: External fertilizers . . . . .	13
2.5 Numerical ESS analysis . . . . .	14
2.6 Results . . . . .	15
2.6.1 Effects of fertilization mode and population size . . . . .	15
2.6.2 Female fitness and sexual conflict . . . . .	16
2.6.3 Effects of traits influencing egg fertilization . . . . .	16
2.7 Discussion . . . . .	17
2.7.1 Evolution of reproductive asynchrony . . . . .	17
2.7.2 Effects of fertilization mode and population density . . . . .	19
2.7.3 Female fitness and sexual conflict . . . . .	20
2.7.4 Effects of traits influencing egg fertilization . . . . .	22
2.7.5 Conclusions . . . . .	22
2.8 Tables . . . . .	24
2.9 Figures . . . . .	26
2.10 Supplementary Figures . . . . .	30
<b>3 The evolution of reproductive phenology in broadcast spawners, and the maintenance of sexually antagonistic polymorphism</b>	<b>33</b>
3.1 Abstract . . . . .	33
3.2 Introduction . . . . .	34

3.3	Methods	36
3.3.1	Fertilization Dynamics	36
3.3.2	A Two-sex, Two-Time-Point Haploid Model of Selection	37
3.3.3	Sexual Conflict and Patterns of Gene Expression	39
3.3.4	Testing Model Assumptions	40
3.4	Results	41
3.4.1	Prevalence of Protected Polymorphism	41
3.4.2	Sexual Conflict and Protected Polymorphism	42
3.4.3	Environmental Gradients	43
3.4.4	Evolution of Within-Individual Variance	44
3.5	Discussion	44
3.5.1	The Evolution of Phenologies	44
3.5.2	Sexual Conflict and Protected Polymorphism	47
3.5.3	Evolution of Within-Individual Variance	47
3.6	Tables	49
3.7	Figures	50
3.8	Appendix A: ESS Conditions	56
3.8.1	Convergence-stability & Hessian Matrices	56
3.9	Appendix B: Quantitative Genetic Simulation Methods	57
3.9.1	Inheritance of individual phenology	57
3.9.2	Reproductive success	58
3.9.3	Patterns of gene expression	58
3.9.4	Environmental gradients and polyspermy	59
3.10	Appendix S1: Mathematica Code	61
3.11	Appendix S2: Numerical results for population genetic models	62
3.12	Appendix S3: Quantitative Genetic Simulation Results	67
3.12.1	Evolution of among- vs. within-individual variance	67
3.12.2	Sexual Conflict	68
3.12.3	Consequences of environmental gradients	69
3.13	Appendix S4: Computer Code	82
<b>4</b>	<b>Sperm-release strategies in external fertilizers: selection during sperm dispersal and sperm competition favour similar reproductive phenotypes</b>	<b>83</b>
4.1	Abstract	83
4.2	Introduction	84
4.3	Methods	86
4.3.1	Study species	86
4.3.2	Estimating spawning durations	86
4.3.3	Flume experiments	86
4.3.4	Analyses	88
4.4	Results	89
4.4.1	Estimating spawning durations	89
4.4.2	Flume experiments	89
4.5	Discussion	90
4.6	Acknowledgements	92
4.7	Tables	93
4.8	Figures	94
4.9	Appendix A: Model selection results	96
4.10	Appendix B: Supplementary figures	98

<b>5</b>	<b>Consequences of genetic linkage for the maintenance of sexually antagonistic polymorphism in hermaphrodites</b>	<b>101</b>
5.1	Abstract	101
5.2	Introduction	102
5.3	Model	103
5.3.1	Data availability	105
5.4	Results	105
5.5	Discussion	106
5.6	Acknowledgments	108
5.7	Tables	109
5.8	Figures	110
5.9	Appendix A: Development of recursions, quasi-equilibrium approx.	112
5.9.1	Recursions	112
5.9.2	QE Approximations	114
5.10	Appendix B: Supplementary figures	116
5.11	Appendix C: Computer Code	120
<b>6</b>	<b>Sexually antagonistic polymorphism and the evolution of dimorphic sexual systems from hermaphroditism</b>	<b>121</b>
6.1	Introduction	122
6.2	Models	124
6.2.1	Gynodioecy	124
6.2.2	Androdioecy	126
6.2.3	Analyses	126
6.2.4	Data availability	128
6.3	Results	129
6.3.1	Invasion into monomorphic populations	129
	Gynodioecy:	129
	Androdioecy:	130
6.3.2	Invasion of unisexuales into polymorphic populations	131
6.3.3	Equilibrium frequencies of unisexuales	131
6.4	Discussion	132
6.4.1	SA Polymorphism and the evolution of dimorphic sexual systems	133
6.4.2	Mating systems and the evolution of dioecy	134
6.4.3	The population genetic basis of the evolution of separate sexes	135
6.5	Tables	137
6.6	Figures	138
6.7	Appendix A: Development of recursions	142
6.7.1	Assumptions	142
6.7.2	Adult genotypic frequencies after inbreeding depression	142
6.7.3	Gynodioecy via dominant male-sterility mutation	143
6.7.4	Gynodioecy via recessive male-sterility mutation	146
6.7.5	Androdioecy via dominant female-sterility mutation	150
6.7.6	Androdioecy via recessive female-sterility mutation	153
6.8	Appendix B: Supplementary figures	156
6.9	Appendix C: Alternative models of inbreeding depression	162

<b>7 Discussion</b>	<b>165</b>
7.1 External Fertilizers and the emergence of SA selection . . . . .	166
7.2 Hermaphrodites and the genetic architecture of sexually antagonistic loci . . . . .	167
<b>A Estimating monotonic biological rates using local linear regression</b>	<b>169</b>
<b>Bibliography</b>	<b>179</b>

*To Elena, Chandra, and Carmen*



## Chapter 1

# Introduction

The great goal of evolutionary biology is to explain how the tremendous genetic and phenotypic diversity observed in natural populations is generated and maintained over time. Owing to fundamental differences in female and male reproductive biology, selection is expected to favour the evolution of different phenotypes in each sex (Parker 1979; Arnqvist and Rowe 2005; but see Kokko and Jennions 2008). Such sex differences in selection can consequently lead to two basic forms of sexual conflict: inter-locus and intra-locus conflict (Arnqvist and Rowe 2005; Bonduriansky and Chenoweth 2009). Inter-locus sexual conflict occurs when there is antagonistic selection between genes that increase female fitness (at the expense of male fitness), and other genes that increase male fitness (at the expense of female fitness). Conversely, intra-locus sexual conflict occurs when pleiotropic effects of genes expressed by both sexes results in sexually antagonistic selection (abbreviated SA selection, hereafter), where beneficial alleles for one sex decrease fitness when expressed in the other.

Because selection acting on one sex can counter-balance opposing selection on the other, SA selection can significantly constrain adaptation to a changing environment. Under some conditions, SA selection can maintain genetic variation that would otherwise be lost if selection were limited to one sex (Kidwell et al. 1977; Connallon and Clark 2012, 2014a). Indeed, SA alleles have been shown to play an important role in the maintenance of genetic variation in fitness, the evolution of reproductive and life-history traits, and genome evolution in a variety of theoretical and empirical contexts (Rice 1992; Prout 2000; Rice and Chippindale 2001; Pischedda and Chippindale 2006; Foerster et al. 2007; Bonduriansky and Chenoweth 2009; Cox and Calsbeek 2010; Fry 2010; Connallon and Clark 2012; Barson et al. 2015; Cheng and Kirkpatrick 2016).

Although sex-specific and SA selection have been studied intensively, previous work has focused largely on a relatively narrow range of reproductive contexts that apply for model animal systems, such as *Drosophila*. In particular, both the theoretical and empirical literature on sexual conflict focuses on species with physically separated sexes (dioecious species), and internal fertilization. Consequently, we know comparatively little about the evolutionary dynamics of sexual conflict in taxonomic groups where these conditions are violated – a major gap in our understanding. External fertilization is the ancestral mode of reproduction among animals (Rouse and Fitzhugh 1994), and occurs in a large and taxonomically diverse group of aquatic species. External fertilizers represent approximately 50% of marine invertebrate biodiversity globally (Monro and Marshall 2015). Similarly, hermaphroditic species, where individuals perform both male and female sex-functions, constitute a massive and taxonomically widespread group including approximately 95% of flowering plants, and 33% of non-insect animal species (Renner 2014; Jarne and Auld 2006).

Moreover, many species with separate sexes are habitual inbreeders. Studies of partially self-fertilizing hermaphrodites therefore have broad relevance for the more general effects of inbreeding on population responses to selection (Crow and Kimura 1970; Pollak 1987). In this thesis, I explore the consequences of sexual conflict and SA selection for the maintenance of genetic variation, and the evolution of reproductive and life-history traits in external fertilizers and simultaneous hermaphrodites.

## 1.1 External fertilizers

Fertilization takes place internally for the vast majority of terrestrial species, but most marine organisms shed gametes into the water column and fertilization takes place in the external environment (Monro and Marshall 2015). Although external fertilizers are extremely diverse and taxonomically widespread within the tree of life, I will focus on the archetypal form of external fertilization — broadcast spawning — which applies in seaweeds, corals, echinoderms, and fish.

The timing of reproduction (reproductive phenology) is a critical life-history trait for all species, but it has profound evolutionary consequences for broadcast spawners. Unlike internal fertilizers, reproduction in broadcast spawners rarely involves physical contact between individuals. Hence, broadcast spawners must time spawning to account for the availability of mates, as well as the favourability of environmental conditions, both of which vary over time. Moreover, fertilization success in broadcast spawners is determined primarily by local gamete concentrations and the fertilization kinetics of sperm-egg interactions. The dynamics of both processes are strongly density-dependent, and play out over very short time-scales (e.g., seconds to minutes). Thus, frequency- and density-dependent effects can be strong, complex, and temporally dynamic in broadcast spawning species (Levitan 1991, 2002, 2004; Rouse and Fitzhugh 1994; Marshall 2002).

As I outline and explore in detail in the following chapters, the reproductive phenology strategies that maximize male fitness in broadcast spawners often differ from those that maximize female fitness. In this context, pleiotropic effects of genes that influence the timing of gamete release in both sexes can give rise to SA selection. The potential for SA selection to act on important life history traits raises several outstanding questions regarding the evolution of reproductive phenology, and the evolutionary dynamics of sexual conflict in external fertilizers. How should we expect reproductive phenologies to evolve in externally fertilizing species relative to internal fertilizers, and how do these predictions compare with well documented empirical patterns? Under what conditions do we expect sexual conflict over the timing of reproduction, and how does sexual conflict influence the evolution of reproductive phenologies? How might the co-evolution of male and female phenologies play out when the adaptive response in each sex is constrained by a shared genetic basis underlying female and male phenological traits? Chapters 2–4 seek to address these unresolved questions using a combination of theoretical and empirical approaches.

In chapter 2, I derive and analyze mathematical models to explore the effect of reproductive mode (internal or external) on the evolution of reproductive phenologies, and especially the population variance in spawning time. The results show that fertilization mode fundamentally alters frequency- and density-dependent selection on the variance in phenology, helping explain observed differences in the phenologies of internal vs. external fertilizers, and suggest that sexual conflict over reproductive timing may be extremely common in broadcast spawners.

In chapter 3, I develop theoretical population and quantitative genetic models of sex-specific selection on reproductive phenology that account for environmental variability as well as the frequency- and density-dependent dynamics of fertilization success in broadcast spawning species. The models explicitly address the consequences sexually dimorphic gene expression, and the influence of frequency-dependent SA selection on the maintenance of polymorphism and the evolution of reproductive phenology. These models demonstrate that the frequency-dependent nature of sperm competition and fertilization kinetics in broadcast spawners generates SA selection and facilitates the maintenance of genetic variation in phenological traits over much of the biologically relevant parameter space.

Finally, in chapter 4, I present an empirical study addressing the effect of selection from the external environment on the reproductive success associated with different male spawning strategies. Using a flow-through flume experiment, I explore how male reproductive success in the absence of sperm competition varies with male energetic investment, and the rate of sperm release (a crucial phenological trait) in the broadcast spawning marine tubeworm *Galeolaria caespitosa*. A key outcome from this experiment was the demonstration that selection from the external environment during sperm dispersal (in the absence of sperm competition) may favour high phenological variances similar to those predicted by the theoretical models developed in chapters 2 and 3. This result suggests that well documented empirical patterns in the reproductive phenologies of broadcast spawners, including slow sperm release rates and sex-specific spawning behaviours, are expected to evolve whether or not males experience sperm competition.

## 1.2 Hermaphrodites

The relevance of SA selection for dioecious species is intuitive because selection acts on physically distinct individuals of each sex. Not surprisingly, the population genetics literature has placed a strong emphasis on the maintenance of SA polymorphism in dioecious species (e.g., Kidwell et al. 1977; Rice 1992; Prout 2000; Connallon and Clark 2012). However, SA selection can also occur in hermaphroditic species, where individuals must perform both male and female sex-functions. In hermaphrodites, alleles with opposing fitness effects through each sex-function, or alleles that affect fitness trade-offs between sex-functions, can create analogous genetic constraints on fitness (Abbott 2011; Jordan and Connallon 2014; Tazzyman and Abbott 2015). Moreover, there is broad scope for SA alleles to constrain fitness in hermaphrodites because individuals must accommodate both sex-functions with a single phenotype (Barrett 2002; Conner 2006; Abbott 2011; Jordan and Connallon 2014). In fact, fitness trade-offs between sex functions have long been considered an essential feature of the evolution of reproductive traits, including floral and inflorescence morphology, as well as sexual and mating systems in hermaphrodites (although the genetic basis of these trade-offs have not always been modeled explicitly) (Charlesworth and Charlesworth, 1978a; Charnov 1982; Lloyd and Webb 1986; Webb and Lloyd 1986; Barrett 2002; Goodwillie et al. 2005; Harder and Barrett 2006; Abbott 2011).

Hermaphroditism carries with it a variety of complicating factors that may influence the fate of SA alleles. Of particular importance is the fact that individuals of many hermaphroditic species may reproduce by outcrossing and by self-fertilization (Goodwillie et al. 2005; Iqic and Kohn 2005; Jarne and Auld 2006; Jordan and Connallon 2014). There are a variety of genomic consequences of such

'mixed-mating' reproductive systems, including reduced effective population size, decreased rates of recombination, and underproduction of heterozygous individuals (Wright et al. 2008). All three factors can impact opportunities for maintaining genetic variation (e.g., chapter 9 in Kimura and Ohta 1971). Self-fertilization should reduce the opportunity for maintaining SA variation under balancing selection, and can introduce a 'female-bias' in the relative importance of selection through each sex-function (Jordan and Connallon 2014; Tazzyman and Abbott 2015).

In addition to mixed-mating, many hermaphroditic species display a variety of dimorphic sexual systems, where populations are composed of a mixture of hermaphroditic and unisexual individuals. Nowhere in the tree of life is this diversity exhibited more dramatically than among flowering plants, where the diversity of sexual systems spans a broad spectrum, ranging from simultaneous hermaphroditism to full dioecy, and includes nearly every possible intermediate state (Darwin 1877; Bawa 1980; Sakai and Weller 1999; Renner 2014). This tremendous diversity in sexual systems suggests that the dynamics of SA genetic variation may differ widely among plant taxa. Such variability may also influence evolutionary transitions between sexual systems (e.g., transitions from hermaphroditism to separate sexes). However, with the exception of simple models of trade-offs between sex functions, previous population genetic theory has largely ignored the consequences of SA selection for the evolution of dimorphic sexual systems.

In chapters 5 and 6, I present new population genetic theory on the maintenance of SA polymorphism in partially self-fertilizing hermaphrodites, and on the potential for evolutionary transitions between reproductive systems (i.e., from hermaphroditism to separate sexes). In both cases, I extend previous theory to a multi-locus context, and emphasize the evolutionary genomic consequences of physical linkage between SA loci.

In chapter 5, I extend recent two-locus SA selection theory developed for dioecious species (Patten et al. 2010) in order to identify conditions under which balancing selection maintains SA polymorphism in simultaneous hermaphrodites. I show that the reduction in the effective rate of recombination caused by self-fertilization significantly increases the opportunity for balancing selection to maintain SA genetic variation, relative to single-locus predictions.

In chapter 6, I develop population genetic models for the evolution of dimorphic sexual systems via the invasion of sex-specific sterility mutations, extending the seminal work of (Charlesworth and Charlesworth, 1978a). Specifically, I explore the effect of linkage between a 'standard' SA locus and a second 'sterility' locus for the invasion of a unisexual sterility allele that completely eliminates either the male or female sex-function. Evolutionary invasion of such sterility alleles give rise to mixed populations comprised of hermaphrodites and females (gynodioecy), or hermaphrodites and males (androdioecy). These mixed populations represent intermediate evolutionary steps along the path to full dioecy. The new results indicate that linkage among SA loci facilitates the invasion and establishment of unisexual sterility alleles, and suggests an altered role for self-fertilization in the evolution of separate sexes from hermaphroditism relative to previous theory (Charlesworth and Charlesworth, 1978a).

### 1.3 Estimating monotonic biological rates

As part of an empirical research project performed in the first two years of my Ph.D. research, I attempted to quantify metabolic costs of reproduction in the broadcast spawning sea urchin *Heliocidaris erythrogramma*. To quantify the costs of reproduction, it was necessary to estimate individual metabolic rates from O<sub>2</sub> consumption nonlinear time-series data. One analytically tractable approach for estimating such rates is by identifying the slope of the most linear region of the time-series data, which is theoretically expected to reflect an individuals' resting metabolic rate. While analyzing these data, it became clear that there was no well-established statistical methodology for this purpose. A detailed literature search also revealed that estimates of this kind are made routinely in many fields within the biological sciences, from ecosystem ecology to biogeochemistry, leading to *ad hoc* and unreproducible results. This methodological gap inspired a collaborative effort between myself and Dr. Diego Barneche (a post-doc at the Monash Centre for Geometric Biology) to develop a statistically robust and reproducible approach for estimating metabolic rates from time-series data. The analysis we developed has now been published as a methods paper in the Journal of Experimental Biology, and as a publicly available R statistical package (LoLinR; <https://github.com/colin-olito/LoLinR>). Because this work did not fit the main theme of my other research, it has been included as an appendix to this thesis (Appendix A) rather than a full research chapter.



## Chapter 2

# Evolutionary consequences of fertilization mode for reproductive phenology and asynchrony<sup>1</sup>

### 2.1 Abstract

Reproductive phenology is a crucial life history trait that is influenced by both environmental and frequency-dependent effects. The fitness benefits of any phenology strategy will depend strongly on other aspects of the life history: one of the most fundamental ways life histories can differ is fertilization mode. Despite the strong potential for fertilization mode to alter selection on phenology, explorations into how these two fundamental life-history traits interact are lacking. We explore theoretically how frequency-dependent effects and fertilization mode influence the evolution of asynchronous reproduction, and the evolutionary stable strategy (ESS) for a population in which individuals' mean and variance in phenology are evolvable traits. We find that when males compete for fertilizations, perfect reproductive synchrony with optimal environmental conditions is never an optimal evolutionary strategy, and asynchronous reproduction is an inevitable consequence of frequency-dependent selection. Fertilization mode qualitatively alters frequency-dependent selection on the variance in phenology, as well as the prevalence of sexual conflict over reproductive timing. Our results contrast with traditional hypotheses that have primarily considered asynchronous reproduction as an adaptive bet-hedging strategy in stochastic environments, and provide a much needed explanation for the emerging picture of reproductive asynchrony observed in many systems.

---

<sup>1</sup>This chapter has been published as: Olito, C., M. Bode, D. J. Marshall. 2015. Evolutionary consequences of fertilization mode for reproductive phenology and asynchrony. *Marine Ecology Progress Series* 537:23–38.

## 2.2 Introduction

Reproductive phenology has myriad consequences for the evolution of plants and animals. The timing of reproduction determines an individual's mating opportunities (Hendry and Day 2005; Elzinga et al. 2007; Weis et al. 2014), the resource budget for mating and offspring development (Stearns 1992; Ejsmond et al. 2010), as well as the environment experienced by both mating adults and offspring (Cushing 1969, 1990; Brunet and Charlesworth 1995; Post et al. 2001; Elzinga et al. 2007). Variation in the timing of reproduction drives assortative mating, changes gene flow, and promotes local adaptation and speciation (Fisher 1958; Hendry and Day 2005; Binks et al. 2012; Weis et al. 2014).

Selection on reproductive phenology (phenology hereafter) is driven by both environmental factors and frequency-dependent effects. Obviously, there is strong selection for reproduction to coincide with environmental conditions that are conducive to mating success and offspring survival. For example, many species time mating so that subsequent offspring development coincides with seasonal resource availability (reviewed in Durant et al. 2007; Lowerre-Barbieri et al. 2011). However, when environmental conditions are unpredictable, theory predicts that within-individual variation in phenology can evolve as an adaptive bet-hedging strategy (Iwasa 1991; Iwasa and Levin 1995). Frequency-dependent effects can be more subtle, and take both positive and negative forms. On one hand, per-capita mate encounter rates and pollinator visitation rates are often positively density-dependent due to Allee effects, or other mechanisms such as patch attractiveness (Allee et al. 1949; Augspurger 1981; Thomson 1981; Fagan et al. 2010; Devaux and Lande 2010). Phenology can also be influenced by positive density dependence when highly synchronous reproduction swamps offspring predators (Augspurger 1981; Ims 1990). On the other hand, negative frequency-dependence occurs when population demographic changes force individuals to compete for a smaller fraction of available resources, mates, pollinators, or fertilizations (Fisher 1958; Birkhead and Møller 1998; Devaux and Lande 2010). While negative frequency-dependence arising from competition for mates has received attention in the context of sex-specific phenologies in hermaphrodites (particularly flowering plants) and some gonochoristic species (e.g., Bulmer 1983; Rathcke and Lacey 1985; Brunet and Charlesworth 1995; Devaux and Lande 2010), most studies of the evolution of asynchronous reproduction emphasize the counter-balancing effects of environmental variation and positive frequency-dependence.

The fitness benefits of any particular phenology strategy will depend strongly on life-history. For example, wind pollinated plants tend to have brief and highly synchronous flowering displays (sometimes on the order of 15–20 min) in order to minimize the amount of pollen wasted by an unpredictable pollen vector (Gregory 1973; Rabinowitz et al. 1981; Friedman and Barrett 2009). Animal pollinated plants, on the other hand, have relatively longer displays that maximize pollen transport efficiency given the foraging behaviours and visitation rates of pollinators (Rabinowitz et al. 1981; Harder and Barrett 1995). One of the most fundamental ways life histories can differ is fertilization mode (Gross and Shine 1981; Rouse and Fitzhugh 1994; Jørgensen et al. 2011). Gametes can either be fertilized while retained inside the female (internal fertilization) or after being shed into the environment (external fertilization). While fertilization mode is almost invariably internal in terrestrial taxa (e.g., flowering plants, mammals, and birds), fertilization mode shows substantial interspecific variation in aquatic groups such as algae, fish, amphibians, and invertebrates at all taxonomic levels (Gross and Shine 1981 (amphibians), Winemiller 1989;

Winemiller and Rose 1992 (fish), Rouse and Fitzhugh 1994 (sabellid worms), Beck 1998 (amphibians), Iyer and Roughgarden 2008 (algae, all animal phyla), Kerr et al. 2011 (scleractinian corals)). Fertilization mode alters selection on, and covaries with, numerous life-history traits, including gamete phenotypes, fertilization probability, mating behaviours, and the degree of parental care, all of which will interact with phenology to determine fitness (Winemiller 1989; Winemiller and Rose 1992; Stockley et al. 1997; Beck 1998). Despite the strong potential for fertilization mode to alter selection on phenology, explorations into how these two fundamental life-history traits interact are lacking.

Here we use both analytic and numerical methods to investigate theoretically how fertilization mode and population density interact to influence selection on phenology. Our results highlight the fundamental importance of negative frequency-dependence arising from among-male competition for mates and fertilizations in maintaining variance in the timing of reproduction, and illustrate how life-history traits such as fertilization mode alter the relative importance of environmental and frequency-dependent effects on the evolution of phenology.

## 2.3 Materials and methods

We use two parallel modelling approaches to study the effects of fertilization mode on the evolution of male spawning phenology. First, we use analytical methods to explore how fertilization mode and population density influence the invasibility of a population that reproduces synchronously at the environmental optimum by an asynchronous mutant. We then complement the analytical results with a numerical analysis of the evolutionary stable strategy (ESS) for a population in which individuals' mean and variance in the timing of reproduction are evolvable traits. Both analyses are based on calculating the relative fitness of a mutant compared to a resident population. The equation describing individuals' fitness has the same basic structure for all models, and has four components:

$$W = \int_t E(t)S(t)F(t)Q(t) dt. \quad (2.1)$$

The first term,  $E(t)$ , describes the rate of egg release by females through time. The second term,  $S(t)$ , describes an individual male's proportional contribution to the total amount of sperm released by all males. The third term,  $F(t)$ , describes the fertilization dynamics resulting from changes in total sperm concentration. The fourth term,  $Q(t)$ , is a catch-all term describing the effect of seasonal changes in environmental conditions influencing density-independent offspring mortality, which we term environmental quality. This could include, for example, environmental conditions at the time of spawning, larval dispersal, or larval settlement, influencing fertilization success or the susceptibility of offspring to various sources of mortality such as dispersal to inhospitable habitats or predation (Denny and Shibata 1989; Morgan and Christy 1995; Christy 2011). This fitness equation is integrated across time for each mating season to calculate an individuals' total fitness. We investigate the effect of fertilization mode on the evolution of male phenology by altering the functional form of  $F(t)$  to reflect biological differences in the dynamics of external versus internal fertilization.

For simplicity, and because selection on males to maximize fertilization success is expected to be intense relative to females (Parker 1982; Birkhead and Møller 1998),

we model the evolution of male phenologies only, and assume the rate of egg release,  $E(t)$ , is constant across generations. Consequently, while the evolution of male phenologies is influenced by the relative fitness of mutant males, female fitness is determined entirely by local sperm concentrations,  $S(t)$ , and environmental quality,  $Q(t)$ , and does not influence trait evolution in our models. In nature environmental and frequency-dependent factors will obviously also influence the evolution of female phenologies, and genetic correlations between male and female phenologies will determine the trajectory of evolution of the population phenology as a whole (Chapman et al. 2003; Bonduriansky and Chenoweth 2009). Modelling the joint evolution of male and female phenologies would require a significant increase in model complexity, and introduce multiple sources of frequency-dependent selection which would be difficult to tease apart. Instead, we choose to focus on males alone as a first step in understanding how fertilization mode might interact with frequency-dependent selection to influence the evolution of phenologies while maintaining analytic tractability and interpretability.

### 2.3.1 Fertilization modes

Fertilization mode in aquatic taxa can be either external or internal. While there is tremendous diversity in the specific biology of fertilization within these broad classifications, we focus on a comparison between two well documented suites of fertilization processes associated with each: external fertilizers susceptible to polyspermy (fertilization of eggs by multiple sperm) at high sperm concentrations, and internal fertilizers that can achieve complete fertilization of eggs at low sperm concentrations. External fertilizers release both eggs and sperm into an aquatic medium, and fertilization success is determined primarily by local sperm concentrations, and therefore the local density of spawning males (Levitan 1991, 2002; Marshall 2002; Levitan 2004). At low sperm concentrations, the probability of an egg being contacted by sperm are low, and few eggs are fertilized (sperm limitation). The probability of successful fertilization increases rapidly with sperm concentration, but for many species, a time lag between when an egg is initially fertilized and when it becomes impermeable to subsequent sperm, egg mortality due to polyspermy can be very high at high sperm concentrations (See Gould and Stephano 2003; Wong and Wessel 2005; Franke et al. 2002; Levitan 2004; Levitan et al. 2004). Polyspermy has been documented under field conditions, or in the laboratory using sperm concentrations expected to occur under field conditions, in a variety of species from diverse phyla, and may therefore be a common problem among externally fertilizing aquatic taxa (Brawley 1992 (Furoid Algae), Pearson and Brawley 1996 (Furoid Algae), Levitan 1998 (Echinoderm), Marshall et al. 2000 (Ascidian), Styan 2000 (Gastropods) and citations therein, Franke et al. 2002 (Echinoderm), Gould and Stephano 2003 (review), Levitan et al. 2004 (Echinoderm), Kupriyanova 2006 (Annelid), Marshall 2002 (Ascidian)). Consequently, the probability of successful mono-spermic fertilization as a function of sperm concentration for species susceptible to polyspermy is roughly bell shaped (Millar and Anderson 2003). For generality and analytic tractability, we use an equation that gives this functional form of polyspermy-induced decreases in successful fertilization success (after Bode and Marshall 2007). We model the probability of successful fertilization for external fertilizers as

$$F_{ext}(S_T) = \left( \frac{A_{ext}S_T}{2} \right)^2 e^{(2-A_{ext}S_T)}, \quad (2.2)$$

where  $S_T$  is the total amount of sperm released by males, and  $A_{ext}$  is a positive shape parameter that determines the steepness of the curve and location of the maximum (See Table 2.1 for descriptions of all terms used in the models; See Appendix 1 in Bode and Marshall 2007 regarding shape parameter  $A_{ext}$ ). Variation in  $A_{ext}$  can result from differences in gamete traits such as the speed and mechanism of polyspermy blocks, the size of eggs, hydrodynamic conditions, and the spatial arrangement of spawning individuals (Levitan 2002, 2004; Marshall et al. 2000; Wong and Wessel 2005; Bode and Marshall 2007).

Internal fertilization can be achieved in several ways, including copulation, physical transfer of spermatophores, and spermcasting, whereby sperm are shed into the water column but eggs are retained in the female (Rouse and Fitzhugh 1994). In contrast to external fertilizers, internally fertilizing species are less likely to suffer either sperm limitation or polyspermy. Sperm limitation will still occur in the extreme case when females fail to find any mates, but otherwise, fertilization rates in internal fertilizers tend to be much higher relative to external fertilizers at similar sperm concentrations (reviewed in Pemberton et al. 2003). Polyspermy is less of a risk for internal fertilizers for several reasons. Most internal fertilizers have evolved rapid blocks to polyspermy because of high sperm concentrations resulting from direct sperm transfer into the female reproductive tract (Gould and Stephano 2003; Wong and Wessel 2005). In many groups, females can also alter the number of sperm that ultimately access their eggs (Wong and Wessel 2005). Therefore the relation between the probability of successful fertilization and local mate density for internal fertilizers is better described by a saturating function with a maximum fertilization probability of 1. For our numerical ESS analyses we model the functional form of this relation using a sigmoidal Holling type III equation:

$$F_{int}(S_T) = \frac{S_T^2}{(A_{int} + S_T^2)}, \quad (2.3)$$

where  $A_{int}$  is a positive shape parameter that defines the function's steepness, and  $S_T$  is again the total sperm released by males. Variation in  $A_{int}$  could result from differences in the efficiency of males at locating potential mates, the duration of copulations, or in the case of some spermcasting species, the efficiency of filter feeding organs at capturing sperm (Pemberton et al. 2003). For our analytic solutions, we consider a different internal fertilization function that has a similar shape, but a more tractable analytic form:

$$f_{int}(S_T) = \frac{S_T}{(A_{int} + S_T)}. \quad (2.4)$$

The only difference between these two functions is the presence of sigmoidal behaviour at very low concentrations for Eq(2.3) (See fig. S1 in the Supplement at [www.int-res.com/articles/suppl/m537p023\\_supp.pdf](http://www.int-res.com/articles/suppl/m537p023_supp.pdf)). For comparison, we also model constant fertilization dynamics, where fertilization success is 100% at all non-zero sperm concentrations.

All three fertilization functions implicitly assume that competition among males for fertilizations follows a fair raffle. Consequently, male density augments the intensity of frequency-dependence by changing each male's share of successful fertilizations.

## 2.4 Analytic solutions

We begin with a simple analytic model that assesses whether a purely synchronous spawning population that reproduces at the environmental optimum can ever be evolutionarily stable. The model proposes a very simple representation of frequency-dependent mating behaviour that captures the fundamentals of synchrony while remaining both analytically tractable and comparable to the more complex ESS model. We consider a population in which females release eggs to coincide with a temporally-varying environment ( $t' \in [0, 1]$ ) which exhibits a single annual maximal quality,  $Q$ , at  $t = 1/2$  which we scale to unity:

$$Q(t) = 4t(1 - t) \quad (2.5)$$

We model environmental quality as the proportion of fertilized eggs that survive to settlement.

Each individual male has  $R$  sperm resources available; an individual's strategy is defined by their choice about how to release these fixed reproductive resources through time. We consider the relative fitness of a single asynchronous mutant that invades a population of  $N - 1$  individuals that spawn synchronously at the environmental maximum. If the relative fitness of this mutant individual is greater than that of the synchronously spawning population, a purely synchronous strategy cannot be evolutionarily stable.

We model the behaviour of the mutant individual using the simplest possible description of asynchrony. Instead of releasing their sperm at the peak female spawning time (and environmental maximum), a small fraction of population,  $d$ , are mutants who release their sperm slightly before the maximum, at  $t = 1/2 - e$ , where  $e$  is the deviation in time from the resident population strategy. The following fitness relationships are all symmetrical functions of  $e$ , and thus our results are equivalent for mutants that release slightly after the maximum. The remainder ( $1 - d$ ) is released at the maximum, with the rest of the population. We assess the three different fertilization success models in turn. For each, we assess the conditions under which a rare, small mutation ( $d = 1; e = 1/2$ ) could invade a population of individuals with purely synchronous spawning strategies. We focus on identifying a critical population size  $N^*$ , above which a mutant strategy will be able to invade, because this will allow us to identify conditions under which synchronously spawning populations are unstable for all three fertilization modes. For this formulation of asynchronous reproduction, the integration in Eq(2.1) becomes the sum of two terms — the fitness of each strategy at the environmental optimum, and their fitness at the slightly earlier release time (the synchronous strategy has no contribution to fitness at this earlier time, since it only reproduces at the environmental maximum).

### 2.4.1 Case 1: Constant fertilization success

The fitness of an individual with a given strategy is equal to the sum of the fertilization success of that individual's sperm across its entire release strategy. If the proportional fertilization rate of eggs is independent of sperm density, the fitness of an individual pursuing the population (i.e., the synchronous) strategy,  $W_p$ , is equal to its share of the total sperm release at the environmental maximum:

$$W_p = \frac{1}{N - d}. \quad (2.6)$$

Note that the total resources available to each individual,  $R$ , do not enter the fitness equation because all individuals are equally resourced.

The fitness of a mutant individual,  $W_m$ , is equal to the sum of its proportional releases at and around the environmental maximum, modified by the lower environmental quality that it experiences when spawning off the maximum:

$$W_m = \frac{(1-d)}{(N-d)} + (1-4e^2). \quad (2.7)$$

A mutant strategy can invade the population and perturb synchronous spawning behaviour in conditions when its relative fitness ( $W_m/W_p$ ) is  $> 1$ . By expressing relative fitness as a function of the population size  $N$  (recall that  $N$  also includes the mutant), we see that the mutant will invade whenever the population is larger than:

$$N^* = d \left( \frac{4e^2 - 2}{4e^2 - 1} \right). \quad (2.8)$$

Invasibility is guaranteed for small values of  $e$  and  $d$  (even for quite large values such as  $e = 0.4$  and  $d = 0.4$ ) because when  $e$  is small then  $N^* = 2d$ . The critical population size is therefore  $< 2$ , and a mutant would be able to invade any synchronously spawning population where fertilisation success is independent of sperm concentration (fig 2.1A).

### 2.4.2 Case 2: Internal fertilizers

By limiting the fertilization success when the total sperm concentration is low (i.e., when fewer individuals are spawning), internal fertilization dynamics will penalize mutant behaviour, and may thereby restore the evolutionary stability of the synchronous strategy. By modifying the fitness function with  $f_{int}(S_T)$ , a synchronously spawning, internally fertilizing individual has fitness:

$$W_p = \frac{1}{A_{int} + N - d} \quad (2.9)$$

while the fitness of the mutant strategy is:

$$W_m = \frac{(1-d)}{A_{int} + N - d} + \frac{d(1-4e^2)}{(A_{int} + d)}. \quad (2.10)$$

From equations (2.9) and (2.10), we can determine that the relative fitness of the mutant is  $> 1$  when the population is larger than:

$$N^* = d - A_{int} + \frac{(A_{int} + d)}{1 - 4e^2}. \quad (2.11)$$

For small asynchronous mutations ( $e, d = 1$ ) we can ignore quadratic terms in  $e$  and make the approximation that  $N^* = 2d$ . When mutations are small,  $N^*$  will always be  $< 2$ , and therefore asynchronous mutants will be able to invade a synchronous population (fig 2.1B).

### 2.4.3 Case 3: External fertilizers

For external fertilizers, the fitness of the synchronous population and mutant strategies are:

$$W_p = \frac{A_{ext} \exp[2 - A_{ext}(N - d)]}{2}, \quad (2.12)$$

and:

$$W_m = \frac{A_{ext} \exp[2 - A_{ext}d]}{2} \left[ (1 - d) \exp[-A_{ext}(N - 2d)] + d(1 - 4e^2) \right]. \quad (2.13)$$

respectively. The relative fitness of the mutant strategy is  $> 1$  when the population is larger than:

$$N^* = 2d - \frac{\ln[1 - 4e^2]}{A_{ext}}. \quad (2.14)$$

Once again we make the approximation that  $e = 1$ , which allows us to approximate Eq(2.14) as  $N^* = 2d$ . This will be  $< 2$  (fig 2.1C), and a synchronous population is therefore always unstable to an invading asynchronous mutant.

## 2.5 Numerical ESS analysis

Population phenologies are the cumulative result of within- and among-individual variation in reproductive timing. Phenologies in our analytic models are described entirely by the temporal deviation ( $d$ ) from the environmental optimum at which mutants release a proportion ( $e$ ) of their sperm resources. However, for organisms that release gametes over time, individual phenologies are perhaps more realistically described by the onset and duration (or mean and variance) of gamete release (Elzinga et al. 2007). We explored the evolutionary consequences of fertilization mode for the mean and variance in sperm release using a classic game-theoretic approach, and model the evolutionary stable strategy (ESS) for mutant males with a spawning phenology defined by a normal distribution  $s(t) = N(t, m, v)$  in a resident population with spawning phenology  $s^* = N(t, m^*, v^*)$  (fig. 2.2A). For a given population size  $N$ , the population phenology, or total amount of sperm released is

$$s_T(t) = s(t) + (N - 1)s^*(t). \quad (2.15)$$

Female phenologies are again assumed to be fixed and to coincide with seasonal changes in environmental conditions. Therefore, egg availability,  $E(t)$ , is defined by a normal distribution  $E(t) = N(t, \mu, \sigma)$ , which we scale to unity. The duration of seasons is arbitrarily scaled to range between 0 and 1. The fitness of the mutant male is the product of the amount of eggs available to be fertilized,  $E(t)$  (fig. 2.2A), and the expected fertilization success they can achieve given their fertilization mode,  $F(t)$  (fig. 2.2B), and the mutant's phenotype relative to the resident population (note that mutants are always modelled to invade a population with the same fertilization mode, we do not address the relative competitive ability of internal vs. external fertilization). Because spawning is temporally explicit, this product is integrated across the season (fig. 2.2C,D). In the example given, in fig. 2.2C,D, both the population and mutant suffer high polyspermy during peak spawning and so are bimodal. However, the mutant has a larger variance, and therefore releases relatively more sperm than population males before and after peak spawning. This strategy allows the mutant to compete more effectively for fertilizations at this time while sacrificing competitive ability during peak spawning, and in this example, results in a relative fitness greater than 1 (area under red curve exceeds area under blue curve). The

same scenario is illustrated for internal fertilizers, but the population fitness curve is unimodal because internal fertilizers do not suffer from polyspermy in our models. The bimodality in the mutant fitness curve is due entirely to negative frequency-dependence resulting from competition for fertilizations. This method results in the overall fitness equation:

$$W(m, v, m^*, v^*) = \int \frac{s(t)}{s_T(t)} F(t) Q(t) dt. \quad (2.16)$$

As in traditional game-theoretic models, the ESS represents the phenology  $(m^*, v^*)$ , such that if all males in the population employed this strategy, no mutant male with a different phenology could achieve a relative fitness  $> 1$  (Maynard Smith 1982). That is, if a population of males release sperm according to the ESS phenology, they cannot be invaded by any mutant with a different mean or variance sperm release rate. Formally, the ESS is defined by the value of the traits  $m^*$  and  $v^*$  and that satisfy :

$$\left. \frac{\partial W(m, v, m^*, v^*)}{\partial m} \right|_{\substack{v = v^* \\ m = m^*}} = 0, \quad (2.17)$$

$$\left. \frac{\partial^2 W(m, v, m^*, v^*)}{\partial m^2} \right|_{\substack{v = v^* \\ m = m^*}} < 0, \quad (2.18)$$

and,

$$\left. \frac{\partial W(m, v, m^*, v^*)}{\partial v} \right|_{\substack{v = v^* \\ m = m^*}} = 0, \quad (2.19)$$

$$\left. \frac{\partial^2 W(m, v, m^*, v^*)}{\partial v^2} \right|_{\substack{v = v^* \\ m = m^*}} < 0. \quad (2.20)$$

The fitness function defined by Eq(2.16) has no closed form solution, thus we solved for the values of  $m^*$  and  $v^*$  that satisfy the ESS conditions numerically.

## 2.6 Results

There are three principal findings of our models. First, our analytic model demonstrates that completely synchronous spawning by males at the environmental optimum is never an ESS due to negative frequency-dependence in males' reproductive success (fig. 2.1). Second, negative frequency-dependence due to among-male competition for fertilizations drives the evolution of spawning away from the environmental optimum through increases in male ESS variance ( $v^*$ ). Third, fertilization mode qualitatively alters the relation between males' ESS variance ( $v^*$ ) and population density ( $N$ ), as well as the prevalence of sexual conflict over the timing of reproduction (fig. 2.3) (See Table 2.2 for a summary of numerical ESS results).

### 2.6.1 Effects of fertilization mode and population size

Fertilization mode, and the associated relation between local sperm concentration and fertilization success strongly influenced  $v^*$ , but had no effect on the ESS mean release time ( $m^*$ ).  $m^*$  was always predicted to coincide with the peak in female

spawning ( $\mu = 0.5$ ), which was at the midpoint of the season in our model. Except at high population densities ( $N$ ), internal fertilizers are predicted to have a higher ESS variance than externally fertilizers (fig. 2.3A,B). As  $N$  increases,  $v^*$  for internal fertilizers asymptotically approaches the expected ESS for males with constant fertilization dynamics. This is because fertilization success for internal fertilizers asymptotes at 1 with increasing  $N$  (fig. 2.2A & Ch2Fig4A,B). For external fertilizers at high population sizes, decreasing fertilization success at peak spawning times due to polyspermy (fig. 2.4C,D) result in  $v^*$  that exceeds those of either internal fertilizers or males with constant fertilization success (fig. 2.3A,B).

### 2.6.2 Female fitness and sexual conflict

Our numerical ESS results suggest that for externally fertilizing species, the male ESS will result in decreased female fitness across most population densities we explored. Specifically, the relation between female fitness (the proportion of eggs fertilized) and population size is convex, with maximum at intermediate population densities (fig. 2.3C,D). At lower densities,  $v^*$  is small relative to  $\sigma$ , which simultaneously prevents females from acquiring fertilizations during adjacent periods of high environmental quality, and inflicts fitness losses due to polyspermy during peak spawning times (fig. 2.4C,D). At high densities,  $v^*$  is large, and although the proportion of eggs lost to polyspermy is high throughout the middle of the season (fig. 2.4C,D), females cannot achieve equivalent fitness due to decreases in environmental quality on the shoulders of the reproductive season.

In contrast to external fertilizers, our model suggests that the strength of sexual conflict over the timing of reproduction in internally fertilizing species will decrease rapidly with increasing population density. The relation between  $N$  and both  $v^*$  and female fitness is a saturating function (fig. 2.3B,D). Thus, as population density increases, the difference between female realized fitness, and their maximum possible fitness decreases asymptotically.

### 2.6.3 Effects of traits influencing egg fertilization

Our results for both  $v^*$  and female fitness do not change qualitatively with the value of  $A_{ext}$  or  $A_{int}$ . Changes in traits or conditions that increase the likelihood of mate encounters, sperm and egg contact, or egg fertilizability (larger  $A$  values) always increase  $v^*$ , as well as increase the steepness of the relation between  $v^*$  and  $N$  (fig. 2.3A,B), and between  $v^*$  and female fitness (fig. 2.3C, D; fig. S2 in the Supplement at [www.int-res.com/articles/suppl/m537p023\\_supp.pdf](http://www.int-res.com/articles/suppl/m537p023_supp.pdf)).

Increases in egg fertilizability (larger  $A_{ext}$ ) shift the location of the female fitness maximum to lower population densities, and increases the steepness of the fitness surface (fig. 2.3C,D). This results in an accompanying shift in the population densities where males and females are not in conflict, but also decreases the range of population densities where sexual conflict is lowest. For internal fertilizers, higher mate encounter rates, or sperm filtering efficiency (higher  $A_{ing}$ ) decrease the strength of sexual conflict at lower population densities, but do not qualitatively alter this relation, or the value female fitness asymptotically approaches with increasing  $N$  (fig. 2.3C, D)

## 2.7 Discussion

### 2.7.1 Evolution of reproductive asynchrony

We found that completely synchronous reproduction by males when environmental conditions are most conducive to offspring survival is never an optimal strategy due to frequency-dependent selection. Specifically, negative frequency-dependent selection on reproductive timing due to among-male competition for fertilizations counterbalanced environmental variation to maintain within- and among-individual variance in phenologies in our models. A corollary of this finding is that asynchrony is an inevitable consequence of frequency-dependent selection when males compete for fertilizations. This result is conceptually similar to predictions from a long history of theoretical models of niche evolution (Roughgarden 1972), and the evolution of continuous traits along environmental gradients (e.g., Lande 1976). In these models, intraspecific competition for resources creates frequency-dependent selection on the trait of interest, while in our model among-male competition for fertilizations drives frequency-dependence. Likewise, the study of flowering phenologies in angiosperms has long acknowledged the potential influence of frequency-dependent processes, such as patch attractiveness, pollinator competition, and seed predation, as well as their interaction with environmental conditions to influence the evolution of phenological variance (e.g., Augspurger 1981; Thomson 1981; Rabinowitz et al. 1981; early literature reviewed in Rathcke and Lacey 1985; Elzinga et al. 2007; Devaux and Lande 2010). The importance of frequency-dependent selection has even been recognized in the evolution of gamete recognition proteins in externally fertilizing marine species (Panhuis et al. 2006; Levitan and Ferrell 2006), but has yet to be thoroughly explored in the context of reproductive phenologies. A fundamental consequence of anisogamy is that sperm from different males compete numerically to fertilize eggs (Parker 1982; Birkhead and Møller 1998) and therefore negative frequency-dependence due to among male competition is likely to be a general mechanism maintaining variance in male reproductive timing.

Despite the potential importance of negative-frequency dependent selection on reproductive phenology, the longstanding view of reproduction in aquatic systems is that it must be highly synchronous and coincident with favourable environmental conditions (see seminal papers by Thorson 1936, 1946, 1950). Similarly, early fisheries models predicted that spawning should evolve to synchronize offspring larval development with favourable environmental conditions (Cushing 1969, 1990; Lowerre-Barbieri et al. 2011). These ideas have remained influential. For example, mass spawning of coral species on the Great Barrier Reef has often been described as synchronous (Harrison et al. 1984; Babcock et al. 1986), as has the reproduction of many marine algae species (Clifton 1997). Synchronous reproduction in crabs and reef fish coincident with diel, lunar, and tidal cycles has been proposed as an adaptive strategy to avoid predation (Morgan and Christy 1995; Christy 2011). Studies of spawning time in many commercially important fish species have documented annual peaks in reproductive activity as measured by spawning stock biomass, and synchronized diel periodicity of spawning behaviours (Lowerre-Barbieri et al. 2011). However, many species thought to have highly synchronous reproduction exhibit greater among- and within-individual variance in phenology than initially thought, and don't necessarily time reproduction to coincide with optimal environmental conditions. Many corals that participate in mass spawning also spawn during multiple periods each year, each lasting up to several months (Baird et al. 2009). Some

species of marine polychaetes have been shown to predominantly spawn when temperatures are sub-optimal for fertilization success (Lewis et al. 2002; Lewis et al. 2003). Weak reproductive synchrony has been documented in a variety of taxa, including sea urchins (Levitan 1988), intertidal ascidians (Marshall 2002), as well as several crab species across a gradient of seasonal resource fluctuation intensity and larval predation by planktivorous fish (Morgan et al. 2011). Likewise, many fisheries species and tropical reef fish are batch spawners that exhibit high individual and population level variance in spawning time and duration, and individuals often skip spawning events (Robertson 1990; Robertson et al. 1990; Sadovy 1996; Lowerre-Barbieri et al. 2011). These studies suggest that reproduction in aquatic systems may be less synchronous than previously thought.

In fact, our understanding of reproductive synchrony in natural populations of aquatic species is extremely limited, especially for external fertilizers. This is because relatively few studies report both the individual and population level data necessary to quantify it. Direct observation of individual reproduction is sometimes possible for internally fertilizing coastal species (e.g., Christy 1978), as well as for brooding fish species with established nests (Robertson 1990; Robertson et al. 1990; Sadovy 1996; Lowerre-Barbieri et al. 2011). However, quantifying reproductive synchrony can be technically difficult for many external fertilizing species. Reproductive synchrony is highly scale-dependent: synchrony only matters at the temporal and spatial scales at which gametes, or reproductively active individuals, interact. For example, individual spawning events in many sea urchin populations take place over one to several hours, but sperm released from individual males dilutes to ineffective concentrations within seconds of being released (Levitan 1988, 1998; Lotterhos and Levitan 2011). This rapid dilution of gametes during advection in externally fertilizing species means reproductive synchrony only matters at small spatial scales. In situ fertilization success declines sharply with the distance to nearest spawning males in several sea urchin species, and is effectively zero when mates are  $> 1.5$  m away (Levitan 1998, 2002). Few studies have managed to measure synchrony at the temporal or spatial scales that matter to the organisms of interest. In a notable exception, Levitan et al. (2011) documented spawning times for individual colonies in populations of three *Montastraea* coral species. Population phenologies lasted 60 min for all three species, but each colony only released gametes for 1 min. Gamete ageing influences within-individual variation in these species — sperm are most effective at fertilizing eggs 30 min after spawning, and die 60–90 min later — but the scale of this variation does not equalize fertilization probabilities for colonies spawning at different times (Levitan et al. 2004). Thus, the precise timing of reproduction with environmental cues does not necessarily result in synchronous reproduction; to detect reproductive asynchrony, the timing of reproduction must be measured on the temporal scale at which competition for fertilization takes place.

Previous explanations for asynchronous reproduction have traditionally invoked stochastic variation in environmental conditions (Iwasa 1991; Iwasa and Levin 1995; Post et al. 2001; Durant et al. 2007; Morgan et al. 2011). In effect, unpredictable environmental conditions represent both changing cues for reproduction, and a moving target for selection on individual phenology (Durant et al. 2007; Christy 2011; Morgan et al. 2011). Previous theory has emphasized that in temporally unpredictable environments, within-individual variance in phenology is an adaptive bet-hedging strategy (Iwasa 1991; Iwasa and Levin 1995). Both bet-hedging and among-male competition for fertilizations could create selection for increased within-individual variance that would push spawning away from the environmental optimum. However, it is unclear what the evolutionary consequences of feedback between these

processes would be. While both are likely to influence the evolution of phenologies simultaneously, our results suggest that among-male competition for mates and fertilizations may act as an important counterbalance to environmental and biotic sources of positive frequency-dependence, and provides a mechanistic link between other life history traits, such as fertilization mode, and the evolution of phenology.

### 2.7.2 Effects of fertilization mode and population density

The effect of population density on our model predictions of phenological variance was mediated by fertilization mode. External fertilizers were predicted to have lower ESS variance than internal fertilizers at lower population densities, but higher variance at high population densities (fig. 2.3A,B). These predictions reflect the fact that phenologies in externally fertilizing males are influenced by selection caused by polyspermy in our model. Males must release sperm synchronously enough to ensure high fertilization success, but if too many males release sperm too synchronously, high local sperm concentrations destroy a large proportion of eggs via polyspermy. Paradoxically, egg mortality due to polyspermy is greatest when environmental conditions are most conducive to offspring survival – peak sperm concentrations occur at the environmental optimum, and egg mortality is therefore highest at this time. At higher densities, increased polyspermy causes the distribution of monospermic fertilizations through time to become increasingly bimodal (fig. 2.4C,D), resulting in stronger selection for higher variance in male phenologies. However, this does not result in reproductive isolation or speciation in our numerical ESS model because male ESS mean release time ( $m^*$ ) remains at the environmental optimum.

At low densities, our model predicts that internal fertilizers will have a higher ESS variance than external fertilizers because of negative frequency-dependence caused by among male competition for fertilizations. Because internal fertilizers can achieve higher fertilization success at lower densities relative to external fertilizers (fig. 2.4A,B; Pemberton et al. 2003), the fitness benefits of outcompeting rival males for fertilizations outweigh the costs of releasing sperm during less favourable environmental conditions. Consequently, internal fertilizers respond more strongly to negative frequency-dependence than external fertilizers at lower densities. Because internal fertilizers generally do not experience egg mortality due to polyspermy (Gould and Stephano 2003; Wong and Wessel 2005), at higher densities the ESS variance for internal fertilizers becomes increasingly constrained by environmental conditions, and asymptotically approaches the value obtained under constant fertilization dynamics. Thus an unanticipated prediction from our model is that, except at very low population densities, internally fertilizing species should more closely track seasonal fluctuations in environmental conditions than externally fertilizing species.

Our numerical ESS predictions are consistent with observed spawning phenologies in many aquatic taxa. For externally fertilizing species susceptible to polyspermy, males are predicted to release sperm more synchronously under sperm-limiting conditions (e.g., low male densities, rapid sperm advection), than under conditions that result in polyspermy (e.g., high densities, aggregated spatial distribution, slow sperm advection). Given the attention that sperm limitation has received as an explanation for synchronous reproduction in external fertilizers, our prediction that polyspermy should create selection for high variances that can exceed even seasonal

environmental fluctuations seems somewhat counterintuitive (Thorson 1950; Levitan 1993; Yund 2000). However, this prediction is consistent with observed spawning phenologies in marine taxa that experience high population densities, or that aggregate during mating. For example, many aggregating sea urchin species spawn sporadically during each lunar month (Levitan 1988), and populations of the gregarious sessile serpulid polychaete *Galeolaria caespitosa*, which can reach population densities of thousands per square meter, spawn continuously during the year (Kupriyanova 2006). Although polyspermy is less important among fishes, many externally fertilizing species that aggregate for mating exhibit similar patterns of asynchronous reproduction (Robertson 1990; Robertson et al. 1990; Sadovy 1996; Lowerre-Barbieri et al. 2011). The prediction that external fertilizers will have a lower ESS variance than internal fertilizers at lower population densities is also consistent with spawning patterns in a variety of taxa. Many internally fertilizing freshwater fish species (e.g., many species of the *Cyprinodontiformes*) are characterized by small population sizes and opportunistic spawning throughout the year (Winnemiller 1989; Gonçalves et al. 2005). Likewise, spermcasting is a common mode of internal fertilization among marine invertebrates from diverse phyla, and males of these species generally release sperm slowly and sporadically over long periods of time (Pemberton et al. 2003).

There have been relatively few studies to explicitly test our models' predictions in aquatic taxa. Marshall and Bolton (2007) showed in a flume experiment that slower sperm release rates resulted in higher fertilization success of multiple downstream batches of eggs in the marine tube worm *Galeolaria caespitosa*, but they did not perform sperm competitive trials. Conversely, Levitan (2005) demonstrated under realistic field conditions that males releasing sperm a longer interval before females enjoy a competitive advantage for fertilization success over other males, but this study did not directly manipulate the duration of sperm release. Among internal fertilizers, there is some experimental evidence from shallow water crab species that supports our models' predictions, albeit through plastic behavioural responses rather than trait evolution. Several studies have demonstrated that male crabs increase the duration of mating behaviours in the presence of male competitors (e.g., Jivoff 1997; Rondeau and Sainte-Marie 2001). Kim et al. (2010) indirectly augmented the strength of among-male competition for mates in a food-supplementation experiment while documenting reproductive phenologies in both sexes for a population of fiddler crabs (*Uca terpsichores*). They found that well-fed males increased both the intensity and duration of mating displays, while female mating phenologies remained unchanged. Thus, male phenological variances in this species may increase with the intensity of among-male competition independent of the timing of female receptivity, a result that is consistent with our prediction that male reproductive phenologies in internal fertilizers should reflect a balance between among-male competition and environmental conditions. For both externally and internally fertilizing species, our model predictions pose a question that has been largely overlooked in aquatic taxa — how are the temporal distributions of male investment in reproduction influenced by the intensity of among-male competition?

### 2.7.3 Female fitness and sexual conflict

Our numerical ESS suggests there may be qualitative differences in the prevalence of sexual conflict over spawning phenology in external versus internal fertilizers. These results are only suggestive because female phenologies were not allowed to evolve in our models. Thus, while the evolution of male phenologies could result

in decreased female fitness in our models, female phenologies were not allowed to evolve in ways that could decrease male fitness, or limit the parameter space explored by males. It is nevertheless interesting that for external fertilizers in our numerical ESS model, the male ESS variance will maximize female fertilization success at intermediate population densities (fig. 2.3C,D; maximum at  $N \approx 58$ , and  $N \approx 58$  for low and high  $A_{ext}$  values respectively), but result in decreased female fitness at both low and high population densities. This apparent conflict is a consequence of female fitness being influenced simultaneously by environmental conditions and egg mortality due to polyspermy. Even at relatively low densities, males are predicted to release sperm over a short period of time, resulting in sperm concentrations that cause some polyspermy during the middle of the season (fig. 2.4C,D). Counter-intuitively, so long as females can still obtain monospermic fertilizations when environmental conditions are relatively good, they enjoy higher total fertilization success at intermediate densities where non-trivial levels of polyspermy occur (figs. 2.3C,D & 2.4C,D). At high densities, females are 'squeezed' between severe egg mortality due to polyspermy during the middle of the season, and decreasing environmental quality on the shoulders of the season, and female fitness begins to decline.

Sexual conflict in external fertilizers is strongly density dependent, and has generally been considered in the context of balancing sperm limitation and polyspermy (Levitan 2004, 2005; Bode and Marshall 2007). At low densities, local sperm concentrations limit fertilization, and both sexes have been predicted to evolve traits that increase fertilization rates (Levitan 1998, 2005; Levitan and Ferrell 2006). At high densities, males experience intense competition for fertilizations, while females experience selection to decrease fertilization rates in order to avoid polyspermy (Franke et al. 2002; Levitan 2002, 2004; Bode and Marshall 2007). For example, polyspermy-mediated sexual conflict has been shown to result in strong frequency-dependent selection on gamete traits influencing fertilization such as egg size and gamete compatibility proteins (Panhuis et al. 2006; Levitan and Ferrell 2006). More recently, Bode and Marshall (2007) showed theoretically that at low densities where sperm is limiting sperm competition should cause males to release less sperm at any given time than would result in complete fertilization of females' eggs. Our results support the idea that external fertilizers experience sexual conflict at most population densities (Bode and Marshall 2007), but suggest that polyspermy-mediated conflict can happen at both low and high densities. The nature of this conflict, however, depends strongly on whether phenologies are constrained by environmental conditions. If phenologies are not constrained by environmental conditions, female fitness will increase with population density despite higher rates of polyspermy. This prediction is in direct contrast to previous models of sexual conflict in external fertilizers, but congruent with empirical studies which have documented non-trivial levels of polyspermy, even under sperm-limited conditions (Franke et al. 2002; Marshall 2002; Levitan 2004). Although sex-specific phenologies were not possible in our models, the prevalence of sexual conflict over reproductive timing suggest that this is a likely evolutionary outcome for this group, an expectation that is consistent with observed differences in male and female spawning behaviours in many externally fertilizing marine invertebrates (Levitan 2005; Lotterhos and Levitan 2011).

For internal fertilizers, the male ESS variance will result in lower female fitness only at low population densities (fig. 2.3B,D). At low densities, competition for fertilizations causes males to release sperm over time such that local sperm concentrations are never high enough to maximize female fertilization success. Our model predicts that males and females will not be in conflict over the timing of reproduction at high densities, when competition among males for fertilizations is strongest,

and sexual conflict over a variety of other traits is well documented (Parker 1979, reviewed in Chapman et al. 2003). While there are many classic examples of sexual conflict in internal fertilizers, very few studies have considered conflict over the timing of reproduction. It would be interesting to see if, as our model suggests, there is indeed little conflict over the timing of reproduction in internally fertilizing species that experience strong sexual conflict and selection on traits affecting pre- and post-copulatory mate choice.

#### 2.7.4 Effects of traits influencing egg fertilization

The results for male ESS variance were robust to changes in the relation between fertilization success and sperm concentration ( $A_{ext}$ ,  $A_{int}$ ), and so may be generally applicable to a variety of species and environmental conditions. Interestingly, our model predicts an evolutionary association between egg phenotype and phenology, particularly for externally fertilizing species. Traits such as egg size, the density of sperm receptor sites on the egg surface, and gamete compatibility proteins can all interact with population density to influence the likelihood of monospermic fertilization (Levitan 2002, 2004; Levitan and Ferrell 2006). Trait values that increase the likelihood of egg fertilization increase male sensitivity to negative frequency-dependent selection on the variance in phenology due to polyspermy and competition for fertilizations, and alter the conditions under which males and females are predicted to be in sexual conflict (fig. 2.3C, D). Thus, our model predicts that species with larger, more fertilizable eggs should reproduce more asynchronously than species with smaller, less fertilizable eggs.

For internal fertilizers, in addition to gamete traits, traits that increase male efficiency at locating and copulating with mates, or filtering sperm, influence phenology primarily through negative frequency-dependence due to among male competition for fertilizations. As with external fertilizers, trait values that increase the likelihood of egg fertilization increase males' sensitivity to negative frequency-dependent selection, resulting in larger variances. However, because internal fertilizers do not suffer the same effects of polyspermy, this effect is most visible at low population densities. When fertilization probabilities are relatively low (e.g., low densities, small eggs, inefficient mate searching), male phenologies should have relatively low variances (but higher than predicted for external fertilizers). Under conditions resulting in high fertilization probabilities (e.g., high densities, large eggs, efficient mate location), selection should favour male phenologies with variance of similar magnitude to prevailing environmental fluctuations (fig. 2.3A, B).

#### 2.7.5 Conclusions

Our analysis expands on traditional hypotheses regarding the evolution of asynchronous reproduction to recognize the importance of negative frequency-dependent selection due to competition among males for fertilizations. We show that when males compete for fertilizations, perfect reproductive synchrony with optimal environmental conditions is never an optimal evolutionary strategy, and asynchronous reproduction is an inevitable consequence of frequency-dependent selection. In addition, our models show that important life-history traits, such as fertilization mode, can alter species' sensitivity to this frequency-dependence and qualitatively alter selection on within- and among-individual variance in phenologies. Our models' predictions are broadly consistent with observed phenologies in many aquatic taxa.

However, more detailed studies that adequately measure variation in both individual and population phenologies at temporal and spatial scales relevant for gamete interactions are needed against which to test our model predictions.

## **Acknowledgements**

We thank C. Venables for valuable discussions and three anonymous reviewers for helpful comments on the manuscript. C.O., M.B., and D.J.M. conceived the study, C.O. and M.B. performed the analyses, and C.O. wrote the manuscript with assistance from M.B. and D.J.M. This work was funded by a Monash University Dean's International Postgraduate Student Scholarship to C.O., and Australian Research Council grants to M.B. and D.J.M.

## 2.8 Tables

TABLE 2.1: Key terms and parameters

Term	Description
<b>General Terms</b>	
$\mu = 0.5$	Environmental quality mean
$\sigma = 0.15$	Environmental quality standard deviation
$t$	Time, within season
$N$	Population density
$A_{ext}$	External fertilization curve shape parameter, determines location of maximum & steepness of curve
$A_{int}$	Internal fertilization curve shape parameter, determines steepness of sigmoidal function
$W_p, W_m$	Fitness of the population, mutant respectively
<b>Analytic models</b>	
$e$	Deviation in time from resident population strategy
$d$	Proportion of mutants adopting asynchronous strategy
$N^*$	Critical population density above which a mutant strategy will be able to invade
<b>Analytic models</b>	
$m, m^*$	Mean sperm release time for mutant, population respectively
$v, v^*$	Standard deviation sperm release time for mutant, population respectively

Key terms and parameters used in models to investigate theoretically how fertilization mode and population density interact to influence selection on phenology. ESS: evolutionary stable strategy

TABLE 2.2: Numerical ESS predictions

Mode	$N$	Process	Egg fertilizability	
			Low	High
External	High	$v^*$	$\uparrow$ (Int > Ext)	$\uparrow$ (Int > Ext)
		Conflict	—	—
	Low	$v^*$	$\downarrow$	$\uparrow$
		Conflict	+	+
Internal	High	$v^*$	$\uparrow$	$\uparrow\uparrow$
		Conflict	—	+
	Low	$v^*$	$\downarrow$	$\downarrow$
		Conflict	+	+

Key to symbols: ( $\uparrow$ ) high variance; ( $\uparrow\uparrow$ ) very high variance; ( $\downarrow$ ) low variance; (+) indicates sexual conflict is predicted to occur; (-) sexual conflict is not predicted.  $N$ : density;  $v^*$ : ESS male sperm release time variance.

## 2.9 Figures

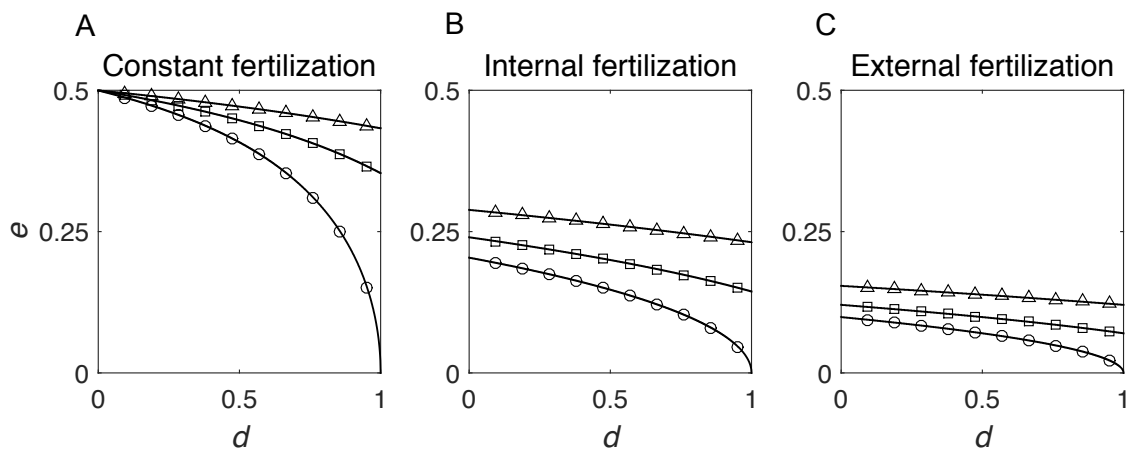


FIGURE 2.1: Mutations that are able to invade populations that exhibit (A) no fertilization dynamics, (B) internal fertilization dynamics and (C) external fertilization dynamics, consisting of ( $\circ$ ) 2, ( $\square$ ) 3, and ( $\triangle$ ) 5 individuals with pure synchronous spawning strategies. Combinations of deviation in time from resident population strategy ( $e$ ) and the proportion of mutants adopting asynchronous strategy ( $d$ ) that can successfully invade are below and to the left of the each of the lines. Panels show model results when egg fertilizability is low (curve shape parameter values:  $A_{ext} = 0.02$ ,  $A_{int} = 10$ ).

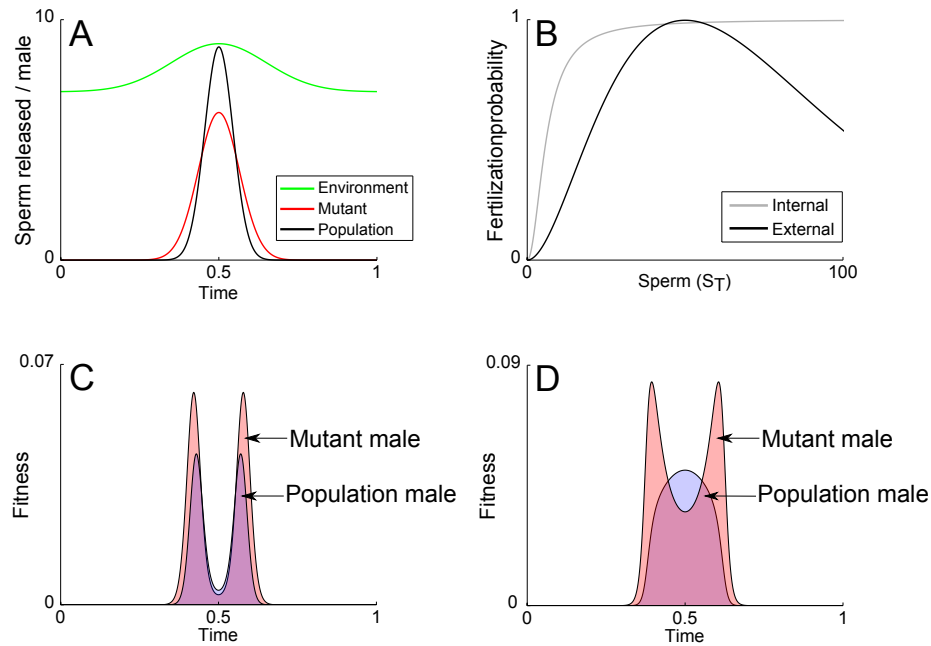


FIGURE 2.2: Influence of negative-frequency dependence and polyspermy on the behaviour of the numerical ESS model. (A) The reproductive phenology of the population (black line) and mutant (red line), with the fluctuation in environmental quality indicated at the top of the figure ( $Q(t) \in [0, 1]$ ). In this example, the mutant has a larger variance than the population. (B) Fertilization functions for external (Eq 2.2) (black line) and internal (Eq 2.3) (grey line) fertilizers.  $S_T$  = total amount of sperm released by males. Bottom panels provide an illustration of how per-male fitness (Eq. 2.16) is calculated for (C) external and (D) internal fertilizers through time for the population (blue curve) and mutant (red curve). In this example, male density is high enough to result in polyspermy at peak spawning, and mutants have a higher variance than the population.

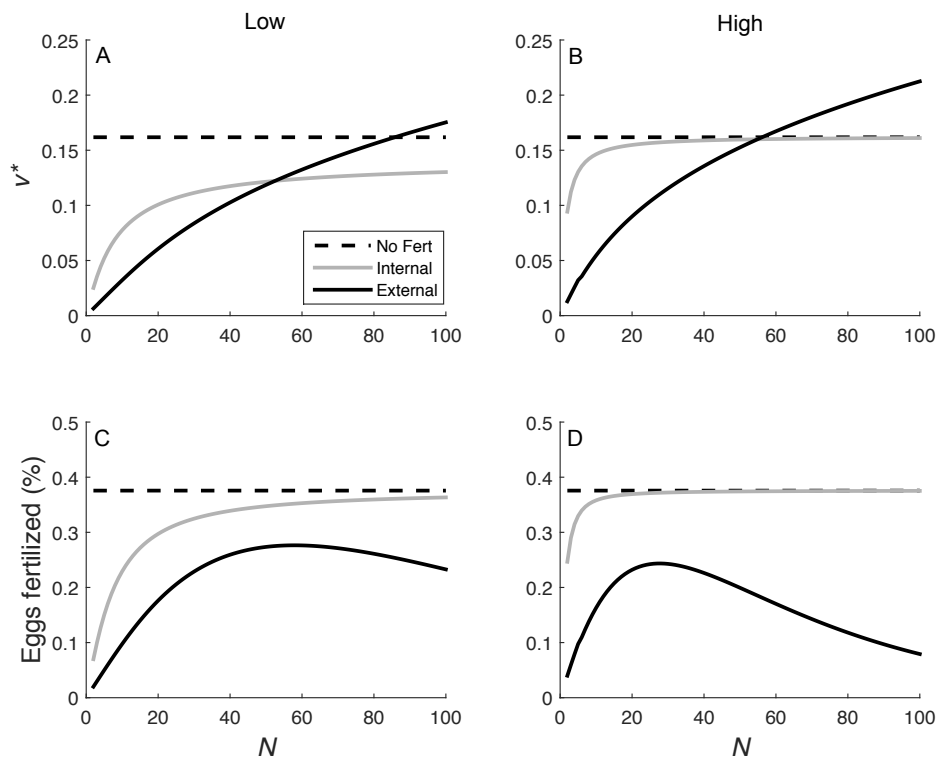


FIGURE 2.3: Male sperm release time variance ( $v^*$ ) when egg fertilizability is (A) low ( $A_{ext} = 0.02$ ,  $A_{int} = 10$ ) and (B) high ( $A_{ext} = 0.04$ ,  $A_{int} = 2$ ), and female fitness with (C) low and (D) high egg fertilizability, as a function of population density ( $N$ ) for external (black) and internal (grey) fertilizers, with constant fertilization dynamics (dashed line).

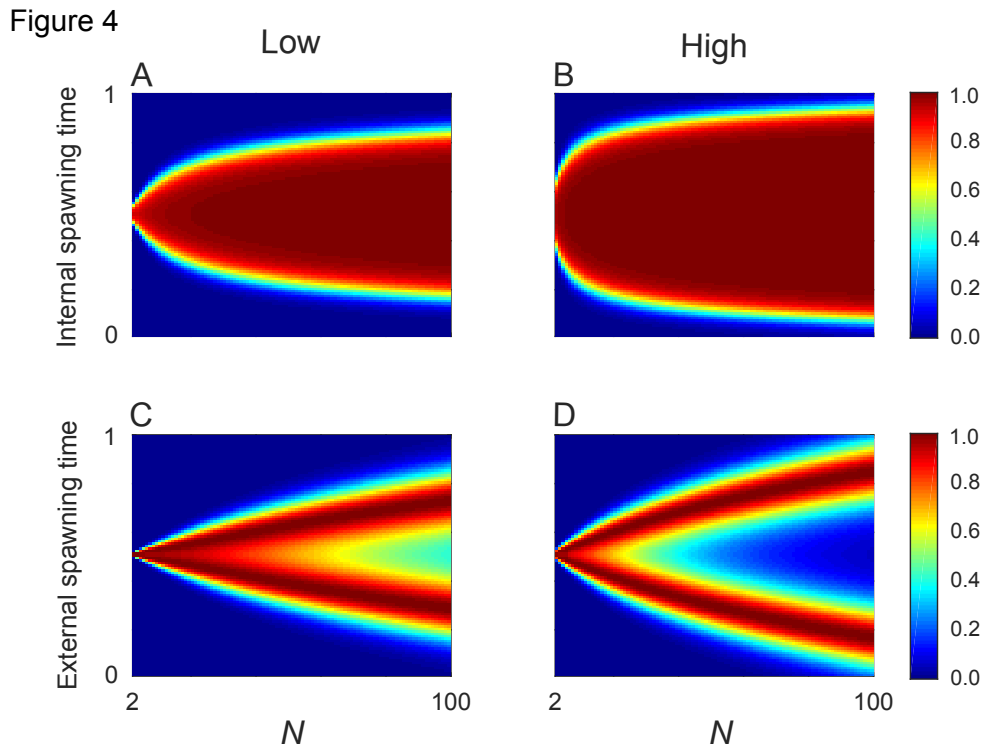


FIGURE 2.4: Probability of successful monospermic fertilization through the reproductive season as a function of population density ( $N$ ) for (A,B) internal and (C,D) external fertilizers. (A,C): low egg fertilizability ( $A_{ext} = 0.02$ ,  $A_{int} = 10$ ); (B,D): high egg fertilizability ( $A_{ext} = 0.04$ ,  $A_{int} = 2$ ). The y-axis represents the reproductive season through time and is scaled arbitrarily to range between 0 and 1. The colour scale indicates the probability of successful fertilization.

## 2.10 Supplementary Figures

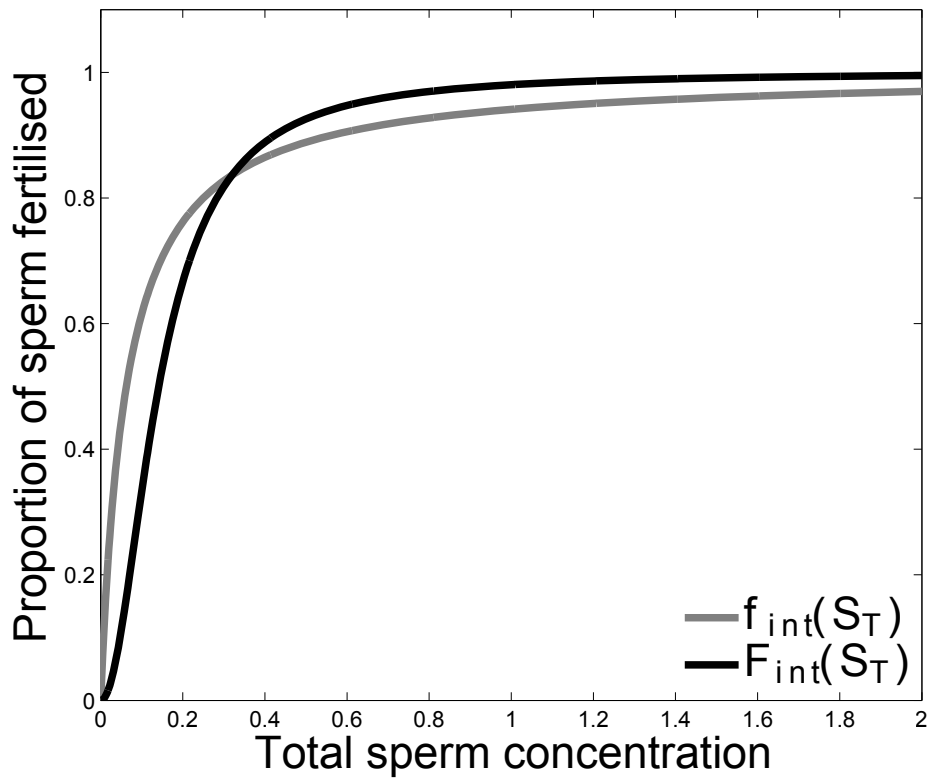


FIGURE 2.S1: Fertilization curves used for internal fertilizers in the analytic (grey line; Eq 2.4) and numerical ESS models (black line; Eq 2.3), as a function of the total sperm concentration ( $S_T$ ). Results are shown for the case of  $A_{int} = 1$  for the function used in the numerical models ( $F_{int}(S_T)$ ). To illustrate the similar form of the two functions, we parameterized the function used in the numerical models ( $f_{int}(S_T)$ ) the by choosing the value of  $A_{int}$  that minimized the squared deviation between the two functions. Note that the functions are very similar, except for sigmoidal behaviour at low sperm concentrations for  $F_{int}(S_T)$ .

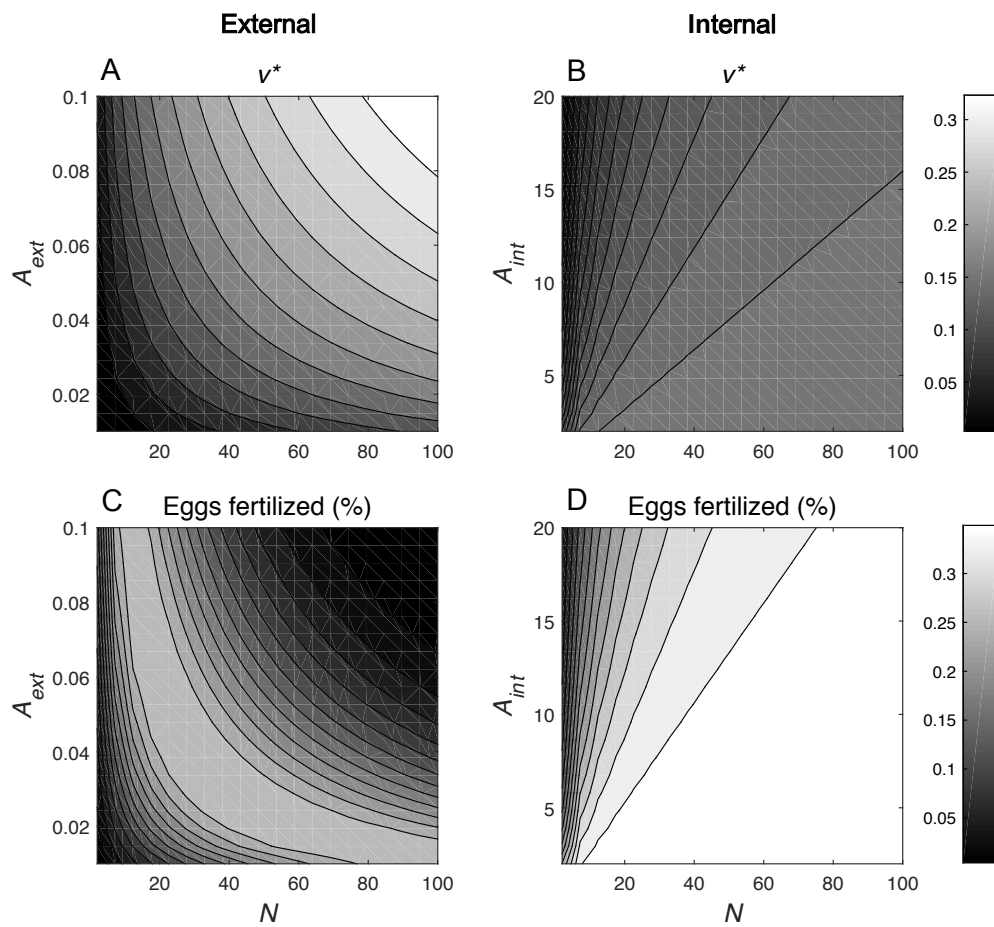


FIGURE 2.S2: Effects of variation in fertilization parameters  $A_{ext}$  and  $A_{int}$  and population density ( $N$ ) on male ESS variance (A,B) and female fitness (C,D) for external and internal fertilizers. For ease of comparison between external and internal fertilizers, plots of  $v^*$  (A,B) and female fitness (C,D) are shown with a common colour scale.



## Chapter 3

# The evolution of reproductive phenology in broadcast spawners, and the maintenance of sexually antagonistic polymorphism<sup>1</sup>

### 3.1 Abstract

Reproductive phenology is a crucial life-history trait that evolves in response to external environmental conditions and frequency- and density-dependent interactions within species. Broadcast spawners — which represent a large fraction of aquatic biodiversity — evolve phenologies that balance strong density-dependent fertilization success against abiotic environmental conditions that are required for successful reproduction. The overall balance between these processes may be particularly complex in dioecious species, where selection on reproductive timing potentially differs between the sexes. Here, we develop a population genetic model of reproductive phenology in a dioecious broadcast spawning species and show that environmental variability and density-dependent fertilization dynamics naturally give rise to profound sex differences in selection on gamete-release strategies. The frequency-dependent nature of sperm competition generates sexually antagonistic selection on reproductive timing and facilitates the maintenance of genetic variation in phenological traits. Selection in females favors monomorphic spawning phenologies that maximize net fertilization success and offspring survival across environmental conditions, whereas selection in males often favors polymorphic phenologies that are primarily shaped by sperm competition. Our model helps explain several well-documented empirical observations in aquatic species, including high intraspecific variance of reproductive phenologies, sex-specific spawning phenologies, and spawning during environmentally suboptimal times.

---

<sup>1</sup>This chapter has been published as: Olito, C., D. J. Marshall, and T. Connallon. 2017. The evolution of reproductive phenology in broadcast spawners, and the maintenance of sexually antagonistic polymorphism. *American Naturalist* 189:153–169.

## 3.2 Introduction

Reproductive phenology is a pivotal life-history trait influencing the evolution of plant and animal species. The timing of reproduction determines mating opportunities (Brunet and Charlesworth 1995; Hendry and Day 2005; Elzinga et al. 2007), the environmental conditions experienced by mating adults and their offspring (Cushing 1969, 1990; Brunet and Charlesworth 1995; Elzinga et al. 2007), as well as each individual's energy budget for growth, reproduction, and development (Stearns 1992; Ejsmond et al. 2010). Indeed, many species experience strong stabilizing selection for reproduction to coincide with environmental conditions that are ideal for mating success and offspring survival (Morgan and Christy 1995; Durant et al. 2007; Lowerre-Barbieri et al. 2011). On the other hand, stochastic environmental conditions and frequency- and density-dependent effects that arise during mating can potentially give rise to selection for increased within-individual variance in phenology (Iwasa and Haccou 1994; Devaux and Lande 2010). For example, while positive density dependence in per capita mate encounter, pollinator visitation, and fertilization rates should select for increased reproductive synchrony between members of a population (Allee et al. 1949; Augspurger 1981; Tomaiuolo et al. 2007; Devaux and Lande 2010), negative frequency- and density-dependent mating success arises when individuals are forced to compete for limited mates, pollinators, or fertilizations; these factors can also generate selection for increased variance in phenology (Fisher 1930; Birkhead and Møller 1998; Levitan 2004; Tomaiuolo et al. 2007; Devaux and Lande 2010).

Although frequency- and density-dependent effects are important for a wide range of aquatic and terrestrial taxa, they are likely to be particularly strong and complex in broadcast spawning species (Levitan 1991, 2002, 2004; Rouse and Fitzhugh 1994; Marshall 2002). Most aquatic organisms shed eggs and sperm directly into the water column (Monro and Marshall 2015), and the consequences of reproductive timing are critical. Spawning strategies must take into account both the availability of mates and fertilization opportunities, as well as the favorability of environmental conditions, which vary over time. As we outline below, reproductive phenology strategies that maximize fitness in broadcast spawning males will often differ from those that maximize female fitness. In this context, pleiotropic effects of loci that influence reproductive timing within both sexes may give rise to sexually antagonistic selection (or intralocus sexual conflict), in which the alleles that benefit one sex prove deleterious when expressed by the other (Kidwell et al. 1977; Rice and Chippindale 2001; Bonduriansky and Chenoweth 2009; Connallon and Clark, 2014b). Developmental genes underlying phenological traits – such as the age of sexual maturity and the timing of reproduction – may experience both differential expression between the sexes and sexually antagonistic selection (McEuan 1988; Levitan 2004; Lotterhos and Levitan 2011; Barson et al. 2015). The timing of gamete release in broadcast spawners therefore provides a broadly relevant arena for examining selection on sexually antagonistic alleles within an explicit ecological context. Importantly, much research on aquatic systems has focused on the consequences of temporally variable environmental conditions and population density for external fertilization and larval mortality (Denny and Shibata 1989; Marshall 2002; Levitan 2004). This ultimately permits us to link the population genetic processes of sex-specific selection to key ecological drivers of the timing of reproduction.

Although external fertilizers are extraordinarily diverse and taxonomically widespread across the tree of life, we focus on the archetypal external fertilizer – the broadcast spawner – which includes seaweeds, corals, sea stars, and many fish taxa.

Broadcast spawning species constitute >50% of marine invertebrates worldwide (Monro and Marshall 2015) and have long served as classic models for the evolution of anisogamy (Parker et al. 1982; Parker 1982). Spawning in broadcasting species has historically been thought to coincide precisely with favorable environmental conditions (e.g., Thorson 1936; Cushing 1969; Harrison et al. 1984; Babcock et al. 1986; Clifton 1997, yet many species exhibit greater variation in reproductive phenology than is expected under this view (McEuan 1988; Marshall 2002; Levitan 2005; Lotterhos and Levitan 2011). Furthermore, many broadcast spawners exhibit protandry, where males release gametes earlier and for longer than females do (McEuan 1988; Levitan 2005; Lotterhos and Levitan 2011). High variance in population phenologies – coupled with sexually dimorphic gamete release strategies – suggests that frequency-dependent, density-dependent, and sex-specific selection may each play critical roles during the evolution of reproductive timing.

For broadcast spawners, individual reproductive success is determined by local gamete concentrations and the kinetics of fertilization. The probability of successful fertilization is governed by the density and reproductive strategies of spawning individuals as well as local hydrodynamic conditions (Denny and Shibata 1989; Levitan 1991, 2002, 2004; Marshall 2002). At low sperm concentrations or rapid advection, the probability of contact between an egg and sperm is low, resulting in sperm-limited fertilization dynamics. At the opposite end of the spectrum, high local sperm concentrations can severely increase egg mortality because of polyspermy, as documented in several aquatic systems (Brawley 1992; Franke et al. 2002; Marshall 2002; Levitan 2004; Levitan et al. 2004). Overall, we expect a bell-shaped relation between population density and the probability of successful fertilization (Millar and Anderson 2003). Sperm-limited contexts should generate sexually concordant selection for increased reproductive synchrony between the sexes, resulting in sperm concentrations that mirror the availability of unfertilized eggs (Tomaiuolo et al. 2007). At high population densities, egg mortality due to polyspermy may lead to strong negative density-dependent selection on spawning time and conflicting selection between the sexes with respect to spawning time (Bode and Marshall 2007; Tomaiuolo et al. 2007; Olito et al. 2015). In synchronously spawning populations, sperm competition may favor the evolution of male gamete release strategies that lead to high rates of polyspermy, suboptimal rates of fertilization, and depressed female fitness (Bode and Marshall 2007; Tomaiuolo et al. 2007; Olito et al. 2015). The evolution of sexually dimorphic reproductive phenologies can potentially resolve this form of sexual conflict. However, such resolutions may involve non-trivial fitness trade-offs between temporally variable sperm concentrations and environmental conditions as well as genetic constraints on the evolution of sexually dimorphic phenotypes (Bode and Marshall 2007; Olito et al. 2015).

In this article, we develop a simple theoretical population genetic model of sex-specific selection on the timing of gamete release phenotypes in a broadcast spawning species. We then explore the robustness of the population genetic model predictions with individual-based quantitative genetic simulations. The models account for environmental variability over time as well as frequency- and density-dependent dynamics of male and female fertilization success. Our models make two important advances on previous theory. First, unlike previous population genetic models of sexually antagonistic selection, we allow selection in both sexes to emerge from underlying processes of frequency- and density-dependent fertilization and spawning phenology. Our models provide a more ecologically grounded approach than classic population genetics models, which typically assign fitness values to genetic variants

arbitrarily rather than explicitly modeling them (see Orr 2005). Second, while previous models of the evolution of phenologies generally assume a perfect correlation between male and female phenotypes (Rathcke and Lacey 1985; Tomaiuolo et al. 2007; Devaux and Lande 2008, 2010; but see Iwasa and Haccou 1994; Brunet and Charlesworth 1995), our population genetic models and quantitative genetic simulations explicitly address the consequences of sexually dimorphic gene expression for the maintenance of genetic variation underlying reproductive phenology. Our new models directly explore the influence of frequency-dependent sexually antagonistic selection on the maintenance of polymorphism and the evolution of reproductive phenology, an antagonistically selected life-history trait.

### 3.3 Methods

Our population genetic model follows the evolution of a dioecious population of broadcast spawners. All individuals are haploid, and generations are discrete and nonoverlapping. Our results are nevertheless likely to apply more generally to hermaphrodite populations that are undergoing obligate outcrossing (Jordan and Connallon 2014). We investigate the conditions permitting balanced polymorphism for a pair of alleles at a single locus that influences reproductive phenology. We do not model long-term evolution under recurrent mutations or substitutions. Hence, our models allow us to identify the evolutionary scenarios that are most and least likely to maintain polymorphism, but they do not assume that a polymorphic state is uninvadable or evolutionarily stable. Indeed, recent theory suggests that adaptation may typically involve the successive invasion of alleles subject to transient balancing selection (Sellis et al. 2011). Furthermore, predictions regarding the long-term evolutionary dynamics from our models would require the strong assumption that population densities and environmental conditions remain stable over similar timescales.

We assume that the ancestral state of the population is sexually monomorphic with regard to spawning phenology. Conditions affecting density-independent offspring and zygote survival are temporally variable, and the reproductive season consists of two time points: one corresponding to the environmental optimum ( $t_0$ ) and the other corresponding to a suboptimal time ( $t_1$ ). All individuals are assumed to have equal resources available for gamete production. Our analysis focuses on the genotypic frequencies ( $1 - p$  and  $p$ ) of wild-type ( $B_1$ ) and mutant ( $B_2$ ) alleles at a single locus influencing the proportion of an individual's gametes that are released at each time point (for a full description of terms, see table 3.1). Within this framework, polymorphism is proportional to among-individual variance in phenology, while intermediate phenotypes are analogous to within-individual variance. Changes in allele frequencies between generations can be caused by two different sources of selection: (1) selection for fertilization success, which is frequency- and density-dependent, and (2) density-independent viability selection based on offspring survival at each time point.

#### 3.3.1 Fertilization Dynamics

A variety of fertilization kinetics models have been derived for external fertilizers. Such models predict the probability of mono- and polyspermic fertilizations as a function of sperm concentration and species-specific gametic traits (Millar and Anderson 2003). For generality and analytic tractability, we model fertilization success

using a modified Ricker equation that gives the same functional form of density-dependent fertilization probability as fertilization kinetics models (after Bode and Marshall 2007; Olito et al. 2015). The probability of successful fertilization is described by the function

$$F(s_t) = \left( \frac{As_t}{2} \right)^2 e^{2-As_t} \quad (3.1)$$

where  $s_t$  is the total amount of sperm released at time  $t_i$  by all males and  $A$  is a positive shape parameter that determines the steepness of the curve and the location of the maximum of the fertilization function. Variation in  $A$  changes the fertilizability of eggs, analogous to changes in egg size or the speed of the polyspermy block (Bode and Marshall 2007; Olito et al. 2015). This changes the population density thresholds at which sperm limitation and polyspermy occur but does not qualitatively alter the behavior of the models. Although the traits influencing  $A$  certainly evolve jointly with phenologies, we focus on the joint evolution of male and female phenologies, given a fixed value of  $A$ , and we present results for only the representative case of  $A = 0.1$ . As in previous models of fertilization dynamics, we assume that sperm greatly outnumber eggs and, therefore, that fertilization probability is independent of egg availability or female density (Vogel et al. 1982; Millar and Anderson 2003). That sperm concentration dominates the fertilization dynamics in external fertilizers has been experimentally demonstrated by numerous studies in diverse taxa (Rothschild and Swann 1951; Vogel et al. 1982; Levitan 1998, 2004; Marshall 2002; Millar and Anderson 2003). While this assumption may be violated if sex ratios are strongly skewed toward females and sperm concentrations are extremely low, cases where eggs outnumber sperm are unlikely. Moreover, populations where this occurs will make minimal contributions to population production because of low fertilization success. We therefore focus our analyses on the scenario where sperm greatly outnumber eggs.

### 3.3.2 A Two-sex, Two-Time-Point Haploid Model of Selection

We begin with a model in which the phenotypic effects of alleles are perfectly correlated between the sexes (hereafter the equal effects model). We subsequently relax this assumption and consider alternative models where phenotypic effects of the alleles differ between the sexes. The phenotypic effects associated with the wild-type ( $B_1$ ) and mutant ( $B_2$ ) alleles are  $\gamma$  and  $\gamma^*$ , respectively, which define the proportion of an individual's gametes that are released at the environmentally unfavorable time point ( $t_1$ );  $1 - \gamma$  and  $1 - \gamma^*$  represent the proportion of gametes released at the favorable time point ( $t_0$ ). Therefore, among the gametes released at each time point ( $t_0$  and  $t_1$ , respectively), the frequency of the mutant genotype is

$$t_0 : \quad g_0 = \frac{p(1 - \gamma^*)}{(1 - p)(1 - \gamma) + p(1 - \gamma^*)}, \quad (3.2a)$$

$$t_1 : \quad g_1 = \frac{p\gamma^*}{(1 - p)\gamma + p\gamma^*}. \quad (3.2b)$$

We define the effective density of males and females as follows. Let  $n_m = N_m a_m$  represent the effective density of males, which takes into account both the number of males ( $N_m$ ) and the total amount of sperm released per male ( $a_m$ ). Likewise, the

effective density of females is  $n_f = N_f a_f$ , where  $N_f$  is the number of females and  $a_f$  is the total number of eggs released per female. For simplicity, we use the terms “population density,” “male density,” and “female density” in the results, but in all cases we are referring to effective density, which takes into account the number of individuals as well as the contributions of each to the gamete pool.

Expressions for effective density can be used to quantify the total number of gametes released by females and males at each time point. The total numbers of sperm released at the two time points are  $s_0 = n_m[(1-p)(1-\gamma) + p(1-\gamma^*)]$  for  $t_0$  and  $s_1 = n_m[(1-p)\gamma + p\gamma^*]$  for  $t_1$ . The number of eggs released at each time point follow from similar expressions. Combining with equation (3.1), the numbers of successfully fertilized eggs at each time point are calculated as

$$t_0 : \quad n_0 = n_f((1-p)(1-\gamma) + p(1-\gamma^*)) \quad (3.3a) \\ \times F\left(n_m((1-p)(1-\gamma) + p(1-\gamma^*))\right)$$

$$t_1 : \quad n_1 = n_f((1-p)\gamma + p\gamma^*) \times F\left(n_m((1-p)\gamma + p\gamma^*)\right) \quad (3.3b)$$

where  $F(\cdot)$  is the fertilization function described in equation (3.1). Successfully fertilized eggs at  $t_1$  experience density-independent mortality at a rate  $d \in [0, 1]$ , resulting from suboptimal environmental conditions. Thus,  $d$  defines the steepness of the environmental gradient. At census, the change in frequency of the mutant allele ( $B_2$ ) due to both sources of selection is

$$\Delta p = g_0 \frac{n_0}{n_0 + n_1(1-d)} + g_1 \frac{n_1(1-d)}{n_0 + n_1(1-d)} - p. \quad (3.4)$$

The corresponding recursion equation is  $p_{t+1} = p(t) + \Delta p$ . We determine the evolutionary fate of a mutant allele by evaluating leading eigenvalues associated with the recursion equation,

$$\lambda = \left. \frac{\partial p_{t+1}}{\partial p_t} \right|_{p=\hat{p}}, \quad (3.5)$$

at the boundary equilibria  $\hat{p} = 0$  and  $\hat{p} = 1$ . Eigenvalues in excess of 1 correspond to unstable equilibria. Evaluating the boundary values of  $\lambda$  allows identification of four possible solution sets: stable equilibrium at  $\hat{p} = 0$  and unstable at  $\hat{p} = 1$ ; stable equilibrium at  $\hat{p} = 1$  and unstable at  $\hat{p} = 0$ ; both boundary equilibria stable; and both boundary equilibria unstable. These boundary eigenvalues roughly correspond to purifying selection against the mutant allele, positive selection for the mutant allele, unstable internal equilibrium, and protected polymorphism (Prout 1968). We explore the prevalence of these different outcomes across male densities ranging between  $n_m \in [0, 100]$  and the full spectrum of possible environmental gradients  $d \in [0, 1]$ .

To further explore the invasibility of wild-type genotypes by mutant alleles as well as the frequency of sexual conflict and protected polymorphism, we evaluated boundary eigenvalues,  $\lambda$ , across  $\gamma \times \gamma^*$  parameter space ( $0 \leq \gamma, \gamma^* \leq 1$ ) at three different male densities ( $n_m = 25, 50, 75$ ) while holding the environmental gradient fixed at an intermediate value of  $d = 0.25$ . These conditions represent biologically interesting and feasible scenarios spanning a gradient of negative frequency- and density-dependent selection and a moderate environmental gradient. At  $n_m = 25$ ,

polyspermy can occur only at the environmentally optimum time, while at  $n_m = 50$  and  $n_m = 75$ , polyspermy can occur at both time points.

In addition to analyzing evolutionary equilibria for the mutant allele frequency,  $p$ , we also examined the evolutionarily stable strategy (ESS) for  $\gamma$  under different densities and environmental gradients. For a given set of conditions regarding the environmental gradient and population density, we specifically identified wild-type phenotypes that prohibit invasion of a new mutant genotype (for ESS methods, see [Appendix A: ESS Conditions](#); [Appendix A: ESS Conditions](#), [Appendix B: Quantitative Genetic Simulation Methods](#) are available online).

### 3.3.3 Sexual Conflict and Patterns of Gene Expression

We subsequently relaxed the assumption of equal phenotypic effects of mutant alleles in each sex and considered three alternative models of sex-specific gene expression. These alternative models serve two purposes. First, they allow for a more general exploration of the evolutionary consequences of sex-specific mutational effects for reproductive phenology. Second, and as described below, they permit us to identify parameter conditions leading to sexually concordant and sexually antagonistic selection on spawning phenology. The three alternative models refer to the expression pattern of the mutant allele,  $B_2$ , corresponding to (1) a female-limited model, (2) a male-limited model, and (3) a model with arbitrary sex-specific expression of the mutant allele. In this way, we explore the cardinal points of possible phenotypic correlations between the sexes (for full derivations of all models, see [Appendix A: ESS Conditions](#); [Appendix A: ESS Conditions](#)—[Appendix B: Quantitative Genetic Simulation Methods](#) are available online). We note that while alternative derivations exist that would fit the verbal definition of sex limited, we have chosen ours for logical consistency with the equal effects model and ease of isolating the response to selection through each sex individually.

In the sex-limited models, mutant individuals of the nonexpressing sex exhibit identical phenotypes to wild-type individuals ( $\gamma$ ). Only mutants of the expressing sex exhibit the modified phenotype ( $\gamma^*$ ). In this way, phenotypic variation and selection on the mutant phenotype is limited to the sex expressing the mutant phenotype. This formulation is also consistent with the assumption in the equal effects model that the ancestral state has no sexual dimorphism in spawning time. Within our modeling framework, we define sexual conflict as a difference in the predicted stability of the boundary equilibria between the female- and male-limited models under equivalent parameter conditions.

The sex-specific model permits individual mutations to differentially affect the phenotypes of male and female carriers. This model requires an additional variable to account for expression of the wild-type and mutant alleles in each sex. We specify sex-specific phenotypic effects with subscripts m and f ( $\gamma_m$ ,  $\gamma_f$ ,  $\gamma_m^*$ , and  $\gamma_f^*$ ;  $\gamma_m$  and  $\gamma_f$  represent the wild-type phenotypes of males and females, and  $\gamma_m^*$  and  $\gamma_f^*$  represent the phenotypes of individuals that carry a mutant allele). In short, the inclusion of these terms enables both male and female mutants to express modified phenotypes from wild-type individuals of the same sex. We assessed the stability of ESS solutions for this model by evaluating the eigenvalues of the convergence stability and Hessian matrices for  $\lambda|_{p=0}$ , where  $\gamma_f^* = \gamma_f$  and  $\gamma_m^* = \gamma_m$  (Otto and Day 2007; [Appendix A: ESS Conditions](#)). We performed the same analyses described above for all models.

In addition to evaluating the boundary values of each  $\lambda$ , we also determined the outcome of the evolutionary invasion analyses by solving for the roots of the difference equation  $\Delta p$  numerically, giving the full solution sets for  $0 \leq \hat{p} \leq 1$ . Our numerical results were sometimes more complex than implied by the eigenvalue analysis, with the emergence of  $\geq 3$  distinct internal equilibria for some parameter conditions. However, the numerical results and boundary values for  $\lambda$  were qualitatively similar over most biologically feasible parameter space, and we present only the boundary results here (for representative numerical results, see [Appendix S2: Numerical results for population genetic models](#)). All analyses of the population genetic models were performed using Mathematica 10 (Wolfram 2014).

### 3.3.4 Testing Model Assumptions

In addition to the haploid models described above, we also derive diploid versions for each model (see [Appendix S1: Mathematica Code](#)). With codominant phenotypic effects of mutant and wild-type alleles (i.e.,  $h = 1/2$ ), the predictions from the diploid and haploid models are equivalent, and we therefore present the results for the haploid case for simplicity. However, in the diploid models, parameter conditions resulting in net over-dominance are possible and would be expected to result in increased balancing selection (Fry 2010). Thus, the haploid results probably represent a conservative prediction for the incidence of balancing selection.

The population genetic models make several other simplifying assumptions that could influence the predictions. In particular, (1) developmental traits influencing phenology are unlikely to be controlled by a single locus and (2) two discrete time points may not adequately capture the consequences of more complex patterns of environmental heterogeneity. To evaluate the robustness of our predictions to these assumptions, we performed individual-based quantitative genetic simulations that conceptually parallel the population genetic models. Specifically, we have expanded the model of flowering phenology described by Devaux and Lande (2010) to model individual spawning phenologies as continuous characters that are governed by two polygenic traits: the individual mean ( $m$ ) and the individual variance ( $v$ ) of gamete release time. Our simulation model expands on Devaux and Lande (2010) by incorporating dioecy and the possibility of varying degrees of genetic correlation between the sexes while retaining the density-dependent fertilization dynamics that are relevant to broadcast spawners (described in eq. 3.1). We simulated the evolution of  $m$  and  $v$  for populations of broadcast spawners under parameter conditions corresponding to a factorial matrix between two magnitudes of polyspermy (low or high) and two degrees of steepness of the environmental gradient (gentle or steep). We also manipulated the shape of the environmental gradient to be either discrete and symmetrical (with two levels of environmental stress, analogous to  $d = 0.25$  or  $0.75$  in the population genetic models) or continuous and Gaussian (as in Devaux and Lande 2010; for detailed simulation methods, see [Appendix B: Quantitative Genetic Simulation Methods](#)).

Simulation results were broadly congruent with predictions of the population genetic models. We touch briefly on these results; for full simulation results, see [Appendix S3: Quantitative Genetic Simulation Results](#). However, while the simulations show that the population genetic model results are not merely a consequence of their simplifying assumptions, a thorough exploration of the evolution of spawning phenologies mediated by polygenic characters remains an interesting avenue for future research.

## 3.4 Results

Our results address four main theoretical questions, which we explore in detail below. First, what fraction of the parameter space leads to protected polymorphism, and how does sex-specific gene expression impact opportunities for balancing selection? Second, what parameter conditions give rise to sexual conflict over the timing of reproduction, and how often does such conflict lead to balancing selection? Third, when is sexually antagonistic selection expected to drive the evolution of spawning during suboptimal environmental conditions? Finally, how do evolutionarily stable spawning strategies (i.e., genotypes that, when fixed, cannot be displaced by a mutant strategy) vary across different population densities and environmental gradients?

### 3.4.1 Prevalence of Protected Polymorphism

Our analyses of the models reveal that negative frequency- and density-dependent selection – which arise from sperm competition and polyspermy – may often generate balancing selection to maintain polymorphism in phenologies. However, the opportunity for balancing selection and protected polymorphism hinges on the pattern of gene expression within each sex. In all four models (i.e., the equal effects, female-limited, male-limited, and sex-specific models), the fate of the mutant allele is sensitive to two density thresholds that determine the incidence of polyspermy. At the lower threshold (at  $n_m \approx 20$  for the parameter condition  $A = 0.1$ ), eggs begin to suffer polyspermy if all males spawn at the same time (e.g.,  $\gamma, \gamma^* = 0$ ). At the higher threshold ( $n_m \approx 40$  when  $A = 0.1$ ), eggs begin to suffer polyspermy at both time points if males release equal amounts of sperm at both time points ( $\gamma, \gamma^* = 0.5$ ).

Stable polymorphism is never maintained in the female-limited model, when selection occurs exclusively through females. Rather, the genetic system always evolves to eliminate or fix the mutant allele (figs. 3.1A, 3.2A). At male densities below the lower threshold, female reproduction is sperm limited, and selection favors high reproductive synchrony with males, leading to increased female spawning at the environmental optimum. As male densities increase and elevate the risk of polyspermy, selection favors female spawning away from the environmental optimum. This occurs because the cost of polyspermy at the environmental optimum outweighs the survival costs to offspring that are produced by spawning at the environmentally suboptimal time.

When at least some selection occurs in males (i.e., in all but the female-limited model), opportunities for maintaining polymorphism increase dramatically. In the male-limited model, the likelihood of balanced polymorphism increases with increased polyspermy (i.e., balancing selection becomes more likely after crossing each population density threshold; fig. 3.1B). Between the two density thresholds, the increase in protected polymorphism in the male-limited model appears to come at the cost of positive selection for the mutant allele. This effect is caused by sperm competition; as males increasingly compete for fertilizations, despite increased rates of polyspermy, selection becomes dominated by the frequency-dependent effects of male-male competition, and selection maintains invading mutant alleles at intermediate frequencies rather than fixing them.

In the equal effects model, where spawning phenotypes are perfectly genetically correlated between the sexes, protected polymorphism occurs only above the upper density threshold, when there is no temporal refuge from polyspermy (fig. 3.1C). The fraction of balanced polymorphism is intermediate between the two sex-limited

models; selection in males can maintain polymorphic mutant alleles that would otherwise be fixed through positive selection in females, an effect that arises at sufficiently high male densities. In the sex-specific model – where selection occurs through both sexes, but the phenotypic effects of mutations may be sexually dimorphic – protected polymorphism can occur at high and low male densities, with increasing incidence of polymorphism with increasing male densities (fig. 3.1D).

Overall, balancing selection is driven exclusively by selection through males, with selection through females tending to remove polymorphism. Balancing selection is most permissible when selection is male limited. When mutations affect the phenotypes of both sexes, we see intermediate opportunities for balancing selection. Mutant alleles are most likely to be maintained when population densities are high.

### 3.4.2 Sexual Conflict and Protected Polymorphism

Strong frequency and density dependence of male fertilization success promotes the maintenance of genetic diversity and generates sexual conflict over the timing of gamete release. The extent of discordance in selection between the sexes hinges on population density. At low population densities (and thus lower sperm concentrations), males and females generally experience concordant selection to synchronize reproduction and maximize fertilization success at the environmentally optimal time. As population densities increase, the interests of males and females diverge sharply, with females experiencing strong selection to minimize polyspermy, and males experiencing frequency-dependent selection to maximize their relative fertilization success. In all models, the fate of mutant alleles reflects the fitness trade-offs resulting from polyspermy, fertilization success, and the environmental gradient. These complex trade-offs often result in asymmetrical invasion plots (fig. 3.2) and divergent evolutionary fates for mutations with female-limited versus male-limited phenotypic effects.

Conflicting selection between the sexes is implied in cases where the evolutionary trajectories of mutant alleles differ between the female- and male-limited models of gene expression. In the female-limited model, mutants releasing more gametes at the environmentally suboptimal time (fig. 3.2A–3.2C, above the diagonal) can invade in two regions of parameter space: (1) when fertilization success at the suboptimal time outweighs the combined fitness costs of polyspermy at the optimal time and poorer environmental conditions at the suboptimal time (e.g., fig. 3.2B, 3.2C, gray regions above the diagonal where  $\gamma < 0.5$ ) and (2) when the fitness cost of sperm limitation at the optimal time exceeds the combined costs of polyspermy and environmental conditions at the suboptimal time (e.g., fig. 3.2A–3.2C, gray regions above the diagonal where  $\gamma > 0.5$ ).

Sperm competition in the male-limited model often drives the evolution of protected polymorphism in regions of parameter space that correspond to positive selection in the female-limited model (fig. 3.2D–3.2F; reflected in fig. 3.1A, 3.1B). The evolutionary outcomes differ between male- and female-limited models because sperm competition leads to frequency-dependent selection in males but not in females. Selection in males can maintain mutant alleles that improve sperm competition against wild-type males but otherwise result in lower net fertilization rates because of polyspermy.

The parameter regions of sexual conflict (and of regions of protected polymorphism in the male-limited model) are determined by the fertilization curve in equation (3.1). The frequency of sexual conflict increases with mutation size (vertical deviation from the diagonal in fig. 3.2), but this relation is sensitive to male density

(fig. 3.3A). The increase in sexual conflict happens because in the regions where sexual conflict occurs, increasing mutation size results in mutants releasing more sperm at the time point where less polyspermy occurs. Mutant alleles can persist at intermediate frequencies when the fitness gains from releasing more sperm at the time point with less polyspermy balance the fitness cost of releasing less sperm at the other time point where sperm competition is strongest. In the limit of arbitrarily large mutation sizes (across all possible values of  $\gamma \times \gamma^*$ ), the overall probability of sexual conflict increases with male density.

In the equal effects model, sexually antagonistic selection constrains the parameter space where protected polymorphism can occur. Conditions for balancing selection are more restrictive when phenotypic effects are tightly correlated between the sexes, relative to the case where selection is male limited. Sexually antagonistic selection does not necessarily result in protected polymorphism, because some mutant alleles that would be maintained by balancing selection in the male-limited model become fixed through directional selection in females. As a result, the equal effects model yields results that are intermediate between the female- and male-limited models (fig. 3.2G–3.2I). The parameter space where polymorphism is predicted to occur becomes quite restricted when male densities are high enough for polyspermy to occur at the environmental optimum only (fig. 3.2E, 3.2H; fig. 3.3A, 3.3B, dashed line). When polyspermy occurs at both time points, intermediate frequencies of the mutant allele minimize polyspermy at both time points, increasing female fitness, thereby increasing the parameter space where polymorphism can occur relative to the male-limited model (fig. 3.2F, 3.2I; fig. 3.3A, 3.3B, solid line). Small-effect mutations generally experience either purifying or positive selection, whereas large-effect mutations are more likely to be maintained as polymorphisms (fig. 3.3B).

We illustrate some features of the sex-specific model's behavior by holding female strategies fixed at the arbitrary value  $\gamma_f = \gamma_f^* = 0.25$  and varying the male strategies associated with each genotype (fig. 3.2J–3.2L). In this example, the majority of explored parameter space results in either positive selection for — or purifying selection against – the mutant allele. When polyspermy can occur at only the environmental optimum, selection can maintain polymorphism for mutations with modest to small effect sizes when male and female phenotypes are similar (fig. 3.2K; where  $\gamma_m, \gamma_m^* \approx 0.25$ ). At high population densities, sperm competition and the incidence of polyspermy at the suboptimal time also increase. Consequently, protected polymorphism occurs only when mutant males are able to compensate for their loss of competitive ability against wild-type males with increased fertilization success at the opposite time point (fig. 3.2K, 3.2L, dark gray region above and below the diagonal, respectively).

### 3.4.3 Environmental Gradients

The steepness of the environmental gradient between spawning time points ( $d$ ) influences the balance of fitness effects associated with spawning at versus away from the environmental optimum. At high densities, negative frequency- and density-dependent fertilization success drives the evolution of stable polymorphism and spawning at the environmentally suboptimal time, even when the fitness costs of doing so are high. The steepness of the environmental gradient influences the population density at which protected polymorphism becomes common. However, the relation between the frequency of balanced polymorphism and population density remains qualitatively similar across all possible parameter values for  $d$  (fig. 3.4). Mutations causing individuals to release more gametes at the suboptimal time  $t_1$

( $\gamma^* > \gamma$ ) were favored at low or high population densities (fig. 3.5). At low densities, fertilization success is sperm limited. In this case, spawning at the suboptimal time is favored only when enough sperm is released that the resulting increase in fertilization success is greater than the survival cost to offspring. At high densities, increased polyspermy at the environmental optimum generates negative density-dependent selection that favors spawning at the suboptimal time, even when the associated reduction in offspring survival is high.

#### 3.4.4 Evolution of Within-Individual Variance

The evolution of within-individual variance (intermediate values of  $\gamma$ ) was strongly density dependent (fig. 3.6; [Appendix S3: Quantitative Genetic Simulation Results](#)). At male densities below  $n_m \approx 50$ , there is no convergence-stable ESS for  $\gamma$ , only a single unstable equilibrium that pushes the evolution of phenologies toward the boundaries of  $\gamma = 0$  and  $\gamma = 1$ , corresponding to no within-individual variance. Thus, low-density populations are predicted to evolve phenologies with no within-individual variance. When male densities are greater than  $n_m \approx 50$  (recall that this corresponds to the density threshold where polyspermy can occur at both time points), two additional equilibria appear: one convergence-stable ESS that approach-

es  $\gamma = 0.5$  with increasing  $n_m$  and a second unstable equilibrium that approaches  $\gamma = 0$  with increasing  $n_m$ . Consequently, high within-individual variance is predicted above the upper density threshold at  $n_m \approx 50$ . The steepness of the environmental gradient modifies the ESS gamete release strategies and unstable equilibrium states, though it does not qualitatively alter their relationships with population density ( $n_m$ ). Increased within-individual variance is predicted to evolve to minimize the fitness costs of polyspermy arising across different time points or spawning opportunities. These general patterns are robust to the specific form gene expression in each sex (see fig. 3.S5 in [Appendix S2: Numerical results for population genetic models](#)).

The evolution of increased within-individual variance is predicted in both the population and the quantitative genetic models when male densities are sufficiently high to result in polyspermy at multiple time points (see [Appendix S3: Quantitative Genetic Simulation Results](#)). Both models for the evolution of within- versus among-individual variance in phenology are similarly influenced by the intensity of polyspermy and changes in environmental conditions between spawning times. However, in contrast to the population genetic models, the quantitative genetic models were sensitive to the gene expression patterns in each sex. In particular, populations tended to have higher within-individual variance in spawning time when phenotypic effects in each sex were uncorrelated (the sex-specific model) than when they were tightly correlated (the equal effects model). Moreover, this result was generally robust to the incidence of polyspermy, or the steepness of the environmental gradient.

## 3.5 Discussion

### 3.5.1 The Evolution of Phenologies

Spawning in marine organisms is traditionally assumed to be highly synchronized between the sexes and to coincide precisely with optimal environmental conditions (Thorson 1936, 1946, 1950; Cushing 1969, 1990; Harrison et al. 1984; Babcock et al.

1986; Clifton 1997; reviewed in Durant et al. 2007; Lowerre-Barbieri et al. 2011). In contrast to this long-held assumption, several studies have documented conspicuous spawning asynchrony or mismatches between spawning time and ideal environmental conditions. These observations come from a diverse range of externally fertilizing species, including corals (Levitan et al. 2004; Levitan et al. 2011; Baird et al. 2009), sea urchins (Levitan 2002, 2004; Lotterhos and Levitan 2011), intertidal ascidians (Marshall 2002), and marine polychaetes (Lewis et al. 2002; Lewis et al. 2003; Kupriyanova 2006). Many species also exhibit sexually dimorphic spawning behaviors, with males typically spawning earlier and for longer than females (McEuan 1988; Levitan 2005; Lotterhos and Levitan 2011). While environmental stochasticity and bet-hedging strategies may explain some of the observed variance in reproductive phenologies (e.g., Iwasa and Haccou 1994; Devaux and Lande 2010), they do not fully address the possible role of negative frequency- and density-dependent selection in the evolution of spawning strategies, nor do they adequately explain the prevalence of sexually dimorphic phenologies within broadcast spawners (Durant et al. 2007; Olito et al. 2015). Our models help to reconcile these empirical patterns with theory. We show that precise synchrony between spawning times and optimal environmental conditions is predicted only under a narrow set of parameter conditions. We also demonstrate that sexually antagonistic selection over the timing of reproduction can select for sexually dimorphic spawning behaviors and potentially maintain variation in population phenologies.

In our models, sexual conflict over the timing of reproduction was predicted to be common, to be density-dependent, and, in many cases, to maintain genetic polymorphism. Selection through females (as in the female-limited gene expression model) favored the evolution of fixed female phenological strategies that reduce the risk of polyspermy, even in cases where fertilization was somewhat sperm limited at suboptimal time points. These results parallel previous predictions regarding frequency-dependent selection on gamete recognition proteins (Levitan and Ferrell 2006). In contrast, protected polymorphism was a common outcome in the male-limited model, which reflects the inherent frequency dependence of sperm competition outcomes (Parker et al. 1982; Parker 1982; Birkhead and Møller 1998). Our results offer an interesting counterpoint to previous studies of sperm competition, which tend to emphasize the evolution of reduced variation around trait values that maximize male competitiveness (e.g., large testes size, ejaculate volume, and competitive sperm morphology; Stockley et al. 1997; reviewed in Wedell et al. 2002). Given its ubiquity, sperm competition offers a potentially common mechanism for generating sexually dimorphic fitness optima and sexually antagonistic selection over traits that affect the fertilization process.

For broadcast spawners, high phenological variances and sexually dimorphic phenologies may be a consequence of sexually antagonistic selection that is driven by sperm competition. While acknowledging the difficulties of detecting sexually antagonistic selection at individual loci (e.g., (Barson et al. 2015)), our model predictions may nevertheless be tested by other means. For example, our models predict that sexual conflict over the timing and duration of spawning should be greatest at high densities. These conditions may, in the long run, give rise to sexually dimorphic phenologies in which males have longer spawning durations and higher among-individual variances than females. Our model predictions could also be tested by estimating the relation between spawning phenotypes (e.g., spawning onset and duration) and the fitness of each sex under sperm-limited versus high-polyspermy conditions. Variances in reproductive success have been shown to differ between males and females across population density gradients (Levitan 2004), and gamete traits

and population phenologies are known to experience strong density- and frequency-dependent selection (Levitan 2002; Levitan and Ferrell 2006; Tomaiuolo et al. 2007). However, these patterns have yet to be linked to sex-specific phenological traits or genes expressed in both sexes.

Our results may also help explain the seemingly counterintuitive observation that some species' reproduction occurs during poor environmental conditions. For example, some marine polychaetes conspicuously spawn when temperatures are suboptimal for fertilization success and larval development (Lewis et al. 2002; Lewis et al. 2003). Seasonal energy budgets and competition among settling larvae have been proposed to explain these patterns. However, these species are also susceptible to polyspermy and occur at high population densities, conditions that lead to spawning away from the environmental optimum in our models. Conceptually, these predictions are loosely analogous to previous theory on the evolution of polygenic traits in sexually dimorphic species (Lande 1980), where sexual selection and positive genetic covariances between the sexes can cause trait values to evolve away from adaptive peaks that are favored by natural selection. In our models, sexual conflict and polyspermy can drive the evolution of spawning in environmental conditions that are unfavorable for survival. In extreme instances, spawning in suboptimal environments can evolve, even when the mortality cost in the poorer environment reaches 95%.

The fitness consequences of a particular phenological strategy should depend on aspects of each species' life history. For example, larger eggs present a bigger target for sperm-egg collisions and lower the effective densities at which polyspermy occurs (Millar and Anderson 2003; Bode and Marshall 2007; Olito et al. 2015; [Appendix B: Quantitative Genetic Simulation Methods](#)). Egg size also covaries strongly with other life-history traits, such as the mode of larval development (Marshall and Keough 2007). Species with nonfeeding (lecithotrophic) larvae have larger eggs (on average) than species with feeding (planktotrophic larvae) and require favorable physicochemical conditions for development (Strathmann 1985; Marshall and Keough 2007). Species with planktotrophic larvae – which have the same physicochemical requirements and additionally rely on planktonic food resources – are more sensitive to environmental conditions during larval development (Vance 1973; Strathmann 1985; Marshall and Keough 2007). The elevated environmental sensitivities of these species should, according to our models, lead to the evolution of relatively low among-individual variances in phenology. In contrast, lecithotrophs should experience selection for increased variance in phenology because of their larger eggs and presumably lower population density thresholds for polyspermy.

Although our models are tailored for broadcast spawners, the results may hold for the evolution of phenologies in other organisms, particularly dioecious and wind-pollinated flowering plants. Positive and negative frequency- and density-dependent pollen transport is a pervasive feature of reproduction in flowering plants resulting from patch attractiveness, competition for pollinator visitation, the dynamics of wind dispersal of pollen, and polyspermy (Allee et al. 1949; Augspurger 1981; Brunet and Charlesworth 1995; Spielman and Scott 2008; Friedman and Barrett 2009; Devaux and Lande 2010). If the consequences of frequency-dependent pollen transport for reproductive success fundamentally differ between sexes or sex roles, there is potential for sexually antagonistic selection to expand opportunities for polymorphism in floral and phenological traits that are expressed in both sexes (Jordan and Connallon 2014). Indeed, similar to the empirical patterns observed in broadcast spawners, males of many dioecious plant species flower earlier and for longer and generally produce larger flowering displays than female plants (Charlesworth et

al. 1987; Brunet and Charlesworth 1995; Kudo 2006). In wind-pollinated species, sex allocation is size dependent and strikingly male biased but is often protogynous (females flower before males; Friedman and Barrett 2009). However, applications of our model predictions to angiosperms must be made with caution because fertilization within this group is internal. While among-male competition during pollen transport superficially resembles that of broadcast spawners, males also compete during the gametophytic stage, with competitive outcomes mediated by interactions with female stylar tissue. These interactions can result in complex fertilization dynamics, including but not limited to negative density dependence (Spielman and Scott 2008; Friedman and Barrett 2009; Harder et al. 2016). Moreover, since the majority of angiosperms are hermaphroditic, floral and phenological traits may be influenced by additional factors, including self-fertilization and selection arising within the context of selfing (Harder and Barrett 1995; Kudo 2006; Friedman and Barrett 2009). Evolutionary responses to negative frequency dependence can also drive adaptive allocation to the less common sex role at any point in the flowering season (Brunet and Charlesworth 1995; Brookes and Jesson 2010; Ishii and Harder 2012).

### 3.5.2 Sexual Conflict and Protected Polymorphism

Population density, gene expression, and mutation effect size each influenced the likelihood of sexually antagonistic selection maintaining polymorphism. At high population densities, mutations with modest to large phenotypic effect sizes were often subject to sexually antagonistic selection (i.e., the female-limited model predicted fixation, and the male-limited model predicted protected polymorphism). In cases where the mutation was expressed by both sexes, polymorphism was maintained in only a subset of the parameter space of sexual conflict. Large-effect mutations were relatively likely to be maintained as protected polymorphisms.

These results complement recent theoretical predictions about mutation size, sexual antagonism, and balancing selection from simple fitness landscape models of sex-specific adaptation (e.g., Fisher's geometric model; Connallon and Clark 2014a, 2014b). Sexually antagonistic selection is a common outcome of adaptation in these models, with mutations of intermediate size most likely to experience balancing selection. Our models expand these predictions by providing an explicit ecological mechanism for fitness trade-offs over female and male spawning strategies. In the current context, sexually antagonistic fitness trade-offs increase with population density because polyspermy decreases the net fitness cost to males of spawning away from the environmental optimum. Large-effect mutations are relatively likely to result in balancing selection because they result in higher sperm concentrations (and relatively high male fertilization success) at the suboptimal time, which helps to offset the cost of lower environmental quality. In contrast, females have no frequency-dependent incentive for incurring environmental fitness costs by spawning at the suboptimal time. While polyspermy may also drive females to spawn away from the environmental optimum, conditions leading them to do so often differ from those that incentivize males.

### 3.5.3 Evolution of Within-Individual Variance

While increased polymorphism leads to increased among-individual variance in our models, the evolution of intermediate gamete release phenotypes (i.e., where individuals spawn across both time points) corresponds to increased within-individual

variance. For flowering plants, density-dependent pollination success (e.g., due to patch attractiveness and competition for pollinators) has been predicted to influence the evolution of population phenologies through evolutionary changes in the individual mean and variance of flowering display times (Elzinga et al. 2007; Devaux and Lande 2008, 2010). Among- and within-individual variance in flowering phenology is predicted to respond differently to positive and negative density-dependent pollinator visitation, with disruptive selection driving increased among-individual variance and stabilizing selection decreasing within-individual variance (Devaux and Lande 2010). Our models partly corroborate these findings for dioecious species. Our models also reveal the effects of genetic correlations between the sexes on the evolution of within- and among-individual variances in population phenology, issues that were not considered by previous theory regarding flowering phenologies in simultaneously hermaphroditic plants. In our models, negative density-dependent fertilization success resulted in the same pattern of increased within-individual variance, independent of among-individual variance in spawning time or the pattern of gene expression in each sex. However, our quantitative genetic simulations gave somewhat different results. The prevalence of sexually antagonistic selection and the evolution of within- and among-individual variance in population phenology depended on disruptive selection because of polyspermy, the severity of the environmental gradient, and the genetic correlation of mutant phenotypic effects between the sexes ([Appendix S3: Quantitative Genetic Simulation Results](#)). Overall, our results suggest that alleles affecting among- individual variance are often under sexually antagonistic selection, that those affecting within-individual variance are under sexually antagonistic selection under some conditions, and that within- and among-individual variance components may respond differently to net stabilizing and disruptive selection, depending on the correlation of phenotypic effects between sexes. A thorough exploration of the joint effects of these processes on the evolution of reproductive phenologies remains an open area for future study.

## Acknowledgements

We thank C. Venable, the editors, and five anonymous reviewers for their helpful comments. We are particularly indebted to S. Proulx for a careful review that greatly improved the models and manuscript. This work was funded by a Monash University Dean's International Postgraduate Student Scholarship to C.O. and Australian Research Council grants to D.J.M. and T.C.

## 3.6 Tables

TABLE 3.1: Key terms and parameters

Term	Description
$B_1, B_2$	Wild-type and mutant alleles
$\gamma, \gamma^*$	Phenotypic values of wild-type and mutant alleles respectively for the equal effects and sex-limited models
$\gamma_f, \gamma_m, \gamma_f^*, \gamma_m^*$	Phenotypic values of wild-type and mutant alleles for the sex-specific model
$(1 - p), p$	Frequency of wild-type and mutant alleles, respectively
$n_f, n_m$	Population density for females and males respectively
$A$	Fertilization function shape parameter
$d$	Difference in environmental quality between time-points

## 3.7 Figures

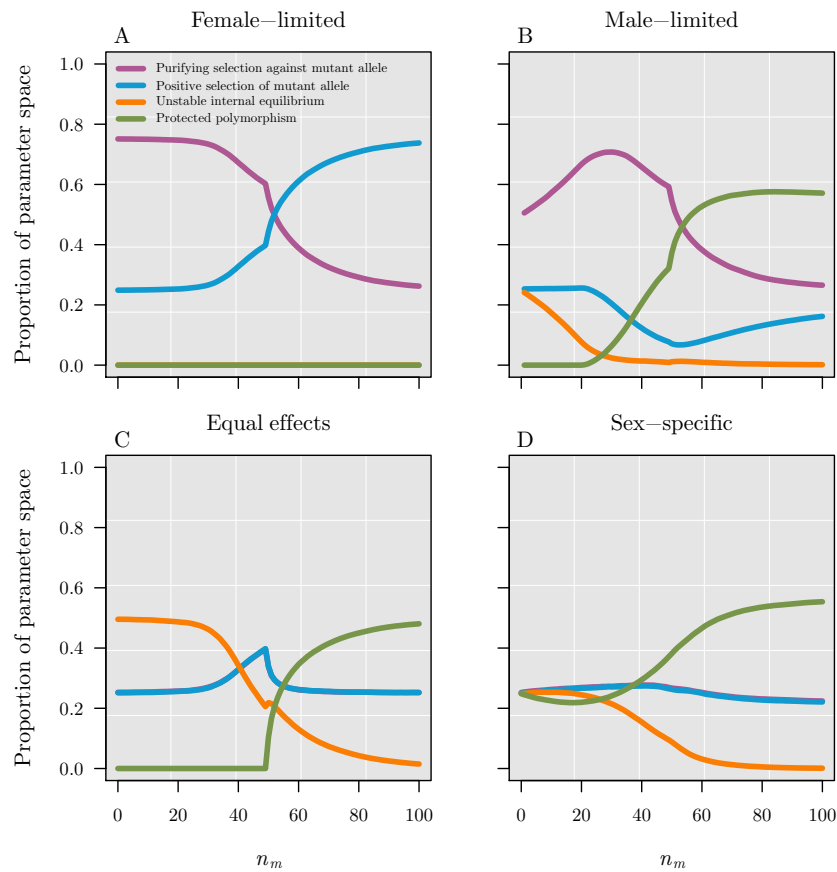


FIGURE 3.1: The proportion of parameter space giving rise to the different outcomes of the evolutionary invasion analysis for each model across  $\gamma \times \gamma^*$  parameter space as a function of male density ( $n_m$ ). Outcomes are based on evaluating the leading eigenvalue,  $\lambda$ , at the boundaries of  $p = 0$  and  $p = 1$ . These results use the parameters  $d = 0.25$ , and  $A = 0.1$ . The line for purifying selection is underneath that of positive selection in panel C.

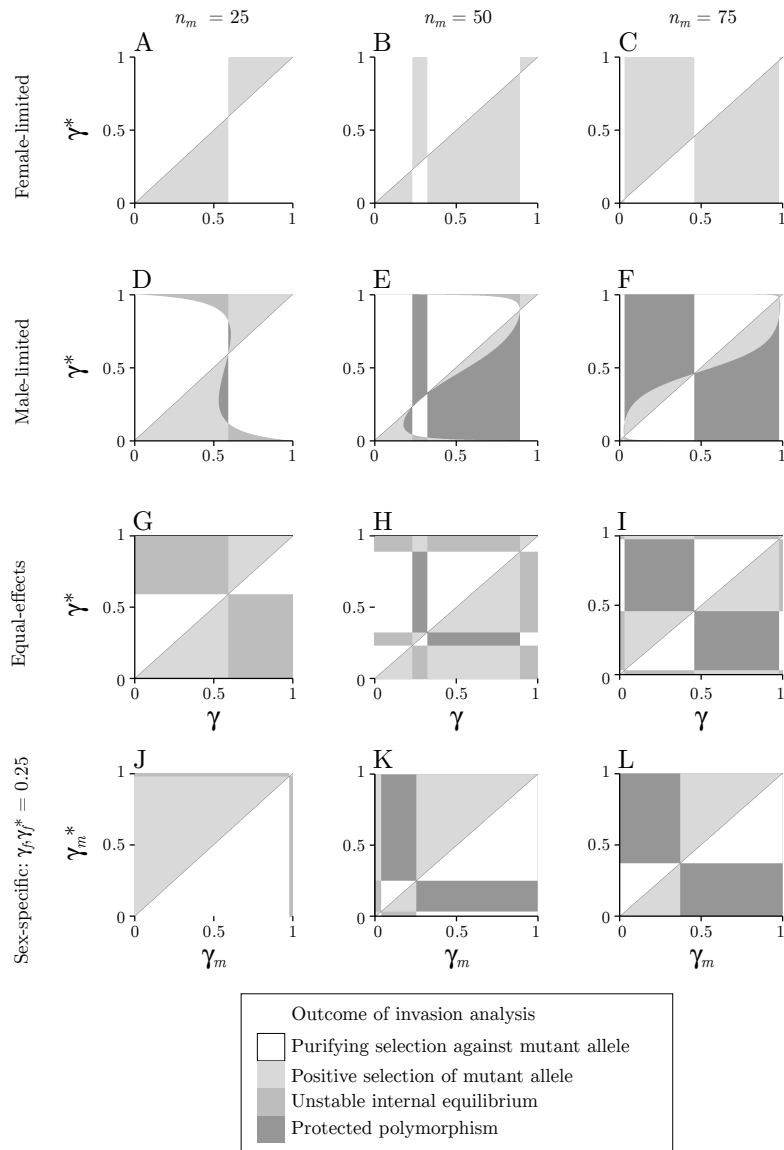


FIGURE 3.2: Outcome of the evolutionary invasion analysis based on evaluating the leading eigenvalue,  $\lambda$ , at the boundaries of  $p = 0$  and  $p = 1$  for each model across  $\gamma \times \gamma^*$  parameter space ( $\gamma_m \times \gamma_m^*$  for the sex-specific model). Vertical deviations from the diagonal represent mutations of different sizes. Results use the parameters  $d = 0.25$ , and  $A = 0.1$ , and the parameters  $\gamma_f, \gamma_f^* = 0.25$  for the sex-specific model.

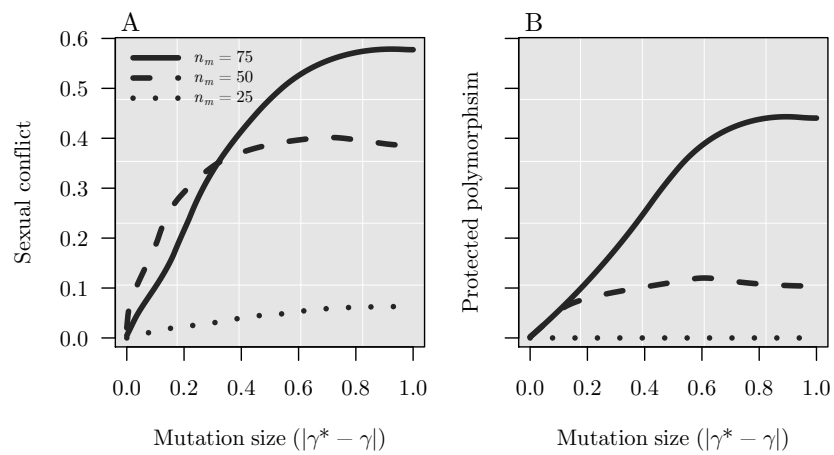


FIGURE 3.3: The frequency of  $A$ , sexual conflict (differences in the boundary signatures for  $\lambda$  between the female- and male-limited models), and  $B$ , protected polymorphism in the equal-effects model, as a function of mutation size ( $|\hat{\gamma}^* - \gamma|$ ) at three different male densities. Note that these results can be recovered directly from the phase-space diagrams in fig 2A-I. Results use the parameters  $d = 0.25$ , and  $A = 0.1$ .

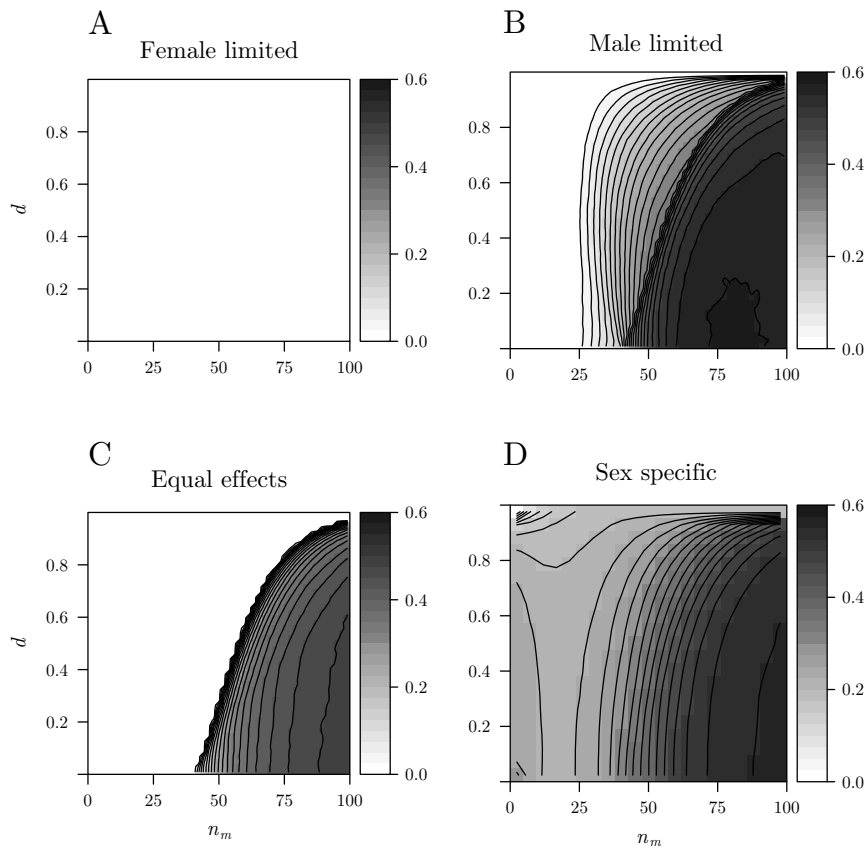


FIGURE 3.4: The proportion of  $\gamma \times \gamma^*$  parameter space resulting protected polymorphism for each model as a function of the environmental gradient ( $d$ ), and male density ( $n_m$ ). Note that the results presented in fig. 3.1 represent a slice through these contours at  $d = 0.25$ . All plots use a common color-scale.

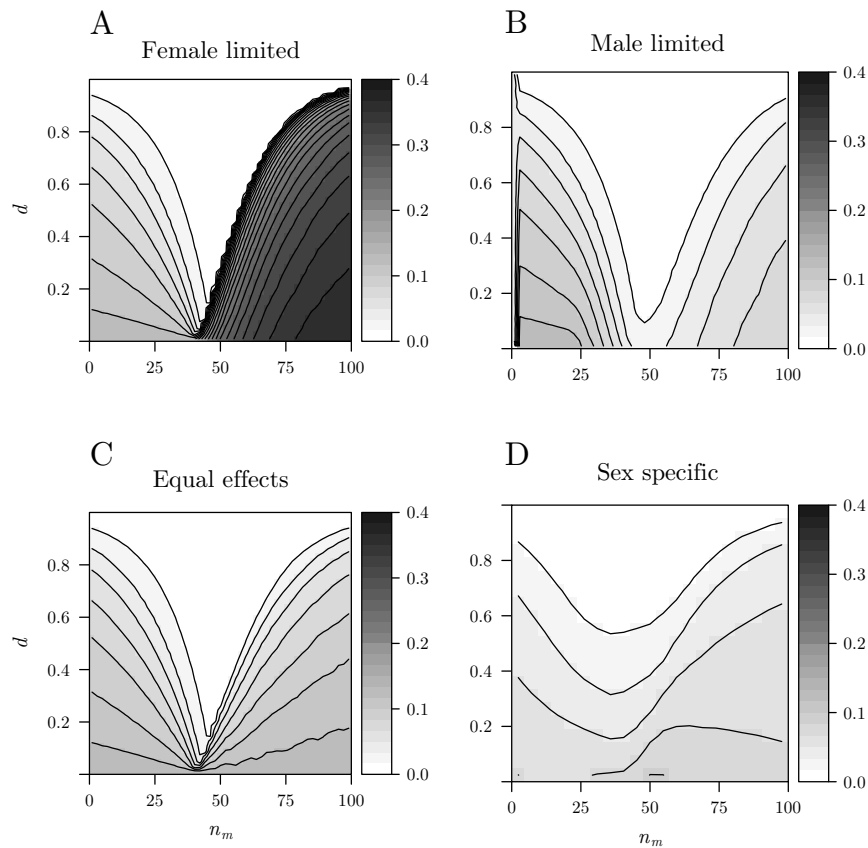


FIGURE 3.5: The proportion of  $\gamma \times \gamma^*$  parameter space resulting in fixation of mutant alleles with greater phenotypic values than the wild-type ( $\gamma^* > \gamma$ ) for each model as a function of the environmental gradient ( $d$ ), and male density ( $n_m$ ). This represents the prevalence of fixation for genotypes that preferentially spawn a greater proportion of their gametes at the environmentally sub-optimal time ( $t_1$ ). Results use the parameter value  $A = 0.1$ , and all plots use a common color-scale.

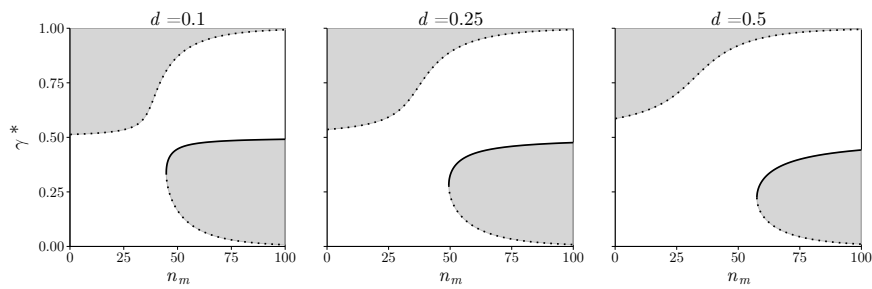


FIGURE 3.6: ESS solutions for  $\gamma$  as a function of male density ( $n_m$ ), at three different environmental gradients ( $d$ ). Solid lines represent the single convergence-stable equilibrium, while dotted lines represent the unstable equilibria. At a given density, populations will evolve away from the unstable equilibria, and towards the stable equilibrium in the vertical axis. These results use the parameter  $A = 0.1$ , and were calculated for the female-limited model. Results for the other three models were nearly identical (See fig. 3.S5).

### 3.8 Appendix A: ESS Conditions

To find the ESS for  $\gamma$ , we evaluated the leading eigenvalue of the recursion equation at  $p = 0$ ,  $\lambda = \frac{\partial p_{t+1}}{\partial p_t} \Big|_{p=0}$ , and solved numerically for the values of  $\gamma$  that satisfied the ESS conditions

$$\frac{\partial \lambda(\gamma^*, \gamma)}{\partial \gamma^*} \Big|_{\gamma^*=\gamma} = 0, \quad \frac{\partial^2 \lambda(\gamma^*, \gamma)}{\partial \gamma^{*2}} \Big|_{\gamma^*=\gamma} < 0.$$

#### 3.8.1 Convergence-stability & Hessian Matrices

To be convergence-stable, the eigenvalues of the convergence-stability matrix,  $\mathbf{C}$ , must have negative real parts, where:

$$\mathbf{C} = \begin{pmatrix} \frac{\partial \left( \frac{\partial \lambda}{\partial \gamma_f^*} \right)}{\partial \gamma_f} & \frac{\partial \left( \frac{\partial \lambda}{\partial \gamma_f^*} \right)}{\partial \gamma_m} \\ \frac{\partial \left( \frac{\partial \lambda}{\partial \gamma_m^*} \right)}{\partial \gamma_f} & \frac{\partial \left( \frac{\partial \lambda}{\partial \gamma_m^*} \right)}{\partial \gamma_m} \end{pmatrix} \quad \gamma_f^* = \gamma_f, \gamma_m^* = \gamma_m \quad (3.A1)$$

In order for  $\lambda$  to be maximized rather than minimized when the mutant strategy is the same as the resident strategy, the eigenvalues of the Hessian matrix,  $\mathbf{H}$ , must not be positive where:

$$\mathbf{H} = \begin{pmatrix} \frac{\partial^2 \lambda}{\partial \gamma_f^{*2}} & \frac{\partial^2 \lambda}{\partial \gamma_f^* \partial \gamma_m^*} \\ \frac{\partial^2 \lambda}{\partial \gamma_f^* \partial \gamma_m^*} & \frac{\partial^2 \lambda}{\partial \gamma_m^{*2}} \end{pmatrix} \quad \gamma_f^* = \gamma_f, \gamma_m^* = \gamma_m \quad (3.A2)$$

## 3.9 Appendix B: Quantitative Genetic Simulation Methods

Here we develop individual-based quantitative genetic simulations that directly parallel the population genetic models described in the main text. These models simulate the evolution of reproductive phenologies in broadcast spawning species due to environmental heterogeneity, density-dependent fertilization success, assortative mating due to spawning time, and patterns of gene expression and genetic variance. We extend the framework developed by Devaux and Lande (2008, 2010) to model within-individual mean spawning time ( $m$ ) and within-individual variance in spawning time ( $v$ ) as independent polygenic traits that together determine individual spawning phenologies. We then explore the responses to selection of these traits under density-dependent fertilization success, as well as different patterns of sex-limited and sex-specific expression of contributing loci. Alternative approaches to modeling reproductive phenologies are possible (e.g. using the onset and duration of gamete release). However we follow the methods described by Devaux and Lande (2010) because they offer an explicit mathematical link between within-individual and population-level variances. Simulations were written and implemented in R (Team 2015; see [Appendix S4: Computer Code](#) for simulation code).

As in the population genetic models, we model reproduction in a population of dioecious individuals with a sex ratio of 1/2. However, unlike our population genetic models, populations are finite in the Quantitative Genetic simulations, with total population size  $N$ . Generations are discrete and non-overlapping, and individuals of the same sex are assumed to have equal resources available for mating. Each generation, the mating season consists of 101 discrete spawning events. Individuals release eggs and sperm through time according to a discretized Gaussian distribution with mean  $m$  and variance  $v$ . Evolution of the population spawning phenology occurs through changes in the distributions of  $m$  and  $v$ . That is, each individual has a specific mean and variance that describes their distribution of gamete release through time, but the traits  $m$  and  $v$  have a mean and variance among individuals of the population.

### 3.9.1 Inheritance of individual phenology

After Devaux and Lande (2010), the within-individual mean,  $m$ , and the log of the within-individual variance,  $\ln(v)$ , of spawning time are both modelled as continuous polygenic traits controlled by  $n = 5$  unlinked and purely additive loci.  $m$  is normally distributed, while  $v$  is log-normally distributed. These traits are influenced by a normally distributed additive environmental effect, with no genotype  $\times$  environment interaction. There is free recombination among all loci for each trait, implemented using the algorithm described in Devaux and Lande (2008). To emphasize the evolutionary responses of  $m$  and  $v$  to selection, we do not model mutation, and populations are initiated with  $2N$  alleles per locus with unique, randomly drawn, phenotypic effects for each trait. For ease of comparison with results presented in Devaux and Lande (2010), and because few estimates of genetic variance or heritability exist for phenological traits in broadcast spawning species (e.g. Hendry and Day 2005), we draw phenotypic effects randomly from normal (for  $m$ ) and log-normal (for  $v$ ) distributions with quantitative genetic parameters based on data from flowering plants (table 3.B1; equivalent to parameter set I in Devaux and Lande (2010)). These parameter values result in equal initial phenotypic variances and heritabilities for these traits  $m$  and  $v$ .

### 3.9.2 Reproductive success

The reproductive season consists of 101 discrete mating events symmetrically distributed about 0 (time units are arbitrary). Reproductive success at each mating event is equal to

$$w_t = Q(t) \cdot F(s_t), \quad (3.B1)$$

where  $Q(t)$  describes the density-independent probability of zygote and offspring survival due to temporally heterogeneous environmental conditions, and  $F(s_t)$  describes the density-dependent probability of successful fertilization (Eq(1) in the main text). We model environmental conditions in two ways. First, we model environmental conditions to be analogous to those used in the population genetic models: discrete and symmetrical with two levels such that no density independent offspring mortality occurs during the middle third of the season, but mortality occurs at a rate  $d$  during the the first and last third of the season. To explore the consequences of relaxing the assumption of discrete environmental conditions, we then model environmental conditions as a generalized Gaussian function

$$Q(t) = \exp \left\{ - \left( \frac{t^2}{2q^2} \right)^\alpha \right\} \quad (3.B2)$$

where  $q$  and  $\alpha$  are shape parameters determining the width and curvature of the environmental quality function. We do not model environmental stochasticity.

The density-dependent probability of successful fertilization of eggs by sperm at each mating event follows Eq.(1) from the main text, where  $s_t$  is the total amount of gametic resources being released by all males in the population at a given mating event  $t_i$ . As before, we assume that sperm greatly outnumber eggs, and therefore that fertilization success is independent of egg density.

We hold the population size,  $N$ , constant across generations. Mating is assortative among mating events, but random within mating events. Accordingly, pairwise mating probabilities between individual males and females at time  $t_i$  are equal to the product of each individual's relative contribution to the total amount of eggs or sperm released by all individuals at time  $t_i$ . We draw  $N$  parent-pairs randomly in proportion to the expected reproductive success among mating events ( $w_t$ ), and the pairwise mating probabilities within mating events, given the individual phenologies of all males and females in the population.

### 3.9.3 Patterns of gene expression

If the same  $n$  loci contribute identically to both male and female phenotypes, genetic variance is expressed equally between the sexes. As in our population genetic models, we relax this assumption of equal phenotypic effects to identify the conditions under which selection on spawning phenology is sexually concordant vs. antagonistic, and to explore the evolutionary consequences for reproductive phenology of different patterns of gene expression. We again consider alternative models corresponding to male- and female-limited, as well as sex-specific expression of genetic variation. In addition, we explore models allowing partially correlated phenotypic effects between males and females.

We manipulate the correlation of phenotypic effects between the sexes by altering the number of shared vs. unshared loci ( $u$ ) contributing to males' and females' phenotypes, while holding the total number of loci controlling phenotypes in each

sex constant at  $n = 5$ . For example, in our model of sex-specific expression  $n = u$ , and individuals of either sex are represented by  $2n$  loci, of which  $n$  are expressed only in females, and the other  $n$  are expressed only in males. Intermediate levels of phenotypic correlation are modelled by setting  $0 < u < n$ .

For the sex-limited models, genetic variance in  $m$  and  $v$  is limited to the sex of interest by modelling  $n = u = 5$  unshared loci, and fixing all individuals of the opposite sex for a single randomly drawn allele per locus. This restricts the evolutionary response to selection to the sex of interest, given the constraints arising from the population phenology for the invariant sex. As in the population genetic models, we define ‘sexual conflict’ as a difference in the evolutionary response of  $m$  and  $v$  to selection between the female- and male-limited models.

Our simulations offer another method to detect a signature of sexually antagonistic selection. In our simulations, we can model partially correlated effects where males and females share some, but not all, of the alleles contributing to  $m$  and  $\ln(v)$  (e.g.  $u = 3$  sex-specific alleles, and  $n - u = 2$  shared alleles). If the form of selection is different between males and females, the distribution of allele effect sizes after selection should differ between shared, and sex-specific locus classes (Connallon and Clark 2014a, 2014b). We can therefore interpret differences in these distributions as a signature of sex-specific selection.

### 3.9.4 Environmental gradients and polyspermy

We explore parameter conditions that mirror those explored in our population genetic models with an important exception (see table 3.B2 for a summary of parameter conditions explored). Although manipulating population size would produce conditions with lower or higher incidence of polyspermy (as manipulating density did in the population genetic models), this would simultaneously alter the relative strength of selection and genetic drift in the simulations because populations are finite. To avoid conflating these processes, we explore the consequences of low and high rates of polyspermy at a fixed population size by manipulating the fertilization shape parameter  $A$  from Eq.(1), which changes the effective densities at which polyspermy occurs (Bode and Marshall 2007; Olito et al. 2015). We also explore the consequences of steep versus gentle environmental gradients in two scenarios. Under discrete and symmetric environmental conditions, we manipulate the steepness of the environmental gradient by varying the parameter  $d$  ( $d = 0.25$  or  $0.75$ ). This changes the difference in environmental quality between the optimal and sub-optimal times, but does not alter the relative duration of optimal and sub-optimal conditions. Under generalized Gaussian environmental conditions, we alter the steepness of the environmental gradient by varying the shape parameter  $q$ . We explore two scenarios corresponding to a brief period where environmental conditions are favourable for reproductive success with a steep environmental gradient, and a longer period of favourable conditions with a more gentle environmental gradient.

We present representative results from a randomly chosen simulation for each model at each set of parameter conditions. For selection to dominate the evolutionary dynamics in the simulations,  $2N_e$  must be far greater than  $T$  (Wright 1931; Lande 1980). For a similar model of assortative mating by flowering time, Devaux and Lande (2008) found that  $2N_e \approx N$ . We ran simulations for  $T = 500$  generations for

populations of  $N = 3000$  individuals. Under these parameter values,  $T \ll 2N_e$ , and the behaviour of the models is driven primarily by selection rather than drift.

TABLE 3.B1: Population Genetic Parameters

Parameter	Mean ( $m$ )	Log-variance ( $\ln(v)$ )
$\bar{g}$	0	$\ln(5) - \ln(1.2)/2$
$G$	2.5	$\ln(1.2)/2$
$\bar{e}$	0	0
$E$	2.5	$\ln(1.2)/2$
$\bar{p}$	0	$\ln(5)$
$P$	5	$\ln(5)$
$h^2$	0.5	0.5

Note: Initial quantitative genetic parameters for  $m$  and  $v$ .  $\bar{g}$  and  $G$  are the mean and variance of the distributions from which random allelic effects are drawn,  $\bar{e}$  and  $E$  are the mean and variance of the environmental effects.  $\bar{p}$  and  $P$  are the resulting mean and variance of phenotypic values, and  $h^2$  is the resulting heritability

TABLE 3.B2: Parameters for simulations

Parameter	Description
$N = 3000$	Population size
$T = 500$	Duration of simulations (generations)
$n = 5$	number of loci
$d = 0.25$ or $0.75$	Discrete environmental shape parameters
$\alpha = 2$ ; $q = 15$ or $40$	Gaussian environmental shape parameters
$A = 0.01$ or $0.1$	Fertilization function shape parameter (from Eq.(1))

### 3.10 Appendix S1: Mathematica Code

Mathematica code with full derivations of all models, and basic results is available in the online supplements to the published article in *The American Naturalist* (<http://www.journals.uchicago.edu/toc/an/current>), or from the author ([colin.olito@gmail.com](mailto:colin.olito@gmail.com)).

### 3.11 Appendix S2: Numerical results for population genetic models

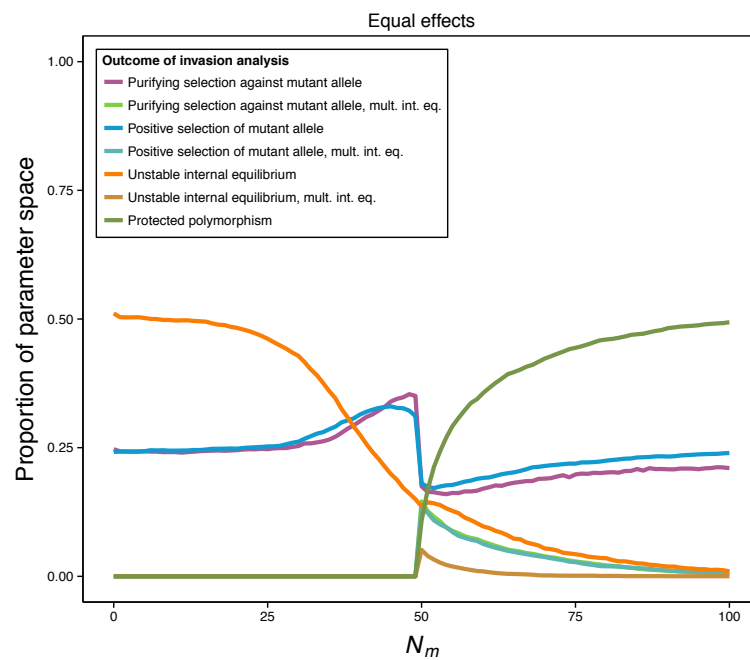


FIGURE 3.S1: The prevalence of different outcomes of the evolutionary invasion analysis for the equal effects model across  $\gamma \times \gamma^*$  parameter space as a function of male density ( $n_m$ ). Outcomes are based on numerical solutions for  $\hat{p}$ , which give full solution sets for  $0 \leq p \leq 1$ . As in fig. 3.1, these results use the parameters  $d = 0.25$ , and  $A = 0.1$ .

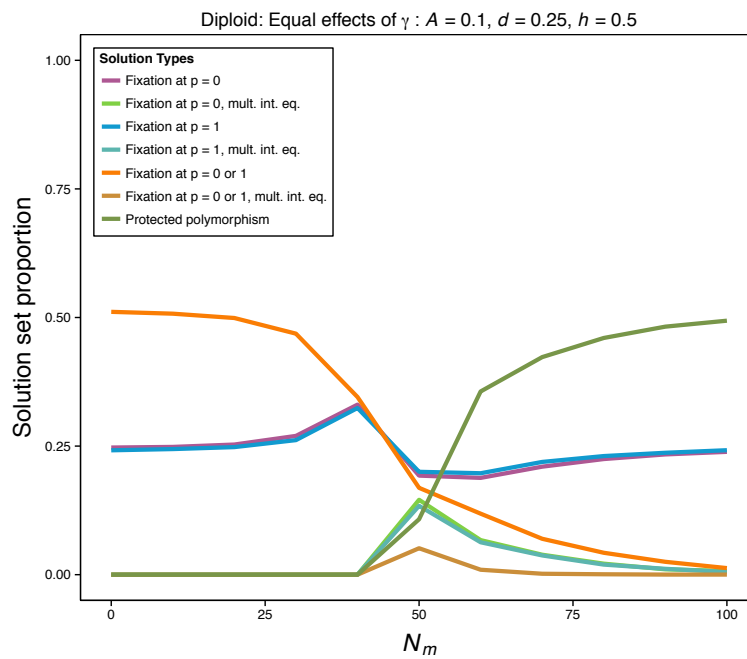


FIGURE 3.S2: Representative numerical results for the Diploid version of the equal effects model under incomplete dominance ( $h = 0.5$ ). The prevalence of different outcomes of the evolutionary invasion analysis are plotted across  $\gamma \times \gamma^*$  parameter space as a function of male density ( $n_m$ ). Outcomes are based on numerical solutions for  $\hat{p}$ , which give full solution sets for  $0 \leq p \leq 1$ . As in fig. 3.S1, these results use the parameters  $d = 0.25$ , and  $A = 0.1$ .

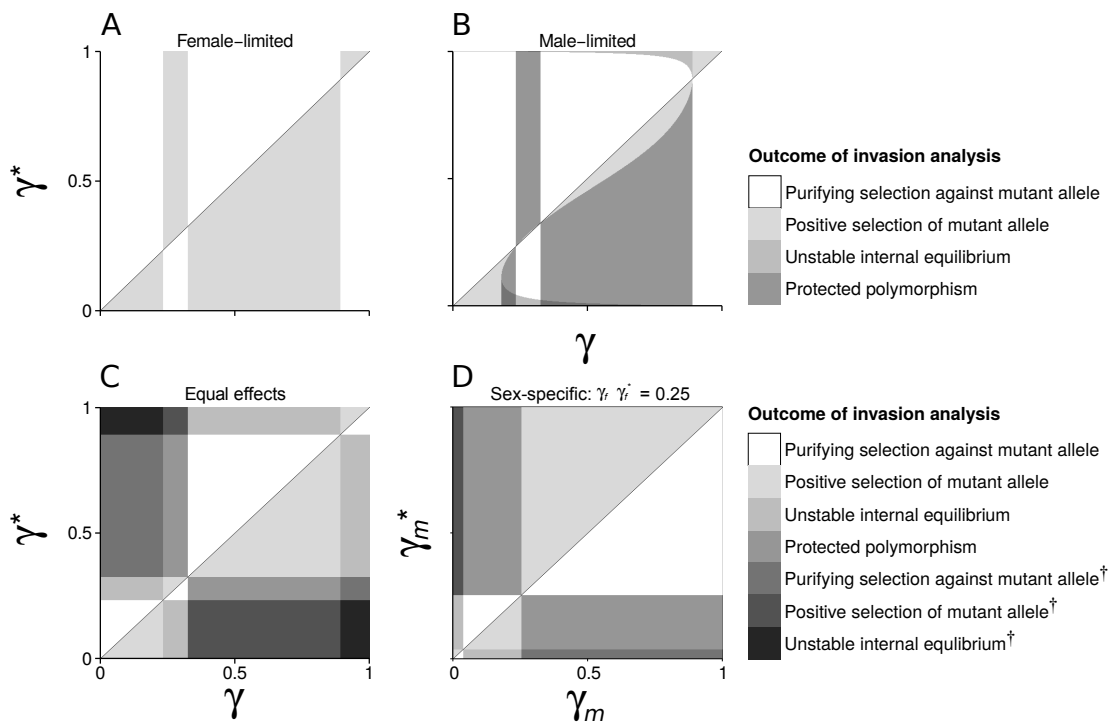


FIGURE 3.S3: Outcomes of the evolutionary invasion analysis based on numerical solutions of the difference equation  $\Delta p$  for each model across  $\gamma \times \gamma^*$  parameter space ( $\gamma_m \times \gamma_m^*$  for the sex-specific model). Vertical deviations from the diagonal represent mutations of different sizes. Results use the parameters  $n_m = n_f = 50$ ,  $d = 0.25$ , and  $A = 0.1$ , and the parameters  $\gamma_f, \gamma_f^* = 0.25$  for the sex-specific model.

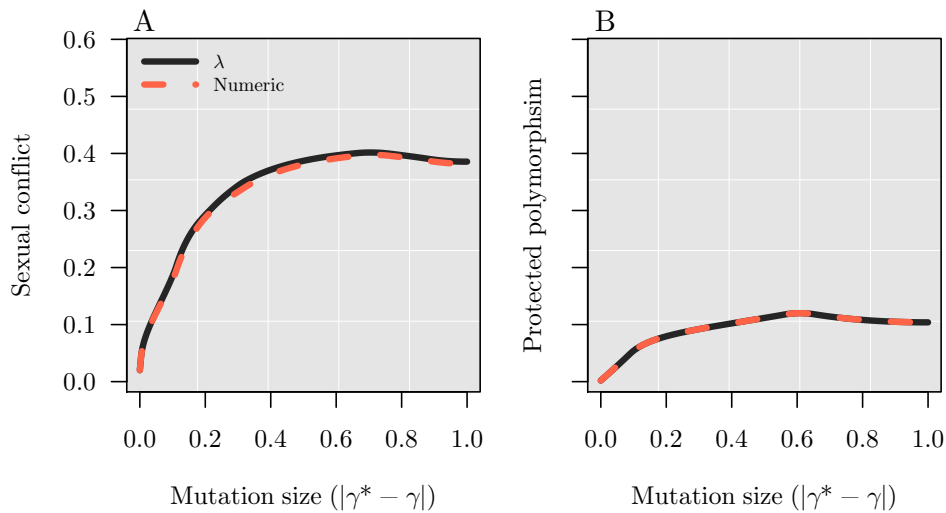


FIGURE 3.S4: Comparison of results using numerical solutions (red dashed lines) vs. boundary stability (black solid lines) for the frequency of  $A$ , sexual conflict (differences in the boundary signatures for  $\lambda$  between the female- and male-limited models), and  $B$ , protected polymorphism in the equal-effects model, as a function of mutation size  $|\gamma^* - \gamma|$ , at  $n_m = 50$ . Note that these results can be recovered directly from the phase-space diagrams in fig 3.S2A-C. Results use the parameters  $d = 0.25$ , and  $A = 0.1$ .

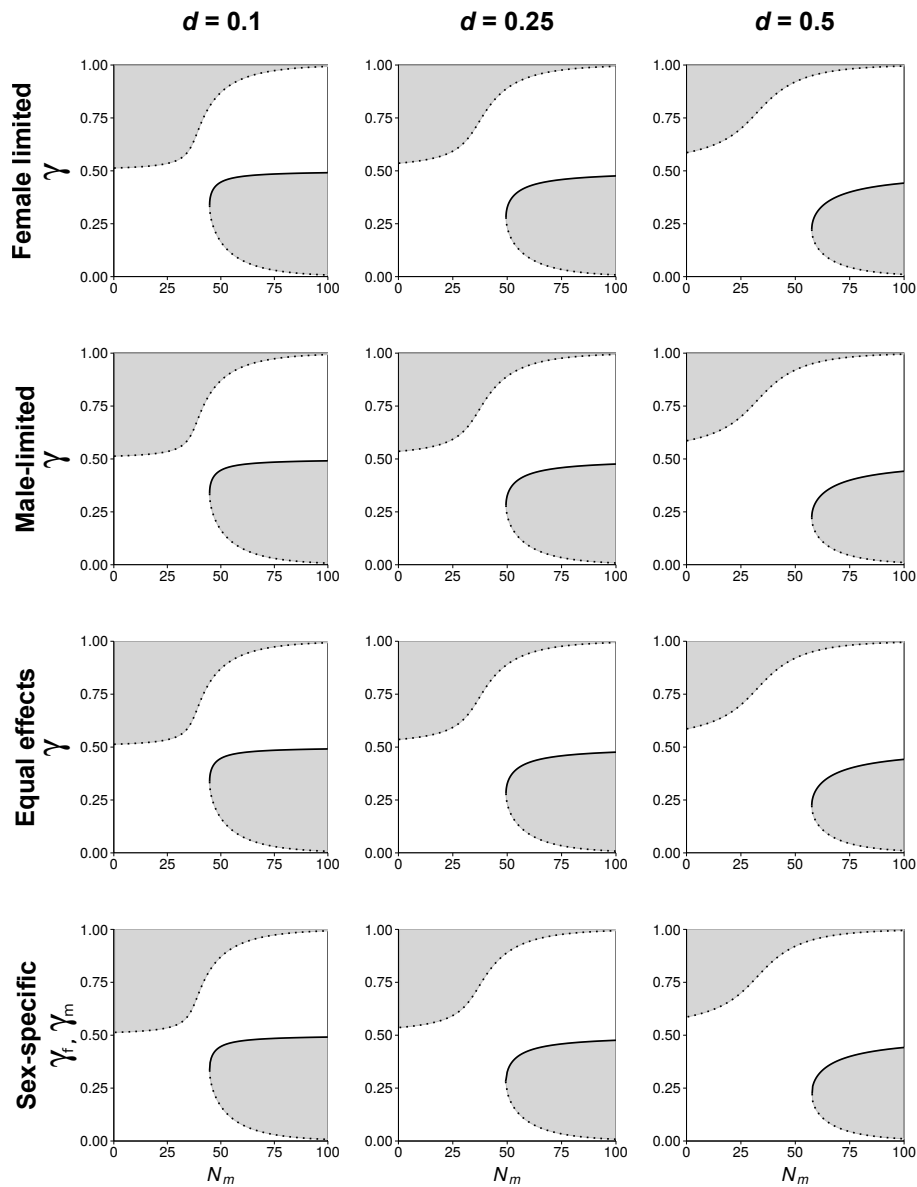


FIGURE 3.S5: ESS solutions for  $\gamma$  as a function of male density ( $n_m$ ) for all four models, at three different environmental gradients ( $d$ ). Solid lines represent the single convergence-stable equilibrium, while dotted lines represent the unstable equilibria. At a given density, populations will evolve away from the unstable equilibria, and towards the stable equilibrium in the vertical axis. These results use the parameter  $A = 0.1$ .

## 3.12 Appendix S3: Quantitative Genetic Simulation Results

The quantitative genetic simulation results were broadly congruent with the population genetic model predictions. In the population genetic models, polymorphism corresponded to greater among-individual variance, while intermediate values of  $\gamma$  correspond to increased within-individual variance. In the quantitative genetic simulations, we are instead interested in the distributions of individual means ( $m$ ) and variances ( $\ln(v)$ ) for males and females. We can rephrase the main theoretical questions outlined in the Results section of the main text as follows:

- 1) Under what conditions do populations evolve increased among- vs. within-individual variance, and how does this change with the pattern of gene expression?
- 2) What are the conditions necessary for sexual conflict over the timing of reproduction, and do analogous conditions to those resulting leading to balanced polymorphism in the population genetic models also lead to higher genetic diversity and among-individual variance in the quantitative genetic context?
- 3) Does sexual conflict generally occur because males experience selection for greater among- or within-individual variance relative to females?
- 4) When is sexually antagonistic selection expected to drive the evolution of mating during unfavourable environmental conditions?

### 3.12.1 Evolution of among- vs. within-individual variance

Under sperm-limited initial conditions, both males and females experience strong selection for lower among- and within-individual variance in spawning time. This outcome was independent of the shape of the environment conditions (discrete or gaussian), the steepness of the environmental gradient, and the pattern of gene expression (fig. 3.S6–3.S9). This was due to strong positive density-dependence in fertilization success when sperm is limiting. However, under these conditions, the sex-specific model always predicted greater within-individual variance and variation in  $\ln(v)$  than the equal effects model (fig. 3.S6–3.S9C,D).

Under polyspermic initial conditions, synchronous spawning results in strong negative density-dependent selection for increased among-individual variance in spawning time (fig. 3.S10–3.S13, High Polyspermy). Under this strong disruptive selection, individual means ( $m$ ) evolved to fill the temporal niche defined by the environmental conditions (higher variation in  $m$  when the environmental gradient is gentle). Higher within-individual variance in spawning time evolved under sex-limited expression, particularly when the environmental gradient was gentle (fig. 3.S10–3.S13C,D).

When environmental conditions were discrete, the evolution of within-individual variance depended on steepness of the environmental gradient for the equal effects and sex-specific models. Lower within-individual variance evolved in the equal effects relative to the sex-specific model, but only when the environmental gradient was steep (fig. 3.S6,3.S7,3.S10,3.S12C,D). When the environmental gradient was gentle, lower within-individual variance evolved for both sexes in the equal effects model, but males evolved higher within-individual variance than females in the sex-specific model (fig. 3.S6,3.S7,3.S10, 3.S11C,D). When the shape of the environmental conditions was Gaussian, lower within-individual variance in the equal effects model only evolved when the environmental gradient was steep (fig. 3.S8,3.S9,3.S12, 3.S13C,D). Under equal expression, when populations experienced polyspermy and were tightly constrained by

a steep environmental gradient they tended to evolve a bimodal distribution of  $m$  as phenologies evolved away from severe polyspermy at during the middle of the season (fig. 3.S9, 3.S13C). Taken together, these results strongly suggest that within- and among-individual components of population variance may respond differently to net stabilizing and disruptive selection due to frequency- and density-dependent factors, depending on the correlation of phenotypic effects between sexes. Further, this occurred under both sperm limited, and polyspermic conditions, an outcome that was not predicted by our population genetic models.

### 3.12.2 Sexual Conflict

As in the population genetic models, the prevalence of sexual conflict was driven by the incidence of polyspermy. Under sperm limited conditions, males and females evolved similar phenologies in the female- and male-limited models (fig. 3.S6–3.S9A,B). This is not surprising, as these conditions result in strong positive density-dependent fertilization success, and a narrow window of favourable environmental conditions. In contrast, sexual conflict was common under polyspermic conditions. In this case, males always evolved higher among-individual variance than females in the respective sex-limited models (fig. 3.S10–3.S13A,B). Males also evolved higher within-individual variances in a gaussian environment when the environmental gradient was steep (fig. 3.S13). These outcomes were congruent with the predictions from the population genetic models (fig. 3.2, fig. 3.6)

The distributions of allele effect sizes in a partially correlated effects model ( $u = 3$  sex-specific loci) generally corroborate the findings from the sex-limited models (fig. 3.S7, 3.S8). Under sperm limited conditions, the distributions of allele effect sizes for  $m$  are mostly indistinguishable between the male-specific, shared, and female-specific locus classes (fig. 3.S14–3.S15A,C). In contrast, there is a signature of strong sexually antagonistic selection on  $m$  under polyspermic conditions (fig. 3.S14–3.S15B,D). Specifically, the distributions are bimodal for shared alleles, but unimodal for the two sex-specific locus classes, with smaller absolute effect sizes. Interestingly, the distributions of allele effect sizes for  $\ln(v)$  differ most under sperm-limiting conditions (particularly with a steep environmental gradient), regardless of whether the shape of the environmental conditions was discrete or gaussian (3.S16–3.S17A,C vs. B,D). Under sperm limited conditions, the effect sizes of alleles at shared loci were generally smaller, and more skewed than those at sex-specific loci. Under polyspermic conditions and a steep environmental gradient, allele effects sizes for  $\ln(v)$  tended to be slightly smaller and more strongly right-skewed than for the sex-specific locus classes (3.S16–3.S17B). However, the distributions become indistinguishable when the environmental gradient is gentle (3.S16–3.S17D). Taken together with the strong difference in the distributions of  $m$  under the same parameter conditions, these results suggests that in our simulations, unless individuals are tightly constrained to spawn during a short window by a steep environmental gradient, the sexual conflict over the timing of reproduction can be largely resolved through the evolution of increased among-individual variance.

Taken together, our results from the sex-limited and correlated-effects models suggest that, despite the fact that males and females are constrained to spawn at roughly the same time, their phenotypic optima generally differ. Males prefer higher among-individual variance than females under polyspermic conditions, and higher within-individual variance under polyspermic conditions as well as under sperm limited conditions, depending on the steepness of the environmental gradient. These differences in phenotypic optima results in sexually antagonistic selection that can

maintain genetic variation in both among- and within-individual components of variance in population phenology.

### 3.12.3 Consequences of environmental gradients

Under polyspermic conditions, among-individual variance in phenology (greater  $\text{Var}(m)$ ) increased to fill the environmental niche defined by the environmental gradient. As discussed above, when selection occurred in males, this among-individual variance was generally higher than when selection acted through females. This increased variance resulted in many individuals having mean spawning times that fell well outside the period of favourable environmental conditions in both the discrete and gaussian environments. This was particularly pronounced for the male-limited and sex-specific models under a steep environmental gradient (fig. 3.S7, 3.S9, 3.S11, 3.S13A,D), where many individuals' mean spawning time corresponded to times of high density-independent mortality rates. These results are directly analogous to the population genetic model results, where protected polymorphism and even fixation of mutant alleles with higher  $\gamma$  could occur if polyspermy was severe at the environmental optimum (fig. 3.4, fig. 3.5).

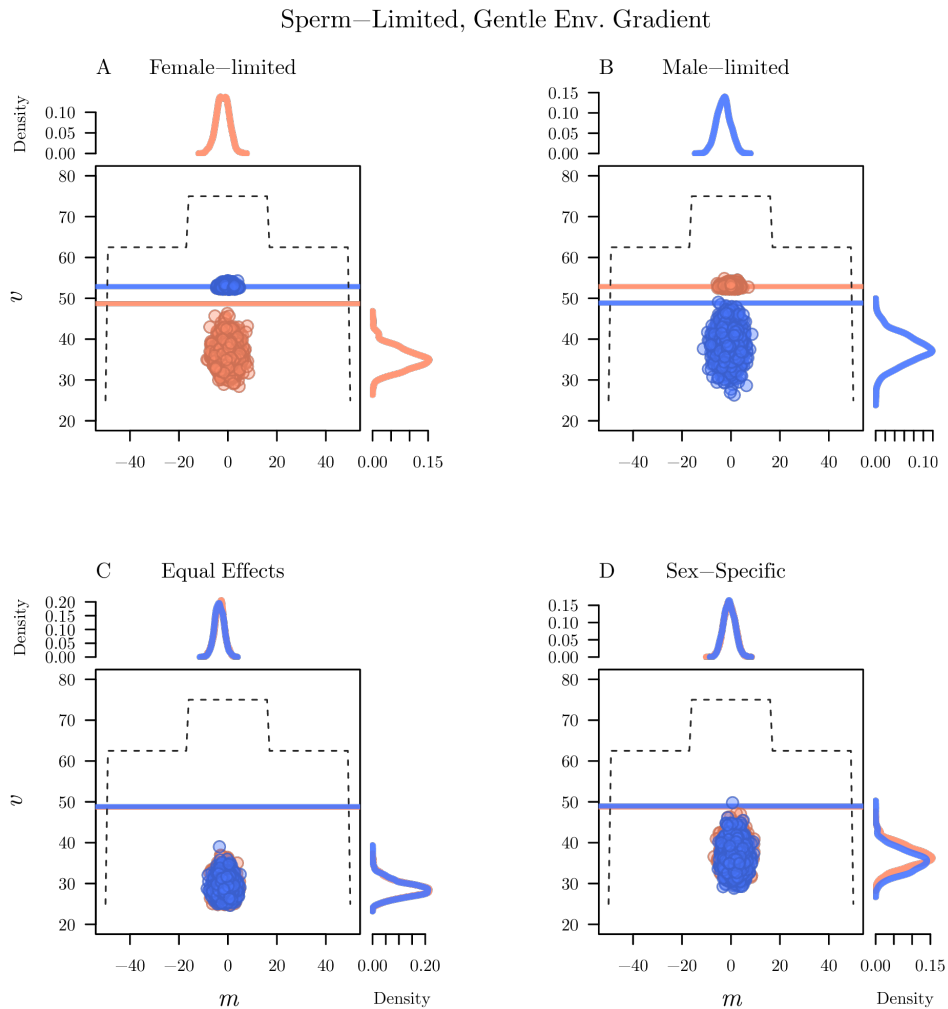


FIGURE 3.S6: Bivariate plots with marginal densities showing the effect of different environmental and fertilization conditions on individual female (orange) and male (blue) spawning phenologies. Results are shown for the case of discrete environmental conditions, and initial conditions of sperm-limitation and a gentle environmental gradient ( $A = 0.01$ ,  $d = 0.25$ ). The environmental quality function ( $Q_t(t)$ ; dotted line) is overlaid to aid comparison, but is not to scale. Horizontal lines indicate the average within-individual variance in spawning time of the initial population for males and females (generation 1). Representative results are plotted for generation 500 from a single simulation.

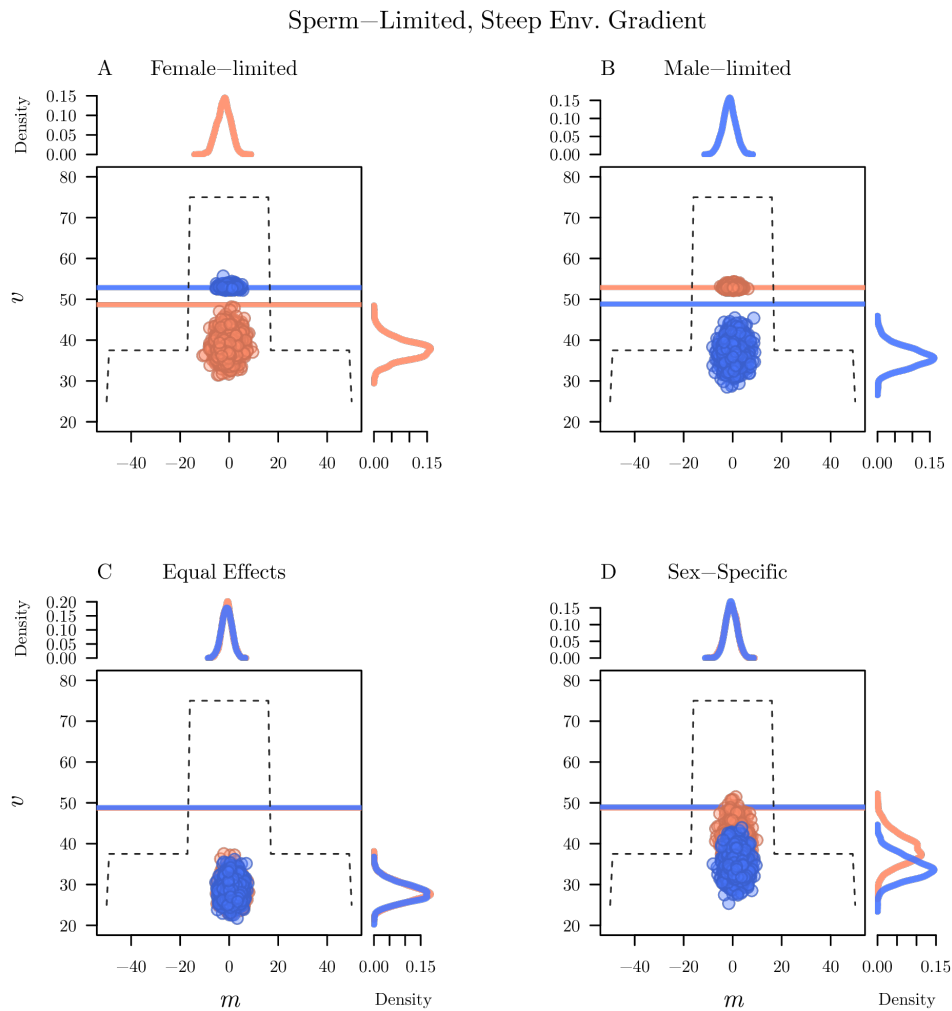


FIGURE 3.S7: Bivariate plots with marginal densities showing the effect of different environmental and fertilization conditions on individual female (orange) and male (blue) spawning phenologies. Results are shown for the case of discrete environmental conditions, and initial conditions of sperm-limitation and a steep environmental gradient ( $A = 0.01$ ,  $d = 0.75$ ). The environmental quality function ( $Q_t(t)$ ; dotted line) is overlaid to aid comparison, but is not to scale. Horizontal lines indicate the average within-individual variance in spawning time of the initial population for males and females (generation 1). Representative results are plotted for generation 500 from a single simulation.

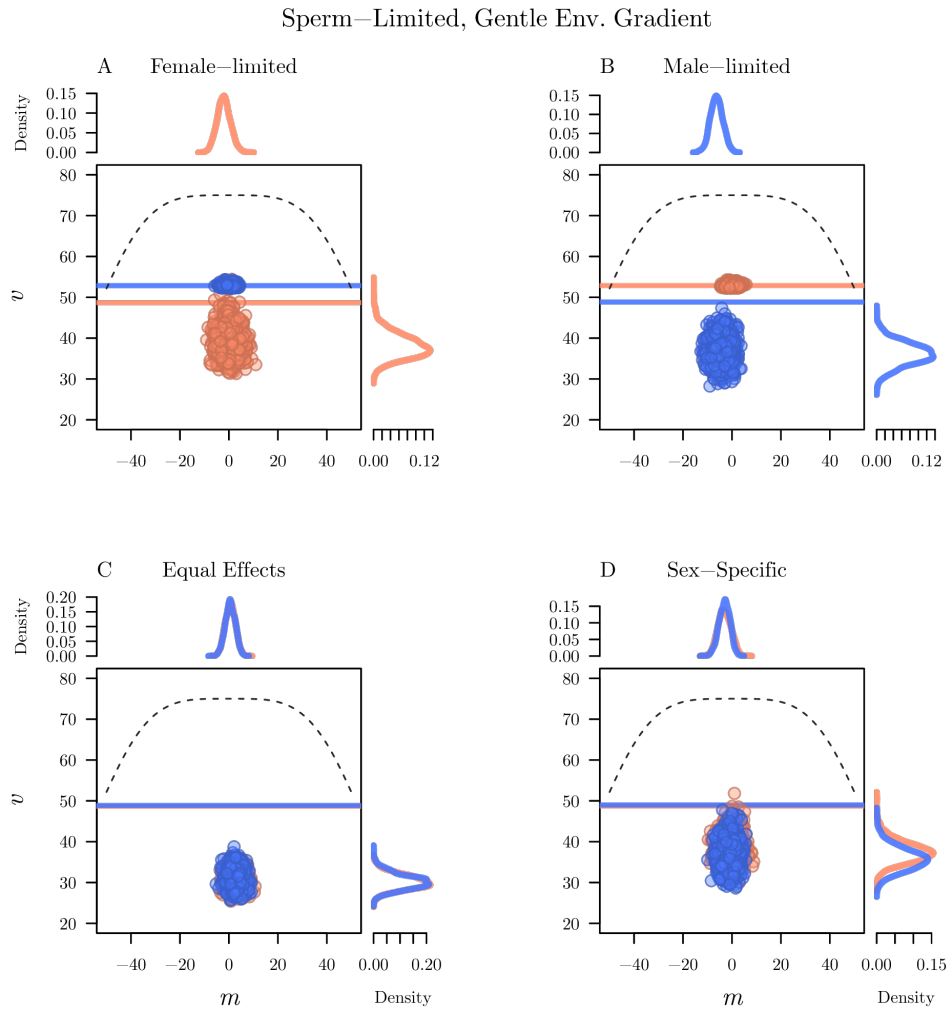


FIGURE 3.S8: Bivariate plots with marginal densities showing the effect of different environmental and fertilization conditions on individual female (orange) and male (blue) spawning phenologies. Results are shown for the case of gaussian environmental conditions, and initial conditions of sperm-limitation and a gentle environmental gradient ( $A = 0.01$ ,  $q = 40$ ). The environmental quality function ( $Q_t(t)$ ; dotted line) is overlaid to aid comparison, but is not to scale. Horizontal lines indicate the average within-individual variance in spawning time of the initial population for males and females (generation 1). Representative results are plotted for generation 500 from a single simulation.

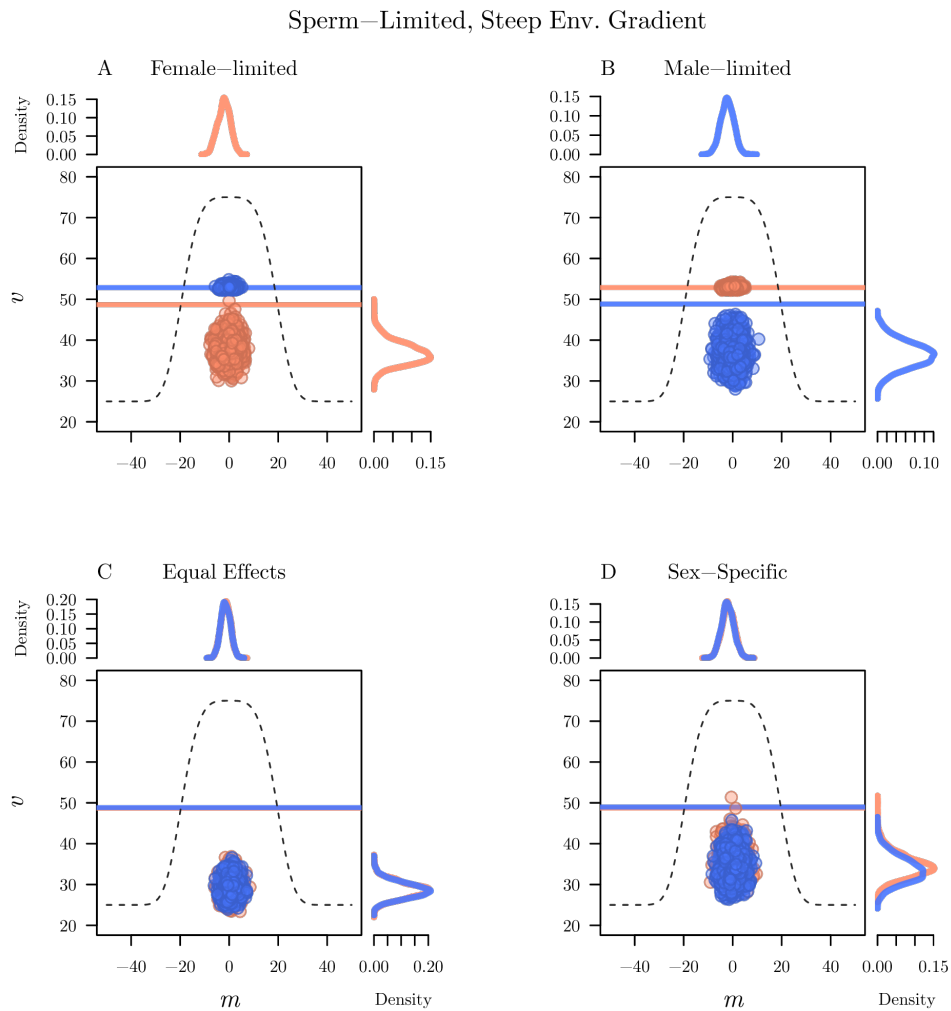


FIGURE 3.S9: Bivariate plots with marginal densities showing the effect of different environmental and fertilization conditions on individual female (orange) and male (blue) spawning phenologies. Results are shown for the case of gaussian environmental conditions, and initial conditions of sperm-limitation and a steep environmental gradient ( $A = 0.01$ ,  $q = 15$ ). The environmental quality function ( $Q_t(t)$ ; dotted line) is overlaid to aid comparison, but is not to scale. Horizontal lines indicate the average within-individual variance in spawning time of the initial population for males and females (generation 1). Representative results are plotted for generation 500 from a single simulation.

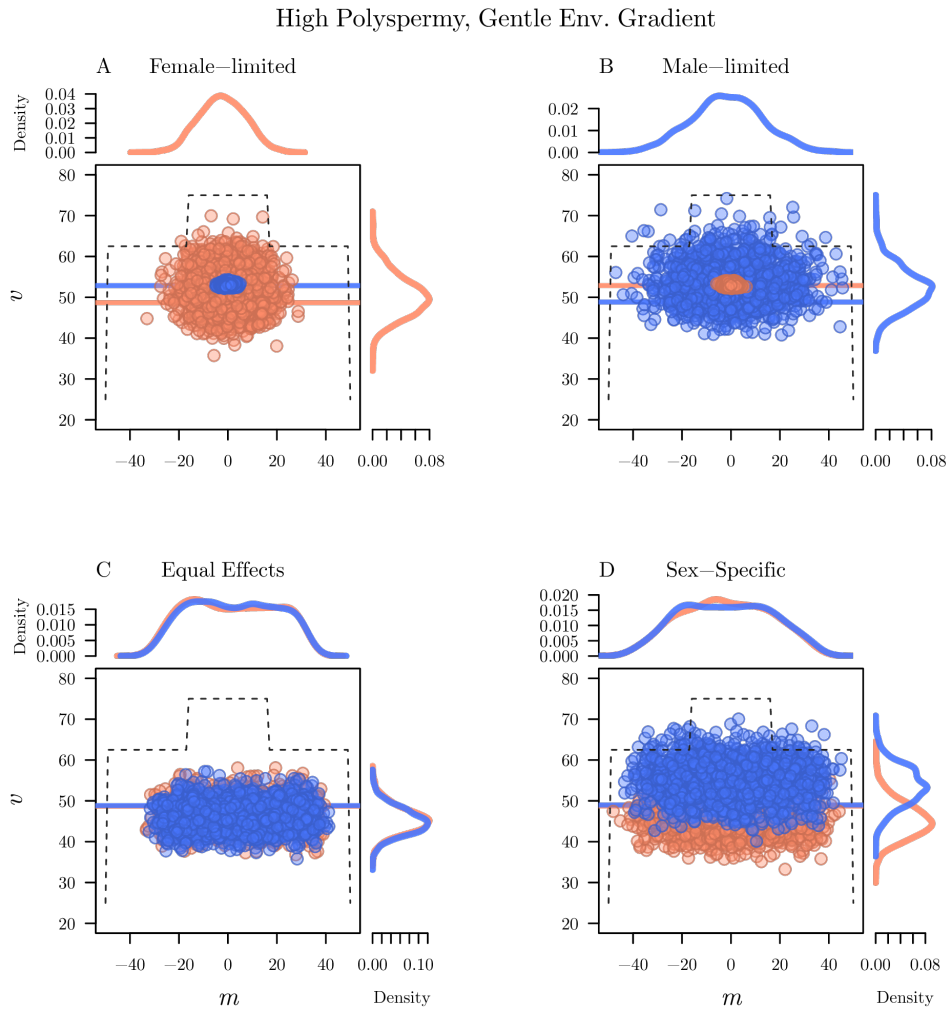


FIGURE 3.S10: Bivariate plots with marginal densities showing the effect of different environmental and fertilization conditions on individual female (orange) and male (blue) spawning phenologies. Results are shown for the case of discrete environmental conditions, and initial conditions of high-polyspermy and a gentle environmental gradient ( $A = 0.1$ ,  $d = 0.25$ ). The environmental quality function ( $Q_t(t)$ ; dotted line) is overlaid to aid comparison, but is not to scale. Horizontal lines indicate the average within-individual variance in spawning time of the initial population for males and females (generation 1). Representative results are plotted for generation 500 from a single simulation.

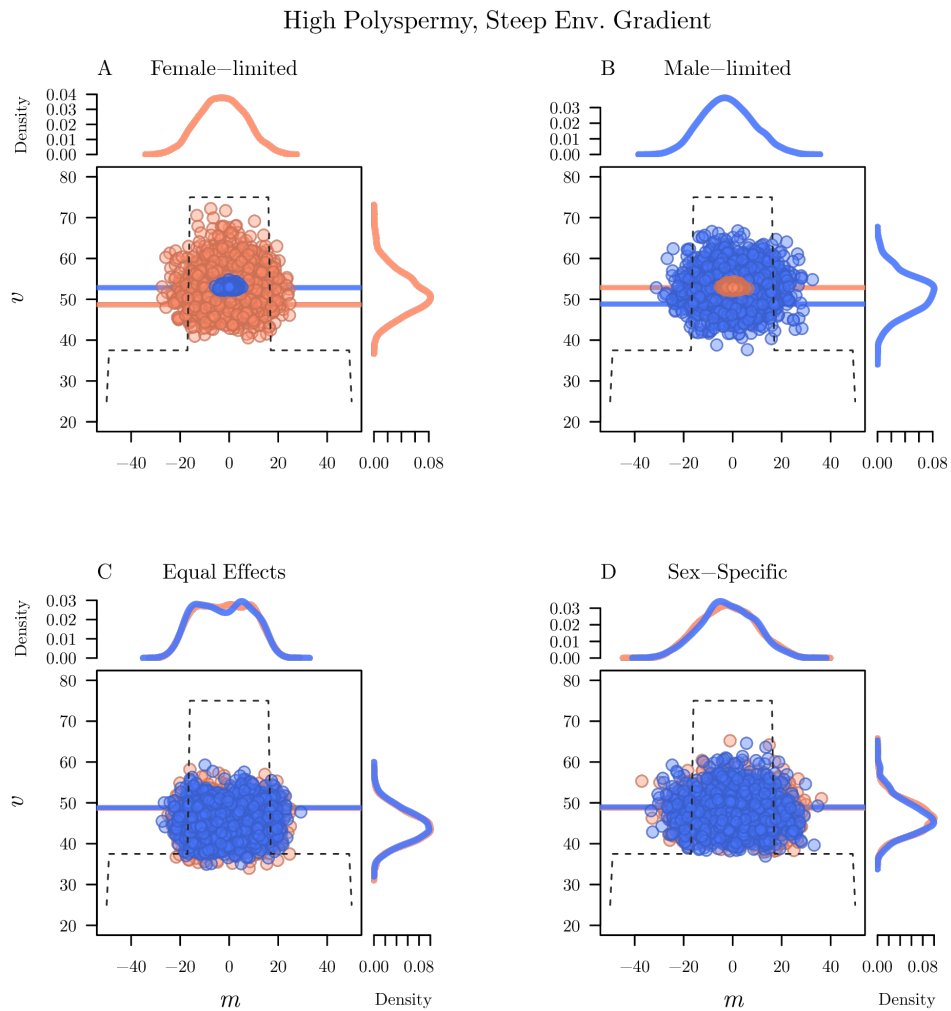


FIGURE 3.S11: Bivariate plots with marginal densities showing the effect of different environmental and fertilization conditions on individual female (orange) and male (blue) spawning phenologies. Results are shown for the case of discrete environmental conditions, and initial conditions of high-polyspermy and a steep environmental gradient ( $A = 0.1$ ,  $d = 0.75$ ). The environmental quality function ( $Q_t(t)$ ; dotted line) is overlaid to aid comparison, but is not to scale. Horizontal lines indicate the average within-individual variance in spawning time of the initial population for males and females (generation 1). Representative results are plotted for generation 500 from a single simulation.

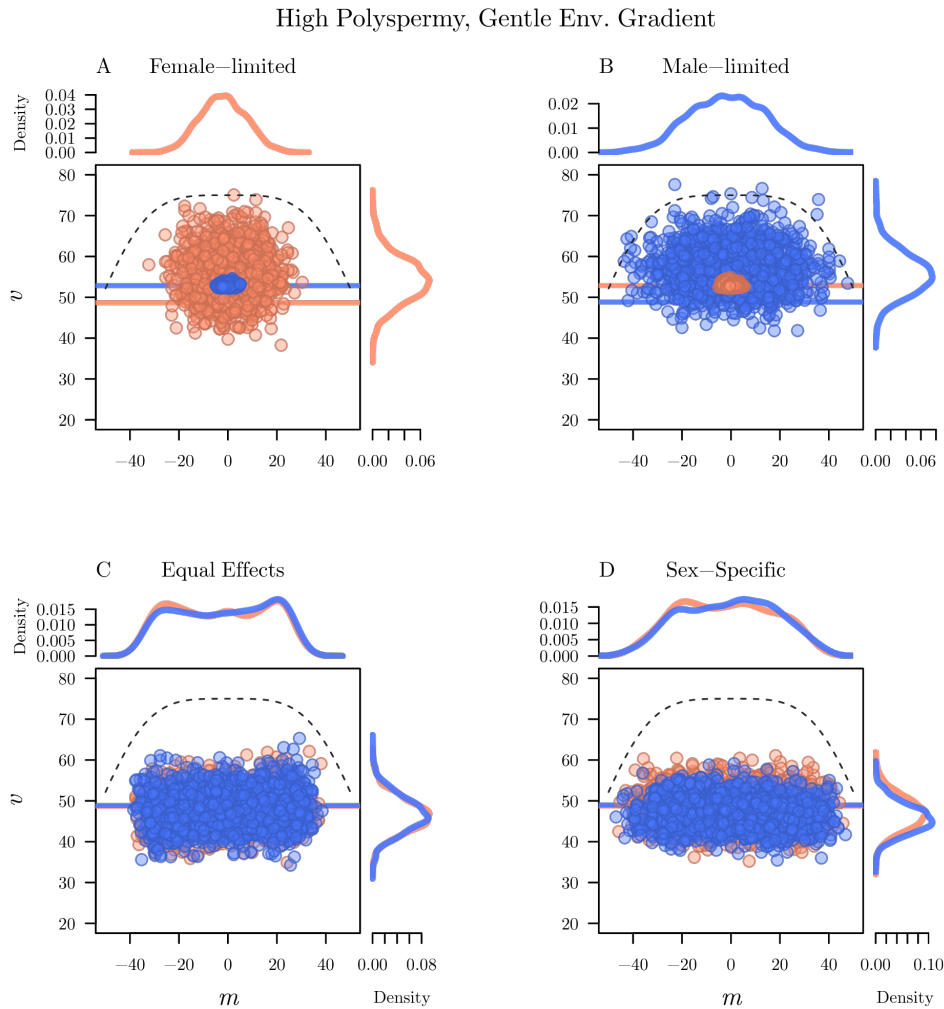


FIGURE 3.S12: Bivariate plots with marginal densities showing the effect of different environmental and fertilization conditions on individual female (orange) and male (blue) spawning phenologies. Results are shown for the case of gaussian environmental conditions, and initial conditions of high-polyspermy and a gentle environmental gradient ( $A = 0.1$ ,  $q = 40$ ). The environmental quality function ( $Q_t(t)$ ; dotted line) is overlaid to aid comparison, but is not to scale. Horizontal lines indicate the average within-individual variance in spawning time of the initial population for males and females (generation 1). Representative results are plotted for generation 500 from a single simulation.

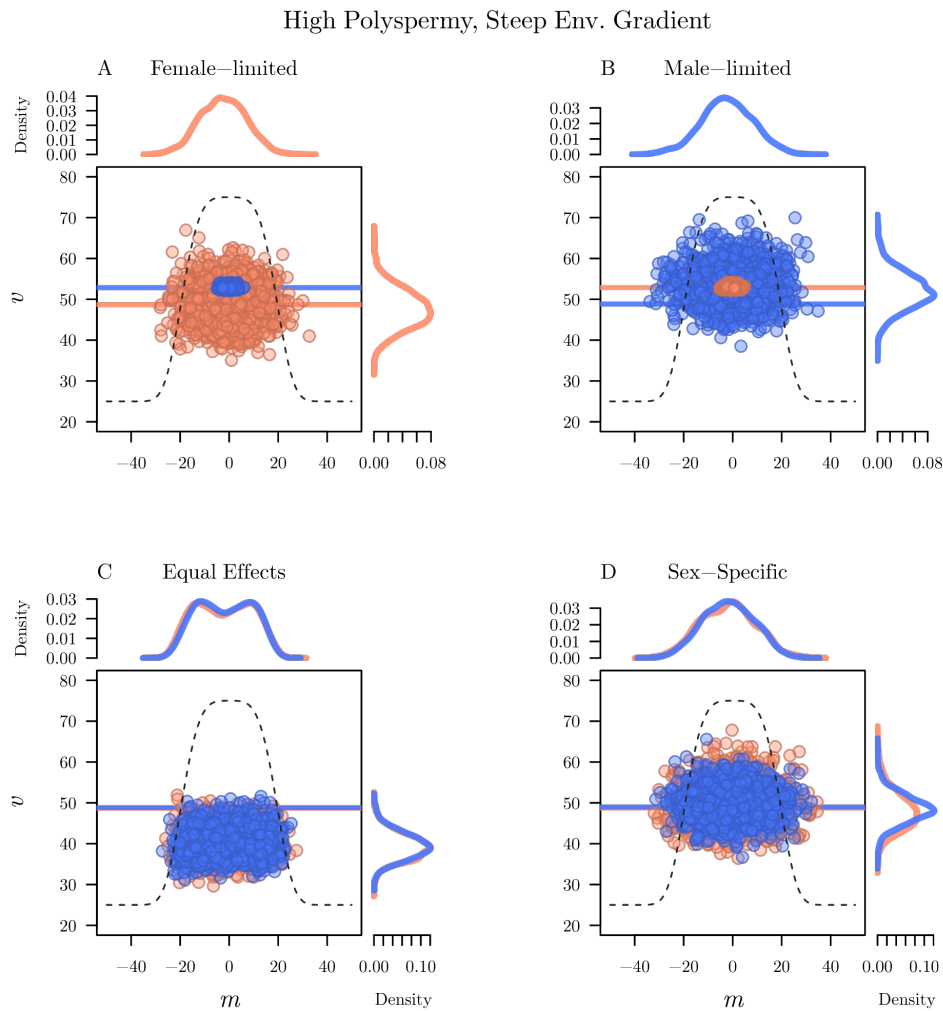


FIGURE 3.S13: Bivariate plots with marginal densities showing the effect of different environmental and fertilization conditions on individual female (orange) and male (blue) spawning phenologies. Results are shown for the case of gaussian environmental conditions, and initial conditions of high-polyspermy and a steep environmental gradient ( $A = 0.1$ ,  $q = 15$ ). The environmental quality function ( $Q_t(t)$ ; dotted line) is overlaid to aid comparison, but is not to scale. Horizontal lines indicate the average within-individual variance in spawning time of the initial population for males and females (generation 1). Representative results are plotted for generation 500 from a single simulation.

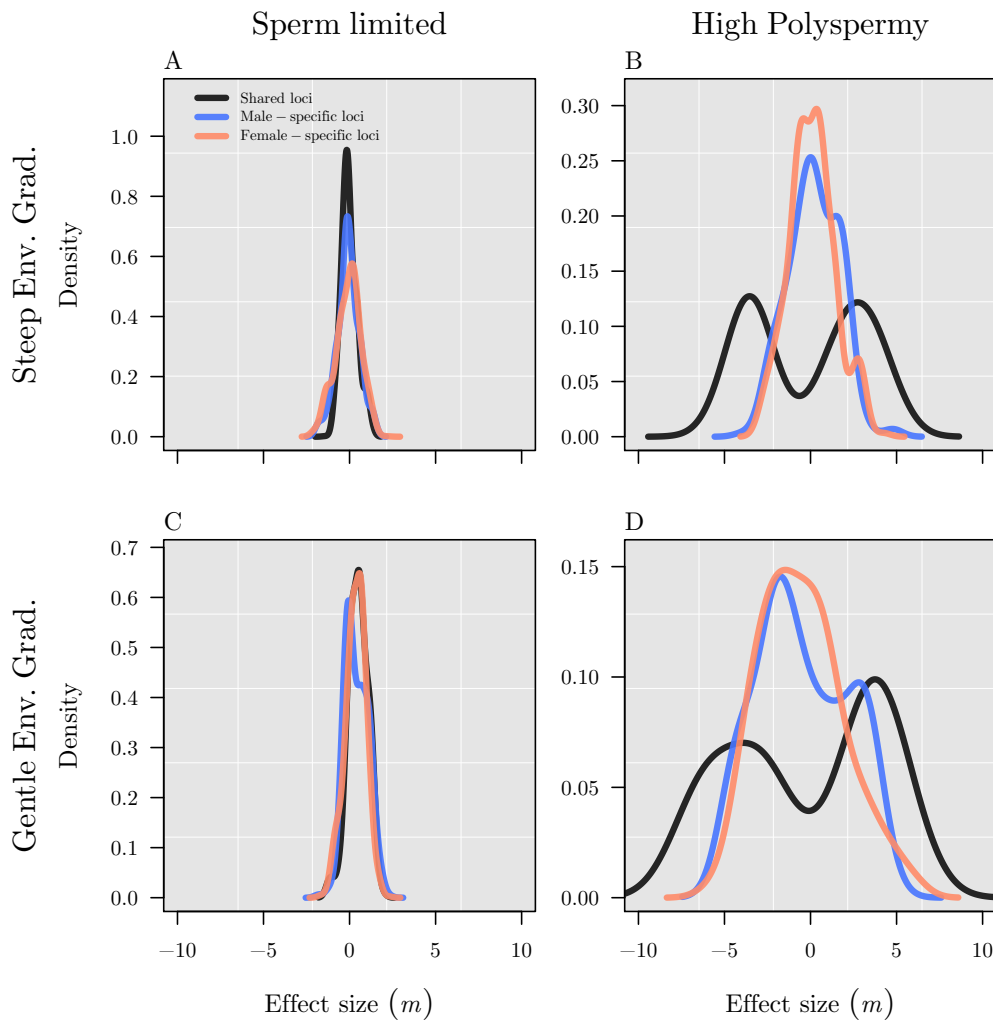


FIGURE 3.S14: Distribution of allele effect sizes for within-individual mean ( $m$ ) for each of the three possible locus classes (shared, female-specific, and male-specific) from a correlated effects model with  $u = 3$  unshared loci. Results are shown for the case of discrete environmental conditions. Representative results are plotted at generation 500 from a single simulation..

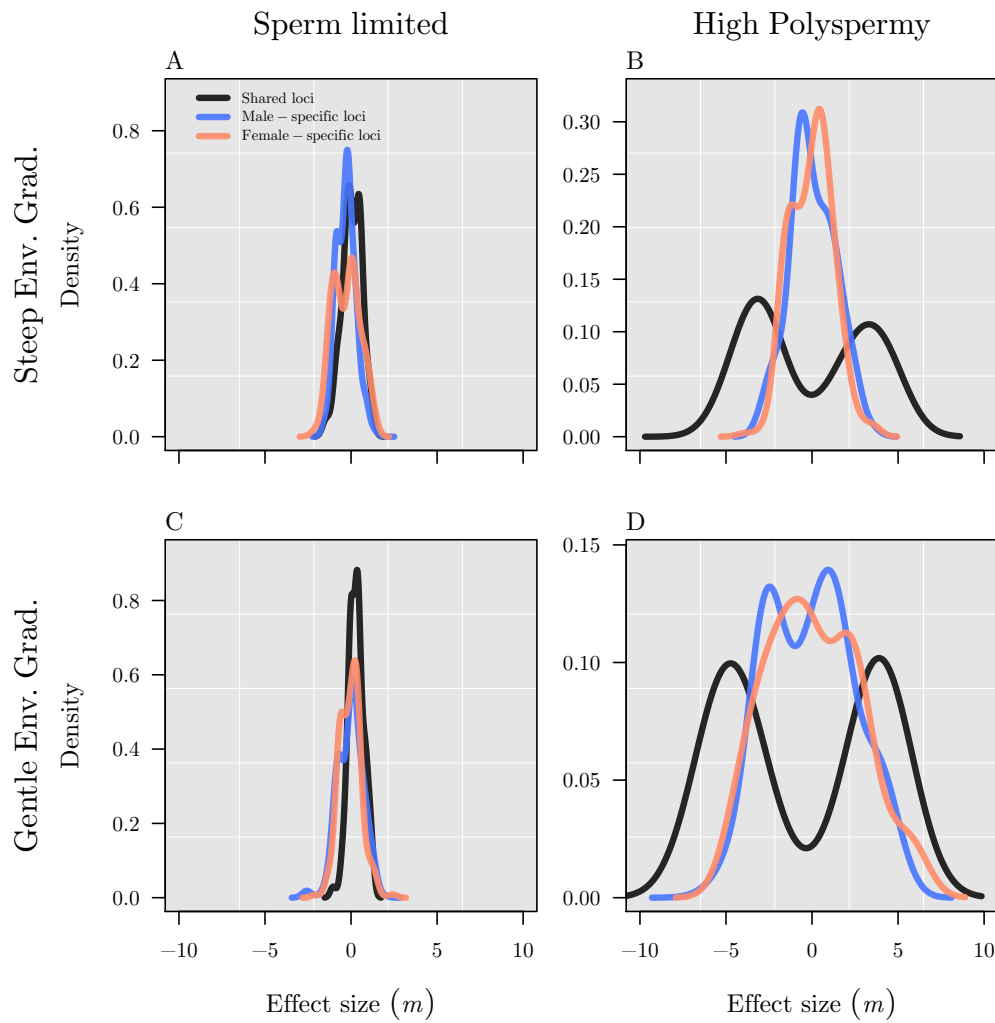


FIGURE 3.S15: Distribution of allele effect sizes for within-individual mean ( $m$ ) for each of the three possible locus classes (shared, female-specific, and male-specific) from a correlated effects model with  $u = 3$  unshared loci. Results are shown for the case of gaussian environmental conditions. Representative results are plotted at generation 500 from a single simulation.

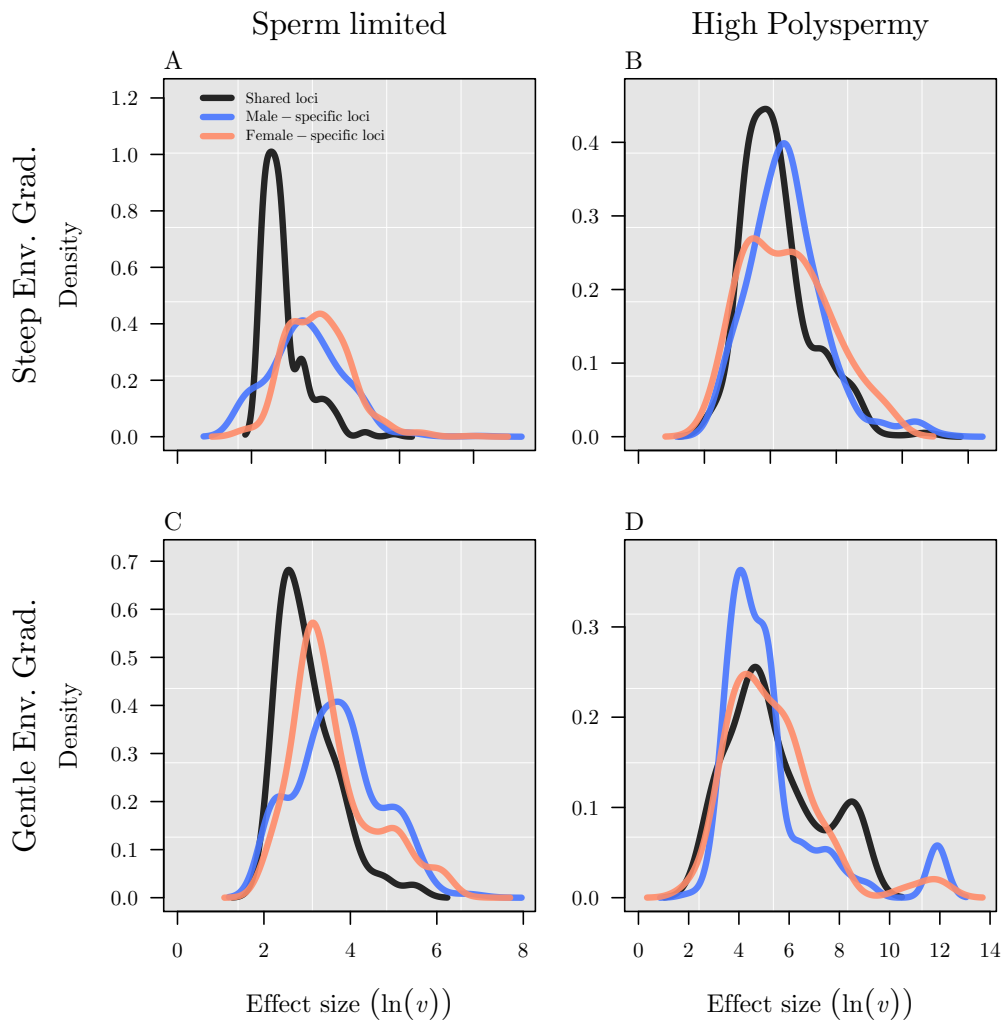


FIGURE 3.S16: Distribution of allele effect sizes for within-individual mean ( $\ln(v)$ ) for each of the three possible locus classes (shared, female-specific, and male-specific) from a correlated effects model with  $u = 3$  unshared loci. Results are shown for the case of discrete environmental conditions. Representative results are plotted at generation 500 from a single simulation.

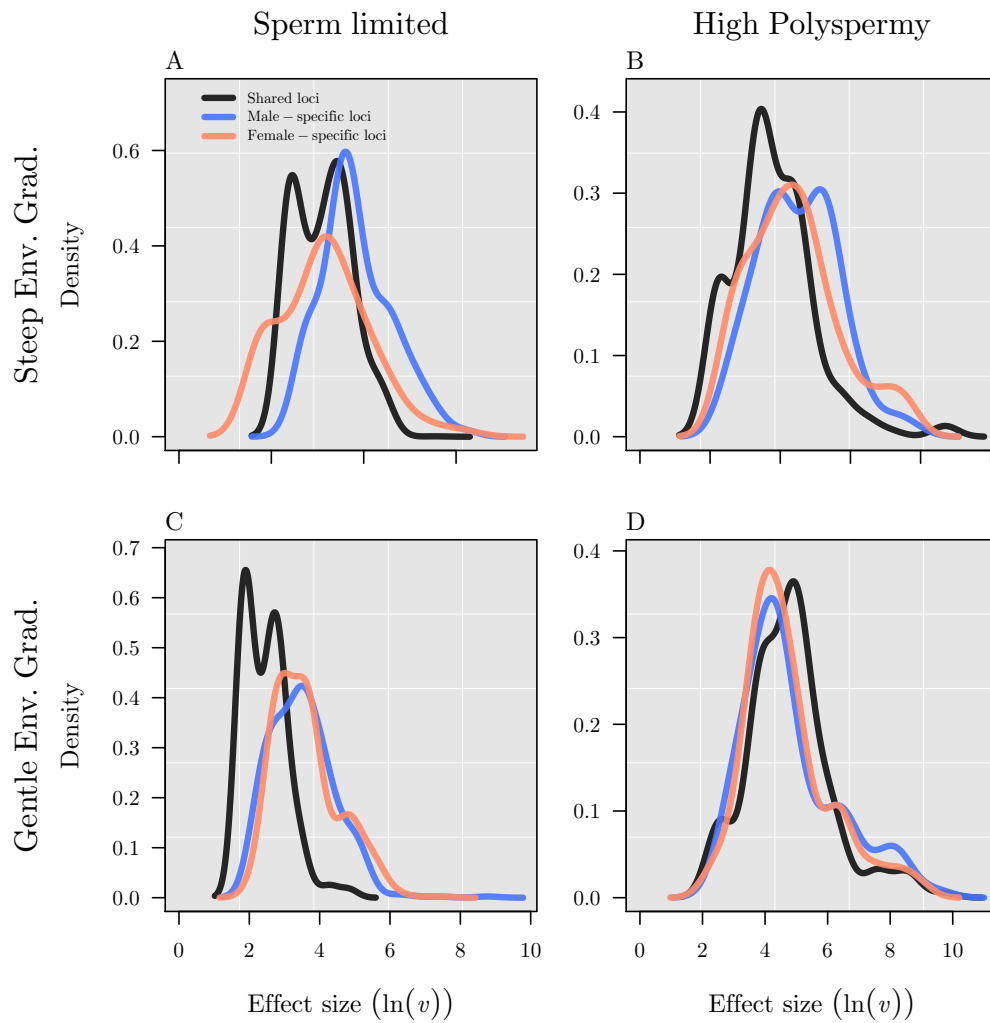


FIGURE 3.S17: Distribution of allele effect sizes for within-individual mean ( $\ln(v)$ ) for each of the three possible locus classes (shared, female-specific, and male-specific) from a correlated effects model with  $u = 3$  unshared loci. Results are shown for the case of gaussian environmental conditions. Representative results are plotted at generation 500 from a single simulation.

### 3.13 Appendix S4: Computer Code

R code for the Quantitative Genetic Simulations is available in the online supplements to the published article in *The American Naturalist* (<http://www.journals.uchicago.edu/toc/an/current>), or from the author ([colin.olito@gmail.com](mailto:colin.olito@gmail.com)).

## Chapter 4

# Sperm-release strategies in external fertilizers: selection during sperm dispersal and sperm competition favour similar reproductive phenotypes

### 4.1 Abstract

The idea that male reproductive strategies evolve primarily in response to sperm competition has become almost axiomatic in evolutionary biology. However, externally fertilizing species, especially broadcast spawners, represent a large and taxonomically diverse group that have long challenged predictions from sperm competition theory – broadcast spawning males often release sperm slowly, with weak resource-dependent allocation to ejaculates despite massive investment in gonads. One possible explanation for these counter-intuitive patterns is that male broadcast spawners experience strong natural selection from the external environment during sperm dispersal. Using a manipulative experiment, we examine how male reproductive success in the absence of sperm competition varies with male energetic investment in ejaculates, and the rate of sperm release, in the broadcast spawning marine invertebrate *Galeolaria caespitosa*. We find that the benefits of fast or slow sperm release rates depend strongly on ejaculate size, but also that the per-gamete fertilization rate decreases precipitously with ejaculate size. Overall, these results suggest that, if males can facultatively adjust ejaculate size, they should always release little sperm, and slowly. Interestingly, these results match recent sperm competition theory developed for broadcast spawners, suggesting that well documented empirical patterns are expected to evolve whether or not males experience sperm competition.

## 4.2 Introduction

Our understanding of male reproductive biology is dominated by the idea that males compete strongly to fertilize females' eggs (Bateman 1948; Parker et al. 1982; Parker 1982). Sperm competition theory (SCT) is the largest and most influential body of theory explaining observed male reproductive phenotypes (Parker et al. 1982; Parker 1982; Wedell et al. 2002), and the existence of sperm competition is often an implicit assumption in the fields of sexual selection and sexual conflict (Birkhead and Møller 1998; Arnqvist and Rowe 2005). Moreover, classic predictions from SCT, such as increased ejaculate investment with competition among species, and facultative adjustment of ejaculate allocation within species, align well with empirical data, particularly for internally fertilizing taxa (reviewed in Wedell et al. 2002).

The amount of resources a male has available for reproduction plays a critical role in determining the outcome of sperm competition because sperm competition always involves some form of raffle competition among competing males' ejaculates (Wedell et al. 2002; Arnqvist and Rowe 2005). Hence, producing more sperm relative to other competing males generally translates into greater siring success (Parker et al. 1982; Parker 1982; Wedell et al. 2002). This has been demonstrated theoretically, and empirically in both plants and animals, where the interplay between male resource availability (generally estimated by age or body size) and mating system strongly influence the optimal male mating strategy (e.g., dominant vs. 'sneaker' males; Parker 1990a, 1990b; Gage et al. 1995), mating rate (Parker, 1990b; Birkhead and Møller 1998; Wedell et al. 2002), ejaculate/pollen allocation strategy (Friedman and Barrett 2009; reviewed in Wedell et al. 2002; Zhang 2006), and body size (e.g., Arnold and Wade 1984). Even sequential hermaphroditism, particularly in animals, is thought to be driven primarily by sex-specific and age-dependent fecundity (Ghiselin 1969; Warner 1975, 1988; Munday et al. 2006).

While resource availability clearly matters for males with internal fertilization, and some externally fertilizing fish species, the consequences of male resource availability are poorly understood for the archetypal external fertilizer – broadcast spawning species. Neglecting broadcast spawners creates a critical gap in our understanding of the evolution of male reproductive strategies because broadcast spawners represent the ancestral mode of reproduction (Rouse and Fitzhugh 1994), and are a large and taxonomically diverse group, representing more than 50% of global marine invertebrate biodiversity (Monro and Marshall 2015). Furthermore, broadcast spawning excludes complicating factors common in internal fertilizers such as cryptic female choice, and have long been used as a model for SCT and the evolution of anisogamy (e.g., Parker et al. 1982; Parker 1982).

There are several tantalizing lines of evidence that suggest the consequences of male reproductive investment are very different for broadcast spawners than for internal fertilizers. Superficially, broadcast spawning species appear well suited to predictions from sperm competition theory. Gametes are released into the water column by multiple individuals, polyandry is common, and sperm competition can be intense (McEuan 1988; Levitan 1998, 2002, 2004; Marshall 2002). However, broadcast spawners often exhibit spawning strategies that differ markedly from classic SCT predictions (Bode and Marshall 2007; Olito et al. 2015; Olito 2016). Many broadcast spawning species have surprisingly long spawning times characterized by slow individual gamete release rates (McEuan 1988; Marshall and Bolton 2007).

Protandry is common among broadcast spawners, with males releasing sperm earlier and longer than females do eggs (McEuan 1988; Lotterhos and Levitan 2011; Levitan 2005; Marshall and Bolton 2007). In some species, large males do not necessarily release more sperm than small males, despite presumably having the resources available to do so (Levitan 1991; Styan 2003). Although these well documented patterns are counter-intuitive from the perspective of SCT, broadcast spawners often exhibit massive investment in gonad tissue relative to even the most extravagant internal fertilizers. For example, the mean size of gonads relative to body mass in the broadcast spawning brittle star *Ophiocoma alexandri* is more than four times the relative gonad size in cape gerbils, who exhibit an especially large GSI among mammals ( $\approx 40\%$  vs.  $\approx 8\%$  gonad mass/body mass percent; Kenagy and Trombulak 1986; Benítez-Villalobos et al. 2012). Thus, the relevance of classic SCT to the evolution of male reproductive phenotypes in broadcast spawners remains unclear.

While some studies have considered the evolution of male broadcast spawning strategies from the perspective of sexual selection (i.e., in the presence of mate competition), few have considered the consequences of natural selection (i.e., from the perspective of what maximized fertilization success in the absence of mate competition) (Levitan 2005; reviewed in Lotterhos and Levitan 2011). Ignoring the potential effects of natural selection is an important omission because there is an expanded opportunity for selection from the external environment to act on male reproductive traits in broadcasters, and the absence of mate competition therefore represents the baseline for what an adaptive spawning strategy should be (Marshall and Bolton 2007). In particular, selection arising from a variety of factors, especially temperature and hydrodynamic conditions, at the time of spawning strongly influence the likelihood that a sperm will make contact with, and possibly fertilize, an egg (Denny and Shibata 1989; Kupriyanova 2006; Kupriyanova and Havenhand 2013). For example, Marshall and Bolton (2007) demonstrated in a flow-through flume experiment that males releasing sperm slowly enjoyed higher fertilization success at downstream egg patches than did fast-releasing males. However, they did not explore the consequences of different levels of male investment in ejaculates. In contrast, Johnson and Yund (2009) found rapidly diminishing returns in male gain curves for a sperm-casting hermaphroditic colonial ascidian (sperm is released, but eggs are retained at spawning), but did not explore alternative spawning strategies (e.g., sperm release rates). These sparse empirical results suggest that natural selection in the absence of sperm competition may provide a simple alternative explanation for many of the well-documented spawning strategies in broadcast spawners that appear counter-intuitive from the perspective of sexual selection alone.

Here we use a manipulative experiment to explore the reproductive success in the absence of sperm competition associated with two important male reproductive traits in the broadcast spawning marine invertebrate *Galeolaria caespitosa*: male energetic investment in ejaculates, and the rate of sperm release. We find that the benefits of any one sperm release strategy depends critically on ejaculate size. We also find that the per-gamete fertilization rate for males decreases dramatically with ejaculate size – highlighting the massive investment required by males to overcome sperm wastage. Our results indicate that if males can facultatively adjust the size of their ejaculates, they should always release very little sperm, and slowly. Crucially, this result matches theory developed for broadcast spawners, suggesting that well documented empirical patterns, and especially slow sperm-release rates, are expected to evolve whether or not males experience sperm competition.

## 4.3 Methods

### 4.3.1 Study species

We studied spawning phenologies and the fertilization success of different male spawning strategies using *Galeolaria caespitosa* Savigny, 1818. *G. caespitosa* is a dioecious sessile polychaete worm common in the intertidal zone throughout southeast Australia. All individuals were collected from pier pilings at the Royal Brighton Yacht Squadron, Port Philip Bay, Victoria. For flume experiments, we used established protocols to collect gametes (e.g., Marshall and Evans 2005a, 2005b). *G. caespitosa* sperm become active immediately upon release, and can remain viable for several hours after spawning (Kupriyanova and Havenhand 2013). To minimize any effects of sperm aging on egg fertilization success, we ensured that all gametes had been freshly spawned no more than 45 min before being used in experiments.

### 4.3.2 Estimating spawning durations

To estimate the duration of individual spawning phenologies, we documented induced, non-traumatic, spawnings in a laboratory setting. A large *G. caespitosa* colony fragment was collected on 16/11/16, and stored overnight in a controlled temperature room at the ambient temperature of Port Philip Bay (17.5°C). The large colony fragment was then sub-divided into small fragments of approx. 50 – 100 individuals that were then induced to spawn by heat shock in a shallow sea-water bath, a common technique for inducing spawning in ripe individuals (Strathmann 1987). Individual spawning males were marked and monitored and the duration of their spawning timed. Water in the bath was gently agitated, and spawning individuals were periodically flushed with seawater using a 1cc syringe. Individual males' spawning phenology was considered complete when no more ejaculate could be seen leaking from the tube with gentle flushing. Approximately 8 – 10 small colony fragments were monitored at once in an experimental run, and we performed 5 experimental runs resulting in 26 documented individual spawning phenologies.

### 4.3.3 Flume experiments

We performed two flume experiments (Exp. 1 and Exp. 2 hereafter) to examine the effect of the amount and rate of sperm released on fertilization success in simulated spawning events. The flume was plexiglass, 240 × 96 × 10 cm (L×W×D), divided into 6 parallel lanes, each 15 cm wide. Filtered seawater sourced from the Mornington Peninsula, Port Philip Bay, was gravity fed from a 20 L constant head tank into a common head for the flume which in turn fed all 6 lanes. Water was not recycled after flowing through the flume. During experimental runs, the flume was filled to a depth of 5 cm, with a constant flow rate of  $\approx 1$  cm per second across all lanes. Laminar flow in each lane was maintained by 10 cm collimators made of drinking straws located 25 cm from the head of each lane (Yund and Meidel 2003). *G. caespitosa* colony fragments for both flume experiments were collected from the Royal Brighton Yacht Squadron between 9/10/2015 and 20/10/2015 for Exp. 1, and between 11/04/2016 and 22/04/2016 for Exp. 2. All flume experiments were conducted in a Controlled Temperature room maintained at 17° C.

In Exp. 1, we examined the effect of releasing different amounts of sperm on fertilization success at a patch of eggs located downstream from the sperm release point. Prior to running the flume, we collected gametes from 12 males and 6 females.

All collected eggs were pooled together and mixed thoroughly to reduce the influence of compatibility effects. Eggs were then divided into 6 aliquots that were gently released onto the bottom of the flume, in the center of each lane, 5 cm downstream from the collimators (25 cm downstream from the sperm release point). *G. caespitosa* eggs are negatively buoyant, and the flow rate in the flume was low enough that eggs were not washed away.

All collected sperm was combined into a single pooled ejaculate, and thoroughly mixed. 0.1 mL of the pooled ejaculate was set aside for sperm enumeration using a haemocytometer. The remaining ejaculate was diluted by a factor of 10, and then sub-divided into 6 aliquots with different volumes corresponding to  $N = 0.5, 1, 1.5, 2, 2.5,$  and 3 times the average amount of sperm released by the individual males used in that experimental run. Thus, the specific amount of sperm released for a given level of  $N$  differed among experimental runs. We intentionally allowed  $N$  to vary among runs in order to harness natural variation in the average amount of sperm collected from males for each experimental run, and sample a broader range of the amount of sperm released, while retaining the same ratios of relative male investment in sperm. Dilutions were performed immediately before initiating an experimental run to minimize sperm aging effects (i.e., after priming the flume, placing eggs, and starting the flow of water). Lane assignments for each level of  $N$ , and the order in which lanes were run, were randomized for each experimental run to account for any lane-specific, or lane order, effects on fertilization success.

During an experimental run, sperm was released from a syringe 15 cm from the head of each lane (10 cm upstream from the collimators), in the center of each lane, immediately above the bottom of the flume. Sperm was released over a period of 15 seconds, and care was taken to release sperm at a steady rate. Note that this necessarily confounded the rate of release with the total amount of sperm released – larger ejaculates were released at faster rates. After all sperm was released, the flume was left to run uninterrupted for 10 min before collecting eggs. Eggs were then washed with fresh filtered seawater, and left to develop in polyethelene test tubes for an additional 2 hours. After incubation, 100 eggs from each lane were examined under an inverted compound microscope, and scored as either unfertilized, fertilized, or polyspermic, based on the presence/absence of raised egg envelopes, regular, or irregular, patterns of cell division. The flume was drained completely and washed with fresh water between each experimental run. We performed 8 experimental runs, yielding a total of  $n = 48$  observations.

In Exp. 2, we examined the effect of a factorial cross between the amount of sperm released, and the rate at which it was released, on fertilization success at two patches of eggs located downstream from the sperm release point. Wherever possible, we used identical protocols to Exp. 1, and describe only the relevant differences here. Eggs from 10 females were collected, combined, and placed on the bottom of the flume in each lane in two patches located 25 cm and 75 cm downstream from the sperm release point. Sperm from 12 males was collected, pooled, diluted by  $10^{-1}$ , and then sub-divided into 6 aliquots with three different volumes corresponding to  $N = 1, 2,$  and 3 times the average amount of sperm released by the individual males used in that experimental run (2 aliquots per level of  $N$ ). For each level of  $N$ , one replicate aliquot was released at a 'fast' rate, corresponding to a single pulse lasting 10 seconds. The second replicate aliquot was released at a 'slow' rate, corresponding to 4 pulses, each lasting 15 seconds, spread out over 4 minutes. Lane assignments and the order of release were again randomized. We performed 10 experimental runs, yielding a total of  $n = 120$  observations (10 runs  $\times$  6 lanes  $\times$  2 egg patches = 120).

#### 4.3.4 Analyses

For both flume experiments, we modeled the number of fertilized eggs ( $n$ ) in a given egg patch as a binomial response variable, where the number of eggs counted in each egg patch ( $E$ ) corresponds to the number of bernoulli trials. We analyzed fertilization success using logistic regression in a Bayesian Linear Mixed Effects Regression framework, with the basic model structure

$$\begin{aligned} n_i &\sim \text{Bin}\left(E_i \mid \text{logit}^{-1}(\mu_i)\right) \\ \mu_i &= \beta\mathbf{X} + \gamma\mathbf{Z} + \epsilon, \end{aligned} \quad (4.1)$$

with priors

$$\begin{aligned} \beta &\sim N(0, 3) \\ \gamma &\sim N(0, \sigma_\gamma) \\ \sigma_\gamma &\sim \text{half-Cauchy}(0, 1), \end{aligned}$$

where  $\beta$  and  $\gamma$  are vectors of regression coefficients for ‘fixed’ and ‘random’ effects,  $\mathbf{X}$  and  $\mathbf{Z}$  are model matrices for the linear predictors, and  $\epsilon$  is the residual error. Although there is little distinction between ‘fixed’ and ‘random’ effects in Bayesian analyses, this model specification allows for flexible heirarchical structure, and direct sampling of the posterior distributions for all parameters rather than maximum likelihood estimates. The number of sperm released,  $Sperm_i$ , was treated as a continuous predictor variable for all analyses. To avoid estimating very small regression coefficients (on the order of  $1 \times 10^{-9}$ ), and to simplify interpretation of parameter estimates, the number of sperm released was Z-transformed prior to analyses. Thus, the units for  $Sperm_i$  coefficients are in standard deviations of the empirical distribution of the number of sperm released in each experiment ( $7.9 \times 10^7$  for Exp. 1;  $8.9 \times 10^7$  for Exp. 2).

For Exp. 1, we fit a simple logistic regression of fertilization success regressed on the number of sperm released ( $\mathbf{X} = Sperm_i$ ), with experimental run as a ‘random’ grouping variable. We then analyzed the full set of nested models arising from the  $\mathbf{Z} = Run \times Sperm_i$  interaction (with all lower-order interactions included). For Exp. 2, we treated the rate of sperm release ( $Rate$ , with two levels: ‘Fast’ or ‘Slow’), and the position of the downstream egg patches ( $EggPos$ , with two levels: ‘25 cm’ or ‘75 cm’) as categorical variables, and modeled fertilization success using a linear model of the three way interaction between of the amount of sperm released, the rate it was released, and the downstream distance to the egg patches ( $\mathbf{X} = Sperm_i \times Rate \times EggPos$ , including lower-order interactions). We again treated experimental run as a ‘random’ grouping variable, and analyzed the nested model set arising from the interaction of  $Run$  with all ‘fixed’ effects (i.e.,  $\mathbf{Z} = Run \times Sperm_i \times Rate \times EggPos$ , including lower-order interactions). We did not drop any of the ‘fixed-effect’ terms in either analysis ( $\mathbf{X}$  was identical for all competing models in each analysis).

Posterior distributions of all model parameters were estimated using Markov Chain Monte Carlo (MCMC) methods implementing a NUTS sampler (Team 2016b). For all models in both analyses we initiated 3 MCMC chains of 2,000 steps, each with a 1,000 step warmup, yielding a total of 3,000 samples (i.e.,  $(2,000 - 1,000) \times 3 = 3,000$ ). Chains were monitored for sampling abnormalities and considered to have

reached convergence when all parameter estimates yielded a scale reduction statistic of  $\hat{R} < 1.01$  (Gelman and Rubin 1992).

For both analyses, we implemented a fully Bayesian model selection procedure using leave-one-out cross-validation using the R package *loo* v.0.1.6 (PSIS-LOO; Behari et al. 2016). For each analysis, we compared the fit of all competing models against one another (i.e., all pairwise model comparisons) using the expected log pointwise predictive density ( $\widehat{elpd}_{loo}$ ), calculated by evaluating the log-likelihood at each of the posterior draws of the parameter values (Hooten and Hobbs 2015; Behari et al. 2016). For each pairwise model comparison, we calculated p-values for the pairwise differences in  $\widehat{elpd}_{loo}$  using standard errors (s.e.) calculated as described in Eq(24) of Behari et al. (2016), and a normal probability density function. Although this method of calculating s.e.'s is most reliable for data sets with many observations (Behari et al. 2016), we obtained similar results using Bayesian bootstrapping methods to estimate either the s.e.'s, or to sample directly from the distribution of pointwise  $\widehat{elpd}_{loo}$  differences. For our final analyses, we selected the model with the fewest parameters that also returned a pairwise difference in prediction accuracy that was not significantly different from the best-fitting model ( $\text{Pr} > 0.05$ ). All statistical analyses were performed in R v.3.2.2 (Team 2016a). All data and code necessary to reproduce the analyses are available at <https://github.com/colin-olito/Fertilization>.

## 4.4 Results

### 4.4.1 Estimating spawning durations

The mean duration of induced male spawning phenologies was  $352.2 \pm 20.0$  sec. (mean  $\pm$  s.e.). This spawning duration was longer than the time taken to release sperm in the *Slow* release strategy for Exp. 1 ( $\approx 4$  min), suggesting that our *Slow* release treatment in Exp. 2 was comparable to the duration of induced spawnings.

### 4.4.2 Flume experiments

The probability of successful fertilization increased with the amount of sperm released down the flume in Exp. 1 (Fig. 4.1;  $\beta_{Sperm} = 0.819$ , HPD interval = [0.736, 0.908]). The maximum fertilization success achieved was 0.87, and rates of abnormal cell cleavage indicative of polyspermy were very low for all runs (1 – 2%), suggesting that our models adequately estimate the probability of successful fertilization for these data, and more complex fertilization kinetics models are unnecessary. The most parsimonious model included only a single random intercepts term for experimental run ( $\mathbf{Z} = Run$ ; see Table 4.A1 in Appendix A: Model selection results for all model comparisons). The *Run* specific intercepts exhibited only moderate variation ( $\sigma_\gamma = 0.765$ ), indicating that the flume was generating repeatable results.

The most parsimonious model from the analysis of Exp. 2 included several interactions between experimental *Run* and ‘fixed’ effects ( $\mathbf{Z} = Run + Run \times Sperm_i + Run \times Rate + Run \times EggPos + Run \times Rate \times EggPos$ ; see Table 4.A2 in Appendix A: Model selection results for all model comparisons). We detected a strong  $Sperm_i \times Rate$  interaction, such that the probability of successful fertilization increased faster with the amount of sperm released for the *Fast* release strategy than the *Slow* release strategy (Table 4.1). We also detected a marginally significant difference in the slope for the 25 cm and 75 cm egg patches for the *Fast* release treatment, with fertilization

success in the distal egg patch (75 cm) increasing faster with the amount of sperm released (Table 4.1; see also Supplementary Figure 4.B1 in Appendix B: Supplementary figures).

From our Exp. 2 results, we calculated the per-gamete increase in the probability of successful fertilization for the *Fast* and *Slow* release strategies (Fig. 4.2). Per-gamete fertilization rate decreased dramatically with the total amount of sperm released for both strategies, but the decrease was slower for the *Fast* release rate strategy (Table 4.1). Simple contrasts between the *Fast* and *Slow* strategy prediction lines showed that when small amounts of sperm are released, the per-gamete fertilization rate is significantly higher for the *Slow* strategy than the *Fast* strategy (see Supplementary Figure 4.B2 in Appendix B: Supplementary figures). Conversely, the *Fast* release strategy achieves higher per-gamete fertilization rates when large amounts of sperm are released.

## 4.5 Discussion

Since the seminal work of Bateman (1948) and the development of SCT in the 1970's, observed patterns of male reproductive investment and allocation in diverse taxa have been interpreted almost exclusively as adaptive strategies under sperm competition (Parker et al. 1982; Parker 1982; Wedell et al. 2002). However, broadcast-spawning species have long presented a challenge to classic SCT predictions by exhibiting counter-intuitive male spawning strategies – specifically, slow sperm release rates and weak resource-dependent allocation to ejaculates, despite massive investment in gonad tissue (McEuan 1988; Marshall and Bolton 2007; Styan 2003; Olito et al. 2015). Although there is some evidence that these strategies can be adaptive in a sperm-competitive context (e.g., Bode and Marshall 2007; Olito et al. 2015; Olito 2016; Lotterhos and Levitan 2011), the potentially crucial role of natural selection from the external environment in shaping the evolution male broadcast spawning strategies has been almost entirely neglected (Marshall and Bolton 2007). Our experimental results using *G. caespitosa* suggest that observed male broadcast spawning strategies are expected to evolve in response to natural selection from the external environment regardless of sperm competition. Two main results stand out from our study which we discuss in detail below: (1) an interaction between the amount and rate at which sperm is released, and (2) a dramatic cost, in terms of per-gamete fertilization success, of releasing large ejaculates.

We found evidence that size- or allocation-dependent sperm release strategies may evolve if males are unable to facultatively adjust ejaculate size, or if they are constrained to participate in few spawning events. Our results indicate that males releasing small ejaculates will achieve higher fertilization success if they release sperm slowly, while males releasing large ejaculates will have greater fertilization success if they release sperm quickly. Although there is some evidence that individuals can facultatively adjust the rate of gamete release (Marshall et al. 2004), we are not aware of any definitive tests of whether male broadcast spawners adjust ejaculate sizes at spawning. Some broadcast spawners may participate in multiple spawning events, expending a fraction of their gametic resources in single events, but again, definitive data is lacking (e.g., Levitan 1988; McEuan 1988; Lotterhos and Levitan 2011). It is worth noting, however, that participation in multiple spawning events requires that females mirror male spawning strategies, a situation that may not always occur, and environmental conditions may constrain spawning to single events (Olito et al. 2015; Olito 2016). It has been demonstrated in two species

of scallop that males of different sizes release similar amounts of sperm, despite the fact that larger males could have released more (Styan 2003). However, these spawnings were chemically induced, and so provide only indirect evidence for facultative adjustment of ejaculate size by large males. Given its central importance in determining optimal male mating strategies, pinning down the extent to which broadcasters facultatively adjust their ejaculate size represents a fundamental issue for future work.

Although there appears to be some potential for the evolution of size- or allocation-dependent sperm release strategies, we also found a massive per-gamete cost associated with releasing large ejaculates. The more sperm males release, the more is wasted during the process of sperm dispersal. Moreover, this pattern was not driven by a saturation effect – none of our experimental runs resulted in complete fertilization, and rates of polyspermy appear to have remained low. While the per-gamete fertilization rate should collapse under conditions resulting in very low overall fertilization success (e.g., very low or very high sperm:egg ratios), our results suggest that for populations with moderate sex ratios ( $\approx 2 : 1$  in our experiments), and intermediate fertilization rates, it should remain high. Taken together, these results suggests that if male broadcast spawners can facultatively adjust their size of their ejaculates, or if they can release sperm over multiple spawning events, the optimal spawning strategy will generally be to release as little sperm as possible, as slowly as possible, during the window of female spawning. Crucially, broadcast spawners incur this cost whether sperm competition is present or not. Moreover, our results suggest that the strength of selection from the external environment during sperm dispersal is likely to be strong, even under conditions that are favourable for fertilization (e.g., laminar, unidirectional flow), while selection from sperm competition is strongly density-dependent (Parker 1982; Levitan 1998; Bode and Marshall 2007). Sperm competition may exaggerate selection for small ejaculates and slow sperm release rates, particularly at high population densities, but selection during sperm dispersal is likely the more consistent force driving the evolution of reproductive phenotypes in broadcast spawners.

Our findings also have interesting implications for the evolution of sequential hermaphroditism in aquatic animals. Protandry, where individuals change their phenotypic and/or functional gender from male to female, is expected to evolve when female fecundity increases faster with size than male fecundity (Ghiselin 1969; Warner 1975, 1988; Munday et al. 2006). This is because individuals can achieve higher life-time fitness by strategically expressing the gender with the highest reproductive success given their body size – small individuals achieve higher reproductive success as males, while larger individuals do so as females. Our results suggest that the dramatic cost of releasing large ejaculates may constrain male size-fecundity curves to be quite shallow in broadcast spawning species, making it more likely that the slope of the female-fecundity curve is steeper than the male. Moreover, size-fecundity curves may be especially constrained if males are unable to facultatively adjust ejaculate size, or if they are constrained to few mating events by environmental conditions or female spawning phenologies (Olito et al. 2015; Olito 2016). Hence, we would predict an evolutionary association between broadcast spawning and protandry among aquatic hermaphrodites. Empirical patterns of reproductive mode and mating system appear consistent with this prediction. Protandry has been documented, and appears common, among several large groups of broadcasting or spermcasting hermaphroditic marine invertebrates including gastropods (e.g., Patelidae, Quesne and Hawkins 2006; Calyptraeidae, Coe 1936; corals, Loya and Sakai 2008, sea stars, and sea cucumbers, Sewell 1994, and references therein). A formal

test of this hypothesis using modern phylogenetic comparative methods would be very interesting.

## **4.6 Acknowledgements**

C.O. thanks C. Venables and C.Y. Chang for fruitful discussions and feedback, and the MEEG lab for assistance with the flume. C.O. and D.J.M. designed the study, C.O. performed the experiments and analyses, and wrote the manuscript with assistance from D.J.M. This work was funded by a Monash University Dean's International Postgraduate Student Scholarship to C.O., an Australian Research Council grants to D.J.M, and by the Monash University Centre for Geometric Biology.

## 4.7 Tables

TABLE 4.1: Parameter estimates of interest and *a priori* contrasts for Exp. 2

Parameter	mean	95% H.P.D. interval	95% Credible Interval
$\beta_{Sperm_i:Slow}$	0.705	(0.626, 0.781)	(0.623, 0.779)
$\beta_{Sperm_i:Fast}$	0.609	(0.518, 0.699)	(0.515, 0.698)
$\beta_{Sperm_i:Fast:25cm}$	0.690	(0.612, 0.774)	(0.604, 0.767)
$\beta_{Sperm_i:Fast:75cm}$	0.720	(0.634, 0.793)	(0.638, 0.792)
$\beta_{Sperm_i:Slow:25cm}$	0.617	(0.530, 0.710)	(0.525, 0.705)
$\beta_{Sperm_i:Slow:75cm}$	0.600	(0.502, 0.700)	(0.496, 0.695)
<i>a priori</i> contrast	mean	95% H.P.D. interval	Pr > 0
$\beta_{Sperm_i:Fast} - \beta_{Sperm_i:Slow}$	0.096	(0.059, 0.133)	<b>1.000</b>
$\beta_{Sperm_i:Fast:25cm} - \beta_{Sperm_i:Fast:75cm}$	-0.029	(-0.067, 0.004)	0.056 <sup>†</sup>
$\beta_{Sperm_i:Slow:25cm} - \beta_{Sperm_i:Slow:75cm}$	0.017	(0.034, 0.076)	0.743
$\beta_{Sperm_i:Fast:25cm} - \beta_{Sperm_i:Slow:25cm}$	0.073	(0.035, 0.106)	<b>1.000</b>
$\beta_{Sperm_i:Fast:75cm} - \beta_{Sperm_i:Slow:75cm}$	0.119	(0.050, 0.192)	<b>1.000</b>

## 4.8 Figures

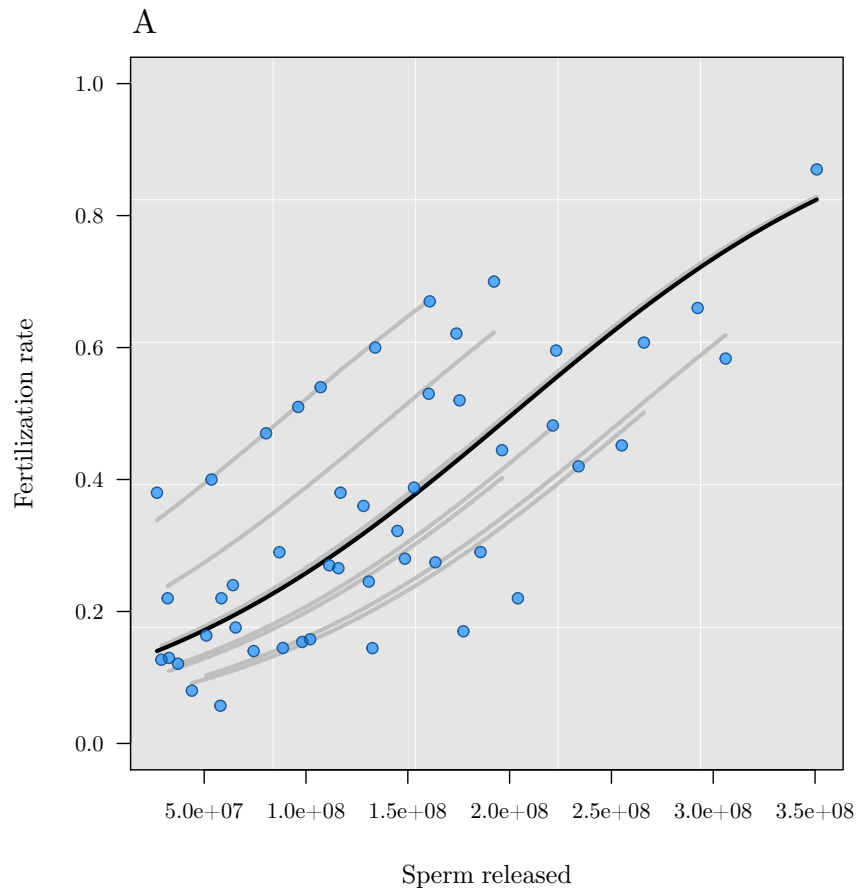


FIGURE 4.1: Fertilization success as a function of the number of sperm released in Exp. 1. Results are shown for the most parsimonious model, which included random intercepts for each experimental run ( $\mathbf{m2} : \mathbf{Z} = \text{Run}$ ), which exhibited only moderate variation ( $\sigma_\gamma = 0.765$ ). Predicted lines are shown for each experimental run (grey lines) in addition to the overall regression (black line). Note that the increase in fertilization success is monotonic, with a maximum of 0.87, and low rates of abnormal cell cleavage were observed for all runs (1 – 2%), indicating that more models adequately approximate the probability of successful fertilization for these data. Credibility intervals have been omitted for clarity.

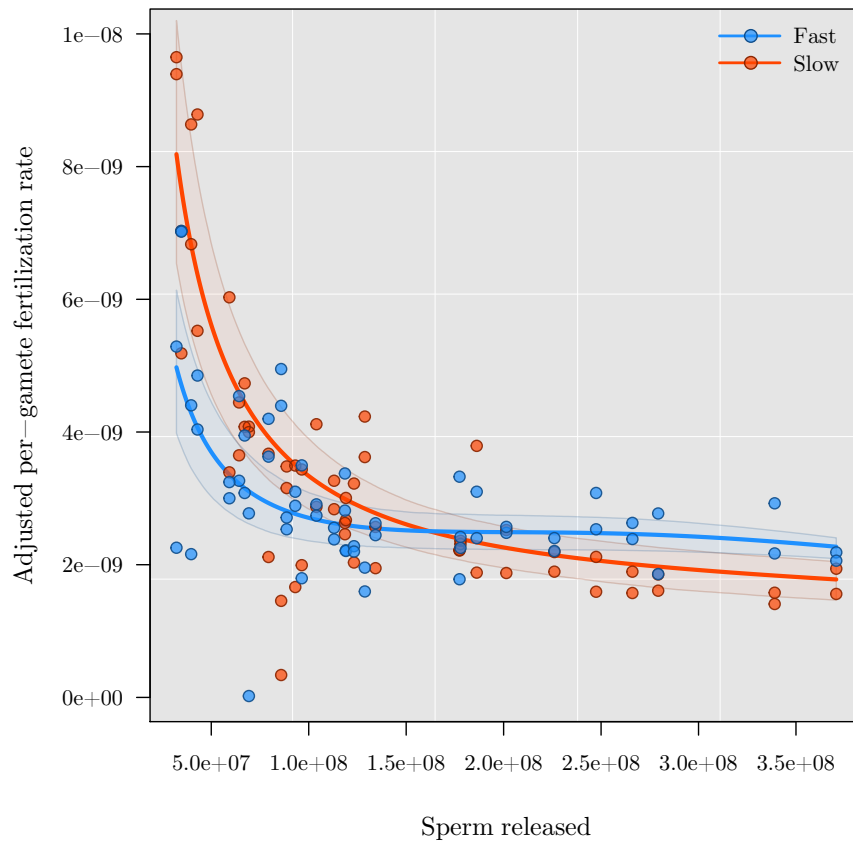


FIGURE 4.2: Results from Exp. 2 showing adjusted per-gamete fertilization success as a function of the amount of sperm released for the Fast and Slow release treatments. Partial regression lines are plotted for the Fast and Slow release treatments (solid lines) with 80% credibility intervals (transparent bands) for the most parsimonious model; data points are adjusted to account for among-run variation (see [Methods](#)).

## 4.9 Appendix A: Model selection results

Model selection for the analysis of Exp. 1 consisted of a comparison between 3 candidate models with the following ‘random effect’  $\mathbf{Z}$  matrices:

$$\mathbf{Z}_{\mathbf{m1}} = \text{Run} + \text{Run} \times \text{Sperm}_i \quad (4.A1)$$

$$\mathbf{Z}_{\mathbf{m2}} = \text{Run} \quad (4.A2)$$

$$\mathbf{Z}_{\mathbf{m3}} = N/A \quad (4.A3)$$

which yielded the following results:

TABLE 4.A1: Model Selection for Exp. 1 analysis

Comparison	$\Delta \widehat{elpd}_{loo}$	<i>s.e.</i> ( $\Delta \widehat{elpd}_{loo}$ )	$\Pr(\Delta \widehat{elpd}_{loo} > 0)$
m1 v. <b>m2</b>	1.485	6.655	0.823
m1 v. m3	134.224	30.675	0.00
m2 v. m3	132.739	31.572	0.00

Model selection for the analysis of Exp. 2 consisted of a comparison between 25 candidate models (m1 through m25, in order of decreasing  $\mathbf{Z}$  matrix complexity; see Supplementary R code for specification of all ‘random effect’  $\mathbf{Z}$  matrices). Here, we present each of the pairwise comparisons with the best-fitting model (according to  $\widehat{elpd}_{100}$ ), and all other candidate models. The most parsimonious model, the one with the fewest terms whose fit to the data is not significantly different from the best-fitting model, is highlighted in bold.

TABLE 4.A2: Model Selection results for Exp. 2

Comparison	$\Delta \widehat{elpd}_{100}$	s.e. ( $\Delta \widehat{elpd}_{100}$ )	$\Pr(\Delta \widehat{elpd}_{100} > 0)$
m2 v. m1	0.605	2.256	0.789
m2 v. m3	5.643	4.260	0.185
m2 v. <b>m12</b>	6.045	10.612	<b>0.569</b>
m2 v. m6	6.518	7.802	0.404
m2 v. m4	7.750	4.292	0.071
m2 v. m9	8.692	7.579	0.251
m2 v. m7	9.455	7.871	0.230
m2 v. m10 <sup>†</sup>	15.727	8.257	0.057
m2 v. m17	36.786	14.180	0.009
m2 v. m11	38.400	12.588	0.002
m2 v. m5	38.548	11.773	0.001
m2 v. m14	38.800	12.712	0.002
m2 v. m8	42.059	11.996	0.000
m2 v. m13	42.276	12.818	0.001
m2 v. m16	43.129	13.303	0.001
m2 v. m19	51.253	20.688	0.013
m2 v. m18	68.478	23.460	0.004
m2 v. m21	78.187	27.890	0.005
m2 v. m15	99.122	23.416	0.000
m2 v. m20	118.226	26.488	0.000
m2 v. m22	121.954	28.257	0.000
m2 v. m23	139.700	28.561	0.000
m2 v. m24	140.445	29.481	0.000
m2 v. m25	322.533	68.962	0.000

Note: Bold indicates the final model selected, while daggers indicate other competitive candidate models with a similar fit to the data, but more terms than the final model.

## 4.10 Appendix B: Supplementary figures

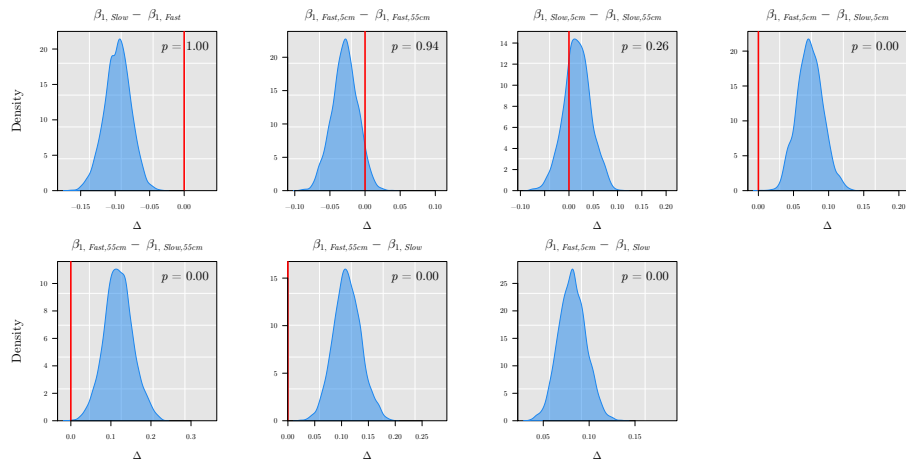


FIGURE 4.B1: Density plots showing the posterior distributions for *a priori* contrasts on the regression coefficients from the analysis of Exp. 2

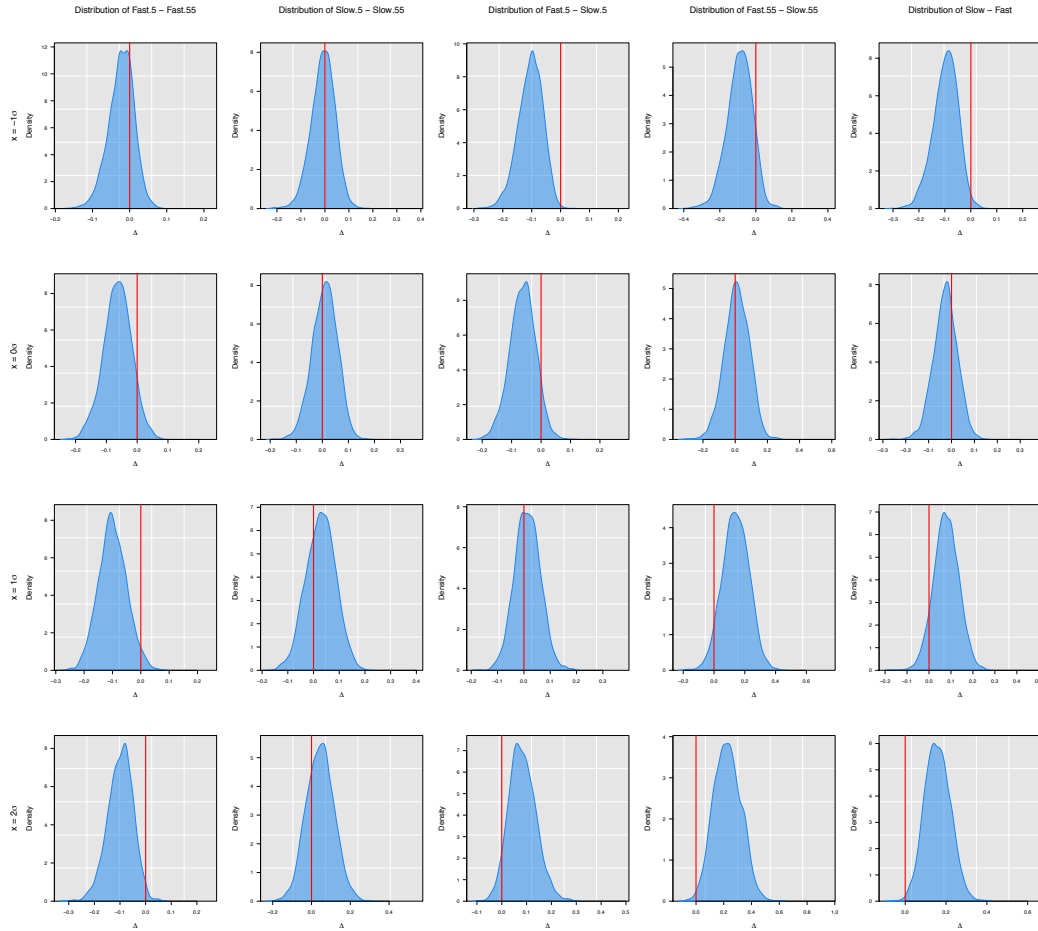


FIGURE 4.B2: Density plots showing the posterior distributions for simple contrasts on the predicted difference in predicted fertilization success for the *Fast* and *Slow* release strategies at different values of the  $Sperm_i$ . Contrasts are calculated at values of  $Sperm_i$  corresponding to  $-1\sigma$ , the mean (0),  $+1\sigma$ , and  $-2\sigma$ , where  $\sigma$  is the empirical standard deviation of the Z-transformed  $Sperm_i$  of the empirical distribution of the number of sperm released in Exp. 2 ( $8.9 \times 10^7$ ).



## Chapter 5

# Consequences of genetic linkage for the maintenance of sexually antagonistic polymorphism in hermaphrodites<sup>1</sup>

### 5.1 Abstract

When selection differs between males and females, pleiotropic effects among genes expressed by both sexes can result in sexually antagonistic selection (SA), where beneficial alleles for one sex are deleterious for the other. For hermaphrodites, alleles with opposing fitness effects through each sex function represent analogous genetic constraints on fitness. Recent theory based on single-locus models predicts that the maintenance of SA genetic variation should be greatly reduced in partially selfing populations. However, selfing also reduces the effective rate of recombination, which should facilitate selection on linked allelic combinations and expand opportunities for balancing selection in a multi-locus context. Here I develop a two-locus model of SA selection for simultaneous hermaphrodites, and explore the joint influence of linkage, self-fertilization, and dominance on the maintenance of SA polymorphism. I find that the effective reduction in recombination caused by selfing significantly expands the parameter space where SA polymorphism can be maintained relative to single-locus models. In particular, linkage facilitates the invasion of male-beneficial alleles, partially compensating for the "female-bias" in the net direction of selection created by selfing. I discuss the implications of accounting for linkage among SA loci for the maintenance of SA genetic variation and mixed mating systems in hermaphrodites.

---

<sup>1</sup>This chapter has been published as: Olito, C. 2016. Consequences of genetic linkage for the maintenance of sexually antagonistic polymorphism in hermaphrodites. *Evolution* 71:458–464.

## 5.2 Introduction

Due to fundamental differences in their reproductive biology, males and females rarely share the same optimal phenotype (Parker 1979; Kokko and Jennions 2008). When phenotypic optima differ between males and females, pleiotropic effects among genes expressed by both sexes can result in sexually antagonistic selection (SA hereafter), where beneficial alleles for one sex have deleterious fitness effects in the other (Kidwell et al. 1977; Rice 1992; Connallon and Clark 2012). SA alleles have been shown to play an important role in the maintenance of genetic variation in fitness, the evolution of reproductive and life-history traits, and genome evolution in a variety of theoretical and empirical contexts (Barson et al. 2015; Bonduriansky and Chenoweth 2009; Cox and Calsbeek 2010; Connallon and Clark 2012; Fry 2010; Prout 2000; Rice 1992; Rice and Chippindale 2001).

The existence of physically separate sexes makes the relevance of SA selection to dioecious species intuitive, and this is reflected in the traditional emphasis on SA polymorphism in this group (e.g. Kidwell et al. 1977; Rice 1992; Prout 2000; Connallon and Clark 2012). However, alleles with opposing fitness effects through male and female sex functions represent analogous genetic constraints on fitness for hermaphrodites (Abbott 2011; Jordan and Connallon 2014; Tazzyman and Abbott 2015). For hermaphroditic individuals, both the male and female sex functions must be accommodated by a single phenotype, and there is ample scope for traits with a shared genetic basis to constrain fitness through each sex function (Abbott 2011; Barrett 2002; Conner 2006; Sicard and Lenhard 2011). Furthermore, fitness trade-offs between sex functions, and thus SA alleles, can have diverse consequences for the evolution of reproductive traits (e.g. floral and inflorescence morphology) as well as sexual and mating systems in hermaphrodites (Lloyd and Webb 1986; Webb and Lloyd 1986; Barrett 2002; Abbott 2011; Charlesworth and Charlesworth, 1978a; Harder and Barrett 2006; Goodwillie et al. 2005).

The fate of SA alleles in hermaphrodites is complicated by the fact that individuals may pass on genes to subsequent generations through a combination of outcrossing and self-fertilization (Goodwillie et al. 2005; Jarne and Auld 2006; Igc and Kohn 2005; Jordan and Connallon 2014). Self-fertilization has several important theoretical consequences for the maintenance of SA genetic variation (Jordan and Connallon 2014; Kimura and Ohta 1971). Selfing diminishes the opportunity for balancing selection to maintain SA polymorphism, and thereby reduces the sensitivity of SA polymorphism to dominance (Jordan and Connallon 2014; Tazzyman and Abbott 2015). If SA alleles influence gamete production and/or gamete quality or performance, selfing also creates a "female-bias" in the net direction of selection because there is reduced opportunity for selection to act via the male sex function (Charlesworth and Charlesworth 1978a; Jordan and Connallon 2014; but see Tazzyman and Abbott 2015 for alternative assumptions regarding selection on selfed gametes). This skews the parameter space where SA polymorphism can be maintained towards female-beneficial alleles (Jordan and Connallon 2014).

Self-fertilization carries with it a variety of other genomic consequences for hermaphrodites, including a reduction in the effective rate of recombination among neighboring loci (reviewed in Wright et al. 2008). The effect of selfing on effective recombination is of particular interest because this should drive selection on linked allelic combinations, potentially preserving polymorphisms that would otherwise experience purifying selection at a single locus (Fisher 1930). For dioecious species, tight linkage between SA loci is predicted to expand the parameter space where SA polymorphism is maintained (Patten et al. 2010). Thus, for hermaphrodites there is

the potential for reduced recombination to compensate for the loss in SA polymorphism due to increased selfing. However, the conditions under which each of these two countervailing effects of self-fertilization will be more influential in maintaining SA polymorphism have yet to be explored.

Here I use a two-locus model of SA selection with partial selfing to investigate the joint influence of linkage, self-fertilization, and dominance on the maintenance of SA polymorphism in hermaphroditic species. In the two-locus context, reduced effective recombination caused by selfing significantly increases the parameter space where balancing selection is predicted to maintain SA polymorphism relative to single-locus models. In particular, linkage expands the conditions where male-beneficial alleles are able to invade, partially compensating for the "female-bias" in selection introduced by selfing.

### 5.3 Model

Consider a genetic system involving two diallelic autosomal loci **A** (with alleles  $A$ ,  $a$ ) and **B** (with alleles  $B$ ,  $b$ ), that recombine at a rate  $r$  in a large population of simultaneous hermaphrodites. The rate of self-fertilization ( $C$ ) in the population is independent of the genotype at the loci in question (a 'fixed' selfing model *sensu* Holden 1979; Caballero and Hill 1992; Jordan and Connallon 2014). Generations are assumed to be discrete and non-overlapping, with selection occurring on diploid adults before fertilization. Let  $x_i$  and  $y_i$  denote the frequencies of the four possible haplotypes  $[AB, Ab, aB, ab]$  among female and male gametes respectively. Both loci are under sexually antagonistic selection such that  $A$  and  $B$  represent male-beneficial alleles, while  $a$  and  $b$  represent female-beneficial alleles (Kidwell et al. 1977). The fitness of offspring formed by the union of the  $i$ th female and  $j$ th male gametic haplotypes,  $w_{k,ij}$  (where  $k \in [m, f]$ ), is assumed to equal the product of the fitnesses at **A** and **B** (Table 5.1; parameterization follows Patten et al. 2010). Following convention for SA models, sex-specific selection coefficients are constrained to be  $0 < s_k < 1$  (e.g. Kidwell et al. 1977).

The evolutionary trajectory of genotype frequencies in this scenario is described by a system of ten recursion equations (Holden 1979; Jordan and Connallon 2014). However, it is possible to approximate the evolutionary trajectories of haplotypes in this system under weak selection (See [Appendix A: Development of recursions, quasi-equilibrium approx](#) in the Supplementary Information). For partially selfing populations under weak selection, the rate of allele frequency change due to selection should be slow relative to the rate at which genotypes approach equilibrium under non-random mating (Nagylaki 1997). Under this assumption, it may be appropriate to use a separation of timescales (Otto and Day 2007), and calculate the quasi-equilibrium (QE) genotypic frequencies in the absence of selection. The genotypic recursions for allele frequency change across generations can then be approximated by substituting into them the QE frequencies, yielding a reduced system of four haplotype recursions.

Using this approach, I model the evolution of the four-haplotype system  $q_i = [AB, Ab, aB, ab]$ , where the QE adult genotypic frequencies are denoted by  $\phi_{ij}$ . The recursions giving the haplotype frequencies in the next generation are then

$$\begin{aligned}
q'_1 &\approx (1 - C) \frac{(x_1 + y_1)}{2} + C \left( \frac{x_1 - r(\phi_{14} - \phi_{23})}{2\bar{w}_f} \right) \\
q'_2 &\approx (1 - C) \frac{(x_2 + y_2)}{2} + C \left( \frac{x_2 + r(\phi_{14} - \phi_{23})}{2\bar{w}_f} \right) \\
q'_3 &\approx (1 - C) \frac{(x_3 + y_3)}{2} + C \left( \frac{x_3 + r(\phi_{14} - \phi_{23})}{2\bar{w}_f} \right) \\
q'_4 &\approx (1 - C) \frac{(x_4 + y_4)}{2} + C \left( \frac{x_4 - r(\phi_{14} - \phi_{23})}{2\bar{w}_f} \right), \tag{5.1}
\end{aligned}$$

where  $x_i$  and  $y_i$  are functions  $f(C, s_k, h_k, \phi_{ij})$  describing the haplotype frequencies in male and female gametes, and  $\bar{w}_f$  is the population average fitness through female function (see [Appendix A: Development of recursions, quasi-equilibrium approx](#) in the Supplementary Information for a full development of the recursions). The QE haplotype recursions approximated deterministic simulations of the genotypic recursions very well, even under strong selection (Figs. 5.S1 and 5.S2; the full set of exact recursions can be found in [Appendix A: Development of recursions, quasi-equilibrium approx](#) in the Supporting Information); I therefore focus the analysis on the analytic QE results.

To identify the parameter conditions under which balancing selection is predicted to maintain SA polymorphism, I evaluate the stability of the system of haplotype recursions, Eq(5.1), for populations initially fixed for male-beneficial or female-beneficial alleles (i.e. stability was assessed at the boundary haplotype frequencies  $[AB] = 1$  and  $[ab] = 1$ ). For these boundary equilibria, one minus the leading eigenvalue of the Jacobian matrix,  $1 - \lambda_L$ , approximates the rate of change of the frequencies of rare haplotypes, and therefore whether new mutations will be able to invade (Otto and Day 2007). Balancing selection is predicted to maintain SA polymorphism when  $\lambda_L > 1$  for both boundary equilibria (Prout 1968). Three candidate leading eigenvalues emerge from the analysis (See [Appendix C: Computer Code](#) in the Supplementary Information). The first two describe invasion at each locus individually, and are identical functions of the sex-specific selection parameters ( $s_k, h_k$ ) and the selfing rate ( $C$ ). Balancing selection at both loci occurs whenever single-locus criteria for balancing selection are met because the selection parameters are identical for both loci (if invasion can occur at one locus, it can also occur at the other). If the two SA loci are physically linked, the conditions for balancing selection differ from the single-locus expectation. This condition is described by the third candidate leading eigenvalue, which involves the recombination rate,  $r$ , in addition to  $s_k, h_k$ , and  $C$ .

I focus the analysis on representative, and biologically plausible, dominance scenarios that have been recently explored in the single-locus context (Kidwell et al. 1977; Fry 2010; Prout 2000; Jordan and Connallon 2014). These correspond to: (1) additive fitness effects ( $h_f = h_m = 1/2$ ), as is commonly observed for small to intermediate effect alleles (Agrawal and Whitlock 2011); and (2) partially recessive fitness effects yielding a "dominance reversal" ( $h_f = h_m = 1/4$ ), which are commonly predicted by a variety of fitness landscape models (Manna et al. 2011; Connallon and Clark, 2014a), and are predicted to evolve under some conditions for SA alleles (Spencer and Priest 2016).

### 5.3.1 Data availability

A full development of all models can be found in Appendix [Appendix A: Development of recursions](#), and all code necessary to reproduce the analyses are available at <https://github.com/colin-olito/twoLocusPartSelf>, or from the author upon request.

## 5.4 Results

Consideration of invasion at a single locus provides a useful baseline for comparison with the two-locus case. Analysis of the first candidate leading eigenvalue yields the general invasion criteria at a single locus, where balancing selection requires that

$$\frac{s_m(C-1)(2h_m(C-1)-C)}{s_m(C-1)(2h_m(C-1)-C) + (C+1)(2-C+2h_f(C-1))} < s_f < \frac{s_m(1-C)(2-C+2h_m(C-1))}{(C+1)(2h_f(C-1)-C)(s_m-1)}. \quad (5.2)$$

Under additive fitness effects ( $h_f = h_m = 1/2$ ), Eq(5.2) reduces to the single-locus invasion criteria given by Jordan and Connallon (2014); and reduces further under obligate outcrossing ( $C = 0$ ) to the classic dioecious result of  $s_m/(1+s_m) < s_f < s_m/(1-s_m)$  (Tazzyman and Abbott 2015; Patten et al. 2010; Kidwell et al. 1977). The corresponding funnel-shaped parameter space where balancing selection at a single locus is predicted to maintain SA polymorphism is shown in Fig. 5.1 by the shaded regions bounded by black solid lines.

Increased self-fertilization broadens the scope for linkage to maintain SA polymorphism that would otherwise be lost in a single-locus model. Analysis of the third candidate leading eigenvalue yields invasion criteria involving both loci that are more complex than the single-locus case. However, under the simplifying assumptions of complete linkage ( $r = 0$ ) and obligate outcrossing ( $C = 0$ ), the third candidate leading eigenvalue yields invasion criteria which are algebraically equivalent to the two-locus dioecious case (Eq (11) in Patten et al. 2010; see [Appendix C: Computer Code](#) in the Supplementary Information). As in Patten et al. (2010), under perfect linkage ( $r = 0$ ), the two-locus invasion criteria expands the parameter space conducive to balancing selection, describing a funnel-shaped region that subsumes the region described by the single-locus criteria. With weaker linkage ( $0 \leq r \leq 0.5$ ), stronger selection is required for the two-locus invasion criteria to expand the parameter space conducive to balancing selection (Fig. 5.1, greyscale lines). This is most restrictive under obligate outcrossing, where linkage must be tight ( $r < 0.2$  for additive effects,  $r < 0.1$  for dominance reversal), for the two-locus invasion criteria to increase SA polymorphism beyond the single-locus case (Fig. 5.1A,D; Patten et al. 2010). If selection on individual SA loci is weak ( $s_f, s_m < 0.1$ ), tight linkage is required to significantly expand the parameter space where balancing selection is predicted beyond that of single-locus models (Figs. 5.S3, 5.S4 in [Appendix B: Supplementary figures](#) in the Supplementary Information). However, the magnitude of the increase is still substantial under tight linkage, particularly for additive fitness effects.

Increased selfing has two important consequences in the two-locus context. As predicted for the single-locus case, selfing biases the net direction of selection towards female interests, reducing the opportunity for male-beneficial alleles to invade at a single locus (Fig. 5.1B,C,E,F; Charlesworth and Charlesworth 1978a; Jordan and Connallon 2014; but see Tazzyman and Abbott 2015). However, the concomitant decrease in effective recombination among double heterozygotes partially compensates for this "female-bias" in selection in several ways. Overall, linkage increases the effective strength of selection at both loci, which is more permissive of balancing selection (Patten et al. 2010). Reduced recombination also slows the break-up of haplotypes pairing male-beneficial with male-beneficial (and female-beneficial with female-beneficial) alleles at both loci, increasing the likelihood that male-beneficial alleles at each locus are paternally inherited (and female-beneficial alleles are maternally inherited) (Patten et al. 2010; Úbeda et al. 2010). With higher selfing, this effectively shelters male-beneficial alleles from increased selection through the female sex function. The net effect is to expand the parameter space where balancing selection is predicted to maintain SA polymorphism, particularly for male-beneficial alleles (Fig. 5.1, upper greyscale lines). The effect of reduced recombination is strongest at higher selfing rates ( $C > 0.5$ ), where interaction between SA loci expands the parameter space where male-beneficial alleles can invade beyond the single-locus case, even under free recombination (Fig. 5.1B-C,E-F, Fig. 5.2B,D).

Under additive fitness effects, the increase in SA polymorphism due to linkage can offset the loss in parameter space attributable to invasion at a single locus up to a selfing rate of about  $C = 0.5$  (Fig. 5.2A). At higher selfing rates ( $C > 0.5$ ), the total parameter space where balancing selection can occur declines, but the relative increase in SA polymorphism predicted by the two-locus model relative to the single-locus case becomes increasingly pronounced, even under free recombination (Fig. 5.2A,B). Under dominance reversal conditions ( $h_f, h_m < 1/2$ ) the sex-specific fitness costs of SA alleles are partially masked, and balancing selection can maintain SA polymorphism over a broader range of parameter conditions due to net overdominance in fitness (Connallon and Clark 2012, 2014a). As a consequence, the effect of linkage is somewhat dampened, and increased selfing always results in a decrease in the total parameter space where SA polymorphism is predicted (Fig. 5.2C). However, the relative increase in the two-locus relative to the single-locus case remains for higher selfing rates ( $C > 0.5$ ), even under free recombination (Fig. 5.2D).

## 5.5 Discussion

Accounting for linkage between SA loci yields several theoretical insights regarding the maintenance of SA polymorphism in hermaphroditic organisms. Provided that either linkage is tight or selection is strong, the reduction in the effective recombination rate due to selfing significantly expands the parameter space where balancing selection is predicted to maintain SA polymorphism beyond that of single-locus models (doubling the parameter space under some conditions). When the sex-specific fitness costs of SA alleles are partially recessive, net overdominance of heterozygotes across both sex functions allows polymorphism to be maintained over a broader range of parameter space than when fitness costs are additive. This alters relative importance of recombination and net overdominance as proximal mechanisms underlying balancing selection at multiple SA loci. However, this does not dramatically influence the role of linkage between SA loci in expanding SA polymorphism relative to single-locus models. Thus, although balancing selection at SA loci

is least likely in highly selfing species, it may still provide a plausible mechanism, along with recurrent mutation (Jordan and Connallon 2014), for the maintenance of genetic variation at linked SA loci in populations with intermediate to high selfing rates.

The joint influence of linkage and self-fertilization on SA polymorphism may have interesting implications for the genomic location of SA loci in hermaphrodites. On one hand, polymorphic SA genes are predicted to be more tightly clustered in the genome than expected at random because linkage facilitates SA polymorphism (Patten et al. 2010; Jordan and Charlesworth 2011). The current results predict that the effect of linkage on the maintenance of SA polymorphism should be stronger in partially selfing species relative to obligately outcrossing ones. This could facilitate increased clustering of polymorphic SA genes in the genomes of partial selfers relative to outcrossers. On the other hand, the reduction in effective rates of recombination due to selfing may have the opposite effect, where interactions between more distant loci are increasingly able to facilitate balancing selection on SA alleles in selfing species. A comparison of the genomic location of SA loci in species with varying rates of self-fertilization would be an interesting direction for future empirical work, particularly given the past emphasis on dioecious species (Bonduriansky and Chenoweth 2009; Abbott 2011).

As the frequency of self-fertilization increases, linkage among SA loci compensates for the increasing "female-bias" in selection and associated decrease in SA polymorphism predicted by single-locus models (Charlesworth and Charlesworth 1978a; Jordan and Connallon 2014; but see discussion of model assumptions below). Compensation for this female bias occurs primarily through an expansion of the parameter space where male-beneficial alleles are able to invade. In this way, linkage among SA loci may have bearing on the prevalence of mixed mating systems. Although many hermaphroditic plants and animals reproduce primarily through either outcrossing or selfing, a large fraction reproduce through a combination of the two (Jarne and Auld 2006; Goodwillie et al. 2005; Iqbal and Kohn 2005). Various theoretical explanations have been proposed for mixed mating strategies, including (but not limited to) reproductive assurance (Lloyd 1979), purging of deleterious alleles and reduced inbreeding depression (Schemske and Lande 1985), reproductive compensation (Harder et al. 2007; Porcher and Lande 2005), and frequency dependence (Holsinger 1991) (reviewed in Goodwillie et al. 2005; Harder and Barrett 2006). The female-bias in selection caused by increased selfing is consistent with the evolution of "selfing syndromes" (Sicard and Lenhard 2011; Jordan and Connallon 2014). However, the concomitant increase in the parameter space where male-beneficial alleles can invade relative to the single-locus case provides an additional mechanism for the persistence of traits promoting male gamete dispersal and performance in partially selfing populations, provided these traits are under SA selection (Barrett 2002; Goodwillie et al. 2005; Harder and Barrett 2006). Given that change in SA allele frequencies is often predicted to be slow and dominated by drift (Connallon and Clark 2011, 2012, 2014a), the loss of male-beneficial alleles may also be slow and stochastic in partially selfing species with linked SA loci, regardless of whether mixed mating is an evolutionary stable strategy.

It should be noted that the increased invasion of male-beneficial alleles predicted by this model is sensitive to the assumption that selection on SA alleles influences the performance of selfed female gametes (Tazzyman and Abbott 2015). The appropriateness of this assumption depends on whether SA fitness costs are incurred primarily through differential gamete production and/or quality and performance

of male and female gametes, or external factors such as conflict with mates (Tazzyman and Abbott 2015). In the absence of selection influencing the performance of selfed female gametes, there is no asymmetry in the net direction of selection, and thus no bias towards the increased invasion of male-beneficial alleles. The scope for linkage to increase SA polymorphism beyond single-locus predictions is also greatly reduced when selection does not influence the performance of selfed gametes (no expansion occurs beyond  $r \approx 1/4$ , even under strong selfing and additive fitness effects; [Appendix C: Computer CodeC](#) in the Supplementary Information). Thus, the mechanisms underlying SA fitness costs can be very important in determining the effect of linkage on the maintenance of SA polymorphism in hermaphrodites.

## 5.6 Acknowledgments

The author thanks C. Venables, J. Cally, and T. Connallon for helpful discussions and feedback, and two anonymous reviewers for their very helpful comments. The idea for this study was conceived during discussion among Drs. Tim Connallon, Crispin Jordan, and Jessica K. Abbott, and the author gratefully acknowledges their encouragement to develop it. This work was funded by a Monash University Dean's International Postgraduate Student Scholarship, and by the Monash University Centre for Geometric Biology.

## 5.7 Tables

TABLE 5.1: Two-locus fitness expressions for the adult female sex function ( $w_{f,ij}$ ) and male sex function ( $w_{m,ij}$ ). Rows and columns indicate the haplotype inherited from mothers and fathers respectively.

Haplotype	$y_1 = AB$	$y_2 = Ab$	$y_3 = aB$	$y_4 = ab$
<b>Females</b>				
$x_1 = AB$	$(1 - s_f)^2$	$(1 - s_f)(1 - h_f s_f)$	$(1 - s_f)(1 - h_f s_f)$	$(1 - h_f s_f)^2$
$x_2 = Ab$	$(1 - s_f)(1 - h_f s_f)$	$(1 - s_f)$	$(1 - h_f s_f)^2$	$(1 - h_f s_f)$
$x_3 = aB$	$(1 - s_f)(1 - h_f s_f)$	$(1 - h_f s_f)^2$	$(1 - s_f)$	$(1 - h_f s_f)$
$x_4 = ab$	$(1 - h_f s_f)^2$	$(1 - h_f s_f)$	$(1 - h_f s_f)$	1
<b>Males</b>				
$x_1 = AB$	1	$(1 - h_m s_m)$	$(1 - h_m s_m)$	$(1 - h_m s_m)^2$
$x_2 = Ab$	$(1 - h_m s_m)$	$(1 - s_m)$	$(1 - h_m s_m)^2$	$(1 - s_m)(1 - h_m s_m)$
$x_3 = aB$	$(1 - h_m s_m)$	$(1 - h_m s_m)^2$	$(1 - s_m)$	$(1 - s_m)(1 - h_f s_f)$
$x_4 = ab$	$(1 - h_m s_m)^2$	$(1 - s_m)(1 - h_m s_m)$	$(1 - s_m)(1 - h_m s_m)$	$(1 - s_m)^2$

## 5.8 Figures

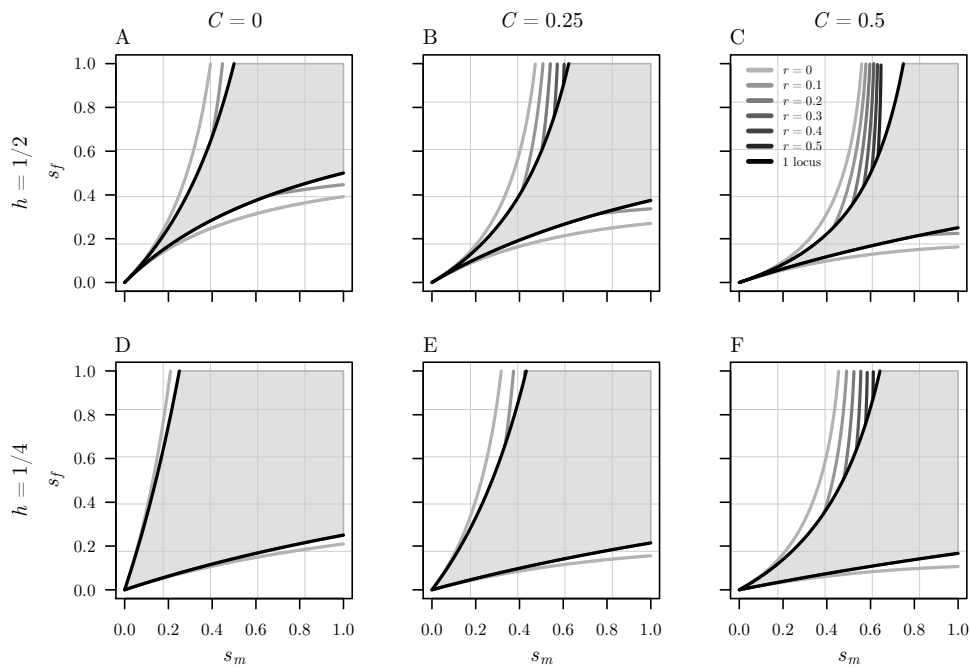


FIGURE 5.1: Self-fertilization increases the scope for genetic linkage to expand the parameter space where balancing selection can maintain SA polymorphism. Results are shown for the conditions of additive allelic effects ( $h_i = 1/2$ ; panels A–C), and dominance reversal ( $h_i = 1/4$ ; panels D–F). In each panel, the shaded region between the black lines indicates the region of sexually antagonistic polymorphism for the single locus case; greyscale lines indicate the thresholds for invasion for female-beneficial (lower lines) and male-beneficial (upper lines) alleles at different recombination rates for the two-locus model.

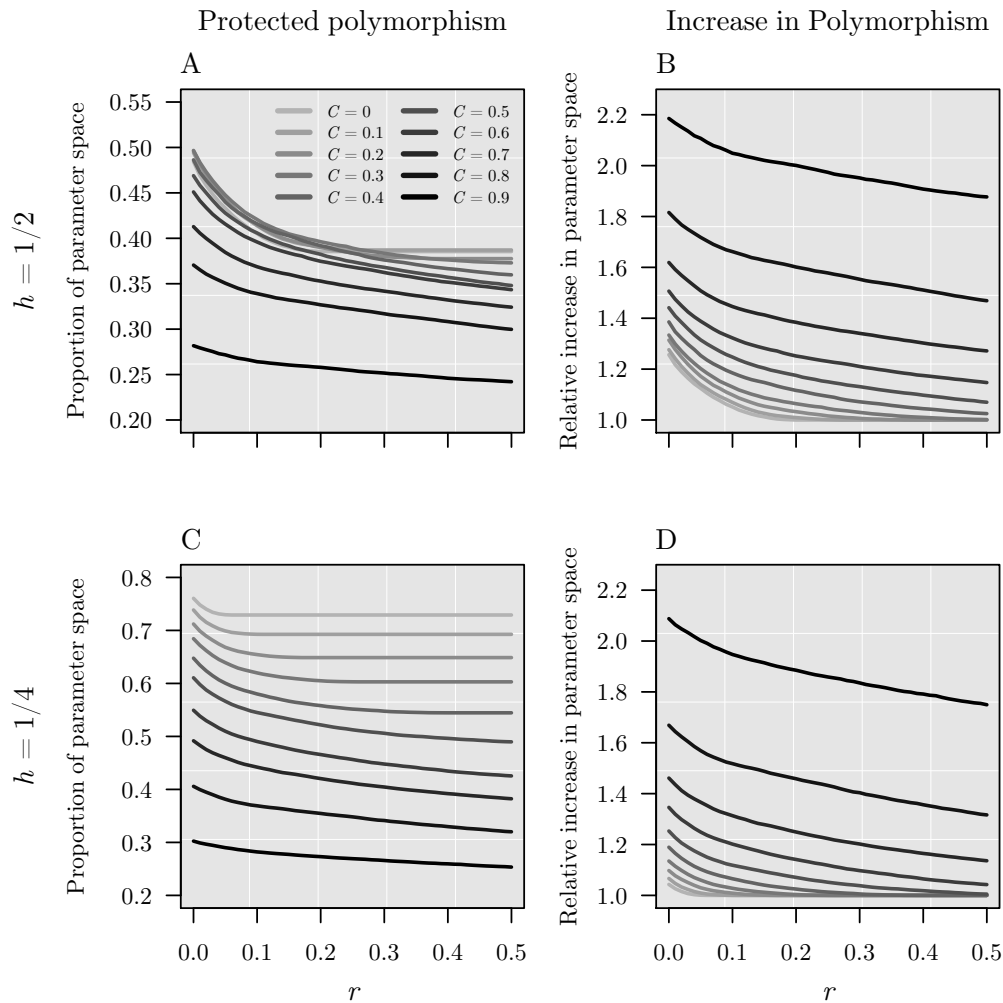


FIGURE 5.2: The proportion of parameter space where SA polymorphism is maintained declines with increased recombination and self-fertilization (panels A,C). The increase in SA polymorphism in the two-locus model relative to the single-locus case also declines with the recombination rate, but increases with the rate of self-fertilization (panels B,D). Results are shown for the conditions of additive allelic effects ( $h_i = 1/2$ ; panels A–B), and dominance reversal ( $h_i = 1/4$ ; panels C–D). Results were obtained by evaluating the leading eigenvalue of the Jacobian matrix of the haplotype recursions for populations initially fixed for the haplotypes  $[AB]$  and  $[ab]$  at 30,000 points distributed uniformly throughout parameter space defined by

$$s_m \times s_f.$$

## 5.9 Appendix A: Development of recursions, quasi-equilibrium approx.

### 5.9.1 Recursions

Consider the genetic system described in the main text. Adult genotypic frequencies formed by the union of the  $i$ th and  $j$ th haplotypes are denoted using  $F_{ij}$ , and the overall haplotype frequencies,  $q_i$  are

$$\begin{aligned} q_1 &= F_{11} + \frac{F_{12} + F_{13} + F_{14}}{2} \\ q_2 &= F_{22} + \frac{F_{12} + F_{23} + F_{24}}{2} \\ q_3 &= F_{33} + \frac{F_{13} + F_{23} + F_{34}}{2} \\ q_4 &= F_{44} + \frac{F_{14} + F_{24} + F_{34}}{2}. \end{aligned} \quad (5.A1)$$

Haplotype frequencies in female gametes are denoted  $x_1 = [AB]$ ,  $x_2 = [Ab]$ ,  $x_3 = [aB]$ , and  $x_4 = [ab]$ , and the corresponding frequencies in male gametes are denoted  $y_1, y_2, y_3$ , and  $y_4$ . The contribution of genotype  $ij$  to the production of offspring in the next generation is denoted by  $F_{ij}^f$ . Given these conditions, the recursion equations for the genotypic frequencies in the next generation are (Holden 1979; Jordan and Connallon 2014)

$$\begin{aligned} F'_{11} &= (1 - C)(x_1y_1) + C \left( F_{11}^f + \frac{F_{12}^f + F_{13}^f + F_{14}^f(1 - r)^2 + F_{23}^f r^2}{4} \right) \\ F'_{12} &= (1 - C)(x_1y_2 + x_2y_1) + C \left( \frac{F_{12}^f + F_{14}^f r(1 - r) + F_{23}^f r(1 - r)}{2} \right) \\ F'_{13} &= (1 - C)(x_1y_3 + x_3y_1) + C \left( \frac{F_{13}^f + F_{14}^f r(1 - r) + F_{23}^f r(1 - r)}{2} \right) \\ F'_{14} &= (1 - C)(x_1y_4 + x_4y_1) + C \left( \frac{F_{14}^f(1 - r)^2 + F_{23}^f r^2}{2} \right) \\ F'_{22} &= (1 - C)(x_2y_2) + C \left( F_{22}^f + \frac{F_{12}^f + F_{14}^f r^2 + F_{23}^f(1 - r)^2 + F_{24}^f}{4} \right) \\ F'_{23} &= (1 - C)(x_2y_3 + x_3y_2) + C \left( \frac{F_{14}^f r^2 + F_{23}^f(1 - r)^2}{2} \right) \\ F'_{24} &= (1 - C)(x_2y_4 + x_4y_2) + C \left( \frac{F_{24}^f + F_{14}^f r(1 - r) + F_{23}^f r(1 - r)}{2} \right) \\ F'_{33} &= (1 - C)(x_3y_3) + C \left( F_{33}^f + \frac{F_{13}^f + F_{14}^f r^2 + F_{23}^f(1 - r)^2 + F_{34}^f}{4} \right) \\ F'_{34} &= (1 - C)(x_3y_4 + x_4y_3) + C \left( \frac{F_{14}^f r(1 - r) + F_{23}^f r(1 - r) + F_{34}^f}{2} \right) \\ F'_{44} &= (1 - C)(x_4y_4) + C \left( F_{44}^f + \frac{F_{14}^f(1 - r)^2 + F_{23}^f r^2 + F_{24}^f + F_{34}^f}{4} \right) \end{aligned} \quad (5.A2)$$

where  $x_i$  are

$$\begin{aligned}
 x_1 &= \frac{2F_{11}w_{f11} + F_{12}w_{f12} + F_{13}w_{f13} + F_{14}w_{f14}}{2\bar{w}_f} - r \left( \frac{F_{14}w_{f14} - F_{23}w_{f23}}{2\bar{w}_f} \right) \\
 x_2 &= \frac{2F_{22}w_{f22} + F_{12}w_{f12} + F_{23}w_{f23} + F_{24}w_{f24}}{2\bar{w}_f} + r \left( \frac{F_{14}w_{f14} - F_{23}w_{f23}}{2\bar{w}_f} \right) \\
 x_3 &= \frac{2F_{33}w_{f33} + F_{34}w_{f34} + F_{13}w_{f13} + F_{23}w_{f23}}{2\bar{w}_f} + r \left( \frac{F_{14}w_{f14} - F_{23}w_{f23}}{2\bar{w}_f} \right) \\
 x_4 &= \frac{2F_{44}w_{f44} + F_{32}w_{f32} + F_{14}w_{f14} + F_{24}w_{f24}}{2\bar{w}_f} - r \left( \frac{F_{14}w_{f14} - F_{23}w_{f23}}{2\bar{w}_f} \right), \quad (5.A3)
 \end{aligned}$$

$y_i$  are

$$\begin{aligned}
 y_1 &= \frac{2F_{11}w_{m11} + F_{12}w_{m12} + F_{13}w_{m13} + F_{14}w_{m14}}{2\bar{w}_m} - r \left( \frac{F_{14}w_{m14} - F_{23}w_{m23}}{2\bar{w}_m} \right) \\
 y_2 &= \frac{2F_{22}w_{m22} + F_{12}w_{m12} + F_{23}w_{m23} + F_{24}w_{m24}}{2\bar{w}_m} + r \left( \frac{F_{14}w_{m14} - F_{23}w_{m23}}{2\bar{w}_m} \right) \\
 y_3 &= \frac{2F_{33}w_{m33} + F_{34}w_{m34} + F_{13}w_{m13} + F_{23}w_{m23}}{2\bar{w}_m} + r \left( \frac{F_{14}w_{m14} - F_{23}w_{m23}}{2\bar{w}_m} \right) \\
 y_4 &= \frac{2F_{44}w_{m44} + F_{32}w_{m32} + F_{14}w_{m14} + F_{24}w_{m24}}{2\bar{w}_m} - r \left( \frac{F_{14}w_{m14} - F_{23}w_{m23}}{2\bar{w}_m} \right), \quad (5.A4)
 \end{aligned}$$

where  $w_{k,ij}$  represent the fitness through each sex function ( $k \in [m, f]$ ) of adults resulting from the union of the  $i$ th and  $j$ th haplotypes, and the population mean fitness through each sex function is

$$\begin{aligned}
 \bar{w}_f &= F_{11}w_{f11} + F_{12}w_{f12} + F_{13}w_{f13} + F_{14}w_{f14} + F_{22}w_{f22} + \\
 &\quad F_{23}w_{f23} + F_{24}w_{f24} + F_{33}w_{f33} + F_{34}w_{f34} + F_{44}w_{f44} \\
 \bar{w}_m &= F_{11}w_{m11} + F_{12}w_{m12} + F_{13}w_{m13} + F_{14}w_{m14} + F_{22}w_{m22} + \\
 &\quad F_{23}w_{m23} + F_{24}w_{m24} + F_{33}w_{m33} + F_{34}w_{m34} + F_{44}w_{m44}. \quad (5.A5)
 \end{aligned}$$

Combining Eqns(A1-A6) and simplifying yields the general haplotype recursion equations:

$$\begin{aligned}
 q'_1 &= F'_{11} + \frac{F'_{12} + F'_{13} + F'_{14}}{2} = (1 - C) \frac{(x_1 + y_1)}{2} + C \left( \frac{x_1 - r(F_{14} - F_{23})}{2\bar{w}_f} \right) \\
 q'_2 &= F'_{22} + \frac{F'_{12} + F'_{23} + F'_{24}}{2} = (1 - C) \frac{(x_2 + y_2)}{2} + C \left( \frac{x_2 + r(F_{14} - F_{23})}{2\bar{w}_f} \right) \\
 q'_3 &= F'_{33} + \frac{F'_{13} + F'_{23} + F'_{34}}{2} = (1 - C) \frac{(x_3 + y_3)}{2} + C \left( \frac{x_3 + r(F_{14} - F_{23})}{2\bar{w}_f} \right) \\
 q'_4 &= F'_{44} + \frac{F'_{14} + F'_{24} + F'_{34}}{2} = (1 - C) \frac{(x_4 + y_4)}{2} + C \left( \frac{x_4 - r(F_{14} - F_{23})}{2\bar{w}_f} \right). \quad (5.A6)
 \end{aligned}$$

### 5.9.2 QE Approximations

After Caballero and Hill (1992), the QE genotypic frequencies for a single locus,  $A$ , are

$$\begin{aligned} F_{AA}^* &= q^2 + \frac{Cq(1-q)}{(2-C)} \\ F_{Aa}^* &= 2q(1-q) - \frac{2Cq(1-q)}{(2-C)} \\ F_{aa}^* &= (1-q)^2 + \frac{Cq(1-q)}{2-C}, \end{aligned} \quad (5.A7)$$

where  $q$  is the allele frequency and  $C$  is the fixed proportion of self fertilization. We can extend these single-locus results for the two-locus model to calculate the QE adult genotypic frequencies formed by the union of the  $i$ th and  $j$ th haplotypes:

$$\begin{aligned} \phi_{11} &= q_1^2 + Cq_1(1-q_1)/(2-C) \\ \phi_{12} &= 4q_1q_2(1-C)/(2-C) \\ \phi_{13} &= 4q_1q_3(1-C)/(2-C) \\ \phi_{14} &= 4q_1q_4(1-C)/(2-C) \\ \phi_{22} &= q_2^2 + Cq_2(1-q_2)/(2-C) \\ \phi_{23} &= 4q_2q_3(1-C)/(2-C) \\ \phi_{24} &= 4q_2q_4(1-C)/(2-C) \\ \phi_{33} &= q_3^2 + Cq_3(1-q_3)/(2-C) \\ \phi_{34} &= 4q_3q_4(1-C)/(2-C) \\ \phi_{44} &= q_4^2 + Cq_4(1-q_4)/(2-C) \end{aligned} \quad (5.A8)$$

Following standard two-locus theory for partially selfing populations (Holden 1979; Otto and Day 2007; Jordan and Connallon 2014), and substituting the QE genotypic frequencies,  $\phi_{ij}$ , yields the haplotype recursions given in Eq(5.1), where  $x_i$  are

$$\begin{aligned} x_1 &= \frac{2\phi_{11}w_{f11} + \phi_{12}w_{f12} + \phi_{13}w_{f13} + \phi_{14}w_{f14}}{2\bar{w}_f} - r \left( \frac{\phi_{14}w_{f14} - \phi_{23}w_{f23}}{2\bar{w}_f} \right) \\ x_2 &= \frac{2\phi_{22}w_{f22} + \phi_{12}w_{f12} + \phi_{23}w_{f23} + \phi_{24}w_{f24}}{2\bar{w}_f} + r \left( \frac{\phi_{14}w_{f14} - \phi_{23}w_{f23}}{2\bar{w}_f} \right) \\ x_3 &= \frac{2\phi_{33}w_{f33} + \phi_{34}w_{f34} + \phi_{13}w_{f13} + \phi_{23}w_{f23}}{2\bar{w}_f} + r \left( \frac{\phi_{14}w_{f14} - \phi_{23}w_{f23}}{2\bar{w}_f} \right) \\ x_4 &= \frac{2\phi_{44}w_{f44} + \phi_{34}w_{f34} + \phi_{13}w_{f13} + \phi_{24}w_{f24}}{2\bar{w}_f} - r \left( \frac{\phi_{14}w_{f14} - \phi_{23}w_{f23}}{2\bar{w}_f} \right) \end{aligned} \quad (5.A9)$$

and  $y_i$  are

$$\begin{aligned}
y_1 &= \frac{2\phi_{11}w_{m11} + \phi_{12}w_{m12} + \phi_{13}w_{m13} + \phi_{14}w_{m14}}{2\bar{w}_m} - r \left( \frac{\phi_{14}w_{m14} - \phi_{23}w_{m23}}{2\bar{w}_m} \right) \\
y_2 &= \frac{2\phi_{22}w_{m22} + \phi_{12}w_{m12} + \phi_{23}w_{m23} + \phi_{24}w_{m24}}{2\bar{w}_m} + r \left( \frac{\phi_{14}w_{m14} - \phi_{23}w_{m23}}{2\bar{w}_m} \right) \\
y_3 &= \frac{2\phi_{33}w_{m33} + \phi_{34}w_{m34} + \phi_{13}w_{m13} + \phi_{23}w_{m23}}{2\bar{w}_m} + r \left( \frac{\phi_{14}w_{m14} - \phi_{23}w_{m23}}{2\bar{w}_m} \right) \\
y_4 &= \frac{2\phi_{44}w_{m44} + \phi_{34}w_{m34} + \phi_{13}w_{m13} + \phi_{24}w_{m24}}{2\bar{w}_m} - r \left( \frac{\phi_{14}w_{m14} - \phi_{23}w_{m23}}{2\bar{w}_m} \right) \quad (5.A10)
\end{aligned}$$

and the population mean fitness through each sex function is

$$\begin{aligned}
\bar{w}_f &= \phi_{11}w_{f11} + \phi_{12}w_{f12} + \phi_{13}w_{f13} + \phi_{14}w_{f14} + \phi_{22}w_{f22} + \\
&\quad \phi_{23}w_{f23} + \phi_{24}w_{f24} + \phi_{33}w_{f33} + \phi_{34}w_{f34} + \phi_{44}w_{f44} \\
\bar{w}_m &= \phi_{11}w_{m11} + \phi_{12}w_{m12} + \phi_{13}w_{m13} + \phi_{14}w_{m14} + \phi_{22}w_{m22} + \\
&\quad \phi_{23}w_{m23} + \phi_{24}w_{m24} + \phi_{33}w_{m33} + \phi_{34}w_{m34} + \phi_{44}w_{m44}. \quad (5.A11)
\end{aligned}$$

## 5.10 Appendix B: Supplementary figures

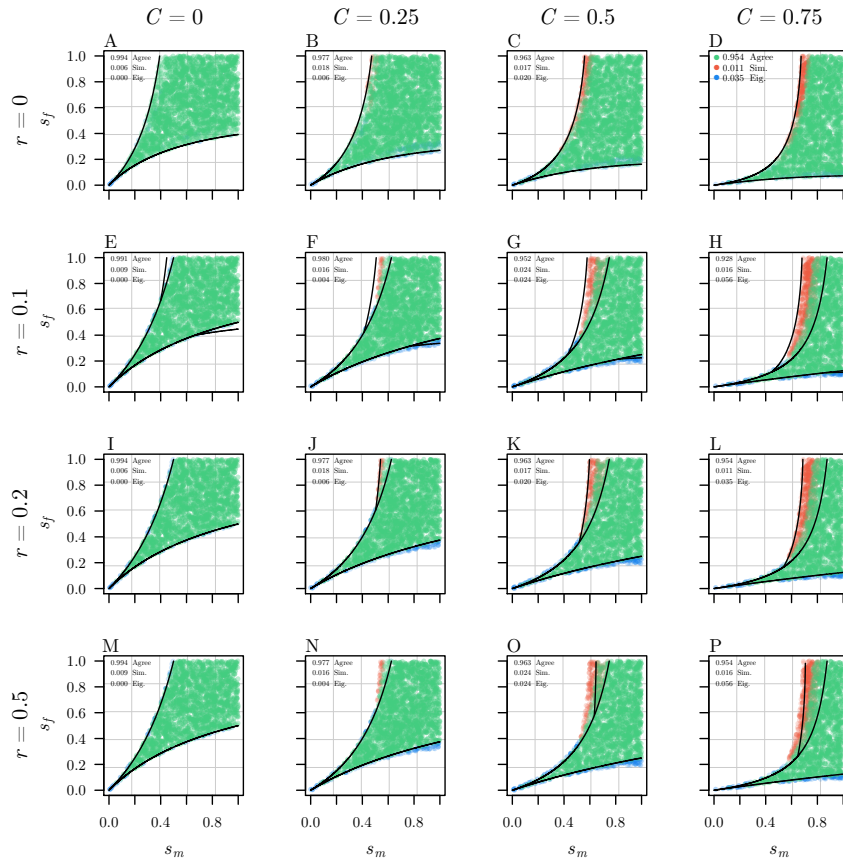


FIGURE 5.S1: Haplotype recursions evaluated at QE, and the resulting invasion conditions, approximate the evolutionary trajectory of the full genotypic recursions very well under additive allelic effects, even under strong selection. Predicted regions of SA polymorphism based on deterministic simulations using the genotypic recursions Eq(5.A2) are compared against the outcome of the invasion analysis for the haplotype recursions using the QE approximation (Eq 5.1) across a gradient of selfing ( $C$ ) and recombination ( $r$ ) rates. Green points indicate parameter conditions where deterministic simulations of the genotypic recursions (Sim.) and the invasion analysis based on eigenvalues for the QE haplotype approximations (Eig.) both predicted polymorphism. Red points indicate regions where the Sim. predicted polymorphism but the Eig. did not; and blue points indicate the opposite. The proportion of each outcome is shown in the upper left corner of each panel. Black solid lines show the invasion conditions based on the haplotype recursions using the QE approximation for the given values of  $C$  and  $r$ , with lines drawn for both the two-locus and single-locus invasion conditions when  $r > 0$ .

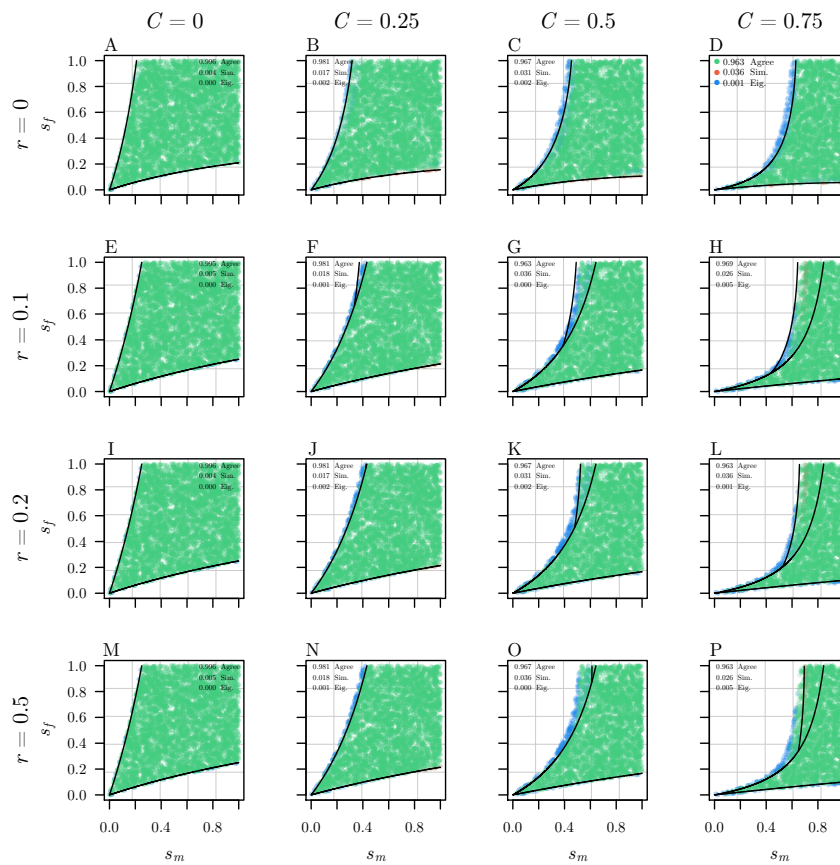


FIGURE 5.S2: Haplotype recursions evaluated at QE, and the resulting invasion conditions, approximate the evolutionary trajectory of the full genotypic recursions very well under allelic effects resulting in dominance reversal, even under strong selection. Predicted regions of SA polymorphism based on deterministic simulations using the genotypic recursions equations (5.A2) are compared against the outcome of the invasion analysis for the haplotype recursions using the QE approximation (Eq 5.1) across a gradient of selfing ( $C$ ) and recombination ( $r$ ) rates. Green points indicate parameter conditions where deterministic simulations of the genotypic recursions (Sim.) and the invasion analysis based on eigenvalues for the QE haplotype approximations (Eig.) both predicted polymorphism. Red points indicate regions where the Sim. predicted polymorphism but the Eig. did not; and blue points indicate the opposite. The proportion of each outcome is shown in the upper left corner of each panel. Black solid lines show the invasion conditions based on the haplotype recursions using the QE approximation for the given values of  $C$  and  $r$ , with lines drawn for both the two-locus and single-locus invasion conditions when  $r > 0$ .

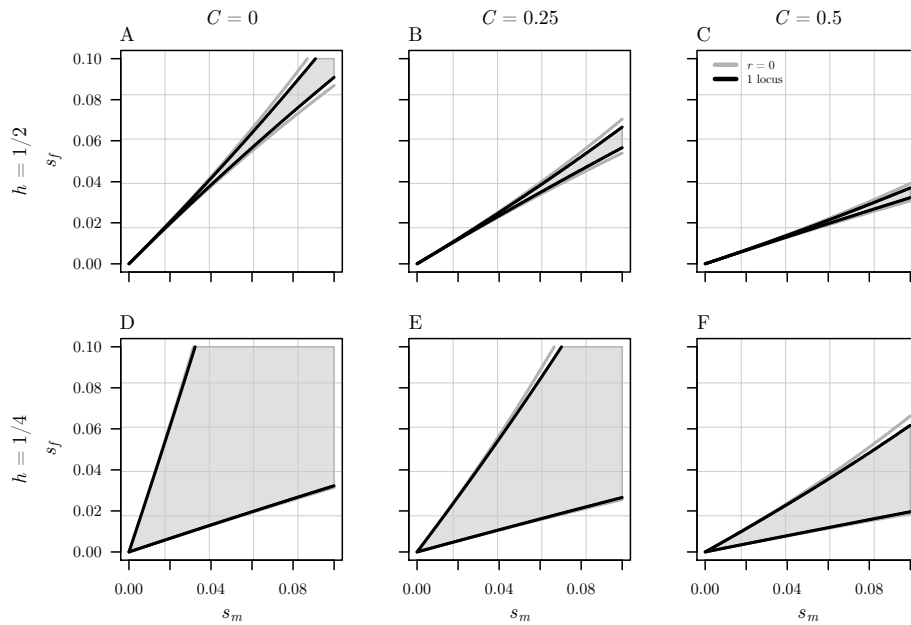


FIGURE 5.S3: Under weak selection ( $s_f, s_m < 0.1$ ), the parameter space where sexually antagonistic polymorphism is maintained is only expanded beyond the single-locus case when there is very tight linkage ( $r \approx 0$ ). Thus, there is little scope for self-fertilization to influence sexually antagonistic polymorphism. Results are shown for the conditions of additive allelic effects ( $h_i = 1/2$ ; panels A–C), and dominance reversal ( $h_i = 1/4$ ; panels D–F). In each panel, the shaded region between the black lines indicates the region of sexually antagonistic polymorphism for the single-locus case; grey lines indicate the thresholds for invasion for female-beneficial (lower lines) and male-beneficial (upper lines) alleles under complete linkage ( $r = 0$ ).

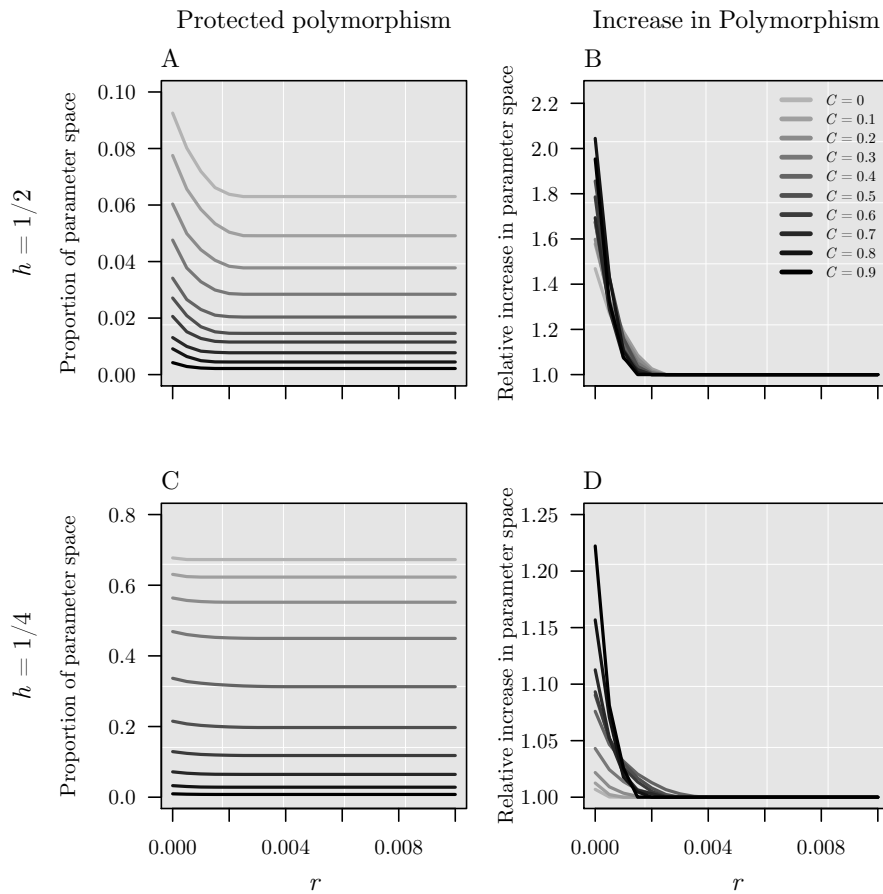


FIGURE 5.S4: Under weak selection, the proportion of parameter space where SA polymorphism is maintained again declines with increased recombination and self-fertilization (panels A,C). The increase in SA polymorphism in the two-locus model relative to the single-locus case also declines with the recombination rate, but increases with the rate of self-fertilization (panels B,D). However, these effects are limited to cases of extremely tight linkage ( $r < 0.004$ ). Results are shown for the conditions of additive allelic effects ( $h_i = 1/2$ ; panels A–B), and dominance reversal ( $h_i = 1/4$ ; panels C–D). Results were obtained by evaluating the leading eigenvalues of  $\mathbf{J}$  for populations initially fixed for the haplotypes  $[AB]$  and  $ab$  at 30,000 points distributed uniformly throughout parameter space defined by  $s_m \times s_f$ , where  $s_f, s_m \in [0, 0.1]$

## 5.11 Appendix C: Computer Code

Additional Supporting Information, including the supplemental Mathematica Notebook (.nb), may be found in the online version of this article at the publisher's website: [http://onlinelibrary.wiley.com/journal/10.1111/\(ISSN\)1558-5646](http://onlinelibrary.wiley.com/journal/10.1111/(ISSN)1558-5646), at <https://github.com/colin-olito/twoLocusPartSelf>, and from the author upon request.

## Chapter 6

# Sexually antagonistic polymorphism and the evolution of dimorphic sexual systems from hermaphroditism

### Abstract

Most flowering plants are hermaphroditic, with each individual expressing both male and female sex functions. Nevertheless, the diversity of plant sexual systems falls along a wide spectrum — from simultaneous hermaphroditism, to physically separate sexes (dioecy), and nearly everything in between. Identifying the evolutionary mechanisms that facilitate transitions between different sexual systems remains a major unresolved question. One evolutionary pathway from hermaphroditism towards separate sexes is via the sequential invasion of "unisexual" sterility alleles that each eliminate female or male sex functions in hermaphrodites, and thereby yield discrete female and male individuals. Classic population genetics theory identifies two key preconditions that facilitate this pathway to dioecy: (1) genetically based allocation trade-offs between female and male sex-functions (a form of "sexual antagonism"); and (2) modest-to-high rates of self-fertilization and inbreeding depression in the ancestral hermaphrodite population. This theory also predicts that transitions to dioecy are most likely to begin by invasion of a male-sterility rather than a female-sterility allele. We extend recent population genetics theory of sexually antagonistic selection to show that physical linkage to a sexually antagonistic locus enhances the invasion of female- and male-sterility alleles, and significantly alters predictions about the role of self-fertilization in the evolution of dioecy. The new model shows that linkage to a sexually antagonistic locus has three consequences for the evolution of sexual systems. First, linkage broadens the conditions for invasion of unisexual sterility alleles, promoting transitions from hermaphroditism to gyno- and andro-dioecy. Second, linkage elevates the equilibrium frequencies of unisexual females or males in mixed-mating populations, thereby promoting subsequent transitions to full dioecy. Third, linkage greatly diminishes effects of ancestral selfing and inbreeding depression on transitions to gyno- and androdioecy. Overall, our results predict that sterility mutations that initiate the evolution of dioecy will evolve in tight linkage with sexually antagonistic loci. We discuss implications of these new results for the evolution of plant mating systems and the early dynamics of sex chromosome evolution.

## 6.1 Introduction

Although the majority of flowering plants are hermaphroditic, where individuals perform both male and female sex-functions, plant sexual systems form a diverse spectrum ranging from simultaneous hermaphroditism, to physically separate sexes (dioecy) (Darwin 1877; Westergaard 1958; Bachtrog et al. 2014). Moreover, this diversity of sexual dimorphism encompasses nearly every possible intermediate state, from hermaphrodites bearing various combinations of perfect and/or single-sex flowers (monoecy), to mixed populations of hermaphrodite and unisexual individuals (subdioecy) (Bawa 1980; Sakai and Weller 1999).

Dioecious sexual systems have evolved from hermaphrodite ancestors repeatedly, and independently, in numerous plant lineages (Westergaard 1958; Sakai and Weller 1999; Charlesworth 2006; Bachtrog et al. 2014; Renner 2014; Goldberg et al. 2017; Käfer et al. 2017). The invasion of unisexual female or male individuals within a population of hermaphrodites – leading to gyno- or androdioecy – is thought to represent the first step in the evolutionary pathway from hermaphroditism to dioecy (Charlesworth and Charlesworth, 1978a; Charlesworth and Charlesworth, 1978b). Unisexuales might arise through invasion of nuclear sterility alleles causing complete loss of one sex-function, or more gradually through gender modifier, or partial sterility alleles (Charlesworth and Charlesworth, 1978a; Charlesworth and Charlesworth, 1978b; Charlesworth 1999). In all cases, at least two mutational steps are required: invasion of male- or female-sterility alleles, resulting in gyno- or androdioecy, and the subsequent invasion of one or more mutations causing sterility for the sex function not affected by the first invading mutation (Westergaard 1958; Charlesworth and Charlesworth, 1978a; Charlesworth and Charlesworth, 1978b; Charlesworth 2006; Charlesworth and Willis 2009; Käfer et al. 2017). Consistent with this two-step pathway to separate sexes, several lines of empirical evidence support the notion that two or more loci are often involved in nuclear plant sex determination systems (Westergaard 1958; Charlesworth 2002, 2006; Renner 2014; Ashman et al. 2015).

Previous theory predicts that evolutionary transitions from hermaphroditism to dioecy are favoured by allocation trade-offs between male and female sex-functions, and by the combination of modest-to-high rates of self-fertilization and inbreeding depression (Lewis 1941; Lloyd 1975, 1976; Charlesworth and Charlesworth, 1978a). This theory also predicts that the invasion of a male sterility allele is more likely to initiate transitions to dioecy than the invasion of a female sterility allele (see Charlesworth 1999, 2006 for comprehensive reviews of relevant theory). The more stringent conditions for the evolution of androdioecy arise because unisexual males must compete with self-fertilizing hermaphrodites to fertilize ovules (Lloyd 1975; Charlesworth and Charlesworth, 1978a; Käfer et al. 2017), and indeed androdioecy is extremely rare relative to gynodioecy among angiosperms (Darwin 1877; Charlesworth and Charlesworth, 1978a; Renner 2014). Additionally, the subsequent invasion of complete or partial sterility mutations resulting in dioecy may often require tight linkage with the first sterility mutation (the "linkage constraint" of Charlesworth and Charlesworth 1978a). The invasion of tightly linked complimentary sterility mutations then sets the stage for the evolution of heteromorphic sex chromosomes, such as a gene-rich X and degenerate Y (Rice 1987; Bachtrog 2006; Charlesworth 2002; Qiu et al. 2013).

The allocation trade-offs between sex-functions favoring transitions to dioecy represent a form of sexual antagonism (SA), and can lead to intra-locus sexual conflict when alleles have pleiotropic effects that are deleterious via one sex-function (e.g., cause decreased pollen production) and beneficial for the other (e.g., cause

increased ovule production) (Jordan and Connallon 2014; Olito 2016). When they cause such reproductive compensation, unisexual sterility alleles can be viewed as a special case of SA alleles that cause partial to complete loss of one sex-function, and possibly increased allocation to the other (Lewis 1941; Lloyd 1975; Charlesworth and Charlesworth, 1978a). In the broader context of SA selection, we might therefore expect that unisexual sterility alleles should behave similarly to SA alleles. For example, their invasion requires adequate allocation to the remaining sex-function to offset the loss of fitness due to sterility and out-compete self-compatible hermaphrodites (Charlesworth and Charlesworth, 1978a). Similarly, the invasion of SA alleles requires that positive selection through one sex-function is not overpowered by purifying selection through the other, and SA alleles can be maintained as polymorphisms when selection through each sex-function is evenly balanced or very strong (Kidwell et al. 1977; Jordan and Connallon 2014).

The invasion conditions for male and female unisexual sterility alleles have been determined in the single-locus context (Charlesworth and Charlesworth, 1978a), yet recent work on SA alleles suggest that multilocus dynamics can substantially alter conditions for invasion and polymorphism at SA loci. In both dioecious and partially selfing hermaphrodite species, tight linkage between two SA loci facilitates the invasion of SA alleles, and expands the parameter space where polymorphism is maintained by balancing selection beyond the predictions of single-locus models (Kidwell et al. 1977; Patten et al. 2010; Úbeda et al. 2010; Olito 2016). Despite the inherent challenges in indentifying SA genes (Connallon and Clark 2012; Barson et al. 2015), there is empirical evidence that such multilocus dynamics may be important in natural populations of hermaphrodites (e.g., chromosomal inversions with SA fitness effects; Lee et al. 2016).

Considering the evolution of sex-specific sterility alleles from the perspective of SA selection theory raises several important questions regarding the role of genomic architecture for the evolution of separate sexes. Does linkage with another SA locus facilitate the invasion of sterility alleles, for example, by promoting selection on linked allelic combinations (i.e., female-beneficial with male-sterility, and male-beneficial with female-sterility alleles)? Does the presence of segregating SA variation expand conditions for the invasion of unisexuals in hermaphrodite populations? Does linkage to SA alleles lead to elevated equilibrium frequencies of unisexuals in the resulting gyno- or androdioecious populations? The idea that linkage with another SA locus should facilitate the invasion of unisexual sterility mutations echoes the premise of the 'linkage constraint' for the evolution of dioecy described by Charlesworth and Charlesworth (1978a), and the role of SA variation for sex chromosome turnover (e.g., vanDoorn and Kirkpatrick 2007, 2010), but focus instead on the initial invasion of unisexuals rather than the subsequent evolution of dioecy or invasion of new sex-determining loci in already dioecious species. Similarly, the logic underlying the invasion of unisexual sterility alleles in hermaphrodites under SA selection is similar to the evolution of sex-ratio adjustment under SA selection in dioecious species (Blackburn et al. 2010). In these models, alleles causing females to produce broods with skewed sex-ratios are predicted to invade when the adjustment in sex ratio compliments the SA alleles the parents carry (e.g., alleles favouring daughters when parents carry female-benefit alleles, and favouring sons when parents carry male-benefit alleles).

Here, we extend population genetic models for the evolution of gyno- and androdioecy from an ancestral population of simultaneous hermaphrodites, and consider the role of linkage between SA loci on transitions away from hermaphroditic sexual systems. We specifically explore the consequences of physical linkage between SA

loci for the invasion and equilibrium frequencies of alleles that cause sex-specific sterility. We show that linkage results in significantly more permissive parameter conditions for the invasion of unisexuals, as well as elevated equilibrium frequencies of unisexuals relative to the predictions of classical, single-locus models. Overall, our results indicate that multi-locus consequences of SA selection facilitate the evolution of dimorphic sexual systems from hermaphroditism, and suggest a hitherto unrecognized role for SA genetic variation during the initial stages of early sex-chromosome evolution.

## 6.2 Models

Following previous population genetic theory, we model the evolution of gynodioecy from an ancestral hermaphroditic population via the invasion of unisexual sterility alleles causing complete male or female sterility (Charlesworth and Charlesworth, 1978a). We restrict our analyses to four scenarios of biological interest: the evolution of gynodioecy via invasion of a (1) completely dominant, or (2) completely recessive male-sterility allele; and the evolution of androdioecy via the invasion of a (3) completely dominant or (4) completely recessive female-sterility allele. These scenarios represent ‘corner cases’ for both the phenotypic effect and the dominance of the sex-specific sterility mutations. Alternative models allowing for partial sterility or dominance will presumably yield evolutionary dynamics that are intermediate between these corner cases. Here we describe in full the simplest model, involving a dominant male-sterility mutation (scenario 1). We subsequently highlight, in brief, the essential differences arising in each of the other three models. Further information on each model, including a development of the full recursions, can be found in [Appendix A: Development of recursions](#).

### 6.2.1 Gynodioecy

Consider a genetic system involving two diallelic autosomal loci, **A** (with alleles  $A$ ,  $a$ ) and **M** (with alleles  $M_1$ ,  $M_2$ ), that recombine at rate  $r$  per meiosis, in a large population that is initially hermaphroditic. Assume that the **A** locus is under sexually antagonistic selection, with the  $A$  allele having female-beneficial (male-deleterious) fitness effects, and the  $a$  allele having male-beneficial (female-deleterious) fitness effects. Also assume that the  $M_1$  allele at the **M** locus has a relative fitness of 1 in both sexes, while the  $M_2$  allele causes sterility through the male sex-function (e.g., via the production of no, or inviable, pollen), and is completely dominant relative to the  $M_1$  allele. Female unisexuals carrying the  $M_2$  allele may be able to re-allocate resources towards ovule production that would otherwise have been used for pollen production (Lloyd 1975, 1976; Charlesworth and Charlesworth 1978a). To account for such reproductive compensation, let  $k$  describe the proportional increase in ovule production in females relative to hermaphrodites, such that  $k = 1$  represents perfect compensation for the loss of the male sex-function via ovule production. In this genetic system, the successful invasion of the  $M_2$  allele represents the evolution of gynodioecy from simultaneous hermaphroditism.

The rate of self-fertilization among hermaphrodite individuals,  $C$ , is not directly influenced by the genotype at the **A** locus. By definition, the genotype at the **M** locus determines whether or not self-fertilization is possible (after Charlesworth and Charlesworth 1978a). Let us also assume a constant population level of inbreeding depression,  $\delta$ , defined as the decrease in the probability of survival of zygotes

formed by self-fertilization relative to those produced by outcrossing. As noted by Charlesworth and Charlesworth (1978a), this assumption only holds for populations at equilibrium, but probably represents a conservative estimate of the effects of inbreeding depression. Generations are assumed to be non-overlapping, and the life-cycle proceeds as follows: fertilization  $\rightarrow$  differential survival due to inbreeding depression  $\rightarrow$  selection  $\rightarrow$  fertilization.

Let  $x_i$  and  $y_i$  denote the frequencies of the four possible haplotypes [ $AM_1, AM_2, aM_1, aM_2$ ] in female and male gametes respectively. The fitness of offspring resulting from the union of the  $i^{\text{th}}$  and  $j^{\text{th}}$  gametic haplotypes, are denoted  $w_{ij}^f$  and  $w_{ij}^m$  respectively, and are assumed to be the product of the fitness expressions for **A** and **M** (Table 6.1). We assume no parent-of-origin effects on fitness, and so index the ten possible pairs of gametic haplotypes where  $i \geq j$  hereafter.

The fact that an individual's genotype at the **M** locus determines whether they are able to self-fertilize complicates the derivation of recursion equations describing evolutionary change in genotype frequencies. We therefore model the change in frequency of each genotype given the mode of transmission (either self-fertilization or outcrossing). This approach yields a system of 20 general recursion equations (10 genotypes  $\times$  two modes of transmission; see [Appendix A: Development of recursions](#) for a full derivation of all recursions). Although more compact approaches have been used for generating recursions in previous models for the evolution of self-fertilization and dioecy (e.g., Charlesworth and Charlesworth 1978a; Charlesworth and Charlesworth 2010), we used the following, expanded expressions as a means of clarifying the pathway and assumptions that underlie each of our models. As shown below, our models reproduce the classical results in special cases where there is only selection at loci segregating for sterility alleles.

When  $M_2$  is completely dominant, the system of recursions reduces considerably. Let  $F_{ij}$  equal the frequency among zygotes of the genotype formed by the union of the  $i^{\text{th}}$  and  $j^{\text{th}}$  haplotypes via outcrossing, and  $G_{ij}$  be the same for zygotes formed via self-fertilization. The genotypic frequencies in the next generation among zygotes formed by outcrossing are then:

$$\begin{aligned}
 F'_{11} &= (1 - S)(x_1y_1) \\
 F'_{12} &= (1 - S)(x_2y_1) \\
 F'_{13} &= (1 - S)(x_1y_3 + x_3y_1) \\
 F'_{14} &= (1 - S)(x_4y_1) \\
 F'_{22} &= 0 \\
 F'_{23} &= (1 - S)(x_2y_3) \\
 F'_{24} &= 0 \\
 F'_{33} &= (1 - S)(x_3y_3) \\
 F'_{34} &= (1 - S)(x_4y_3) \\
 F'_{44} &= 0,
 \end{aligned} \tag{6.1}$$

where  $x_i$  and  $y_i$  are functions  $x_i = f(F_{ij}, G_{ij}, w_{ij}^f, C, \delta, r)$  and  $y_i = f(F_{ij}, G_{ij}, w_{ij}^m, C, \delta)$  describing the haplotype frequencies among ovules and pollen, and  $S$  is the proportion of all ovules produced by the population that are self-fertilized. Note that  $y_2 = y_4 = 0$  because these male gametic haplotypes cannot be produced when  $M_2$  is dominant, and the recombination rate. Because  $y_2$  and  $y_4$  cannot be produced under

this dominance scenario, males cannot produce offspring that are double heterozygotes, and the recombination rate therefore does not feature in equations describing haplotype frequencies among pollen ( $y_i$ ). The genotypic frequencies in the next generation among zygotes formed by self-fertilization are

$$\begin{aligned} G'_{11} &= S(o_{11}^S + o_{13}^S/4) \\ G'_{13} &= S(o_{13}^S/2) \\ G'_{33} &= S(o_{33}^S + o_{13}^S/4), \end{aligned} \quad (6.2)$$

where  $o_{ij}^S$  are functions  $f(F_{ij}, G_{ij}, w_{ij}^f, C, \delta)$  describing the proportional contribution of each genotype to self-fertilized ovules. All  $G'_{ij} = 0$  where  $ij \neq [11, 13, 33]$ .

The basic form of the recursions does not change when  $M_2$  is completely recessive, but there are two notable differences. Because only  $M_2M_2$  homozygotes are unisexual females, none of the recursions reduce to zero, and the recombination rate enters into the nonzero  $G'_{ij}$  recursions. For the same reason, all  $x_i$  and  $y_i$  describing the haplotype frequencies among ovules and pollen become nonzero functions  $f(F_{ij}, G_{ij}, w_{ij}^m, C, \delta, r)$  including the recombination rate.

### 6.2.2 Androdioecy

The successful invasion of a dominant  $M_2$  allele causing complete female-sterility (e.g., production of no, or inviable, ovules) represents the evolution of androdioecy. In contrast to the models of gynodioecy described above, the reproductive compensation term,  $k$ , now describes the proportional increase in pollen production by males relative to hermaphrodites. The fitness expressions,  $w_{ij}^f$  and  $w_{ij}^m$  resemble those described in Table 6.1, except the fitness effects of the  $\mathbf{M}$  locus apply to the female rather than male sex-function.

The genotype  $\times$  transmission mode recursions for the models of androdioecy are very similar to those described for the models of gynodioecy, with a few key differences. When  $M_2$  is dominant,  $x_i$  and  $y_i$  are again functions describing the haplotype frequencies among ovules and pollen, but now the recombination rate drops out of the expressions for  $x_i = f(F_{ij}, G_{ij}, w_{ij}^f, C, \delta)$ , comes into the expressions for  $y_i = f(F_{ij}, G_{ij}, w_{ij}^m, C, \delta, r)$ , and  $x_2 = x_4 = 0$ . The genotypic frequencies in the next generation among zygotes formed by outcross fertilization,  $F'_{ij}$ , are otherwise identical to Eq(6.1), but now account for the fact that heterozygotes at the  $\mathbf{M}$  locus do not produce ovules. The form of the  $G'_{ij}$  recursions remain unchanged from Eq(6.2).

When the  $M_2$  female-sterility allele is completely recessive, only  $M_2M_2$  homozygotes are unisexual males. The form of the recursions is very similar to the case of gynodioecy with a recessive sterility allele. The fitness effects arising from the  $\mathbf{M}$  locus now only affect the female sex-function, and all  $x_i$  and  $y_i$  describing the haplotype frequencies among outcrossed ovules and pollen become nonzero functions  $f(F_{ij}, G_{ij}, w_{ij}^f, C, \delta, r)$  including the recombination rate.

### 6.2.3 Analyses

Our analyses address three main theoretical questions: (1) Does linkage to SA loci expand conditions for the evolutionary invasion of unisexual sterility? (2) How does

linkage to SA loci affect the frequency of unisexual individuals in andro- and gynodioecious populations? (3) How does the invasion of sterility alleles impact evolutionary dynamics, including conditions for polymorphism at SA loci? As in previous models of sexually antagonistic selection (e.g., Kidwell et al. 1977; Prout 2000; Jordan and Connallon 2014), we limit our analyses to the representative, and biologically interesting cases of additive fitness effects ( $h_m = h_f = 1/2$ ), and dominance reversals ( $h_m = h_f < 1/2$ ) at the **A** locus. These scenarios are of particular interest because additive fitness effects are commonly observed for alleles with small to intermediate fitness effects (Agrawal and Whitlock 2011), and dominance reversals are often predicted by fitness landscape models of dominance (Manna et al. 2011; Connallon and Clark, 2014b).

We first examine the case where **A** is monomorphic, and identify the parameter conditions where balancing selection is predicted to maintain stable polymorphism at **A** and unisexuals are able to invade. We evaluate the stability of the system of recursions for a population initially fixed for the female-beneficial or male-beneficial allele at the **A** locus, and the  $M_1$  allele at the **M** locus. These conditions correspond to initial equilibrium genotypic frequencies among outcrossed and selfed zygotes of  $F_{11} = (1 - C)[AAM_1M_1] = 1$ ,  $F_{33} = (1 - C)[aaM_1M_1] = 1$ , and  $G_{11} = C[AAM_1M_1] = 1$ , and  $G_{33} = C[aaM_1M_1] = 1$ . Under these initial conditions, the fate of new mutations is determined by the rate of change of the frequencies of rare genotypes, which can be approximated by one minus the leading eigenvalue of the Jacobian matrix of the system of recursions,  $1 - \lambda_L$  (Otto and Day 2007). Balancing selection is predicted to maintain polymorphism when  $\lambda_L > 1$  for both boundary equilibria (Prout 1968; Otto and Day 2007). For the models involving dominant male- and female-sterility alleles, this analysis yields three analytically tractable candidate leading eigenvalues describing the invasion of a new mutation at each locus independently ( $\lambda_A$  and  $\lambda_M$ ), and the joint invasion of a double-mutant haplotype ( $\lambda_{AM}$ ). When sterility alleles are recessive, analysis of the eigenvalues yield inconclusive results for invasion of unisexuals because heterozygotes at the **M** locus are entirely sheltered from selection. We therefore present analytic results based on the eigenvalue analyses for the models of dominant sterility alleles only.

To explore how segregating SA variation influences the invasion of unisexuals into populations of hermaphrodites, we evaluated whether the  $M_2$  allele could invade populations initially at polymorphic single-locus equilibrium for **A** and fixed for  $M_1$  at **M**. Specifically, we evaluated whether  $\lambda_M|_{F_{ij}^*, G_{ij}^*} > 1$  and  $\lambda_{AM}|_{F_{ij}^*, G_{ij}^*} > 1$ , where  $F_{ij}^*$  correspond to the single-locus equilibrium genotypic frequencies

$$\begin{aligned} F_{11}^* &= (1 - C)[AAM_1M_1], & G_{11}^* &= C[AAM_1M_1] \\ F_{13}^* &= (1 - C)[AaM_1M_1], & G_{13}^* &= C[AaM_1M_1] \\ F_{33}^* &= (1 - C)[aaM_1M_1], & G_{33}^* &= C[aaM_1M_1], \end{aligned} \quad (6.3)$$

and all other  $F_{ij}^* = G_{ij}^* = 0$ . Assuming obligate outcrossing and additive effects, analytic solutions are possible for the single-locus allele frequencies at **A** among males and females ( $\hat{p}_f, \hat{p}_m$ ; Kidwell et al. 1977). This is not possible for partial selfing, or in the case of dominance reversal. However, under these conditions, the single-locus equilibrium frequencies can be estimated using weak selection approximations for  $\hat{p}$  ( $s_m, s_f \ll 1$ ), which we then use to calculate  $F_{ij}^*$  and  $G_{ij}^*$ . For example, under complete dominance reversal ( $h_f = h_m = 0$ ), the single-locus equilibrium frequency of a male-beneficial allele under weak selection can be approximated as  $\hat{p}_{DR} \approx s_m / (s_f + s_m)$  (Connallon and Jordan 2016). More complex expressions can be

found for the case of incomplete dominance reversal (e.g.,  $h_f = h_m = 1/4$ ; Jordan and Connallon 2014; Olito 2016). In both cases, the approximations perform reasonably well when selection is not especially strong ( $s_f, s_m \leq 0.5$ ; Jordan and Connallon 2014; Connallon and Jordan 2016; Olito 2016).

To determine the equilibrium frequencies of SA alleles,  $M_2$ , and unisexuals invading polymorphic populations, we performed deterministic simulations of the recursions  $F'_{ij}$ ,  $G'_{ij}$  using the initial genotypic frequencies described by Eq(6.3). We focus our analysis on the comparison of equilibrium frequencies of unisexuals from our models with the corresponding exact single-locus equilibrium frequencies,  $\hat{Z}$ , given by Charlesworth and Charlesworth (1978a) for cases of relatively tight linkage between the **A** and **M** ( $r \leq 0.1$ ). We emphasize tight linkage for two reasons. First, this represents the parameter conditions where our model predictions should differ most from those of single-locus models; with higher recombination, the predictions from the one- and two-locus models converge. Second, tight or complete linkage should approximate the biologically plausible scenario where SA loci, including a sex-specific sterility locus, are involved in a chromosomal inversion (Lee et al. 2016).

In single-locus models of gynodioecy and androdioecy, the equilibrium frequency of unisexuals is determined by the reproductive compensation term,  $k$ , and the compound parameter  $C\delta$  (Charlesworth and Charlesworth, 1978a). However, if inbreeding depression is caused primarily by recessive deleterious mutations, as current data suggest (Charlesworth and Willis 2009), there should be strong negative covariance between  $C$  and  $\delta$  as increased selfing more effectively purges deleterious recessives. In the simplest case, the mutation load due to deleterious recessive mutations at a single locus in a completely selfing population should be roughly half that of a randomly mating outcrossing population ( $\mu$  versus  $2\mu$ , where  $\mu$  is the genome-wide mutation rate; Ohta and Cockerham 1974). To account for negative covariance between  $C$  and  $\delta$ , and thereby explore more biologically meaningful parameter space, we constrain inbreeding depression for our simulations to be a linear declining function of the selfing rate:  $\delta = \delta^*(1 - C/2)$ , where  $\delta^*$  represents the hypothetical severity of inbreeding depression if selfing were enforced on a completely outcrossing population ( $\delta^* \in [0, 1]$ ). More complex expressions for  $\delta$  yielded qualitatively similar results (See Appendix C: Alternative models of inbreeding depression).

Finally, it was important to account for the fact that  $C$  and  $\delta$  also influence the maintenance of SA polymorphism and the equilibrium frequencies of the SA alleles at **A** (Jordan and Connallon 2014; Olito 2016). We therefore ran simulations using values of  $s_f$  and  $s_m$  corresponding to single-locus equilibrium frequencies of  $1/2$  for the two SA alleles ( $p = [A], q = [a]; p = q = 1/2$ ). Thus, our simulations explore the invasion of the male- or female-sterility allele,  $M_2$ , into hermaphroditic populations initially at highly polymorphic single-locus equilibrium at **A**.

#### 6.2.4 Data availability

A full development of all models can be found in Appendix A: Development of recursions, and all code necessary to reproduce the analyses are available at <https://github.com/colin-olito/dioecySA>, or from the author upon request.

## 6.3 Results

### 6.3.1 Invasion into monomorphic populations

#### Gynodioecy:

We begin with the evolution of gynodioecy by the invasion of a dominant male-sterility allele,  $M_2$ , into populations initially fixed for the  $AAM_1M_1$  and  $aaM_1M_1$  genotypes. We focus on results for additive fitness effects at the **A** locus, and discuss the effect of dominance reversals at the end of each section of the results. Solving for the conditions where  $\lambda_A > 1$ , we were able to recover the well known single-locus invasion criteria for SA alleles under obligate outcrossing (Kidwell et al. 1977) and partial selfing (Jordan and Connallon 2014; Olito 2016), with either additive fitness effects, or dominance reversal. Solving  $\lambda_M > 1$  for  $k$  also yields the classic single-locus criterion for the invasion of females into a population of hermaphrodites (Eq(4) in Charlesworth and Charlesworth 1978a):

$$\hat{k} > 1 - 2C\delta. \quad (6.4)$$

The invasion conditions for a mutant haplotype bearing  $M_2$  depend on whether the population is initially fixed for the female-beneficial ( $A$ ) or male-beneficial ( $a$ ) allele at **A**. In both cases, solving  $\lambda_{AM} > 1$  for  $k$  yield expressions  $f(C, \delta, s_f, r)$  of the same basic form as Eq(6.4), in which  $k$  is a decreasing function of  $C\delta$ . For populations initially fixed for  $A$ , the haplotype invasion conditions are always more restrictive (requiring larger  $k$ ) than those described by Eq(6.4), except in the limit of complete linkage and no selection against  $a$  ( $r \rightarrow 0$  and  $s_f \rightarrow 0$ ). In contrast, for populations initially fixed for the male-beneficial allele,  $a$ , the invasion conditions become more permissive with either lower recombination, or stronger selection against  $a$ . Specifically, the condition for the spread of mutant  $AM_2$  haplotypes becomes more permissive than Eq(6.4) when

$$\frac{2r}{1+r} < s_f. \quad (6.5)$$

Eq(6.5) shows that the invasion of females into a population of hermaphrodites can be quite sensitive to linkage with a nearby SA locus. When selection is relatively weak ( $s_f = 0.1$ ), even modest linkage ( $r \approx 0.05$ ) can reduce the amount of reproductive compensation necessary for females to invade relative to the single-locus prediction.

Linkage with a male-sterility locus also influences the invasion of female-beneficial SA alleles. For example, under obligate outcrossing and additive fitness effects, the single-locus invasion condition for the female-beneficial allele,  $A$ , is  $s_f > s_m / (1 + s_m)$  (Kidwell et al. 1977; also from  $\lambda_A$ ). Substituting for  $s_f$  in Eq(6.5) and solving for  $r$  yields the degree of linkage necessary to expand the invasion conditions for a female-benefit allele beyond the single-locus criterion:

$$r < \frac{s_m}{2 + s_m}. \quad (6.6)$$

By the same method, the criterion for the invasion of a female-beneficial allele under partial selfing and additive fitness effects will become more permissive than the single-locus criterion when

$$r < \frac{s_m(1 - C)}{2 + s_m + C(2 - s_m - 4\delta)}. \quad (6.7)$$

Eq(6.7) shows that the scope for linkage between SA loci to expand the parameter space where female-beneficial alleles can invade is reduced with higher selfing (larger  $C$ ), but inbreeding depression (larger  $\delta$ ) can compensate for this effect by 'enforcing' outcross reproduction. This outcome arises directly from the increasing "female bias" in selection caused by selfing. With higher selfing, there is simply less parameter space where linkage with a male-sterility locus can facilitate the invasion of the female-beneficial allele (Jordan and Connallon 2014; Olito 2016).

### Androdioecy:

We performed a stability analysis for the model for the evolution of androdioecy via the invasion of a dominant female-sterility allele,  $M_2$ , into populations initially fixed for the  $AAM_1M_1$  genotype or the  $aaM_1M_1$  genotype. As before, analysis of  $\lambda_A$  recovered the single-locus invasion criteria for SA alleles under obligate outcrossing and partial selfing under both additive fitness effects and dominance reversal conditions. Likewise, solving  $\lambda_M > 1$  for  $k$  yielded the familiar invasion criterion for males into a population of hermaphrodites (Eq(8) in Charlesworth and Charlesworth 1978a),

$$\hat{k} > \frac{1 + C(1 - 2\delta)}{(1 - C)}. \quad (6.8)$$

Not surprisingly, the invasion conditions for mutant haplotypes bearing  $M_2$  again depended on the initial fixed genotype of the hermaphrodite population, and solving  $\lambda_{AM} > 1$  for  $k$  yields expressions  $f(C, \delta, s_m, r)$  of the same form as Eq(6.8). Mirroring the results of the previous model, the conditions satisfying  $\lambda_{AM} > 1$  for the invasion of a mutant haplotype were always more restrictive than Eq(6.8) when the population was initially fixed for the male-beneficial allele ( $a$ ; except when  $s_m \rightarrow 0$  and  $r \rightarrow 0$ ), and more permissive for populations initially fixed for the female-beneficial allele ( $A$ ). In fact, replacing  $s_f$  with  $s_m$  in Eq(6.5) gives the conditions under which invasion of males via the spread of mutant  $aM_1$  haplotypes become more permissive than the single locus criteria described by Eq(6.8). Thus, although the conditions necessary for the evolution of androdioecy are more restrictive than for gynodioecy overall, linkage to a SA locus similarly impacts the invasion conditions for female-sterility alleles and for male-sterility alleles.

The effect of linkage with a female-sterility locus on the invasion of male-beneficial SA alleles is nearly identical for the case of obligate outcrossing. This is due to the symmetry of the single-locus SA invasion conditions (Kidwell et al. 1977). In this case, substituting  $s_m$  in for  $s_f$  in Eq(6.6) gives the conditions where invasion of male-beneficial alleles becomes more permissive than the single-locus predictions. However, the case is altered substantially in partially selfing populations. For example, assuming additive fitness effects, linkage to a female-sterility locus expands the invasion conditions of male-beneficial alleles at an SA locus when

$$r < \frac{s_f + s_f C(1 - 2\delta)}{2 + s_f - 2C + s_f C(1 - 2\delta)}. \quad (6.9)$$

The right hand side of Eq(6.9) increases with both  $C$  and  $s_f$  such that, for  $C > 1/3$ , there is always some expansion of the parameter space where male-beneficial alleles can invade beyond the single-locus expectation, even under free-recombination with the female-sterility locus ( $r = 1/2$ ).

### 6.3.2 Invasion of unisexuals into polymorphic populations

Three factors determine the fate of new sterility mutations in populations that are initially polymorphic at **A**: the degree of reproductive compensation ( $k$ ), the rate of recombination ( $r$ ), and the selfing rate ( $C$ ). Unisexuals are always able to invade populations with segregating SA variation if either Eq(6.4) (for gynodioecy) or Eq(6.8) (for androdioecy) are satisfied (fig. 6.1; light blue lines). Unisexuals can still invade when  $k < \hat{k}$ , provided there is some linkage between **A** and **M**. For example, under obligate outcrossing and tight linkage, unisexuals can invade a polymorphic population across  $\approx 69\%$  of relevant parameter space (defined by  $s_f \times s_m$  where  $0 < s_f, s_m \leq 0.5$ , and  $F_{ij}^* > 0$ ), despite a 10% reduction in gamete production relative to hermaphrodites (fig. 6.1A,D). With smaller reductions in relative gamete production, unisexuals can invade across a greater fraction of parameter space, even when linkage is quite weak (e.g.,  $\approx 38\%$  when  $k = \hat{k} \times 0.95$  and  $r = 0.2$ ).

Unisexuals can invade under similar conditions if the selfing rate among hermaphrodites is relatively low and inbreeding depression is relatively high ( $C = 1/4$ ,  $\delta = 4/5$ ) (fig. 6.1B,E). This because under these conditions the majority of offspring are produced through outcrossing rather than selfing. For populations with relatively high selfing rates among hermaphrodites and low inbreeding depression ( $C = 3/4$ ,  $\delta = 1/5$ ), major differences between the models of gynodioecy and androdioecy emerge. Most notably, much tighter linkage is required for the male-sterility mutation to spread when  $k < \hat{k}$ . Even then, unisexual females will only invade if the reduction in ovule production by females relative to hermaphrodites is quite small (fig. 6.1C,F). In contrast, the invasion of female-sterility mutations does not become sensitive to  $r$ , and unisexual males can invade over similar fractions of parameter space as in predominantly outcrossing populations. This contrast in the effect of selfing between the models of gynodioecy and androdioecy is a consequence of the increasing female-bias in the net direction of SA selection caused by increased selfing among hermaphrodites (Charlesworth and Charlesworth, 1978a; Jordan and Connallon 2014; Olito 2016). As individuals self-fertilize at a greater rate, there is reduced scope for selection to act on traits influencing performance via the male sex function (e.g., traits pollen export). Analogous to previous results for linked SA loci (Olito 2016), as the female-bias in SA selection increases with selfing, there is greater scope for linkage to a male-beneficial SA allele to facilitate invasion of a female-sterility mutation.

In the models of both gynodioecy and androdioecy, the loss of parameter space where unisexuals can invade is determined by the rate of recombination, the degree of reproductive compensation, and the relative strength of selection through each sex-function. With weaker linkage between **A** and **M**, invasion of unisexuals requires stronger SA selection coefficients that must also be increasingly biased toward the gender of the invading unisexuals. Hence, the invasion of male-sterility alleles requires female-biased selection, while the invasion of female-sterility requires male-biased selection (see figs. S1–S6 in Appendix B: Supplementary figures).

### 6.3.3 Equilibrium frequencies of unisexuals

When unisexual sterility alleles arise in linkage with another polymorphic SA locus, it can result in elevated equilibrium frequencies of unisexuals relative to single-locus predictions. If reproductive compensation by unisexuals satisfies the conditions for single-locus invasion of  $M_2$  (i.e.,  $k \geq \hat{k}$ ), the increase in the equilibrium frequency of unisexuals relative to single-locus predictions can be quite large (fig. 6.2, greyscale

lines). As long as linkage among the SA loci remains relatively tight ( $r < 0.05$ ), the effect is strongest in predominantly outcrossing populations, and becomes weaker with increasing selfing rates among hermaphrodite individuals (with concomitant decrease in inbreeding depression; see [Models](#)). With weaker linkage, the two-locus predictions converge on those of the single-locus models. Although the single-locus invasion condition for the  $M_2$  allele ( $\hat{k}$ ) is significantly higher for androdioecy than gynodioecy (Eq.6.4 vs. Eq.6.8), linkage among SA loci results in similarly elevated equilibrium frequencies of unisexuals in either model.

When linkage exists among SA loci, unisexual sterility alleles can still invade when reproductive compensation falls below the single-locus threshold for invasion ( $k < \hat{k}$ ; fig. 6.3). Under tight linkage, the increase in equilibrium unisexual frequencies is again greatest for predominantly outcrossing populations, and decreases as the rate of self-fertilization among hermaphrodite individuals increases (fig. 6.3A,C). This effect diminishes with weaker linkage, where equilibrium unisexual frequencies drop to 0 with smaller and smaller decreases in reproductive compensation relative to the single locus invasion criterion (fig. 6.3B,D). In this case, the decrease in equilibrium male frequencies in the model of androdioecy was more sensitive to reductions in  $k$  relative to  $\hat{k}$  than for the model of gynodioecy. Under weaker linkage or lower reproductive compensation, equilibrium frequencies of unisexuals are predicted to be highest for populations with intermediate selfing rates. This pattern results from three counterbalancing effects arising from our assumption that inbreeding depression,  $\delta$ , decreases with the selfing rate,  $C$ , in our simulations. On one hand, higher selfing rates favour the invasion of unisexuals by increasing the rate at which  $M_2M_2$  homozygotes (unisexuals in the recessive models) are formed from rare  $M_2$  mutants increases, and lowers inbreeding depression. On the other hand, unisexuals can only reproduce by outcrossing, and higher selfing eventually limits their contribution to the genetic composition of the next generation.

## 6.4 Discussion

The first theoretical insight provided by our models is that linkage to SA loci facilitates the invasion of unisexual sterility alleles, and elevates the equilibrium frequencies of unisexuals relative to single-locus predictions. The second is that when linkage is relatively tight, this effect is greatest for predominantly outcrossing populations – suggesting that the ancestral hermaphrodite selfing rate may play a different role in the evolution of separate sexes than predicted by the classic models of (Charlesworth and Charlesworth, 1978a). Overall, these predictions suggest that the unisexual sterility alleles driving the evolution of dimorphic sexual systems are likely to evolve in genomic regions harboring polymorphic SA loci. When this occurs, elevated frequencies of unisexuals in the resulting gyno- and androdioecious populations are more likely to evolve than previously predicted, facilitating subsequent transitions to separate sexes (Charlesworth and Charlesworth, 1978a). Below, we discuss the implications of our findings, and suggest empirical tests of our predictions, in three main contexts: SA polymorphism and the evolution of gyno- and androdioecy, hermaphrodite mating systems and the evolution of dioecy, and the population genetic basis of the evolution of separate sexes.

### 6.4.1 SA Polymorphism and the evolution of dimorphic sexual systems

Although dioecy is relatively uncommon among angiosperms (represented in  $\approx 7\%$  of genera), the fantastic diversity and repeated evolution of dimorphic sexual systems in flowering plants begs a genetical explanation (Renner 2014; Käfer et al. 2017). Several evolutionary pathways, and a variety of genetic mechanisms, lead from hermaphroditism to separate sexes, but all ultimately involve the evolutionary invasion of at least two unisexual sterility alleles (Charlesworth and Charlesworth, 1978a; Charlesworth and Charlesworth, 1978b; Renner 2014; Ashman et al. 2015). When accompanied by allocation trade-offs between sex-functions, unisexual sterility alleles are an important class of SA allele, yet previous theory has not considered the potential influence of standing SA genetic variation, or genetic architecture, on their invasion and establishment in hermaphroditic populations. Our theoretical results suggest that physical linkage among SA loci can strongly influence the evolution of gyno- or androdioecy from hermaphroditism, expanding the conditions under which dimorphic sexual systems, and ultimately separate sexes, are predicted to evolve.

Classical theoretical predictions, based on single-locus models, suggest that conditions for the evolution of dioecy may be stringent (Lloyd 1975, 1976; Charlesworth and Charlesworth, 1978a; Käfer et al. 2017). For unisexual sterility alleles to invade, the resulting unisexuals must adequately compensate for the loss of a sex function through increased gamete production. On the other hand, we find that the conditions for the spread of unisexual sterility alleles can be quite permissive – especially if the sterility mutation arises on a haplotype bearing a complimentary SA allele (e.g., one that is beneficial for the same sex-function as the invading unisexuals). In this case, invasion requires only modest linkage for biologically plausible selection coefficients (e.g.,  $s_f, s_m \leq 0.1$ ). When linkage does exist, the fitness effects of the complimentary SA allele help offset the loss of a sex function, and reduce the amount of reproductive compensation required by unisexuals to invade the population (i.e., relative to single-locus predictions; Charlesworth and Charlesworth 1978a). These results are similar to other multilocus models of sex-specific selection and mutations, which show that predominantly female-harming mutations tend to accumulate on haplotypes carrying male-benefit alleles (Connallon and Jordan 2016). An important corollary of this result is that the conditions for the maintenance of SA polymorphism are also expanded by linkage to sex-specific sterility mutations. Hence, new unisexual sterility mutations underpinning dimorphic sexual systems are most likely to evolve in tight linkage with other SA loci, and should simultaneously promote the maintenance of SA polymorphism at linked loci.

The amount of standing SA genetic variation should directly influence the potential for hermaphroditic populations to evolve dimorphic sexual systems. Although the invasion conditions for unisexual sterility alleles into populations without segregating SA variation are generally favourable, the waiting time for double mutants with the necessary haplotype (e.g., female-beneficial–male-sterile) to appear could be long (Weinreich and Chao 2005; Connallon and Clark 2010). However, we find that the invasion conditions for unisexual sterility alleles are still quite permissive when there is standing SA genetic variation in hermaphroditic populations. Although it is not yet clear how much SA genetic variation for fitness is harbored by hermaphroditic species, three features of SA selection suggest that this is not an unlikely scenario, particularly in large populations. First, balancing selection is predicted to maintain SA polymorphism in partially selfing populations over a broad spectrum of parameter conditions, particularly when SA loci are linked (Patten et

al. 2010; Jordan and Connallon 2014; Olito 2016). Second, net directional selection under SA is predicted to be small, even when fitness effects in each sex are large, resulting in relatively long persistence times of SA alleles (Connallon and Clark 2012). This facilitates the formation of double-mutant haplotypes (e.g., Weinreich and Chao 2005), and leads to an elevated contribution of SA alleles to fitness variance compared to other classes of mutations (e.g., unconditionally beneficial or deleterious alleles; Connallon and Clark 2012). Third, although definitively indentifying SA loci is challenging, there is empirical evidence suggesting that segregating SA allele frequencies can be non-trivial, even in partially selfing hermaphroditic populations (Barson et al. 2015; Lee et al. 2016). Additional studies attempting to quantify the degree of SA genetic variation in hermaphroditic species would help clarify the potential for dimorphic sexual systems to evolve from hermaphroditism, especially if they were to target species exhibiting intraspecific variation in the degree or frequency of dimorphic sexual systems (e.g., many of the species reviewed in Sakai and Weller 1999; Barrett 2010; Renner 2014).

#### 6.4.2 Mating systems and the evolution of dioecy

The interplay between hermaphrodite mating systems and reproductive compensation is a key factor influencing the evolution of separate sexes in flowering plants, especially via the gynodioecy pathway (Darwin 1877; Charlesworth and Charlesworth, 1978a). Prior theory predicts that the evolution of gynodioecy is driven by the combination of reproductive compensation by unisexuals, and avoidance of inbreeding depression, and is therefore most likely to occur in partially selfing populations (Lewis 1942; Lloyd 1975; Charlesworth and Charlesworth, 1978a; Käfer et al. 2017). This follows directly from the structure of Eq(6.4) where  $\hat{k}$  is determined entirely by the product of the selfing rate and inbreeding depression ( $C\delta$ ). In contrast, the evolution of androdioecy is predicted to require significantly higher reproductive compensation, especially in partially selfing populations, because invading males must still compete with selfing hermaphrodites to fertilize ovules (Charlesworth and Charlesworth, 1978b; Käfer et al. 2017).

The population selfing rate plays a similarly critical role in our models. Linkage to a SA locus both expands conditions for invasion, and elevates the equilibrium frequencies, of unisexual individuals. Yet the effect of linkage, relative to single-locus models, is particularly pronounced in hermaphrodite populations with low rates of self-fertilization, and least pronounced in those with high selfing rates. The evolution of higher equilibrium frequencies of females in the gynodioecy model is particularly important as this should facilitate the subsequent evolution of dioecy via invasion of partial female-sterility mutations (Charlesworth and Charlesworth, 1978a; Charlesworth and Charlesworth, 1978b; Charlesworth 1999, 2006). The major implication is that when male-sterility mutations do arise in linkage with other SA loci, single-locus theory may significantly underestimate the potential for gynodioecy, and subsequently dioecy, to evolve in predominantly outcrossing species. Moreover, outcrossing hermaphrodite populations are more likely to harbor segregating SA genetic variation than selfing ones (Jordan and Connallon 2014; Olito 2016). The ancestral mating systems in which linkage to a polymorphic SA locus is predicted to have the largest effect on evolutionary transitions to dioecy are also the ones that are most likely to harbor segregating SA variation.

For the evolution of androdioecy, modest linkage to an SA locus broadens the conditions for invasion of female-sterility alleles, even for highly selfing populations. Linkage also increases equilibrium conditions frequencies of unisexual males

(given invasion), particularly in populations with low selfing-rates. Thus, when linkage exists between a female-sterility allele and another SA locus, single-locus theory may underestimate the potential for the evolution of androdioecy, and subsequently, of dioecy. However, our models agree with previous theory that the conditions for invasion of female-sterility alleles in partially selfing populations are still quite stringent, requiring very high reproductive compensation (large  $k$ ; Charlesworth and Charlesworth 1978a, Eq(6.8)). Overall, linkage with an SA locus will always facilitate the invasion of female-sterility mutations, but the evolution of androdioecy, and dioecy via the androdioecy pathway, is still expected to be quite rare relative to gynodioecy (Charlesworth and Charlesworth, 1978a; Charlesworth 2006; Käfer et al. 2017; Renner 2014).

Despite the longstanding theoretical prediction of a strong correlation between the hermaphrodite mating system and dioecy, empirical evidence for this association remains equivocal (Charlesworth 1985, 2006; Renner 2014). Our predictions suggest a partial explanation for this weak association. In species where unisexual sterility alleles arise in linkage with another SA locus, evolutionary transitions to dimorphic sexual systems should be elevated in taxa with predominantly outcrossing hermaphrodite ancestors. However, not all transitions to dioecy will have occurred by our proposed mechanism, and the net effect will be a weakened correlation between the ancestral hermaphrodite selfing rate, and dioecy. In light of our results, a re-examination of the evolutionary association between angiosperm mating and sexual systems using modern phylogenetic comparative methods would be most interesting, and would help identify species where our proposed mechanism for the evolution of gynodioecy is most likely to have played a role (e.g., species with dimorphic sexual systems that appear to have evolved from predominantly outcrossing ancestors).

### 6.4.3 The population genetic basis of the evolution of separate sexes

Our results also have implications for the role of SA alleles during the early stages of sex chromosome evolution. The process of sex chromosome origin and differentiation into distinct X and Y (or Z and W) chromosomes is thought to proceed by the following series of steps. First, a sex-determining locus originates on an ordinary pair of autosomes. Second, SA genes linked to the sex-determining locus accumulate over time. Third, this linked SA variation drives the evolution suppressed recombination between the neo sex-chromosomes, generally via chromosomal inversions. Fourth, the non-recombining sex chromosome degenerates (usually). Finally, mechanisms of dosage compensation evolve in response to the loss of coding regions on the degenerate sex chromosome (sometimes) (Rice 1987; Charlesworth 2002; Bachtrog 2006; Qiu et al. 2013; Bachtrog et al. 2014).

A key assumption that the emergence of a sex-determining locus is the first step in this process traces back (again) to classic population genetic theory of unisexual sterility alleles. The key prediction is that after the invasion of a recessive male-sterility allele (yielding gynodioecy), the subsequent invasion of dominant gender modifiers leading to full dioecy require tight linkage to the first male-sterility locus (the linkage constraint of Charlesworth and Charlesworth 1978a). This process leads to a tightly coupled pair of sex-determining loci, effectively a single sex determining locus. Once this sex determining locus arises, further differentiation following the steps outlined above can result in heteromorphic sex chromosomes.

Our theoretical results suggest a previously unrecognized, or at least underappreciated, role for SA genetic variation in hermaphroditic taxa during these initial

stages of sex-chromosome evolution. Our finding that linkage with a polymorphic SA locus facilitates the invasion of unisexual sterility alleles strongly suggests that the accumulation of SA genetic variation may actually precede the origin of sex-determination loci. In other words, SA may represent the first (rather than a subsequent) step in the origin and evolution of new sex chromosome systems. This process is similar to prior theory regarding sex chromosome turnover (vanDoorn and Kirkpatrick 2007, 2010), but is distinct in that it begins with SA variation in hermaphroditic populations, and deals with the invasion of unisexual sterility alleles rather than master sex-determining loci. In addition, our finding that linkage drives the evolution of elevated equilibrium frequencies of unisexual females should also facilitate the subsequent evolution of dioecy via tightly linked gender modifiers yielding separate sexes (Charlesworth and Charlesworth, 1978a). The resulting complex of linked SA and sterility loci effectively establishes a nascent sex-determining-region on the neo sex-chromosome pair. If pre-existing SA polymorphism at the linked SA locus survives the transition to dioecy, the process of accumulating SA variation prior to recombination suppression will have already begun – setting the stage for the subsequent accumulation of linked SA genetic variation and recombination suppression leading to sex-chromosome differentiation (Charlesworth and Charlesworth, 1978a; Rice 1987; Bachtrog 2006; Qiu et al. 2013). Given the crucial role of linkage in each of these steps, it seems plausible that the degree of SA genetic variation present when an initial male-sterility mutation arises may help explain the large variation in the rate and extent of sex-chromosome differentiation in angiosperms (Charlesworth 2002; Renner 2014; Bachtrog et al. 2014).

## 6.5 Tables

TABLE 6.1: Fitness expressions for diploid adults prior to reproduction for the model of a dominant male-sterility mutation ( $w_{ij}^f$  denotes fitness effects through the female sex-function,  $w_{ij}^m$  for male sex-function).

Haplotype	$AM_1$	$AM_2$	$aM_1$	$aM_2$
Female sex-function				
$AM_1$	1	$(1+k)$	$(1-h_f s_f)$	$(1-h_f s_f)(1+k)$
$AM_2$	—	$(1+k)$	$(1-h_f s_f)(1+k)$	$(1-h_f s_f)(1+k)$
$aM_1$	—	—	$(1-s_f)$	$(1-s_f)(1+k)$
$aM_2$	—	—	—	$(1-s_f)(1+k)$
Male sex-function				
$AM_1$	$(1-s_m)$	0	$(1-h_m s_m)$	0
$AM_2$	—	0	0	0
$aM_1$	—	—	1	0
$aM_2$	—	—	—	0

Note: Rows and columns indicate the  $i$ th and  $j$ th gametic haplotype respectively. The lower triangle of each matrix is the reflection of the upper triangle, and is omitted for simplicity and consistency with the  $i \geq j$  row/column indexing used throughout the article.

## 6.6 Figures

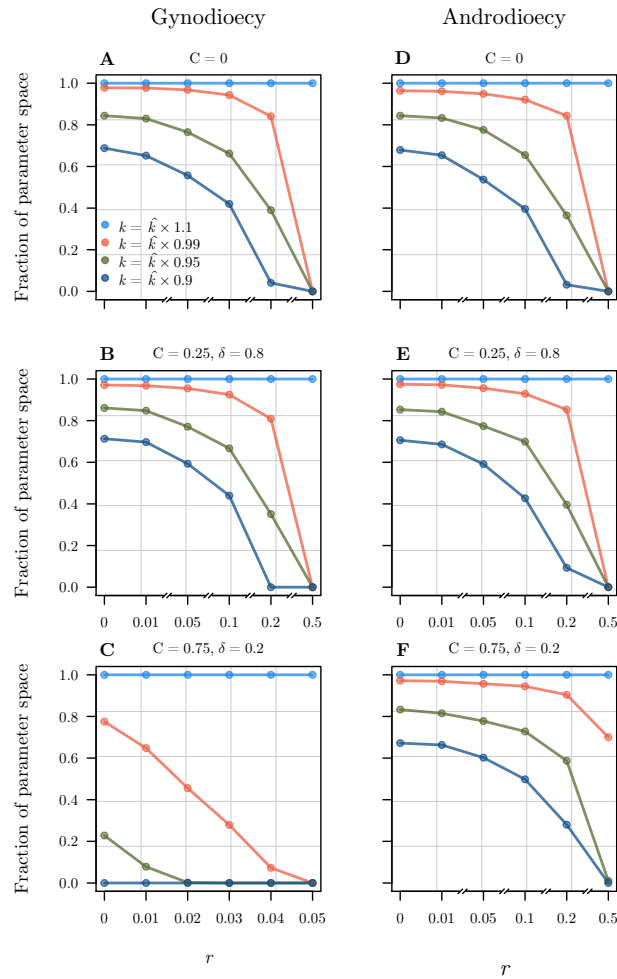


FIGURE 6.1: Invasion of unisexuals into populations with pre-existing SA polymorphism. Plots show the fraction of parameter space (defined by  $s_f \times s_m |E_{ij}^*, G_{ij}^* > 0$  and  $0 < s_f, s_m \leq 0.5$ ) where a dominant sex-specific sterility allele at  $\mathbf{M}$ , can invade populations initially at single-locus equilibrium frequencies for  $\mathbf{A}$  with additive fitness effects ( $h_f = h_m = 1/2$ ), plotted as a function of the recombination rate  $r$ . Panels A–C show results from the model of gynodioecy via invasion of a male-sterility allele, while panels D–F show results for the model of androdioecy via invasion of a female-sterility allele. For each panel, results are shown for different values of reproductive compensation,  $k$ , chosen as a fraction of the single-locus invasion criterion for  $M_2$  defined by Eq(6.4) and Eq(6.8) for the models of gynodioecy and androdioecy respectively. Hence, the orange, green, and dark blue lines show scenarios where unisexuals experience a decrease in gamete production relative to hermaphrodites of 1, 5, and 10%. Note the different scale for the x-axis in panels C and F. Results were obtained by evaluating the three candidate leading eigenvalues ( $\lambda_{\mathbf{A}}, \lambda_{\mathbf{M}}, \lambda_{\mathbf{AM}}$ ) of the Jacobian matrix of the genotype  $\times$  transmission mode recursions for populations at the above initial conditions for 1000 points uniformly distributed throughout the relevant  $s_f \times s_m$  parameter space.

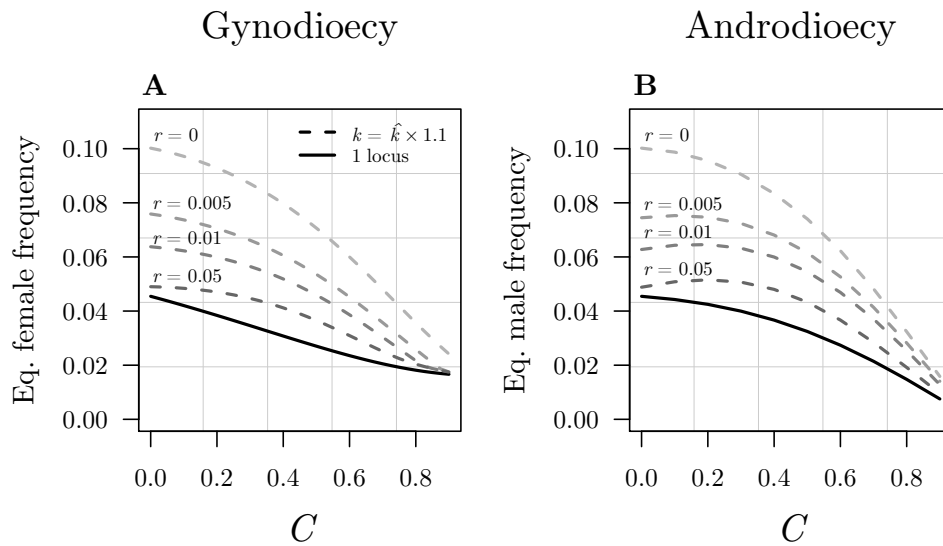


FIGURE 6.2: Equilibrium frequencies of unisexual (A) females, and (B) males, compared with single-locus predictions when reproductive compensation is above the single-locus threshold (i.e.,  $k > \hat{k}$ ). Results are shown for the models of gyno- and androdioecy via invasion of recessive unisexual sterility alleles, additive fitness effects at **A** ( $h_f = h_m = 0.5$ , using selection coefficients of  $s_m = 0.1$  (for the model of gynodioecy) and  $s_f = 0.1$  (for the model of androdioecy), and inbreeding depression that follows  $\delta = \delta^*(1 - C/2)$  (see [Models](#)). Plots illustrate the increase in equilibrium frequencies of unisexuals predicted by our two-locus models (dashed greyscale lines) relative to the corresponding exact single-locus equilibrium frequencies (solid black line;  $\hat{Z}$  predicted by Charlesworth and Charlesworth 1978a). Results are shown for four different levels of recombination, highlighting that with weaker linkage, the two-locus predictions converge on those of the single-locus model.

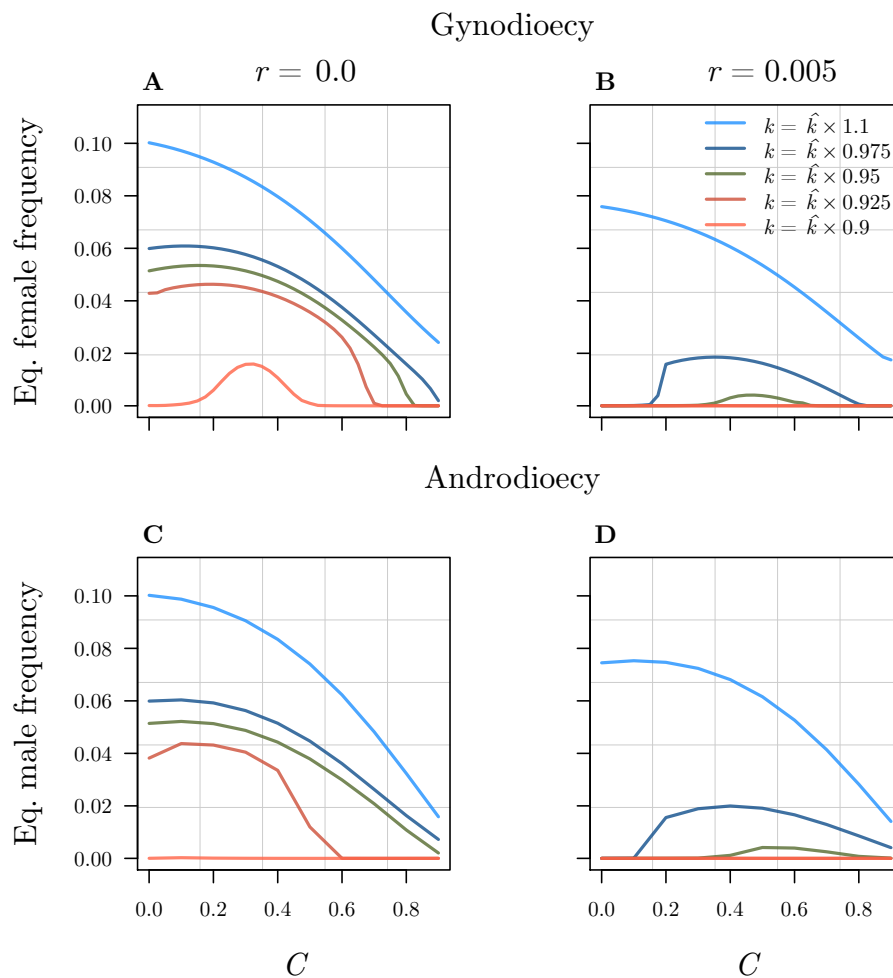


FIGURE 6.3: Equilibrium frequencies of unisexual (A–B) females and (C–D) males across a gradient of reproductive compensation. Results are shown for the models of gyno- and androdioecy via invasion of recessive unisexual sterility alleles, additive fitness effects at A ( $h_f = h_m = 0.5$ , using selection coefficients of  $s_m = 0.1$  (for the model of gynodioecy) and  $s_f = 0.1$  (for the model of androdioecy), and inbreeding depression that decreases linearly with the selfing rate:  $\delta = \delta^*(1 - C/2)$  (see [Models](#)). Plots show the equilibrium frequencies of unisexuals predicted by our models for five different levels of reproductive compensation, calculated as a fraction of the single-locus invasion criterion for  $M_2$  defined by Eq(6.4) and Eq(6.8). Note that the single-locus equilibrium frequency of unisexuals always equals 0 when  $k < \hat{k}$ . Hence, the lines corresponding to  $k < \hat{k}$  illustrate how linkage among SA loci expands the parameter space where unisexual sterility alleles can invade beyond the predictions of the single-locus models.

## 6.7 Appendix A: Development of recursions

Here, we fully develop the system of genotype  $\times$  transmission mode recursion equations underlying each of the four models described in the main text: the evolution of gynodioecy via invasion of a (1) completely dominant, or (2) completely recessive male-sterility allele; and the evolution of androdioecy via the invasion of a (3) completely dominant or (4) completely recessive female-sterility allele. We start by briefly re-iterating the main assumptions of the models. We then describe the calculation of adult frequencies after inbreeding depression, as this is the same for all four models. We then walk through the derivation of each of the four models in turn. Where possible, we highlight only essential differences between models rather than re-deriving identical equations.

### 6.7.1 Assumptions

Consider the genetic system described in the main text – two diallelic autosomal loci, **A** (with alleles  $A, a$ ) and **M** (with alleles  $M_1, M_2$ ), that recombine at rate  $r$  per meiosis, in a large, initially hermaphroditic, population. Assume that the **A** locus is under sexually antagonistic selection, with the  $A$  allele having female-beneficial (male-deleterious) fitness effects, and the  $a$  allele having male-beneficial (female-deleterious) fitness effects. Assume also that the  $M_1$  allele at the **M** locus has a relative fitness of 1 for both sex-functions, while the  $M_2$  allele causes complete sterility through one sex function (e.g., via cessation of production, or the production of inviable pollen or ovules). The population rate of self-fertilization,  $C$ , is assumed to be independent of the genotype at the **A** locus, while the genotype at the **M** locus determines whether or not a genotype is capable of self-fertilization. We also assume a constant population level of inbreeding depression,  $\delta$ , and that a vanishingly small amount of pollen is adequate for successful self-fertilization. Generations are assumed to be non-overlapping, and the life-cycle for all models proceeds as follows: fertilization  $\rightarrow$  inbreeding depression  $\rightarrow$  selection  $\rightarrow$  fertilization.

### 6.7.2 Adult genotypic frequencies after inbreeding depression

There are four possible combinations of alleles at the **A** and **M** loci that can be found on any chromosome:  $AM_1, AM_2, aM_1, aM_2$ . Let  $x_i$  and  $y_j$  denote the haplotype frequencies  $[AM_1, AM_2, aM_1, aM_2]$  in female and male gametes respectively. The calculation of adult genotypic frequencies after inbreeding is identical for all models. Let  $F_{ij}$  denote the frequency among offspring of the genotype formed by the union of the  $i$ th and  $j$ th gametic haplotypes via outcrossing. Similarly, let  $G_{ij}$  denote the frequency among offspring of the genotype formed by the union of the  $i$ th and  $j$ th gametic haplotype via self-fertilization. We assume no parent-of-origin effects on fitness, and so index the ten possible pairs of gametic haplotypes where  $i \geq j$  hereafter. The frequency of each genotype among adults after inbreeding depression,  $F_{ij}^A$ , will then be:

$$F_{ij}^A = \frac{F_{ij} + G_{ij}(1 - \delta)}{D}, \quad (6.A1)$$

where

$$\bar{D} = \sum_{i=1}^4 \sum_{j=i}^4 F_{ij} + \sum_{i=1}^4 \sum_{j=i}^4 G_{ij}(1 - \delta). \quad (6.A2)$$

### 6.7.3 Gynodioecy via dominant male-sterility mutation

For the model of the evolution of gynodioecy via the invasion of a completely dominant male-sterility mutation at **M**, the successful invasion of the  $M_2$  allele, either alone or coupled with an allele at the **A** locus as a haplotype, represents the evolution of gynodioecy from simultaneous hermaphroditism. The fitness expressions for adult genotype  $ij$  through the female and male sex-function can be expressed in  $4 \times 4$  matrices, with elements  $w_{ij}^f$  (for female-function), and  $w_{ij}^m$  (for male-function), yielding Table 1 from the main text:

TABLE 6.A1: Fitness expressions for diploid adults prior to reproduction for the model of a dominant male-sterility mutation ( $w_{ij}^f$  denotes fitness effects through the female sex-function,  $w_{ij}^m$  for male sex-function).

Haplotype	$AM_1$	$AM_2$	$aM_1$	$aM_2$
Female-function				
$AM_1$	1	$(1 + k)$	$(1 - h_f s_f)$	$(1 - h_f s_f)(1 + k)$
$AM_2$	–	$(1 + k)$	$(1 - h_f s_f)(1 + k)$	$(1 - h_f s_f)(1 + k)$
$aM_1$	–	–	$(1 - s_f)$	$(1 - s_f)(1 + k)$
$aM_2$	–	–	–	$(1 - s_f)(1 + k)$
Male-function				
$AM_1$	$(1 - s_m)$	0	$(1 - h_m s_m)$	0
$AM_2$	–	0	0	0
$aM_1$	–	–	1	0
$aM_2$	–	–	–	0

Note: Rows and columns indicate the  $i$ th and  $j$ th gametic haplotype respectively. The lower triangle of each matrix is the reflection of the upper triangle, and is omitted for simplicity and consistency with the  $i \geq j$  row/column indexing used throughout the article.

The total number of ovules produced by the population at reproduction will be proportional to

$$O_T = \sum_{i=1}^4 \sum_{j=i}^4 F_{ij}^A w_{ij}^f. \quad (6.A3)$$

Because  $M_2$  is assumed to be completely dominant, only those genotypes that are homozygous for  $M_1$  are phenotypically hermaphrodite, and therefore able to self-fertilize. The proportion of ovules that are self-fertilized will therefore be proportional to

$$S = C \left( \frac{F_{11}^A w_{11}^f + F_{13}^A w_{13}^f + F_{33}^A w_{33}^f}{O_T} \right). \quad (6.A4)$$

The proportion of ovules fertilized via outcrossing is the complement of  $S$ , and will be proportional to

$$(1 - S) = \left( \frac{(1 - C)(F_{11}^A w_{11}^f + F_{13}^A w_{13}^f + F_{33}^A w_{33}^f) + U}{O_T} \right), \quad (6.A5)$$

where  $U = F_{12}^A w_{12}^f + F_{14}^A w_{14}^f + F_{22}^A w_{22}^f + F_{23}^A w_{23}^f + F_{24}^A w_{24}^f + F_{34}^A w_{34}^f + F_{44}^A w_{44}^f$  is the total frequency of unisexual females (all genotypes either heterozygous or homozygous for  $M_2$ ).

Only the three genotypes that are homozygous for  $M_1$  are phenotypically hermaphrodite and able to self-fertilize. The proportional contribution of self-fertilized offspring by each of these genotypes are then:

$$\begin{aligned} o_{11}^S &= C \left( \frac{F_{11}^A w_{11}^f}{O_T^S} \right) \\ o_{13}^S &= C \left( \frac{F_{13}^A w_{13}^f}{O_T^S} \right) \\ o_{33}^S &= C \left( \frac{F_{33}^A w_{33}^f}{O_T^S} \right), \end{aligned} \quad (6.A6)$$

where  $O_T^S = C(F_{11}^A w_{11}^f + F_{13}^A w_{13}^f + F_{33}^A w_{33}^f)$ , and simplify down to the relative genotypic frequencies after selection.  $o_{ij}^S = 0$  for all genotypes that are phenotypically unisexual (female). The relevant genotypic recursions (Eq(2) in the main text) describing the frequency in the next generation of each genotype among zygotes derived from self-fertilization are then:

$$\begin{aligned} G'_{11} &= S(o_{11}^S + o_{13}^S/4) \\ G'_{13} &= S(o_{13}^S/2) \\ G'_{33} &= S(o_{33}^S + o_{13}^S/4), \end{aligned} \quad (6.A7)$$

and all  $G'_{ij} = 0$  where  $ij \neq [11, 13, 33]$ .

The genotypic frequency recursions for offspring derived via outcrossing follows similar logic. The proportional contribution of each genotype to the pool of outcrossed ovules are

$$\begin{aligned} o_{11}^X &= (1 - C)(F_{11}^A w_{11}^f)/O_T^X \\ o_{12}^X &= (F_{12}^A w_{12}^f)/O_T^X \\ o_{13}^X &= (1 - C)(F_{13}^A w_{13}^f)/O_T^X \\ o_{14}^X &= (F_{14}^A w_{14}^f)/O_T^X \\ o_{22}^X &= (F_{22}^A w_{22}^f)/O_T^X \\ o_{23}^X &= (F_{23}^A w_{23}^f)/O_T^X \\ o_{24}^X &= (F_{24}^A w_{24}^f)/O_T^X \\ o_{33}^X &= (1 - C)(F_{33}^A w_{33}^f)/O_T^X \\ o_{34}^X &= (F_{34}^A w_{34}^f)/O_T^X \\ o_{44}^X &= (F_{44}^A w_{44}^f)/O_T^X, \end{aligned} \quad (6.A8)$$

where  $O_T^X = (1 - S)O_T$ . Only those genotypes that are phenotypically hermaphrodite are able to sire outcross offspring. The proportional contribution of each genotype that is phenotypically hermaphrodite to the pool of outcrossed pollen is equal to the

relative genotypic frequencies after selection:

$$\begin{aligned} p_{11}^X &= (F_{11}^A w_{11}^m) / P_T^X \\ p_{13}^X &= (F_{13}^A w_{13}^m) / P_T^X \\ p_{33}^X &= (F_{33}^A w_{33}^m) / P_T^X, \end{aligned} \quad (6.A9)$$

where  $P_T^X = F_{11}^A w_{11}^m + F_{13}^A w_{13}^m + F_{33}^A w_{33}^m$ . From the relative genotypic contributions to the pool of outcrossed ovules ( $o_{ij}^X$ ) and pollen ( $p_{ij}^X$ ), we can then calculate the haplotype frequencies among outcrossed ovules ( $x_i$ ) and pollen ( $y_i$ ) following standard two-locus theory. The haplotype frequencies among outcrossed ovules,  $x_i$ , are

$$\begin{aligned} x_1 &= o_{11}^X + \frac{o_{12}^X + o_{13}^X + o_{14}^X}{2} - r \left( \frac{o_{14}^X - o_{23}^X}{2} \right) \\ x_2 &= o_{22}^X + \frac{o_{12}^X + o_{23}^X + o_{24}^X}{2} + r \left( \frac{o_{14}^X - o_{23}^X}{2} \right) \\ x_3 &= o_{33}^X + \frac{o_{13}^X + o_{23}^X + o_{34}^X}{2} + r \left( \frac{o_{14}^X - o_{23}^X}{2} \right) \\ x_4 &= o_{44}^X + \frac{o_{14}^X + o_{24}^X + o_{34}^X}{2} - r \left( \frac{o_{14}^X - o_{23}^X}{2} \right), \end{aligned} \quad (6.A10)$$

and the haplotype frequencies among the pool of outcrossed pollen,  $y_i$ , are

$$\begin{aligned} y_1 &= p_{11}^X + p_{13}^X / 2 \\ y_2 &= 0 \\ y_3 &= p_{33}^X + p_{13}^X / 2 \\ y_4 &= 0. \end{aligned} \quad (6.A11)$$

The genotypic recursions describing the frequency in the next generation of each genotype among zygotes derived from outcrossing are calculated from these haplotype frequencies as:

$$\begin{aligned} F'_{11} &= (1 - S)(x_1 y_1) \\ F'_{12} &= (1 - S)(x_2 y_1) \\ F'_{13} &= (1 - S)(x_1 y_3 + x_3 y_1) \\ F'_{14} &= (1 - S)(x_4 y_1) \\ F'_{22} &= 0 \\ F'_{23} &= (1 - S)(x_2 y_3) \\ F'_{24} &= 0 \\ F'_{33} &= (1 - S)(x_3 y_3) \\ F'_{34} &= (1 - S)(x_4 y_3) \\ F'_{44} &= 0. \end{aligned} \quad (6.A12)$$

### 6.7.4 Gynodioecy via recessive male-sterility mutation

For the model of the evolution of gynodioecy via the invasion of a completely recessive male-sterility mutation at **M**, only genotypes that are homozygous for the  $M_2$  allele are phenotypically female. As described above, the adult genotypic frequencies,  $F_{ij}^A$ , are described by Equations 6.A1 and 6.A2. Now, the fitness expressions associated with each  $F_{ij}^A$  through the female and male sex-function are:

TABLE 6.A2: Fitness expressions for diploid adults prior to reproduction for the model of a recessive male-sterility mutation ( $w_{ij}^f$  denotes fitness effects through the female sex-function,  $w_{ij}^m$  for male sex-function).

Haplotype	$AM_1$	$AM_2$	$aM_1$	$aM_2$
Female-function				
$AM_1$	1	1	$(1 - h_f s_f)$	$(1 - h_f s_f)$
$AM_2$	—	$(1 + k)$	$(1 - h_f s_f)$	$(1 - h_f s_f)(1 + k)$
$aM_1$	—	—	$(1 - s_f)$	$(1 - s_f)$
$aM_2$	—	—	—	$(1 - s_f)(1 + k)$
Male-function				
$AM_1$	$(1 - s_m)$	$(1 - s_m)$	$(1 - h_m s_m)$	$(1 - h_m s_m)$
$AM_2$	—	0	$(1 - h_m s_m)$	0
$aM_1$	—	—	1	1
$aM_2$	—	—	—	0

Note: Rows and columns indicate the  $i$ th and  $j$ th gametic haplotype respectively. The lower triangle of each matrix is the reflection of the upper triangle, and is omitted for simplicity and consistency with the  $i \geq j$  row/column indexing used throughout the article.

The total number of ovules produced by the population at reproduction will again be proportional to

$$O_T = \sum_{i=1}^4 \sum_{j=i}^4 F_{ij}^A w_{ij}^f. \quad (6.A13)$$

Since the  $M_2$  allele is now assumed to be completely recessive, all genotypes not homozygous for  $M_2$  are phenotypically hermaphrodite, and therefore able to self-fertilize. The proportion of ovules that are self-fertilized will therefore be proportional to

$$S = C \left( \frac{F_{11}^A w_{11}^f + F_{12}^A w_{12}^f + F_{13}^A w_{13}^f + F_{14}^A w_{14}^f + F_{23}^A w_{23}^f + F_{33}^A w_{33}^f + F_{34}^A w_{34}^f}{O_T} \right), \quad (6.A14)$$

and the proportion of ovules fertilized via outcrossing is the complement of  $S$ :

$$(1 - S) = \left( \frac{(1 - C)(F_{11}^A w_{11}^f + F_{12}^A w_{12}^f + F_{13}^A w_{13}^f + F_{14}^A w_{14}^f + F_{23}^A w_{23}^f + F_{33}^A w_{33}^f + F_{34}^A w_{34}^f) + U}{O_T} \right), \quad (6.A15)$$

where  $U = F_{22}^A w_{22}^f + F_{24}^A w_{24}^f + F_{44}^A w_{44}^f$  is the total frequency of all unisexual females (all genotypes homozygous for  $M_2$ ).

The proportional contribution of each genotype to the pool of self-fertilized offspring is then:

$$\begin{aligned}
o_{11}^S &= C\left(\frac{F_{11}^A w_{11}^f}{O_T^S}\right) \\
o_{12}^S &= C\left(\frac{F_{12}^A w_{12}^f}{O_T^S}\right) \\
o_{13}^S &= C\left(\frac{F_{13}^A w_{13}^f}{O_T^S}\right) \\
o_{14}^S &= C\left(\frac{F_{14}^A w_{14}^f}{O_T^S}\right) \\
o_{23}^S &= C\left(\frac{F_{23}^A w_{23}^f}{O_T^S}\right) \\
o_{33}^S &= C\left(\frac{F_{33}^A w_{33}^f}{O_T^S}\right) \\
o_{34}^S &= C\left(\frac{F_{34}^A w_{34}^f}{O_T^S}\right), \tag{6.A16}
\end{aligned}$$

where  $o_{ij}^S = 0$  where  $ij \in [22, 24, 44]$ , and  $O_T^S = S \times O_T$ . The resulting genotypic recursions describing the frequency in the next generation of each genotype among zygotes derived from self-fertilization are then:

$$\begin{aligned}
G'_{11} &= S\left(o_{11}^S + \frac{o_{12}^S + o_{13}^S + o_{14}^S(1-r)^2 + o_{23}^S r^2}{4}\right) \tag{6.A17} \\
G'_{12} &= S\left(\frac{o_{12}^S + o_{14}^S r(1-r) + o_{23}^S r(1-r)}{2}\right) \\
G'_{13} &= S\left(\frac{o_{13}^S + o_{14}^S r(1-r) + o_{23}^S r(1-r)}{2}\right) \\
G'_{14} &= S\left(\frac{o_{14}^S(1-r)^2 + o_{23}^S r^2}{2}\right) \\
G'_{22} &= S\left(\frac{o_{12}^S + o_{13}^S + o_{14}^S r^2 + o_{23}^S(1-r)^2}{4}\right) \\
G'_{23} &= S\left(\frac{o_{14}^S r^2 + o_{23}^S(1-r)^2}{2}\right) \\
G'_{24} &= S\left(\frac{o_{14}^S r(1-r) + o_{23}^S r(1-r)}{2}\right) \\
G'_{33} &= S\left(o_{33}^S + \frac{o_{13}^S + o_{14}^S r^2 + o_{23}^S(1-r)^2 + o_{34}^S}{4}\right) \\
G'_{34} &= S\left(\frac{o_{14}^S r(1-r) + o_{23}^S r(1-r) + o_{34}^S}{2}\right) \\
G'_{44} &= S\left(\frac{o_{34}^S + o_{14}^S(1-r)^2 + o_{23}^S r^2}{4}\right). \tag{6.A18}
\end{aligned}$$

The genotypic frequency recursions for offspring derived via outcrossing are derived in similar fashion. The proportional contribution of each genotype to the pool

of outcrossed ovules are

$$\begin{aligned}
o_{11}^X &= (1 - C)(F_{11}^A w_{11}^f) / O_T^X \\
o_{12}^X &= (1 - C)(F_{12}^A w_{12}^f) / O_T^X \\
o_{13}^X &= (1 - C)(F_{13}^A w_{13}^f) / O_T^X \\
o_{14}^X &= (1 - C)(F_{14}^A w_{14}^f) / O_T^X \\
o_{22}^X &= (F_{22}^A w_{22}^f) / O_T^X \\
o_{23}^X &= (1 - C)(F_{23}^A w_{23}^f) / O_T^X \\
o_{24}^X &= (F_{24}^A w_{24}^f) / O_T^X \\
o_{33}^X &= (1 - C)(F_{33}^A w_{33}^f) / O_T^X \\
o_{34}^X &= (1 - C)(F_{34}^A w_{34}^f) / O_T^X \\
o_{44}^X &= (F_{44}^A w_{44}^f) / O_T^X,
\end{aligned} \tag{6.A19}$$

where  $O_T^X = (1 - S)O_T$ . The proportional contribution of each genotype that is phenotypically hermaphrodite to the pool of outcrossed pollen is equal to the relative genotypic frequencies after selection:

$$\begin{aligned}
p_{11}^X &= (F_{11}^A w_{11}^f) / P_T^X \\
p_{12}^X &= (F_{12}^A w_{12}^f) / P_T^X \\
p_{13}^X &= (F_{13}^A w_{13}^f) / P_T^X \\
p_{14}^X &= (F_{14}^A w_{14}^f) / P_T^X \\
p_{23}^X &= (F_{23}^A w_{23}^f) / P_T^X \\
p_{34}^X &= (F_{34}^A w_{34}^f) / P_T^X,
\end{aligned} \tag{6.A20}$$

where  $p_{ij}^X = 0$  where  $ij \in [22, 24, 44]$ , and  $P_T^X = \sum_{i=1}^4 \sum_{j=i}^4 p_{ij}^X$ . The haplotype frequencies among outcrossed ovules ( $x_i$ ) are then:

$$\begin{aligned}
x_1 &= o_{11}^X + \frac{o_{12}^X + o_{13}^X + o_{14}^X}{2} - r \left( \frac{o_{14}^X - o_{23}^X}{2} \right) \\
x_2 &= o_{22}^X + \frac{o_{12}^X + o_{23}^X + o_{24}^X}{2} + r \left( \frac{o_{14}^X - o_{23}^X}{2} \right) \\
x_3 &= o_{33}^X + \frac{o_{13}^X + o_{23}^X + o_{34}^X}{2} + r \left( \frac{o_{14}^X - o_{23}^X}{2} \right) \\
x_4 &= o_{44}^X + \frac{o_{14}^X + o_{24}^X + o_{34}^X}{2} - r \left( \frac{o_{14}^X - o_{23}^X}{2} \right),
\end{aligned} \tag{6.A21}$$

and the haplotype frequencies among the pool of outcrossed pollen ( $y_i$ ) are:

$$\begin{aligned}
 y_1 &= p_{11}^X + \frac{p_{12}^X + p_{13}^X + p_{14}^X}{2} - r \left( \frac{p_{14}^X - p_{23}^X}{2} \right) \\
 y_2 &= \frac{p_{12}^X p_{23}^X}{2} + r \left( \frac{p_{14}^X - p_{23}^X}{2} \right) \\
 y_3 &= p_{33}^X + \frac{p_{13}^X + p_{23}^X + p_{34}^X}{2} + r \left( \frac{p_{14}^X - p_{23}^X}{2} \right) \\
 y_4 &= \frac{p_{14}^X p_{34}^X}{2} - r \left( \frac{p_{14}^X - p_{23}^X}{2} \right).
 \end{aligned} \tag{6.A22}$$

The genotypic recursions describing the frequency in the next generation of each genotype among zygotes derived from outcrossing are calculated from these haplotype frequencies as:

$$\begin{aligned}
 F'_{11} &= (1 - S)(x_1 y_1) \\
 F'_{12} &= (1 - S)(x_1 y_2 + x_2 y_1) \\
 F'_{13} &= (1 - S)(x_1 y_3 + x_3 y_1) \\
 F'_{14} &= (1 - S)(x_1 y_4 + x_4 y_1) \\
 F'_{22} &= (1 - S)(x_2 y_2) \\
 F'_{23} &= (1 - S)(x_2 y_3 + x_3 y_2) \\
 F'_{24} &= (1 - S)(x_2 y_4 + x_4 y_2) \\
 F'_{33} &= (1 - S)(x_3 y_3) \\
 F'_{34} &= (1 - S)(x_3 y_4 + x_4 y_3) \\
 F'_{44} &= (1 - S)(x_4 y_4).
 \end{aligned} \tag{6.A23}$$

### 6.7.5 Androdioecy via dominant female-sterility mutation

The model of Androdioecy via the invasion of a dominant female-sterility mutation is very similar in structure to the model of gynodioecy via a dominant male-sterility mutation. Adult genotypic frequencies again follow equations 6.A1 and 6.A2. With a dominant female-sterility mutation, any genotype carrying the  $M_2$  allele will be phenotypically male. The fitness expressions corresponding to each  $F_{ij}^A$  are:

TABLE 6.A3: Fitness expressions for diploid adults prior to reproduction for the model of a dominant female-sterility mutation ( $w_{ij}^f$  denotes fitness effects through the female sex-function,  $w_{ij}^m$  for male sex-function).

Haplotype	$AM_1$	$AM_2$	$aM_1$	$aM_2$
Female-function				
$AM_1$	1	0	$(1 - h_f s_f)$	0
$AM_2$	—	0	0	0
$aM_1$	—	—	$(1 - s_f)$	0
$aM_2$	—	—	—	0
Male-function				
$AM_1$	$(1 - s_m)$	$(1 - s_m)(1 + k)$	$(1 - h_m s_m)$	$(1 - h_m s_m)(1 + k)$
$AM_2$	—	$(1 - s_m)(1 + k)$	$(1 - h_m s_m)(1 + k)$	$(1 - h_m s_m)(1 + k)$
$aM_1$	—	—	1	$(1 + k)$
$aM_2$	—	—	—	$(1 + k)$

Note: Rows and columns indicate the  $i$ th and  $j$ th gametic haplotype respectively. The lower triangle of each matrix is the reflection of the upper triangle, and is omitted for simplicity and consistency with the  $i \geq j$  row/column indexing used throughout the article.

Because only phenotypically hermaphroditic individuals can produce ovules, the total number of ovules produced by the population at reproduction will be proportional to

$$O_T = F_{11}^A w_{11}^f + F_{13}^A w_{13}^f + F_{33}^A w_{33}^f. \quad (6.A24)$$

The proportion of ovules that are self-fertilized will therefore be proportional to

$$S = \frac{C(O_T)}{O_T}, \quad (6.A25)$$

and the proportion of ovules fertilized via outcrossing is the complement of  $S$ :

$$(1 - S) = \frac{(1 - C)O_T}{O_T}. \quad (6.A26)$$

Because only those genotypes homozygous for  $M_1$  can self-fertilize, the structure of the recursions for selfed zygotes are the same as for the model of gynodioecy via invasion of a dominant male-sterility mutation. That is, the proportional contribution of each adult genotype to the pool of selfed ovules,  $o_{ij}^S$  follow Eq(6.A6), and the resulting recursions,  $G'_{ij}$  follow Eq(6.A7). However, the case is altered for outcrossed offspring. The proportional contributions to the pool of outcrossed ovules for each genotype are:

$$\begin{aligned}
o_{11}^X &= (1 - C)(F_{11}^A w_{11}^f) / O_T^X \\
o_{13}^X &= (1 - C)(F_{13}^A w_{13}^f) / O_T^X \\
o_{33}^X &= (1 - C)(F_{33}^A w_{33}^f) / O_T^X,
\end{aligned} \tag{6.A27}$$

where  $O_T^X = (1 - S)O_T$ . The proportional contribution of each genotype to the pool of outcrossed pollen after selection is:

$$\begin{aligned}
p_{11}^X &= (F_{11}^A w_{11}^f) / P_T^X \\
p_{12}^X &= (F_{12}^A w_{12}^f) / P_T^X \\
p_{13}^X &= (F_{13}^A w_{13}^f) / P_T^X \\
p_{14}^X &= (F_{14}^A w_{14}^f) / P_T^X \\
p_{22}^X &= (F_{22}^A w_{22}^f) / P_T^X \\
p_{23}^X &= (F_{23}^A w_{23}^f) / P_T^X \\
p_{24}^X &= (F_{24}^A w_{24}^f) / P_T^X \\
p_{33}^X &= (F_{33}^A w_{33}^f) / P_T^X \\
p_{34}^X &= (F_{34}^A w_{34}^f) / P_T^X \\
p_{44}^X &= (F_{44}^A w_{44}^f) / P_T^X,
\end{aligned} \tag{6.A28}$$

where  $P_T^X = \sum_{i=1}^4 \sum_{j=i}^4 p_{ij}^X$ . The resulting haplotype frequencies among outcrossed ovules ( $x_i$ ) and pollen ( $y_i$ ) are then:

$$\begin{aligned}
x_1 &= o_{11}^X + o_{13}^X / 2 \\
x_2 &= 0 \\
x_3 &= o_{33}^X + o_{13}^X / 2 \\
x_4 &= 0.
\end{aligned} \tag{6.A29}$$

and the haplotype frequencies among the pool of outcrossed pollen are

$$\begin{aligned}
x_1 &= p_{11}^X + \frac{p_{12}^X + p_{13}^X + p_{14}^X}{2} - r \left( \frac{p_{14}^X - p_{23}^X}{2} \right) \\
x_2 &= p_{22}^X + \frac{p_{12}^X + p_{23}^X + p_{24}^X}{2} + r \left( \frac{p_{14}^X - p_{23}^X}{2} \right) \\
x_3 &= p_{33}^X + \frac{p_{13}^X + p_{23}^X + p_{34}^X}{2} + r \left( \frac{p_{14}^X - p_{23}^X}{2} \right) \\
x_4 &= p_{44}^X + \frac{p_{14}^X + p_{24}^X + p_{34}^X}{2} - r \left( \frac{p_{14}^X - p_{23}^X}{2} \right),
\end{aligned} \tag{6.A30}$$

The genotypic recursions describing the frequency in the next generation of each

genotype among zygotes derived from outcrossing are calculated from these haplo-type frequencies as:

$$\begin{aligned}F'_{11} &= (1 - S)(x_1y_1) \\F'_{12} &= (1 - S)(x_1y_2) \\F'_{13} &= (1 - S)(x_1y_3 + x_3y_1) \\F'_{14} &= (1 - S)(x_1y_4) \\F'_{22} &= 0 \\F'_{23} &= (1 - S)(x_3y_2) \\F'_{24} &= 0 \\F'_{33} &= (1 - S)(x_3y_3) \\F'_{34} &= (1 - S)(x_3y_4) \\F'_{44} &= 0.\end{aligned}\tag{6.A31}$$

### 6.7.6 Androdioecy via recessive female-sterility mutation

For the model of the evolution of androdioecy via the invasion of a completely recessive female-sterility mutation at  $\mathbf{M}$ , only genotypes homozygous for the  $M_2$  allele are phenotypically male. Again, the adult genotypic frequencies,  $F_{ij}^A$ , are described by Equations 6.A1 and 6.A2. Now, the fitness expressions associated with each  $F_{ij}^A$  through the female and male sex-function are:

TABLE 6.A4: Fitness expressions for diploid adults prior to reproduction for the model of a recessive female-sterility mutation ( $w_{ij}^f$  denotes fitness effects through the female sex-function,  $w_{ij}^m$  for male sex-function).

Haplotype	$AM_1$	$AM_2$	$aM_1$	$aM_2$
Female-function				
$AM_1$	1	1	$(1 - h_f s_f)$	$(1 - h_f s_f)$
$AM_2$	—	0	$(1 - h_f s_f)$	0
$aM_1$	—	—	$(1 - s_f)$	$(1 - s_f)$
$aM_2$	—	—	—	0
Male-function				
$AM_1$	$(1 - s_m)$	$(1 - s_m)$	$(1 - h_m s_m)$	$(1 - h_m s_m)$
$AM_2$	—	$(1 - s_m)(1 + k)$	$(1 - h_m s_m)$	$(1 - h_m s_m)(1 + k)$
$aM_1$	—	—	1	1
$aM_2$	—	—	—	$(1 + k)$

Note: Rows and columns indicate the  $i$ th and  $j$ th gametic haplotype respectively. The lower triangle of each matrix is the reflection of the upper triangle, and is omitted for simplicity and consistency with the  $i \geq j$  row/column indexing used throughout the article.

Only individuals not homozygous for  $M_2$  are phenotypically hermaphrodite, and thus able to produce ovules. The total number of ovules produced by the population at reproduction is therefore proportional to

$$O_T = F_{11}^A w_{11}^f + F_{12}^A w_{12}^f + F_{13}^A w_{13}^f + F_{14}^A w_{14}^f + F_{23}^A w_{23}^f + F_{33}^A w_{33}^f + F_{34}^A w_{34}^f. \quad (6.A32)$$

The proportion of ovules that are self-fertilized will therefore be proportional to

$$S = \frac{C(O_T)}{O_T}, \quad (6.A33)$$

and the proportion of ovules fertilized via outcrossing is the complement of  $S$ :

$$(1 - S) = \frac{(1 - C)O_T}{O_T}. \quad (6.A34)$$

As before, the structure of the equations describing genotypic frequency change among selfed offspring for the model of androdioecy via a recessive female-sterility mutation are similar to the model of gynodioecy via a recessive male-sterility mutation. The proportional contribution of self-fertilized offspring by each of the phenotypically hermaphrodite genotypes,  $o_{ij}^S$ , follows Eq(6.A16), and the genotypic recursions for self-fertilized zygotes,  $G'_{ij}$  follow Eq(6.A17).

The genotypic frequency recursions for offspring derived via outcrossing proceeds as follows. The proportional contribution of each genotype to the pool of

outcrossed ovules are

$$\begin{aligned}
o_{11}^X &= (1 - C)(F_{11}^A w_{11}^f) / O_T^X \\
o_{12}^X &= (1 - C)(F_{12}^A w_{12}^f) / O_T^X \\
o_{13}^X &= (1 - C)(F_{13}^A w_{13}^f) / O_T^X \\
o_{14}^X &= (1 - C)(F_{14}^A w_{14}^f) / O_T^X \\
o_{23}^X &= (1 - C)(F_{23}^A w_{23}^f) / O_T^X \\
o_{33}^X &= (1 - C)(F_{33}^A w_{33}^f) / O_T^X \\
o_{34}^X &= (1 - C)(F_{34}^A w_{34}^f) / O_T^X,
\end{aligned} \tag{6.A35}$$

where  $o_{ij}^X = 0$  where  $ij \in [22, 24, 44]$ , and  $O_T^X = (1 - S)O_T$ . The proportional contribution of each genotype that is phenotypically hermaphrodite to the pool of outcrossed pollen is equal to the relative genotypic frequencies after selection:

$$\begin{aligned}
p_{11}^X &= (F_{11}^A w_{11}^f) / P_T^X \\
p_{12}^X &= (F_{12}^A w_{12}^f) / P_T^X \\
p_{13}^X &= (F_{13}^A w_{13}^f) / P_T^X \\
p_{14}^X &= (F_{14}^A w_{14}^f) / P_T^X \\
p_{22}^X &= (F_{22}^A w_{22}^f) / P_T^X \\
p_{23}^X &= (F_{23}^A w_{23}^f) / P_T^X \\
p_{24}^X &= (F_{24}^A w_{24}^f) / P_T^X \\
p_{34}^X &= (F_{34}^A w_{34}^f) / P_T^X \\
p_{44}^X &= (F_{44}^A w_{44}^f) / P_T^X,
\end{aligned} \tag{6.A36}$$

where  $P_T^X = \sum_{i=1}^4 \sum_{j=i}^4 p_{ij}^X$ . The haplotype frequencies among outcrossed ovules ( $x_i$ ) are then:

$$\begin{aligned}
x_1 &= o_{11}^X + \frac{o_{12}^X + o_{13}^X + o_{14}^X}{2} - r \left( \frac{o_{14}^X - o_{23}^X}{2} \right) \\
x_2 &= \frac{o_{12}^X o_{23}^X}{2} + r \left( \frac{o_{14}^X - o_{23}^X}{2} \right) \\
x_3 &= o_{33}^X + \frac{o_{13}^X + o_{23}^X + o_{34}^X}{2} + r \left( \frac{o_{14}^X - o_{23}^X}{2} \right) \\
x_4 &= \frac{o_{14}^X o_{34}^X}{2} - r \left( \frac{o_{14}^X - o_{23}^X}{2} \right).
\end{aligned} \tag{6.A37}$$

and the haplotype frequencies among the pool of outcrossed pollen ( $y_i$ ) are:

$$\begin{aligned}
 y_1 &= p_{11}^X + \frac{p_{12}^X + p_{13}^X + p_{14}^X}{2} - r \left( \frac{p_{14}^X - p_{23}^X}{2} \right) \\
 y_2 &= p_{22}^X + \frac{p_{12}^X + p_{23}^X + p_{24}^X}{2} + r \left( \frac{p_{14}^X - p_{23}^X}{2} \right) \\
 y_3 &= p_{33}^X + \frac{p_{13}^X + p_{23}^X + p_{34}^X}{2} + r \left( \frac{p_{14}^X - p_{23}^X}{2} \right) \\
 y_4 &= p_{44}^X + \frac{p_{14}^X + p_{24}^X + p_{34}^X}{2} - r \left( \frac{p_{14}^X - p_{23}^X}{2} \right), \tag{6.A38}
 \end{aligned}$$

The genotypic recursions describing the frequency in the next generation of each genotype among zygotes derived from outcrossing are calculated from these haplotype frequencies following Eq(6.A23).

## 6.8 Appendix B: Supplementary figures

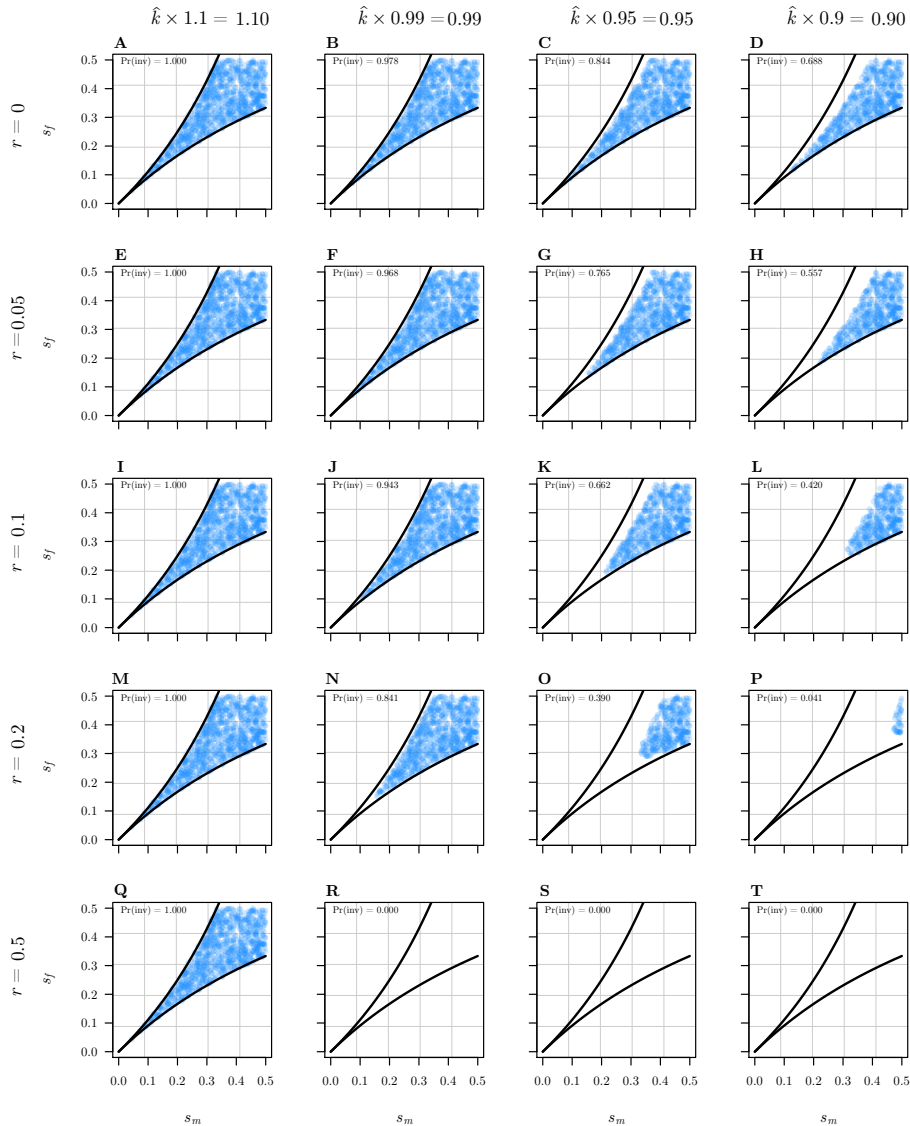


FIGURE S1: Invasion of dominant male-sterility mutations into populations with segregating SA variation under obligate outcrossing. Plots show the regions of parameter space (defined by  $s_f \times s_m | F_{ij}^*, G_{ij}^* > 0$  and  $0 < s_f, s_m \leq 0.5$ ) where a dominant male-sterility allele at **M**, can invade populations initially at single-locus equilibrium frequencies for **A** with additive fitness effects ( $h_f = h_m = 1/2$ ). Results were obtained by evaluating the three candidate leading eigenvalues ( $\lambda_M, \lambda_{AM}$ ) of the Jacobian matrix of the genotype  $\times$  transmission mode recursions for populations at the above initial conditions for 1000 points uniformly distributed throughout the relevant  $s_f \times s_m$  parameter space. Blue points indicate parameter sets where  $\lambda_M - 1 > 0$ , and/or  $\lambda_{AM} - 1 > 0$ . Solid black lines represent the corresponding single-locus invasion criteria for SA alleles.

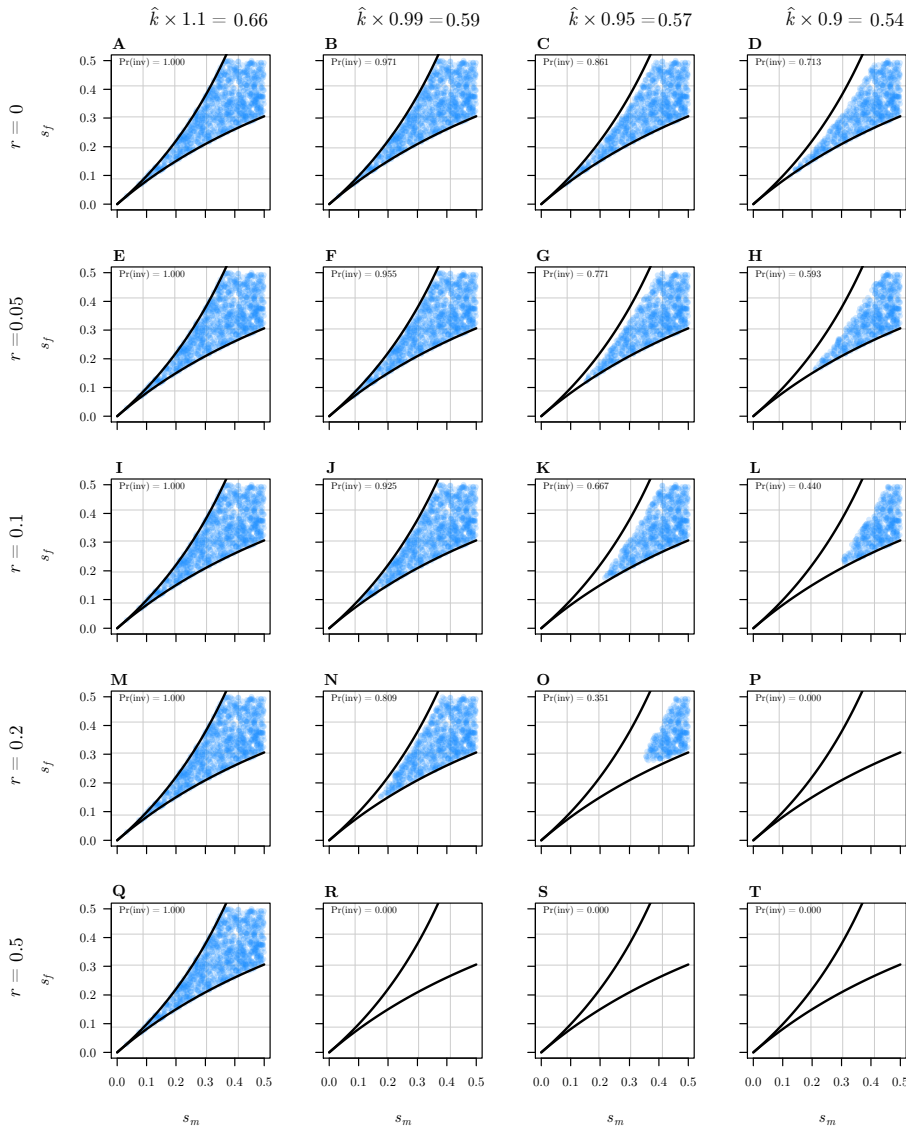


FIGURE S2: Invasion of dominant male-sterility mutations into populations with segregating SA variation under conditions of low selfing ( $C = 0.25$ ) and high inbreeding depression ( $\delta = 0.8$ ). Plots show the regions of parameter space (defined by  $s_f \times s_m | F_{ij}^*, G_{ij}^* > 0$  and  $0 < s_f, s_m \leq 0.5$ ) where a dominant male-sterility allele at **M**, can invade populations initially at single-locus equilibrium frequencies for **A** with additive fitness effects ( $h_f = h_m = 1/2$ ). Results were obtained by evaluating the three candidate leading eigenvalues ( $\lambda_M, \lambda_{AM}$ ) of the Jacobian matrix of the genotype  $\times$  transmission mode recursions for populations at the above initial conditions for 1000 points uniformly distributed throughout the relevant  $s_f \times s_m$  parameter space. Blue points indicate parameter sets where  $\lambda_M - 1 > 0$ , and/or  $\lambda_{AM} - 1 > 0$ . Solid black lines represent the corresponding single-locus invasion criteria for SA alleles.

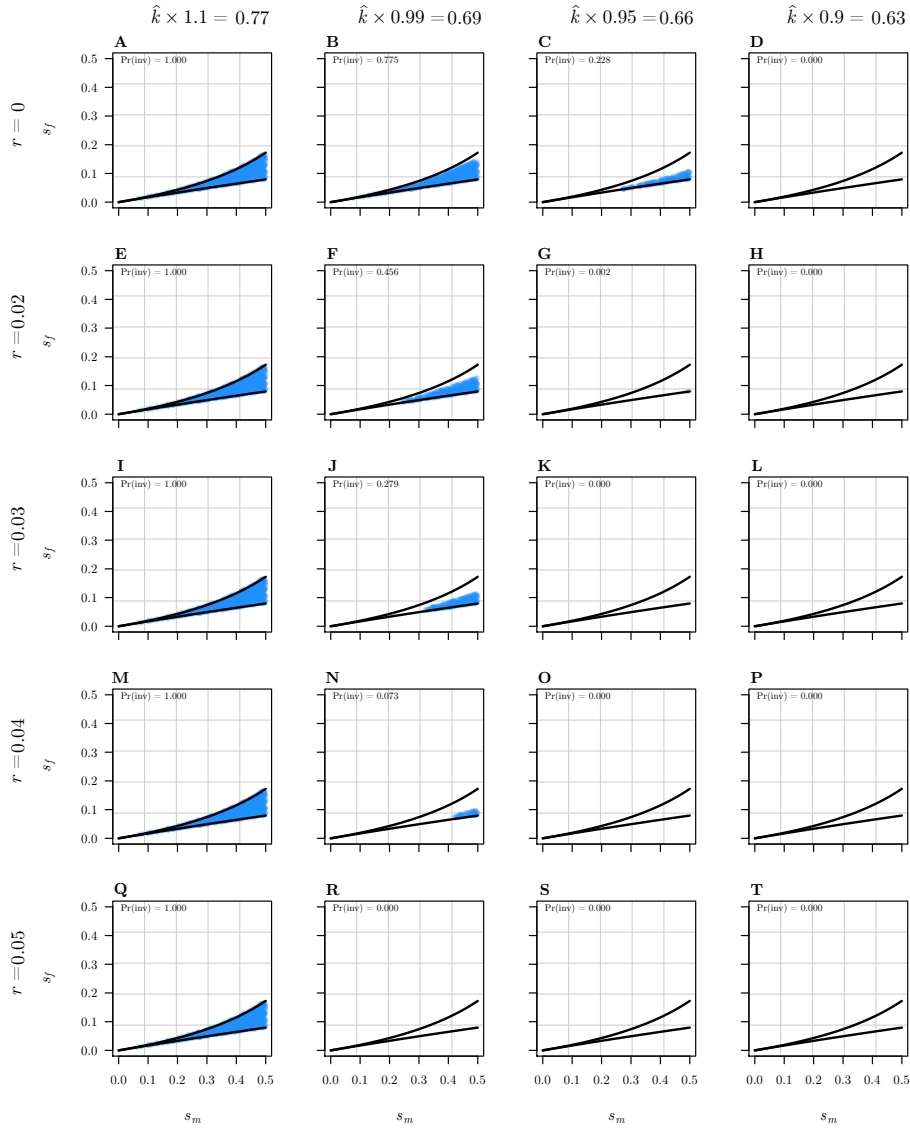


FIGURE S3: Invasion of dominant male-sterility mutations into populations with segregating SA variation under conditions of high selfing ( $C = 0.75$ ) and low inbreeding depression ( $\delta = 0.2$ ). Plots show the regions of parameter space (defined by  $s_f \times s_m |F_{ij}^*, G_{ij}^*| > 0$  and  $0 < s_f, s_m \leq 0.5$ ) where a dominant male-sterility allele at **M**, can invade populations initially at single-locus equilibrium frequencies for **A** with additive fitness effects ( $h_f = h_m = 1/2$ ). Results were obtained by evaluating the three candidate leading eigenvalues ( $\lambda_M, \lambda_{AM}$ ) of the Jacobian matrix of the genotype  $\times$  transmission mode recursions for populations at the above initial conditions for 1000 points uniformly distributed throughout the relevant  $s_f \times s_m$  parameter space. Blue points indicate parameter sets where  $\lambda_M - 1 > 0$ , and/or  $\lambda_{AM} - 1 > 0$ . Solid black lines represent the corresponding single-locus invasion criteria for SA alleles.

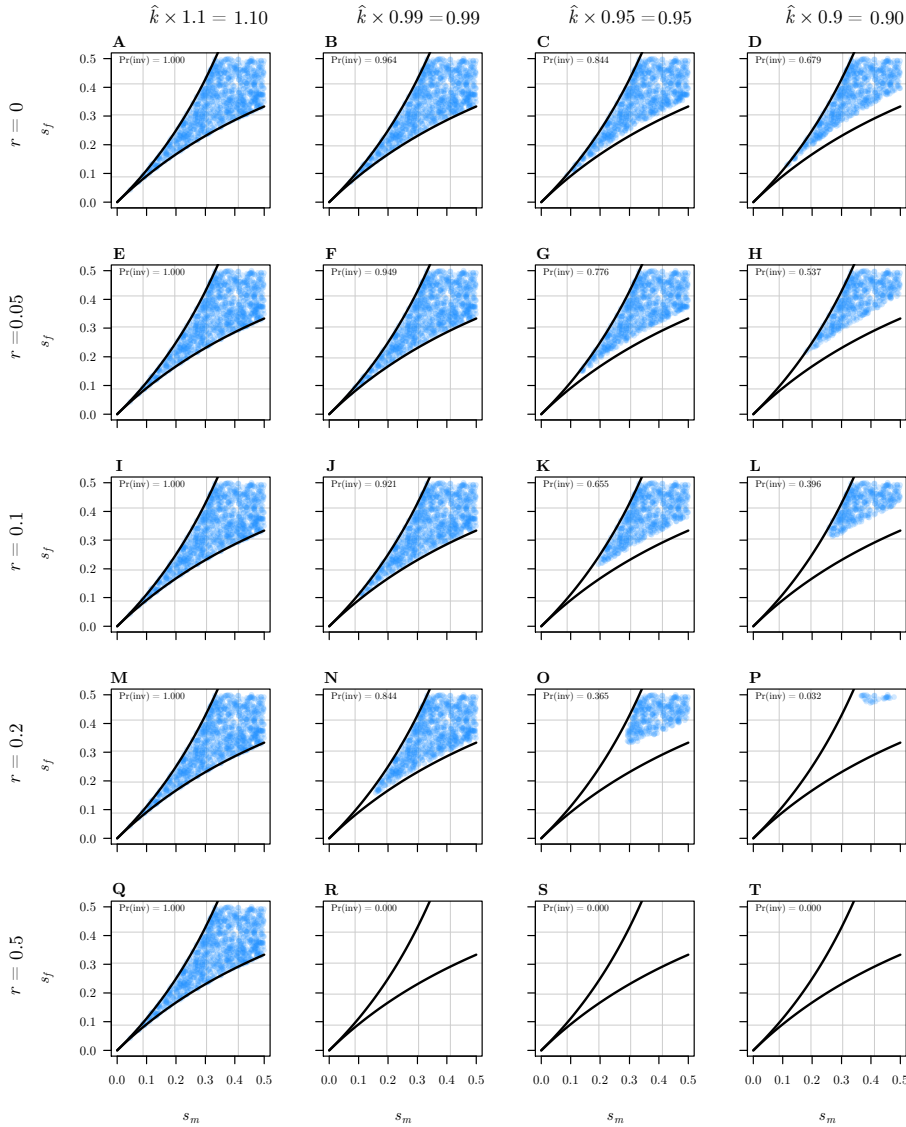


FIGURE S4: Invasion of dominant female-sterility mutations into populations with segregating SA variation under obligate outcrossing. Plots show the regions of parameter space (defined by  $s_f \times s_m | F_{ij}^*, G_{ij}^* > 0$  and  $0 < s_f, s_m \leq 0.5$ ) where a dominant male-sterility allele at **M**, can invade populations initially at single-locus equilibrium frequencies for **A** with additive fitness effects ( $h_f = h_m = 1/2$ ). Results were obtained by evaluating the three candidate leading eigenvalues ( $\lambda_{\mathbf{M}}, \lambda_{\mathbf{AM}}$ ) of the Jacobian matrix of the genotype  $\times$  transmission mode recursions for populations at the above initial conditions for 1000 points uniformly distributed throughout the relevant  $s_f \times s_m$  parameter space. Blue points indicate parameter sets where  $\lambda_{\mathbf{M}} - 1 > 0$ , and/or  $\lambda_{\mathbf{AM}} - 1 > 0$ . Solid black lines represent the corresponding single-locus invasion criteria for SA alleles.

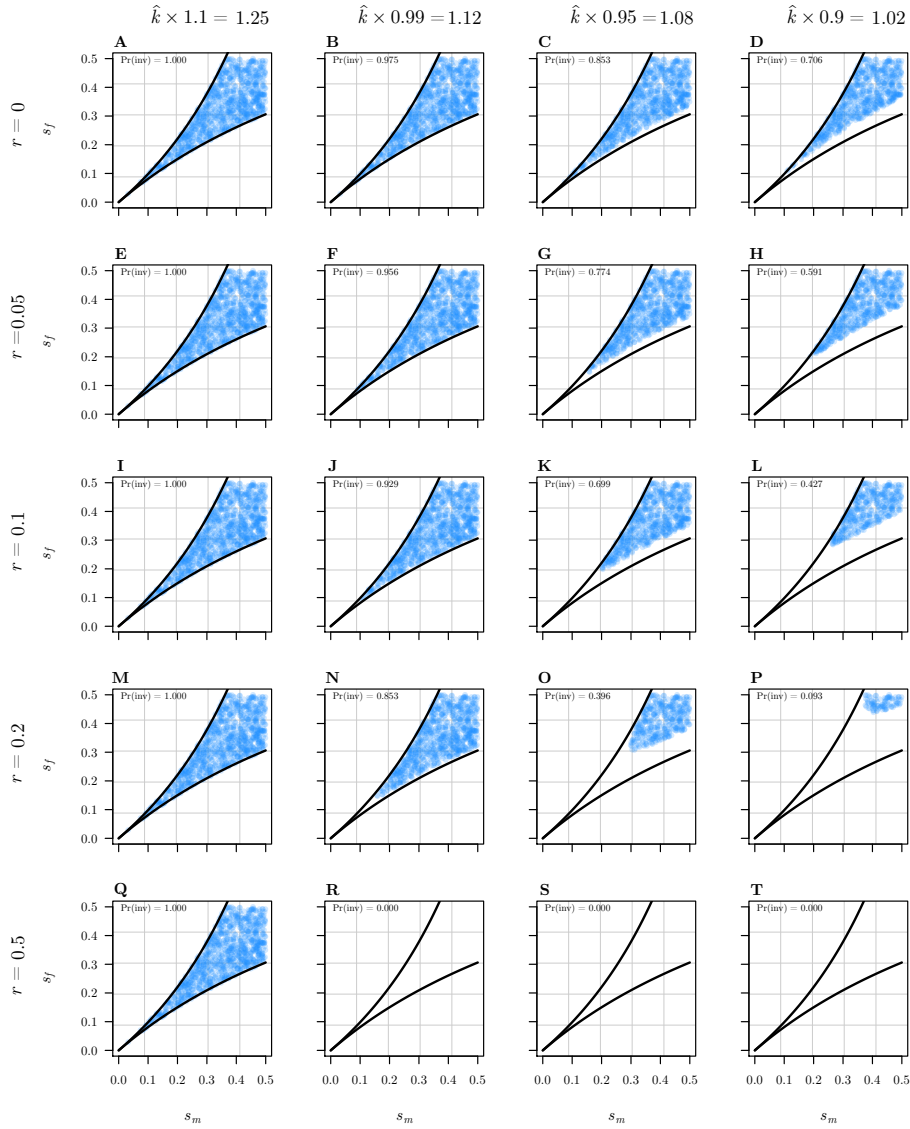


FIGURE S5: Invasion of dominant female-sterility mutations into populations with segregating SA variation under conditions of low selfing ( $C = 0.25$ ) and high inbreeding depression ( $\delta = 0.8$ ). Plots show the regions of parameter space (defined by  $s_f \times s_m |F_{ij}^*, G_{ij}^*| > 0$  and  $0 < s_f, s_m \leq 0.5$ ) where a dominant male-sterility allele at **M**, can invade populations initially at single-locus equilibrium frequencies for **A** with additive fitness effects ( $h_f = h_m = 1/2$ ). Results were obtained by evaluating the three candidate leading eigenvalues ( $\lambda_{\mathbf{M}}, \lambda_{\mathbf{AM}}$ ) of the Jacobian matrix of the genotype  $\times$  transmission mode recursions for populations at the above initial conditions for 1000 points uniformly distributed throughout the relevant  $s_f \times s_m$  parameter space. Blue points indicate parameter sets where  $\lambda_{\mathbf{M}} - 1 > 0$ , and/or  $\lambda_{\mathbf{AM}} - 1 > 0$ . Solid black lines represent the corresponding single-locus invasion criteria for SA alleles.

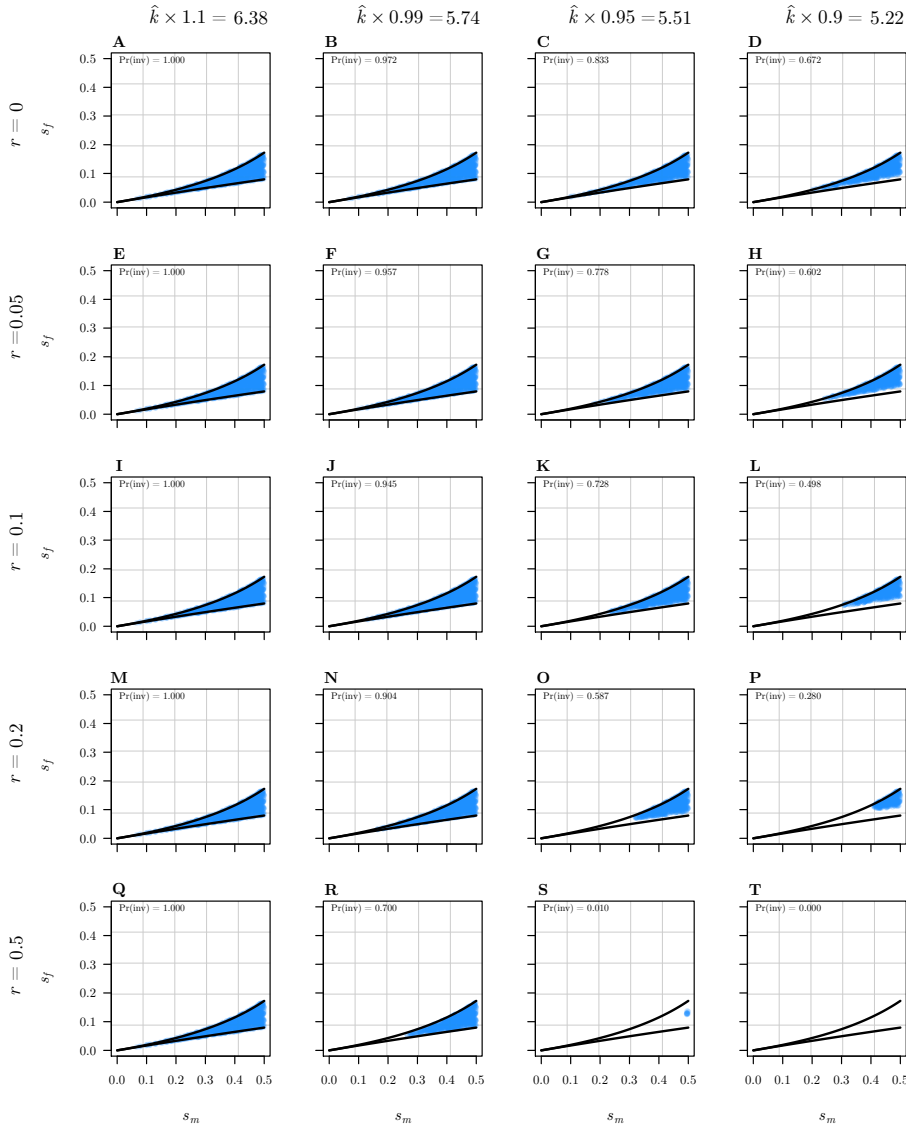


FIGURE S6: Invasion of dominant female-sterility mutations into populations with segregating SA variation under conditions of high selfing ( $C = 0.75$ ) and low inbreeding depression ( $\delta = 0.2$ ). Plots show the regions of parameter space (defined by  $s_f \times s_m | F_{ij}^*, G_{ij}^* > 0$  and  $0 < s_f, s_m \leq 0.5$ ) where a dominant male-sterility allele at **M**, can invade populations initially at single-locus equilibrium frequencies for **A** with additive fitness effects ( $h_f = h_m = 1/2$ ). Results were obtained by evaluating the three candidate leading eigenvalues ( $\lambda_{\mathbf{M}}, \lambda_{\mathbf{AM}}$ ) of the Jacobian matrix of the genotype  $\times$  transmission mode recursions for populations at the above initial conditions for 1000 points uniformly distributed throughout the relevant  $s_f \times s_m$  parameter space. Blue points indicate parameter sets where  $\lambda_{\mathbf{M}} - 1 > 0$ , and/or  $\lambda_{\mathbf{AM}} - 1 > 0$ . Solid black lines represent the corresponding single-locus invasion criteria for SA alleles.

## 6.9 Appendix C: Alternative models of inbreeding depression

As explained in the main text, we attempted to account for negative covariance between  $C$  and  $\delta$  in our deterministic simulations, as might be expected if inbreeding depression is caused by recessive deleterious mutations (Charlesworth and Willis 2009). We did this by constraining inbreeding depression to follow a simple linear function of the selfing rate  $\delta = \delta^*(1 - C/2)$ , where  $\delta^*$  represents the hypothetical severity of inbreeding depression if selfing were enforced on a completely outcrossing population ( $\delta^* \in [0, 1]$ ). Here we briefly address the consequences of relaxing this assumption.

In the simplest case, the mutation load due to deleterious recessive mutations at a single locus in a completely selfing population should be roughly half that of a randomly mating outcrossing population ( $\mu$  versus  $2\mu$ , where  $\mu$  is the genome-wide mutation rate; Ohta and Cockerham 1974). Moreover, the single-locus mutation load is predicted to follow a negative decelerating curve as a function of the population selfing rate (Ohta and Cockerham 1974). To capture these main features, first we define a simple function describing the mutation load due to recessive deleterious mutations,

$$L = \frac{a(1 - C)}{C + a(1 - C)}, \quad (\text{C1})$$

where  $C$  is the population selfing rate, and  $a$  is a shape parameter determining the curvature of the line. When  $a = 1$ , Eq(C1) yields a straight line. For  $a < 1$  the function is concave up (Fig. S7A), and for  $a > 1$  it is concave downward. We then incorporate Eq(C1) into a simple expression for inbreeding depression,

$$\delta = \delta^* - \delta^*b(1 - L), \quad (\text{C2})$$

where  $\delta^*$  represents the hypothetical severity of inbreeding depression in an obligately outcrossing population ( $\delta^* \in [0, 1]$ ), and  $b$  is a shape parameter determining how far  $\delta$  will drop relative to  $\delta^*$  under complete selfing ( $C = 1$ ). This flexible function allows us to define an initial level of inbreeding depression under obligate outcrossing ( $\delta^*$ ), how far inbreeding depression will decline under complete selfing ( $b$ ), and the curvature of the line connecting these two endpoints ( $a$ ). Given that in a completely selfing population  $L$  is expected to be roughly half that in an obligately outcrossing one, we constrain  $b$  to equal  $1/2$ . Note that when  $a = 1$  and  $b = 1/2$ , Eq(C2) yields  $\delta = \delta^*(1 - C/2)$ , as defined in the main text. Altering the curvature of Eq(C1) to be concave upward has only a minor effect on the results, and does not alter the main conclusions from our simulations (fig. S7B).

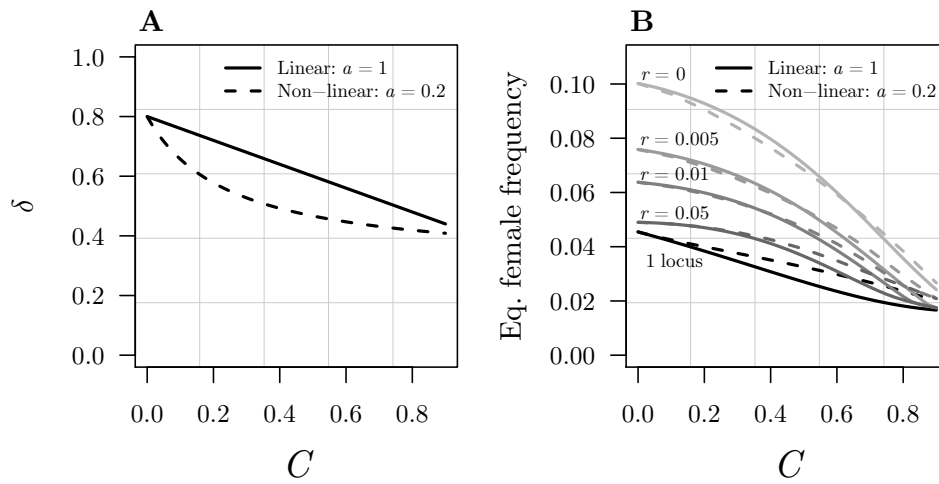


FIGURE S7: Comparison of linear versus non-linear models of inbreeding depression,  $\delta$ , as a function of the hermaphrodite selfing rate,  $C$ . Panel (A) shows the linear ( $a = 1$ ; solid line) vs. non-linear ( $a = 0.2$ ; dashed line) functions for  $\delta$ . For both examples, we assume inbreeding depression of  $\delta^* = 0.8$  in a completely outcrossing population, and inbreeding depression will be half this value in a completely selfing population ( $b = 0.5$  for both lines). Panel (B) illustrates the effect of using the linear and non-linear models of  $\delta$  for the simulation results presented in fig. 6.2 of the main text – equilibrium frequencies of unisexual females compared with single-locus predictions when reproductive compensation is above the single-locus threshold (i.e.,  $k > \hat{k}$ ). Results are shown for the model of gynodioecy via invasion of a recessive male-sterility allele, with additive fitness effects at **A** ( $h_f = h_m = 0.5$ ), using a selection coefficient of  $s_m = 0.1$ , and the same linear (solid lines) vs. nonlinear (dashed lines) functions of inbreeding depression as shown in panel (A).



## Chapter 7

# Discussion

In this thesis, I have explored the evolutionary consequences of sex-specific and sexually antagonistic (SA) selection in two non-traditional contexts: external fertilization and hermaphroditism. In external fertilizers, I focused on the evolution of a crucial life-history trait — the timing of reproduction (reproductive phenology) — and how selection from the external environment, and differential selection on male and female mating strategies, can maintain variation in phenological traits (Chapters 2–4). In hermaphrodites, I focused more explicitly on the population genetic consequences of SA selection for the maintenance of polymorphism, and for the evolution of separate sexes (Chapters 5 & 6). The unifying theme of this work is the generality and importance of SA selection for the evolution of genomes and mating systems.

Sexually Antagonistic selection represents a classic theoretical scenario in population genetics for the maintenance of genetic polymorphism. Early single-locus models formalized the logic that when genes expressed in both sexes experience opposing selection, polymorphism can be maintained when alleles that would otherwise experience purifying selection in one sex are held at intermediate frequencies by positive selection in the other sex (Haldane 1926; Owen 1953; Kidwell et al. 1977). However, it is still unclear how important or general SA selection is for the maintenance of genetic variation in fitness. This is because under realistic assumptions about the strength of selection at individual loci, the conditions permitting polymorphism in classical models are often restrictive (Prout 2000; Patten and Haig 2009; but see e.g., Fry 2010). In the absence of favorable conditions of genetic dominance (see Fry 2010), SA selection is only expected to maintain genetic variation when selection is strong or exceptionally well balanced in strength between females and males (Kidwell et al. 1977; see, for example, fig. B3 in chapter 5). Nevertheless, high levels of SA fitness variation have been observed in lab and natural populations in a variety of taxa (Rice 1992; Chippindale et al. 2001; Pischedda and Chippindale 2006; Foerster et al. 2007; Delcourt et al. 2009; Cheng and Kirkpatrick 2016). This apparent disagreement between classical theory and data has prompted recent theory work exploring mechanisms that may promote the maintenance of SA genetic variance for fitness, including interactions between recurrent mutation and genetic drift, as well as genetic conditions that expand opportunities for balancing selection (e.g., Patten and Haig 2009; Arnqvist 2011; Connallon and Clark 2012, 2014b; Spencer and Priest 2016).

Within this context, my thesis research makes three major contributions. First, by focusing on external fertilizers and hermaphrodites, my work expands the range of biological contexts in which we predict selection to maintain SA genetic variation beyond the traditional case of internally fertilizing dioecious species. Second, by addressing the underlying biology of selection over spawning phenologies in external fertilizers, I demonstrate how SA selection and the maintenance of variation in phenological traits commonly arises from biologically realistic conditions.

Finally, by extending recent SA theory in hermaphrodites to a multi-locus context, I show how the parameter conditions permitting SA polymorphism are expanded by linkage between SA loci. I also explore the consequences of this polymorphism for evolutionary transitions from hermaphroditism to separate sexes.

## 7.1 External Fertilizers and the emergence of SA selection

Traditional population genetic models tell us very little about the ecological conditions that lead to different selection regimes and population genetic outcomes. This is because they begin by assigning arbitrary selection coefficients to genetic variants, and predict the evolutionary trajectory of allele frequencies given these selection coefficients (Orr 2005). With the exception of one previous study (Connallon and Clark, 2014b), SA selection theory has followed this tradition, making it difficult to infer the importance of SA selection for the maintenance of genetic variation in fitness (e.g., Owen 1953; Kidwell et al. 1977). Despite offering an attractive theoretical explanation for the high levels of SA fitness variation observed in lab and natural populations in a variety of taxa, few studies have linked the ecological drivers of selection with the population genetic parameters that are predicted to result in balancing selection.

In my theoretical work on external fertilizers patterns of selection emerge naturally from the underlying biology of frequency- and density-dependent fertilization dynamics of male and female spawning phenologies (chapters 2–3). In this way, it links the population genetic processes of sex-specific selection and the maintenance of SA polymorphism with the key ecological drivers of reproductive phenology. These models predicted SA selection over the timing of reproduction as a common outcome under biologically realistic outcome of fertilization dynamics in broadcast spawners. Specifically, SA selection was predicted to be positively density-dependent, and often leading to balancing selection that maintained variation in population phenologies. Importantly, these predictions were consistent with well-documented patterns in the phenologies of broadcast spawning species, which exhibit high population variances in phenologies and sexually dimorphic spawning strategies (McEuan 1988; Levitan 2005; Lotterhos and Levitan 2011). The match between theory and observations suggest that SA selection may indeed play a key role in shaping the evolution of reproductive phenologies in such taxa.

Another important implication of these models is that a population must reach a relatively high density (and presumably well adapted) before sexual antagonism emerges. This result parallels recent work on the prevalence of sexual antagonism in poorly versus well-adapted populations (e.g. Berger et al. 2014; Long et al. 2012; ). The relative importance of sexually antagonistic selection for adaptation is expected to change under novel or stressful conditions, as new conditions augments selection on sexually antagonistic loci, and exposes mutations with conditional fitness effects to increased selection (Berger et al. 2014; Long et al. 2012; Whitlock and Agrawal 2009). Theory predicts that the genetic and demographic factors that facilitate local adaptation also promote sexual antagonism. Consequently, sexually antagonistic selection is predicted to decline towards species' range margins as migration, rather than sexual antagonism, becomes the dominant constraint on adaptation (Connallon 2015). For many broadcast spawning species, dense and potentially well adapted populations are more likely to experience polyspermy, which creates antagonistic selection over the timing of reproduction due to the frequency-dependence of sperm

competition (Levitan 1991, 2002, 2004; Levitan and Ferrell 2006). In contrast, reproductive success in small, marginal populations will generally be sperm-limited, creating strong congruent selection for synchronized spawning in both males and females (Franke et al. 2002; Levitan 1991, 2002, 2004). Our models therefore suggest an ecologically explicit mechanism for why well adapted populations of broadcast spawners might be more likely to experience sexual antagonism.

## 7.2 Hermaphrodites and the genetic architecture of sexually antagonistic loci

The theory of sexual conflict and sexually antagonistic selection has traditionally been dedicated to species with separate sexes (dioecious species). My research on SA selection in simultaneous hermaphrodites extends this body of theory to include non-traditional — but quite common — mating systems. At the same time, this work explores the consequences of genetic architecture for the maintenance of SA genetic variation. In this way, it extends recent two-locus theory in dioecious species, which has shown that genetic linkage between SA loci expands the conditions where balancing selection maintaining SA polymorphisms (Patten et al. 2010). This work provides contrasting insights from recent single-locus theory of SA selection in hermaphrodites, which predicts that self-fertilization significantly reduces the opportunities for balancing selection on SA loci (Jordan and Connallon 2014; Tazzyman and Abbott 2015). Instead, these models suggest that when there is linkage between SA loci, the reduction in the effective rate of recombination caused by selfing can significantly expand the parameter space where SA polymorphism can be maintained (chapter 5). Moreover, linkage among SA loci promotes the invasion of male-beneficial alleles, and can partially counteract the bias in favour of female-benefit alleles that arises in single-locus models of sexual antagonism with selfing.

One particularly interesting implication of these results is that linked clusters of SA genes may contribute disproportionately to the maintenance of mixed-mating systems in hermaphroditic species. Determining the mechanisms for the maintenance of intermediate selfing rates is a long-standing question in the evolutionary biology of hermaphrodites (Darwin 1877; Lloyd 1979; Goodwillie et al. 2005; Harder and Barrett 2006; Jarne and Auld 2006). The prediction that linkage among SA loci can offset the increasing female-bias in selection introduced by selfing suggests that SA selection could be an important mechanism maintaining pollen dispersal traits in species with mixed mating systems. Interestingly, this is true whether or not partial selfing is expected to be the long-term evolutionary outcome of mating system evolution. Such interactions between mating system and sex-specific selection warrant further theoretical attention.

That linkage pairing multiple male-benefit alleles (or multiple female-benefit alleles) in a single haplotype facilitates their invasion suggests that linkage may also play an important role in other contexts. In chapter 6, I show that linkage pairing a sex-specific sterility mutation with a complimentary SA allele at another locus should facilitate the invasion of separate sexes from hermaphroditism. Previous theory regarding the invasion of unisexuals into hermaphrodite populations has emphasized its importance as a means of inbreeding avoidance (Charlesworth and Charlesworth, 1978a; Käfer et al. 2017). The importance of inbreeding avoidance is reflected in the critical role of both the ancestral hermaphrodite population selfing rate, and inbreeding depression in these models (Charlesworth and Charlesworth,

1978a). As I show in chapter 6, linkage with SA loci alters these predictions, indicating a lesser role for selfing and inbreeding depression in creating the conditions necessary for unisexuals to invade. Crucially, these models suggest that the sex-specific sterility mutations responsible for the evolution of separate sexes are likely to evolve in tight linkage with loci that are polymorphic for SA alleles. Previous models have shown that the subsequent evolution of complete dioecy requires tight linkage between sex-specific sterility loci and gender modifiers (Charlesworth and Charlesworth, 1978a). Hence, a key insight from the new theory is that the existence of segregating SA polymorphisms in hermaphrodite populations is expected to play a role facilitating the evolution of sex-determining regions and neo-sex chromosomes during evolutionary transitions from hermaphroditism to separate sexes.

## Appendix A

# Estimating monotonic biological rates using local linear regression<sup>1</sup>

---

<sup>1</sup>This chapter has been published as: Olito, C., C. W. White, D. J. Marshall, and D. M. Barneche. 2017. Estimating monotonic biological rates using local linear regression. *J. Exp. Biol.* 220:759–764. Please see the online version of the article, and all supplementary materials, at the publisher's website: [here](#).

## METHODS &amp; TECHNIQUES

# Estimating monotonic rates from biological data using local linear regression

Colin Olito\*, Craig R. White, Dustin J. Marshall and Diego R. Barneche

## ABSTRACT

Accessing many fundamental questions in biology begins with empirical estimation of simple monotonic rates of underlying biological processes. Across a variety of disciplines, ranging from physiology to biogeochemistry, these rates are routinely estimated from non-linear and noisy time series data using linear regression and *ad hoc* manual truncation of non-linearities. Here, we introduce the R package LoLinR, a flexible toolkit to implement local linear regression techniques to objectively and reproducibly estimate monotonic biological rates from non-linear time series data, and demonstrate possible applications using metabolic rate data. LoLinR provides methods to easily and reliably estimate monotonic rates from time series data in a way that is statistically robust, facilitates reproducible research and is applicable to a wide variety of research disciplines in the biological sciences.

**KEY WORDS:** Biological rates, Time series, Local linear regression, Autocorrelation, Linearity, Reproducible research

## INTRODUCTION

Living organisms, the communities they form and the environments they inhabit are all temporally dynamic systems. Consequently, many fundamental questions in biology begin with estimating the rates of underlying biological processes. When non-linearity is of biological interest and accurately represents the rate of interest, then non-linear, function-valued approaches may be most appropriate (Marshall et al., 2013; Stinchcombe et al., 2012). Non-linear approaches can be further generalized using function regression if the question also requires accounting for change in parameters as a function of other variables (Yen et al., 2015). However, in many cases, there is a putatively linear rate that we wish to estimate free of artifactual non-linear regions (e.g. Fig. 1). In these cases, researchers often reduce experimental complexity by holding state variables constant in order to estimate monotonic rates, which are then used in subsequent analyses. For example, the metabolic theory of ecology (MTE) seeks to explain ecological patterns by scaling the size dependence and temperature dependence of metabolic rates from individuals to ecosystems (Brown et al., 2004; Gillooly et al., 2001). The study of MTE therefore begins with estimates of metabolic rate at standardized temperatures (e.g. Barneche et al., 2014; Brown et al., 2004; Gillooly et al., 2001; White et al., 2011a,b). Similarly, predicting the impacts of climate change on ecosystem processes, such as community primary productivity, begins with estimates of O<sub>2</sub> production rates (Tanaka et al., 2013; Yvon-Durocher et al., 2015). Other examples

include estimates of leaf respiration rate (Shapiro et al., 2004), ecosystem functioning (Ross et al., 2013), and components of biogeochemical cycles including denitrification (Song et al., 2011), CO<sub>2</sub> and CH<sub>4</sub> gas emissions (e.g. Larmola et al., 2013). Thus, accurate estimates of biological rates provide the foundation for many branches of biology but, surprisingly, there are few systematic approaches to estimating monotonic rates from biological data.

Biological rates are routinely estimated from non-linear or noisy time series using linear regression. For example, many studies in physiology, ecosystem ecology and biogeochemistry monitor reactant consumption in closed chambers at standardized temperatures, and use the resulting, often non-linear, time series to estimate the rate of interest (e.g. Larmola et al., 2013; Ross et al., 2013; Song et al., 2011; Tanaka et al., 2013; White et al., 2011a,b; Yvon-Durocher et al., 2015). There are several problems with this approach. First, the data used rarely meet the criteria for linear regression to be an appropriate analytic tool. The first measures in a time series are often noisy as equipment/samples/organisms equilibrate after setup, while at the end of the time series, rates can change because of saturation effects or the exhaustion of a limiting resource (e.g. Fig. 1). Consequently, naive linear regression of a full time series can conflate the biological rate of interest with undesired effects. Second, common *ad hoc* methods to ameliorate this problem, such as manually truncating non-linear portions of the time series, introduce subjectivity into the analysis, and may reduce statistical power by removing useful data. Last, published studies rarely provide both the raw data and the specific methods necessary to reproduce reported results. This makes it difficult or impossible to evaluate the appropriateness of the methods, and is particularly problematic in a new era that demands scientific transparency and reproducibility (Fang et al., 2012; Grieneisen and Zhang, 2012). The need to estimate monotonic rates from time series data will only increase as technological advances continue to make collection of high-resolution data easy and cost effective. This presents biologists with a non-trivial challenge: to reliably estimate biological rates in a way that is statistically robust and fully reproducible.

Here, we introduce the LoLinR package for R (R Development Core Team, 2016), which provides a suite of simple functions to implement local linear regressions to estimate monotonic rates from time series data. We describe the general approach to reproducible and statistically robust estimation of monotonic rates, and the specific methods used in the package. We then walk through two example analyses to illustrate the utility of the package, as well as important analytic considerations and pitfalls (all computer code necessary to reproduce the analyses and figures in this article are available in Scripts S1 and S2; additional examples are available through <https://github.com/colin-olito/LoLinR>).

## MATERIALS AND METHODS

We first describe the base function around which the LoLinR package is built, then detail the component linearity metrics underpinning the function. The methods provided in the LoLinR package are a

Centre for Geometric Biology, School of Biological Sciences, Monash University, Clayton, VIC 3800, Australia.

\*Author for correspondence (colin.olito@gmail.com)

 C.O., 0000-0001-6883-0367; C.R.W., 0000-0002-0200-2187; D.R.B., 0000-0002-4568-2362

Received 26 August 2016; Accepted 14 December 2016

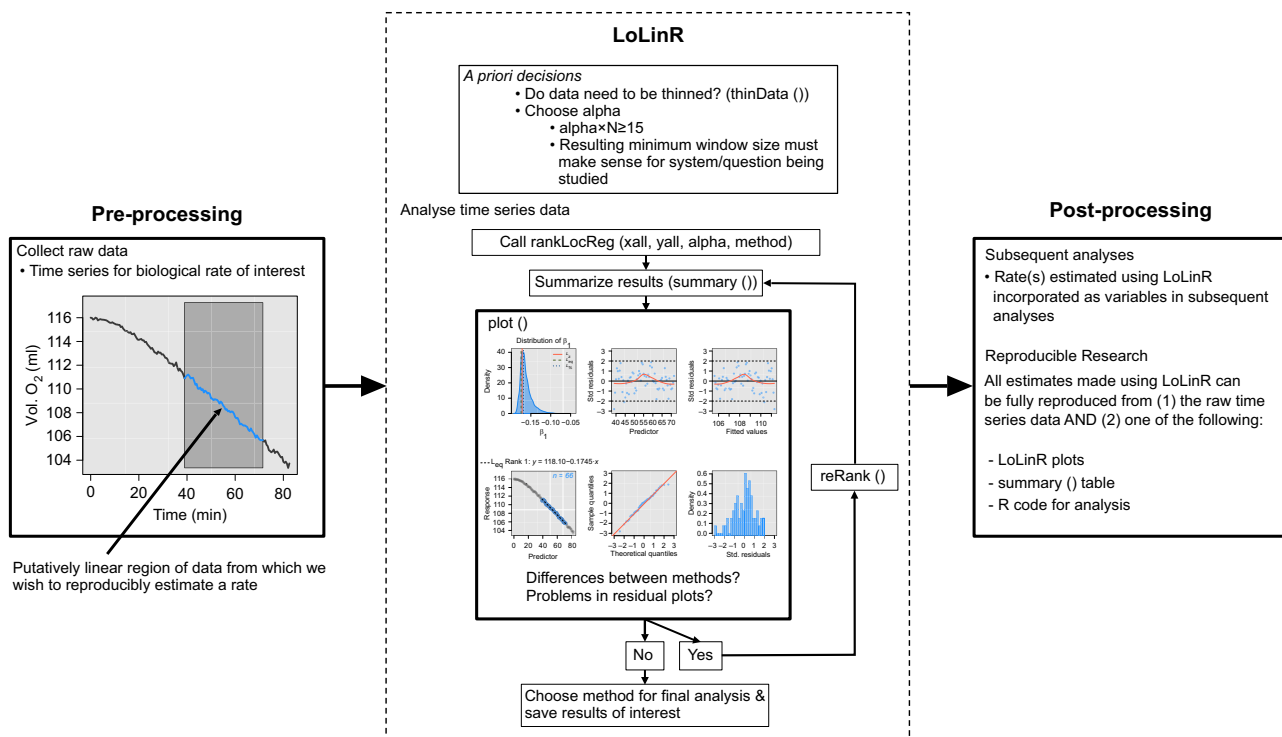


**Fig. 1. Schematic diagram showing a typical LoLinR workflow, as well as how using LoLinR to estimate biological rates would fit into an experimental project workflow.** In this example,  $O_2$  saturation data are being used to estimate metabolic rate for an individual sea urchin (*Heliocidaris erythrogramma*; C.O. and D.J.M., unpublished data). The putatively linear region of interest occurs after equipment equilibration, but before the urchin begins to show physiological responses to declining oxygen. Crucially, any estimate made using LoLinR can be easily reproduced from two pieces of information: (1) the raw time series data, and (2) LoLinR plots or summary tables or the R code used to implement the analysis. Each of these can be very easily compiled into appendices for published studies, making LoLinR analyses very easy to reproduce.

modification of traditional Loess regression techniques built around the wrapper function rankLocReg. While Loess techniques are designed primarily for data interpolation and visualization, rankLocReg stores relevant data from all possible local regressions of ordered subsets (adjacent points) of a full time series, given a minimum window size. The function returns an object of class rankLocReg, which includes a ranked list of the most linear subsets of the data, as well as corresponding data for each local regression. A call to rankLocReg implements three steps: (1) define the minimum window size, (2) fit local regressions and (3) rank local regressions.

The only user-defined constraint imposed on the analysis is alpha, which defines the minimum window size used to fit local regressions, expressed as a proportion of the total number of observations in the full data set (analogous to a traditional Loess smoothing parameter). At a minimum, alpha must take into account the total number of observations in the full data set,  $N$ , such that  $(\alpha \times N) \geq 15$  (Harrell, 2001). Ideally,  $(\alpha \times N)$  should also represent a biologically meaningful interval for the given data set. A call to rankLocReg fits all possible local regressions with  $n \geq (\alpha \times N)$  adjacent observations using ordinary least squares.

To quantify linearity for each of the local regressions, we define the combined linearity metric  $L$ , which represents a weighted sum of three component metrics. The first metric is the skewness of the standardized residuals for the local regression, estimated as the Fisher–Pearson standardized third moment coefficient:

$$S = \frac{n}{(n-1) \times (n-2)} \times \sum \left[ \left( \frac{x - \bar{x}}{\sigma(x)} \right)^3 \right], \quad (1)$$

where  $\sigma(x)$  is the sample standard deviation of  $x$ . The second metric is the range of the 95% confidence interval (CI) for the slope of the local regression  $\beta_1$ :

$$CI \text{ range} = \left( \beta_1 + t_{0.975}^* \times \frac{\sigma}{\sqrt{n}} \right) - \left( \beta_1 - t_{0.025}^* \times \frac{\sigma}{\sqrt{n}} \right), \quad (2)$$

where  $\sigma$  is the sample standard deviation and  $n$  is the number of observations used in the local regression, and the asterisks indicate the ‘critical’  $t$ -values associated with the 97.5th and 2.5th percentiles. The third and final metric is a modified Breusch–Godfrey statistic:

$$R_{BG}^2 = \frac{nR^2}{n}, \quad (3)$$

for serial correlation of the standardized residuals of the local regression up to order  $(n-k-1)$  (where  $k$  is the number of parameters in the fitted model – usually 2). We divide the traditional  $nR^2$  Breusch–Godfrey statistic by  $n$  to remove the multiplicative effect of sample size. We do this because we wish to compare the variance explained by local regressions with different sample sizes, rather than perform a significance test for an asymptotically  $\chi_{d.f.=n}^2$  distributed variable with fixed sample size  $n$ . It is also possible to account for autocorrelation using generalized linear models with a specified correlation structure. However, the  $R_{BG}^2$  metric accounts for serial correlation up to the maximum lag of  $(n-k-1)$  inclusive, and does not require additional assumptions made by alternative correlation structures. Each of the three component metrics,  $x$ , are  $\mathbf{Z}$  standardized against the minimum value (or minimum absolute

value for  $S$ ) obtained from all  $i$  fitted local regressions as:

$$\mathbf{Z}_{\min}[x_i] = \frac{x_i - \min(x)}{\sigma(x)},$$

$$\mathbf{Z}_{\min(\text{abs})}[x_i] = \frac{x_i - \min(\text{abs}(x))}{\sigma(x)},$$
(4)

where  $\sigma$  is the sample standard deviation, ensuring that all component metrics have a common scale, and smaller values of each correspond to greater linearity of the associated local regression. Thus, the combined linearity metric without any further weighting of the component metrics is defined as:

$$L_Z = \mathbf{Z}_{\min(\text{abs})}[S] + \mathbf{Z}_{\min}[\text{CI range}] + \mathbf{Z}_{\min}[R_{\text{BG}}^2].$$
(5)

$L_Z$  implicitly weights the contributions of each component metric by the relative magnitudes of their empirical variances for a given data set. For the many cases where the empirical distributions of the component metrics differ, we define and strongly recommend two alternative weighting methods:  $L_{\text{eq}}$  and  $L_{\%}$ .  $L_{\text{eq}}$  enforces equal weights by dividing the  $\mathbf{Z}_{\min}$  scores for each metric by their maximum value before summing.  $L_{\%}$  sums the percentile-ranks of the  $\mathbf{Z}_{\min}$  scores for each component metric. The choice of weighting method will ultimately depend on the specific characteristics of each data set, the alpha value used for the rankLocReg analysis, and the biology of the system being studied.

When used with rankLocReg objects, the plot function generates several diagnostic plots to help determine the most appropriate method for a given analysis. Users can examine results from alternative  $L$  metrics by using the reRank function. Fig. 1 provides a schematic overview of a typical workflow using LoLinR to estimate biological rates. Crucially, analyses using LoLinR can be fully reproduced from (1) the time series data and (2) any one of the following: summary plots, summary tables or the R code used to perform the analysis. All are easily included as appendices or supplementary material to published articles, making LoLinR analyses extremely easy to reproduce.

## RESULTS AND DISCUSSION

### Larval metabolic rate

The first example is from a study of allometric scaling of metabolic rate during larval development in two bryozoan species (*Bugula neritina* and *Watersipora subquortata*; Pettersen et al., 2015). Metabolic rate was estimated for individual larva from  $\text{O}_2$  saturation time series collected using closed chambers. Fig. 2A provides an example of the analytical challenge presented by these data. The full time series is clearly non-linear: the rate of  $\text{O}_2$  consumption initially decelerates as the chamber and larva equilibrate after handling. There is also a subtle acceleration towards the end of the time series, probably resulting from a physiological response by the larva to declining  $\text{O}_2$  availability (Lagos et al., 2015), or accumulation of bacterial biofilm that began to consume oxygen. Any estimate of  $\text{O}_2$  consumption rate including these non-linearities would be conflated

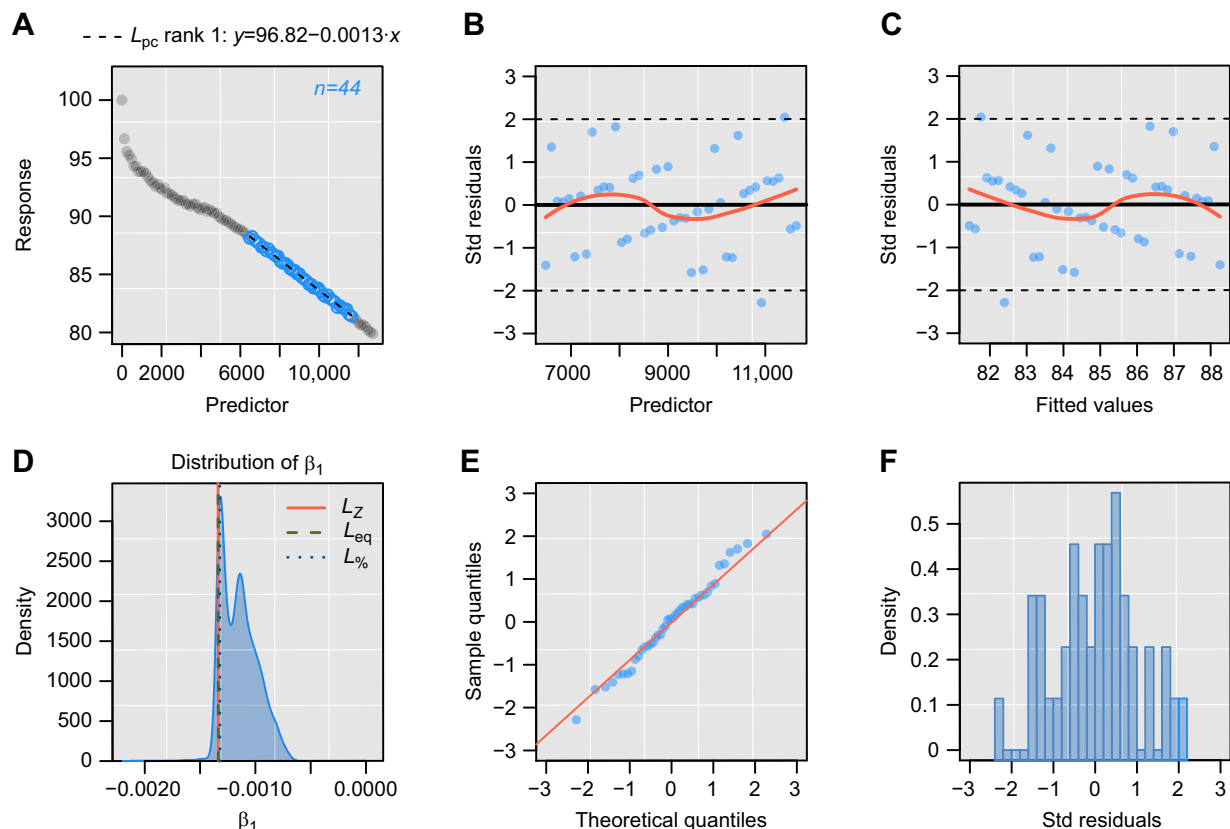


**Fig. 2.** Diagnostic plots generated by the plot command for the  $L_{\%}$  rank 1 local regression for the *Bugula* larva respiration time series data. Data are from Pettersen et al. (2015). The output plots show: (A) the full time series, with the rank 1 local regression highlighted in blue, along with the associated regression equation and number of observations; (B) standardized residuals for the chosen local regression, regressed against the predictor variable (time in seconds for the *Bugula* data set); (C) standardized residuals regressed against the fitted values; (D) density plot with empirical distribution of local regression slopes ( $\beta_1$ ), benchmarked against the slopes of the rank 1 local regressions for each  $L$  metric; (E) normal–quantile–quantile plot for the rank 1 local regression; and (F) a histogram of the distribution of the standardized residuals for the rank 1 local regression.

with these other processes. However, truncating the data to exclude these non-linearities is subjective and difficult, especially for the subtle curvature towards the end of the data set. Ultimately, we wish to identify the region where the relationship between  $O_2$  concentration and time is most linear, and estimate its slope.

Using the LoLinR package, we can analyse this data set with the call:

```
library(LoLinR)
data(BugulaData)
BugulaRegs <- rankLocReg(
  xall=BugulaData$Time.s, yall=BugulaData$Dl,
  alpha=0.2, method="eq")
```

which implements the rankLocReg function with a minimum window size of  $\alpha=0.2$ , and uses the linearity metric  $L_{eq}$  to rank local regressions. This alpha value results in a minimum window size of  $(\alpha \times N)=22$  for this data set. This call returns an object of class rankLocReg which includes a ranked list of all possible local regressions, the number of local regressions fitted and several summary statistics. Examination of the summary output and the distribution of local regression slopes (Fig. 2D, density plot) indicates that both the  $L_Z$  and  $L_{eq}$  weighting methods return the same rank 1 local regression, while the  $L_{\%}$  method returns a slightly different result. However, all three methods identify local regressions in the later half of the time series, where the rate of  $O_2$  consumption has stabilized. The  $L_{\%}$  rank 1 local regression includes a larger subset of the data ( $n=44$  observations) than the other two methods ( $n=26$ ), and all three rank 1 local regressions have nearly identical slopes ( $L_Z$ ,  $L_{eq}$ :  $\beta_1=-0.00133$ ;  $L_{\%}$ :  $\beta_1=-0.00132$ ). Given the similarity of the results, we would recommend using the  $L_{\%}$  method in this case, because it provides greater statistical power for the estimation of  $\beta_1$ , the parameter of interest. Inspection of the chosen local regression and accompanying residual plots also suggests that other than some autocorrelation, which is expected in time series data, there are no other major concerns (Fig. 2C–F).

A comparison of this result with common alternative approaches highlights the usefulness of the methods. Naive linear regression of the full time series yields an estimate of  $\beta_1=-0.00119$ , indicating that non-linearities, particularly early in the time series, result in under-estimation of the metabolic rate. Estimates obtained by linear regression of manually truncated subsections of these data (with the same window size of  $n=22$  observations) can range from  $\beta_1=-0.00212$  to  $\beta_1=-0.00067$ , more than a threefold difference in the estimate of metabolic rate. In addition to being methodologically

opaque and conflating the desired rate with other experimental and biological processes, these common *ad hoc* methods can give highly inaccurate estimates.

### Flow-through respirometry

The second example is a study of the metabolic costs of living in the Arctic for great cormorants (*Phalacrocorax carbo*) (White et al., 2011a). In this study, metabolic rate was estimated for individual birds using flow-through respirometry protocols (see supplementary material in White et al., 2011a). These techniques generate time series of the rate of  $O_2$  consumption ( $\dot{V}_{O_2}$ , ml  $O_2$   $kg^{-1}$   $min^{-1}$ ) rather than  $O_2$  saturation or concentration. For these data, the analytic goal was to estimate resting metabolic rate, which should correspond to the subset of the time series where  $\dot{V}_{O_2}$  is lowest and most linear. Conventional methods for estimating  $\dot{V}_{O_2}$  from flow-through respirometry data are based on analysis of the distribution of sequences of adjacent data points, and the minimum running average of subsets of adjacent points with varying numbers of included observations (e.g. Withers, 2001). Here, we illustrate how rankLocReg can be used to estimate resting metabolic rate from these data by leveraging the statistical framework of local linear regression and examining the distribution of standardized residuals.

We analyse a representative  $\dot{V}_{O_2}$  time series for an individual cormorant. The time series is non-linear with large spikes occurring when the animal is physically active inside the chamber, but there appears to be a region of relative stability between 2.5 and 5.25 h (Fig. 3). We analyse the thinned data with a call to rankLocReg using  $\alpha=0.1$ . This ensures that the minimum window size corresponds to approximately 30 min, and a minimum of 15 observations for the local regressions. Although we are not necessarily interested in the slopes of the local regressions ( $\beta_1$ ), an examination of the distribution of  $\beta_1$  highlights the fact that the  $L_{\%}$  metric returns a different rank 1 local regression from the other two  $L$  metrics (Fig. 3A). For these data, the  $L_Z$  and  $L_{eq}$  metrics misidentify the most stable subset of these data (a consequence of strongly skewed empirical distribution of  $R_{BG}^2$ ) (Fig. 3B; Fig. S1). However,  $L_{\%}$  identifies a period of approximately 2 h where  $\dot{V}_{O_2}$  is most stable (Fig. 3C). The average (or median)  $\dot{V}_{O_2}$  during this period is easily recovered using the summary for this analysis, and returns an estimate of  $\dot{V}_{O_2}$ . This estimate is similar to those obtained using conventional methods ( $\dot{V}_{O_2}=33.90$  and  $35.57$  ml  $kg^{-1}$   $min^{-1}$ ; Fig. S2; see Withers, 2001, for detailed methods), as well as the median of the full time series ( $36.71$  ml  $kg^{-1}$   $min^{-1}$ ), but has two

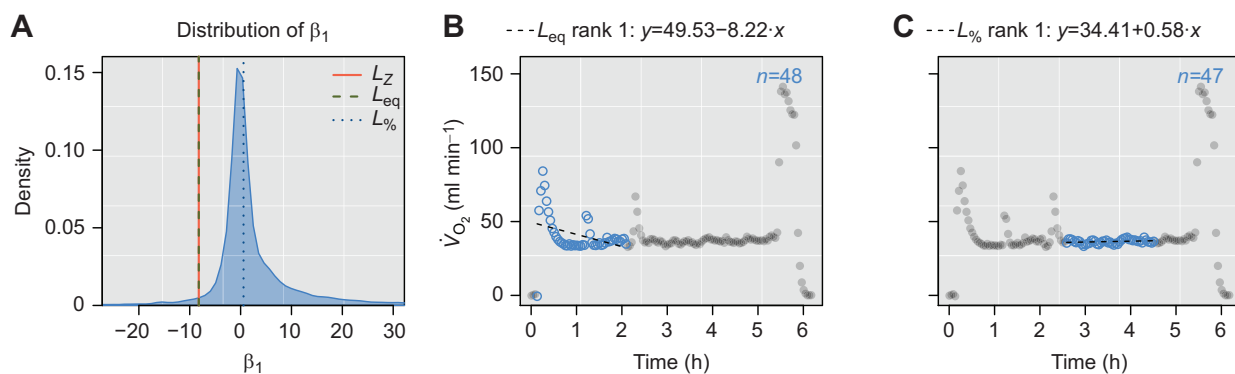


**Fig. 3. Diagnostic plots of flow-through respirometry data from great cormorants.** Data are from White et al. (2011a). Plots show: (A) the distribution of local regression slopes ( $\beta_1$ ; note that long tails on the distribution have been truncated to emphasize differences in the  $L$  metric benchmarks); (B) the  $L_{eq}$  rank 1 local regression, which misidentifies the subset of data where  $O_2$  consumption was most stable; and (C) the  $L_{\%}$  rank 1 local regression, which identifies a reasonable subset of the full time series where the rate of  $O_2$  consumption is most stable.

distinct advantages. First, the  $L$  metrics provide an objective measure of linearity to identify periods of stability in the  $\dot{V}_{O_2}$  time series. Second, the  $L$  metrics do not preferentially select the smallest possible subset of the time series to estimate resting metabolic rate, resulting in an estimate that is based on more observations, and therefore has more statistical power ( $n=47$  using LoLinR;  $n=11$  or 18 using conventional methods).

## Appendix

### Quantifying LoLinR performance using simulated data

An informative comparison between the methods provided in LoLinR and common alternatives is deceptively difficult for at least two reasons. First, the most common alternative methods (e.g. eyeballing the data to select a linear region and then running a linear regression, or the methods described in Withers, 2001) simply cannot be reliably compared with LoLinR because they are not objectively reproducible. Second, generating appropriate simulated data for the types of analyses LoLinR is designed to assist with (i.e. where some subset of a time series is indeed linear, or expected to be linear, but the rest is arbitrarily non-linear) is a non-trivial problem. This is particularly problematic when the specific nature of the non-linearity has a strong influence on the behaviour of the methods that LoLinR might be compared against (e.g. naive linear regression of full data sets). As a first step towards providing objective validation and comparison of our methods, we provide functions to generate simulated data and analyse the performance of rankLocReg (see Script S1). However, we emphasize that this is not a comprehensive sensitivity analysis, but rather a starting point for validating our methods and making future comparisons with other reproducible methods. Here, we briefly describe how simulated data were generated, and how the performance of rankLocReg was assessed.

We generated simulated data that roughly resemble O<sub>2</sub> consumption data (similar to the ‘Larval metabolic rate’ example in Results and Discussion), with an initial phase of acceleration/deceleration which then stabilizes as a straight line. Simulated data sets are composed of 100 observations. The first 50 observations are non-linear, following a sine wave from the apex (or trough) at  $\pm\pi/2$  to the inflection point at  $\pm\pi$ . The second 50 observations are linear, following  $y=\beta_0+\beta_1x$ , where  $\beta_0$  is equal to the 50th observation (the last of the non-linear subset), and the regression slope is uniformly distributed on the intervals  $\beta_1\in[-0.028, -0.004] \cup [0.004, 0.028]$ . We add a small amount of normally distributed noise to the entire data set [ $\epsilon\sim\mathcal{N}(0, 0.05)$ ] to simulate random variation present in real-time series data. We analyse each randomly generated data set using rankLocReg, with  $\alpha=0.2$ .

To quantify the performance of rankLocReg, we use three simple metrics. (1) The difference between the actual slope of the linear subset of the simulated data and the slope of the local linear regressions identified by rankLocReg ( $\Delta_i=\beta_i-\beta_{\text{real}}$ ), where  $i$  indicates each of the  $L$  methods used by rankLocReg ( $i\in[Z, \text{eq}, \%]$ ). As each of the three  $L$  metrics performs differently for different data sets, we also compare the difference between the real regression slope and the best of the three local regressions identified by rankLocReg (i.e. the one with the smallest  $\Delta_i$ ), which we designate  $\Delta_{\text{best}}$ . (2) The proportion of the linear subset of the data that is correctly included in the local linear regressions identified by rankLocReg. (3) The proportion of the observations included in local linear regressions that correctly include the linear subset of the data.

### Results summary

For this particular type of simulated test data, rankLocReg performs remarkably well, particularly in comparison with a naive linear

regression of the full data sets. The result of this specific comparison is not surprising, however, as the curvature in the first half of the simulated data results in systematic bias of  $\beta_{\text{naive}}$  towards 0. This is reflected in Fig. S3A, where the distribution of  $\Delta_{\text{naive}}$  is right skewed with a thicker tail than the distribution of  $\Delta_{\text{best}}$ . In contrast,  $\Delta_{\text{best}}$  is tightly distributed about 0, with a few outliers in the right tail. Each of the three  $L$  metrics performs similarly, although the local regressions identified using the  $L_{\%}$  methods are generally better at recovering regression slopes that are more similar to  $\beta_{\text{real}}$  (Fig. S3B). As expected, the absolute values of  $\beta_{\text{real}}$  also influence the performance of rankLocReg. Overall, rankLocReg performs better when  $\beta_{\text{real}}$  is further from 0 (Fig. S3C). Specifically, when  $\beta_{\text{real}}$  is negative but close to 0, rankLocReg tends to choose regressions that include the non-linear portion of the data, with slopes that are more steeply negative than  $\beta_{\text{real}}$ . When  $\beta_{\text{real}}$  is positive but close to 0, rankLocReg tends to choose local regressions with more steeply positive slopes than  $\beta_{\text{real}}$  for the same reasons. This behaviour makes sense because the 95% CI for  $\beta_1$  is used to calculate the  $L$  metrics used by rankLocReg, which becomes increasingly inflated as  $\beta_{\text{real}}$  approaches 0.

rankLocReg also does a reasonably good job of correctly identifying the truly linear subset of these simulated data. This is encouraging, particularly because the curvature of the simulated data in this example should make this rather difficult. This is because the second half of the non-linear portion of the simulated data is increasingly linear (with a slope of  $\beta_1\approx\pm 0.016$  on the  $x$ -scale used for this analysis) as they approach the inflection point of the sine wave at  $\pm\pi$ . Thus, it should be difficult for rankLocReg to distinguish between the end of the non-linear subset of the data and the truly linear subset. However, at least one of the  $L$  methods implemented by rankLocReg (i.e. the ‘best’ local regression with the smallest  $\Delta$  value) generally included a large fraction of the truly linear subset of the data (Fig. S3D). However, there was quite a bit of variability in the performance of each of the  $L$  methods (Fig. S3E). The  $L_Z$  and  $L_{\text{eq}}$  methods in particular either performed very well or very poorly at identifying the truly linear subset of the data. In contrast, the  $L_{\%}$  method generally identified at least half of the truly linear subset (Fig. S3E). The ability of rankLocReg to correctly identify the truly linear subset of the data was again sensitive to the absolute value of  $\beta_{\text{real}}$ . Specifically, even the ‘best’ local regression mis-identified the truly linear subset more frequently as  $\beta_{\text{real}}$  approached 0 (Fig. S3F).

rankLocReg also performed well at identifying local regressions that correctly include the truly linear subset of the data. For a large majority of simulated data sets, more than half of the observations included in the ‘best’ local regression identified by rankLocReg were part of the truly linear subset of the data (Fig. S3G). However, there was again significant variability in the performance of each of the three  $L$  methods (Fig. S3H). The  $L_{\%}$  method clearly performed the best in this respect, generally choosing local regressions with the majority of observations falling within the truly linear subset of the data (Fig. S3H). However, the  $L_Z$  method generally performed very poorly, choosing local regressions that badly mis-identified the linear subset of the data, or choosing local regressions of which only half of the included observations were actually part of the truly linear subset (Fig. S3H). The  $L_{\text{eq}}$  method also performed poorly, but was better at identifying local regressions, with the majority of observations falling within the truly linear subset of the data (Fig. S3H). Once again, the performance of even the ‘best’ local regression became worse as  $\beta_{\text{real}}$  approached 0. The variability in the performance of the three  $L$  methods is almost certainly a direct consequence of the difficulty in distinguishing between the end of the non-linear and the beginning of the linear subsets of these

simulated data. This is particularly clear for  $L_{\%}$ , which often identified local regressions that spanned both the non-linear and linear portions of the data.

Four main conclusions emerge from this limited test of the performance of rankLocReg against simulated data. First, rankLocReg performs better than naive linear regression of full time series at estimating the slope of a linear subset of the time series. Second, this analysis strongly supports our recommendations in the Materials and Methods and Results and Discussion sections that  $L_{\%}$  be used as the preferred weighting method.  $L_{\%}$  is generally more robust and does a better job than the other methods of choosing local regressions that both accurately estimate  $\beta_{\text{real}}$  and correctly include the truly linear subset of these simulated data. Third, rankLocReg becomes progressively better at accurately estimating  $\beta_{\text{real}}$  values that are further from 0 (and presumably further from 1 as well). Fourth, this analysis highlights that while there can be significant variation in the performance of each of the three  $L$  metric weighting methods, it is rare that all three mis-identify the truly linear subset of the time series. Taken together, these results indicate that the methods provided in LoLinR perform well for their intended purpose for the type of data simulated here.

#### Acknowledgements

The authors thank A. Pettersen and G. Yvon-Durocher for graciously providing data, and two anonymous reviewers.

#### Competing interests

The authors declare no competing or financial interests.

#### Author contributions

Conceptualization: C.O. and D.R.B.; Methodology: C.O. and D.R.B.; Software: C.O. and D.R.B.; Writing – original draft preparation: C.O.; Writing – review and editing: C.R.W., D.J.M. and D.R.B.; Funding acquisition: D.J.M. and C.R.W.

#### Funding

This work was funded by a Monash University Dean's International Postgraduate Student Scholarship to C.O., Australian Research Council grants to D.J.M. and C.R.W., and a Monash University Centre for Geometric Biology Post-Doctoral Fellowship to D.R.B.

#### Data accessibility

All data used in this study are included in the LoLinR package and available at <https://github.com/colin-olito/LoLinR>.

#### Supplementary information

Supplementary information available online at <http://jeb.biologists.org/lookup/doi/10.1242/jeb.148775.supplemental>

#### References

- Barneche, D. R., Kulbicki, M., Floeter, S. R., Friedlander, A. M., Maina, J. and Allen, A. P. (2014). Scaling metabolism from individuals to reef-fish communities at broad spatial scales. *Ecol. Lett.* **17**, 1067-1076.
- Brown, J. H., Gillooly, J. F., Allen, A. P., Savage, V. M. and West, G. B. (2004). Toward a metabolic theory of ecology. *Ecology* **85**, 1771-1789.
- Fang, F. C., Steen, R. G. and Casadevall, A. (2012). Misconduct accounts for the majority of retracted scientific publications. *Proc. Natl. Acad. Sci. USA* **109**, 17028-17033.
- Gillooly, J. F., Brown, J. H., West, G. B., Savage, V. M. and Charnov, E. L. (2001). Effects of size and temperature on metabolic rate. *Science* **293**, 2248-2251.
- Grieneisen, M. L. and Zhang, M. (2012). A comprehensive survey of retracted articles from the scholarly literature. *PLoS ONE* **7**, e44118.
- Harrell, F. E. (2001). *Regression Modelling Strategies with Applications to Linear Models, Logistic Regression and Survival Analysis*. New York, USA: Springer.
- Lagos, M. E., White, C. R. and Marshall, D. J. (2015). Avoiding low-oxygen environments: oxytaxis as a mechanism of habitat selection in a marine invertebrate. *Mar. Ecol. Prog. Ser.* **540**, 99-107.
- Larmola, T., Bubier, J. L., Kobyljanec, C., Basiliko, N., Juutinen, S., Humphreys, E., Preston, M. and Moore, T. R. (2013). Vegetation feedbacks of nutrient addition lead to a weaker carbon sink in an ombrotrophic bog. *Glob. Change Biol.* **19**, 3729-3739.
- Marshall, D. J., Bode, M. and White, C. R. (2013). Estimating physiological tolerances - a comparison of traditional approaches to nonlinear regression techniques. *J. Exp. Biol.* **216**, 2178-2182.
- Pettersen, A. K., White, C. R. and Marshall, D. J. (2015). Why does offspring size affect performance? Integrating metabolic scaling with life-history theory. *Proc. R. Soc. B Biol. Sci.* **282**, 20151946.
- R Core Team (2016). R: A language and environment for statistical computing. R Foundation for Statistical Computing, Vienna, Austria. URL <https://R-project.org/>
- Ross, D. J., Longmore, A. R. and Keough, M. J. (2013). Spatially variable effects of a marine pest on ecosystem function. *Oecologia* **172**, 525-538.
- Shapiro, J. B., Griffin, K. L., Lewis, J. D. and Tissue, D. T. (2004). Response of *Xanthium strumarium* leaf respiration in the light to elevated CO<sub>2</sub> concentration, nitrogen availability, and temperature. *New Phytol.* **162**, 377-386.
- Song, K., Lee, S.-H. and Kang, H. (2011). Denitrification rates and community structure of denitrifying bacteria in newly constructed wetland. *Eur. J. Soil Biol.* **47**, 24-29.
- Stinchcombe, J. R. and Kirkpatrick, M. and Function-valued Traits Working Group (2012). Genetics and evolution of function-valued traits: understanding environmentally responsive phenotypes. *Trends Ecol. Evol.* **27**, 637-647.
- Tanaka, T., Alliouane, S., Bellerby, R. G. B., Czerny, J., de Kluijver, A., Riebesell, U., Schulz, K. G., Silyakova, A. and Gattuso, J.-P. (2013). Effect of increased pCO<sub>2</sub> on the planktonic metabolic balance during a mesocosm experiment in an Arctic fjord. *Biogeosciences* **10**, 315-325.
- White, C. R., Grémillet, D., Green, J. A., Martin, G. R. Butler, P. J. (2011a). Metabolic rate throughout the annual cycle reveals the demands of an Arctic existence in Great Cormorants. *Ecology* **92**, 475-486.
- White, C. R., Kearney, M. R., Matthews, P. G. D., Kooijman, S. A. L. M. and Marshall, D. J. (2011b). A manipulative test of competing theories for metabolic scaling. *Am. Nat.* **178**, 746-754.
- Withers, P. C. (2001). Design, calibration, and calculation for flow-through respirometry systems. *Aust. J. Zool.* **49**, 445-461.
- Yen, J. D. L., Thomson, J. R., Paganin, D. M., Keith, J. M. and MacNally, R. (2015). Function regression in ecology and evolution: FREE. *Methods Ecol. Evol.* **6**, 17-26.
- Yvon-Durocher, G., Allen, A. P., Cellamare, M., Dossena, M., Gaston, K. J., Leitao, M., Montoya, J. M., Reuman, D. C., Woodward, G. and Trimmer, M. (2015). Five years of experimental warming increases the biodiversity and productivity of phytoplankton. *PLoS Biol.* **13**, e1002324.

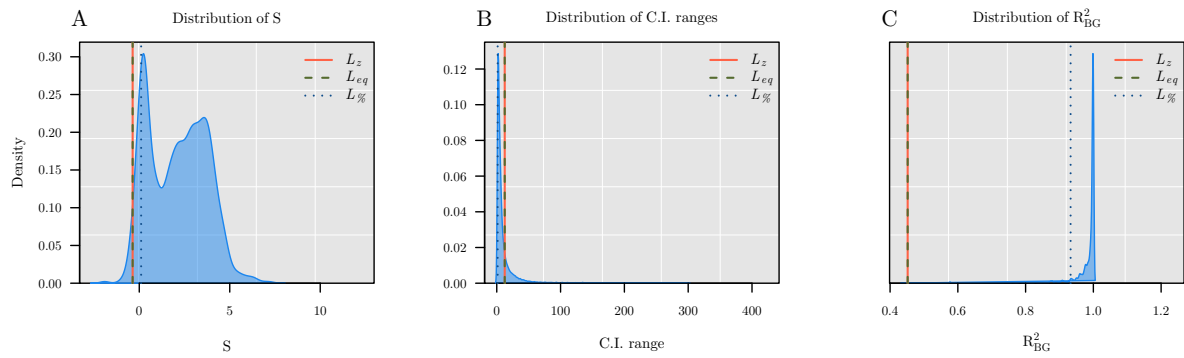


Fig. S1. Empirical distributions of the component metrics A)  $S$ ; B)  $C.I. range$ ; and C)  $R^2_{BG}$  for the analysis of resting metabolic rate in Great Cormorants (raw data thinned using `thinData(CormorantData, by=3)`, and a call to `rankLocReg` using `alpha=0.1`). Note the extremely long tail in the distribution of  $R^2_{BG}$  (panel C), and the large discrepancy between the  $L_{\%}$  benchmark and the other metrics.

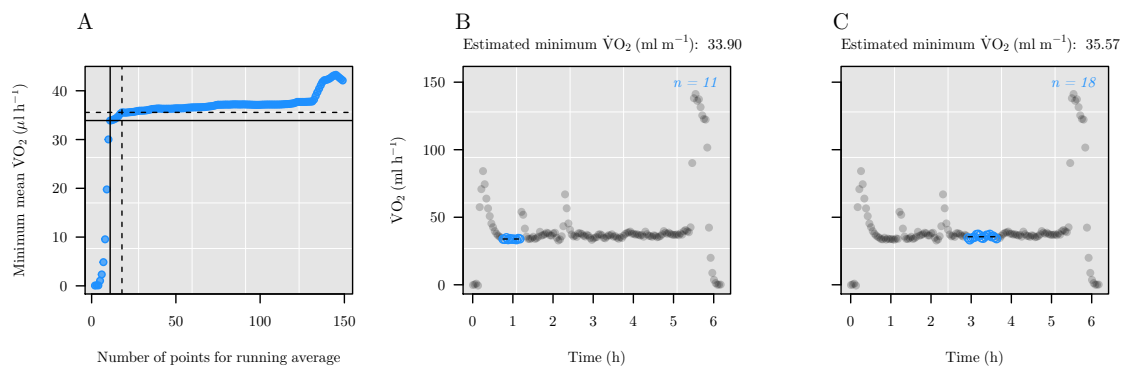


Fig. S2. A graphical summary of conventional methods of estimating resting metabolic rate from  $\dot{V}O_2$  time series data (after Withers, 2001). Panel A shows the minimum estimated  $\dot{V}O_2$  as a function of the number of adjacent observations used to calculate the running average. After a rapid increase in the minimum  $\dot{V}O_2$  with increasing observations up to  $n = 11$  (solid black cross), there is a brief region with an intermediate slope, before the plot plateaus at  $n = 18$  (dotted cross). Using these methods, a researcher could potentially justify using the running average associated with either of these two points as an estimate of resting metabolic rate. Panels A and B show the full time series, with the subsets associated with  $n = 11$  and  $n = 18$  respectively highlighted in blue. Note that both subsets are much smaller than the number of observations included in the  $L_{\%}$  rank 1 local regression identified by `rankLocReg` (Fig. 3).

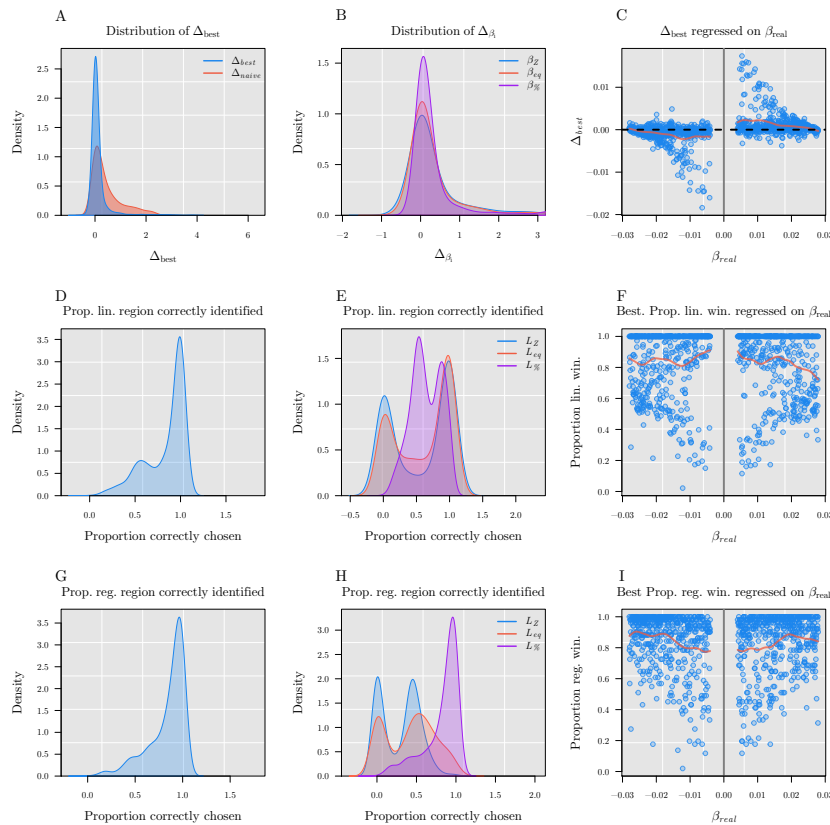


Fig. S3. Graphical summary of the performance of LoLinR methods using certain types of simulated data. Panels A-C show results for the performance metric  $\Delta$ ; panels D-F show results for the proportion of the linear subset of the data that are correctly included in the local regressions identified by rankLocReg; and panels G-I show results for the proportion of the local regression identified by rankLocReg that correctly includes the linear subset of the simulated data. The first column of panels (A,D,G) show the distributions for each performance metric of the 'best' local regression identified by rankLocReg (the local regression with the smallest  $\Delta$ ). Note that the x-axes are scaled in units of  $\beta_{real}$ ; thus, in panel A, a  $\Delta$  value of 2 indicates that  $\Delta_{best}$  was twice as large as the real slope of the simulated data ( $\beta_{real}$ ). Panel A shows a comparison between the performance of rankLocReg and a naive regression by comparing the distributions of  $\Delta_{best}$  and  $\Delta_{naive}$ . As expected, the slopes identified by naive regression are systematically biased by the non-linearity present in the simulated data, while rankLocReg is better able to identify slopes that are closer to the  $\beta_{real}$ . The second column of panels (B,E,H) show the distributions of each performance metric for each of the three  $L$  metric methods provided in rankLocReg. The third column of panels (C,F,I) show scatter plots of each performance metrics regressed on the actual slope of the simulated data ( $\beta_{real}$ ), with smoothing splines overlaid to help visualize any trends. This is to visualize that, as expected, rankLocReg performs better as the slope of the linear region is further from 0. Note that in panel B long right tails have been truncated to better visualize the peaks of the distributions

# Bibliography

- Abbott, J. K. 2011. Intralocus sexual conflict and sexually antagonistic genetic variation in hermaphroditic animals. *Proc. Roy. Soc. B.* 278:161–169.
- Agrawal, A. F., and M. C. Whitlock. 2011. Inferences about the distribution of dominance drawn from yeast gene knockout data. *Genetics* 178:553–566.
- Allee, W. C., et al. 1949. *Principles of animal ecology*. Philadelphia, PA, USA: Saunders.
- Arnold, G., and L. Wade. 1984. On the measurement of natural and sexual selection: applications. *Evolution* 38:720–734.
- Arnqvist, G. 2011. Assortative mating by fitness and sexually antagonistic genetic variation. *Evolution* 65:2111–2116.
- Arnqvist, G., and L. Rowe. 2005. *Sexual conflict*. Princeton, NJ, USA: Princeton University Press.
- Ashman, T.-L., et al. 2015. Multilocus sex determination revealed in two populations of gynodioecious wild strawberry, *Fragaria vesca* subs. *bracteata*. *G3* 5:2759–2773.
- Augspurger, C. K. 1981. Reproductive synchrony of a tropical shrub: experimental studies on effects of pollinators and seed predators on *Hybanthus prunifolius* (Violaceae). *Ecology* 62:775–788.
- Babcock, R. C., et al. 1986. Synchronous spawnings of 105 scleractinian coral species on the Great Barrier Reef. *Marine Biology* 90:379–394.
- Bachtrog, D. 2006. A dynamic view of sex chromosome evolution. *Curr. Op. Gen. Devel.* 16:578–585.
- Bachtrog, D., et al. 2014. Sex determination: why so many ways of doing it? *PLoS Biology* 12 (7): e1001899.
- Baird, A. H., J. R. Guest, and B. L. Willis. 2009. Patterns in reproductive biology of scleractinian corals. *Ann. Rev. Ecol. Evol. Syst.* 2009:551–571.
- Barrett, S. C. H. 2010. Darwin's legacy: the forms, function, and sexual diversity of flowers. *Phil. Trans. Roy. Soc. B.* 365:351–368.
- . 2002. Sexual interference of the floral kind. *Heredity* 88:154–159.
- Barson, N. J., et al. 2015. Sex-dependent dominance at a single locus maintains variation in age at maturity in salmon. *Nature* 528:405–408.
- Bateman, D. 1948. Intra-sexual selection in *Drosophila*. *Heredity* 2:349–368.
- Bawa, K. F. 1980. Evolution of dioecy in flowering plants. *Ann. Rev. Ecol. Syst.* 11:15–39.
- Beck, C. W. 1998. Mode of fertilization and parental care in anurans. *Animal Behaviour* 55:439–449.
- Behtari, A., A. Gelman, and J. Gabry. 2016. Practical Bayesian model evaluation using leave-one-out cross-validation and WAIC. *Statistical Computing* doi:10.1007/s11222-016-9696-4.

- Benítez-Villalobos, F., C. Aguilar-Duarte, and O. H. Avila-Poveda. 2012. Reproductive biology of *Opiocoma aethiops* and *O. alexandri* (Echinodermata: Ophiuroidea) from Estacahuite Bay, Oaxaca, Mexico. *Aquatic Biology* 17:119–128.
- Berger, D., et al. 2014. Intralocus sexual conflict and environmental stress. *Evolution* 68:2184–2196.
- Binks, R. M., et al. 2012. More than bindin divergence: reproductive isolation between sympatric subspecies of a sea urchin by asynchronous spawning. *Evolution* 66:3545–3557.
- Birkhead, T. R., and A. P. Møller. 1998. *Sperm competition and sexual selection*. London, UK: Academic Press.
- Blackburn, G. S., A. Y. K. Albert, and S. P. Otto. 2010. The evolution of sex ratio adjustment in the presence of sexually antagonistic selection. *The American Naturalist* 176:264–275.
- Bode, M., and D. J. Marshall. 2007. The quick and the dead? Sperm competition and sexual conflict in the sea. *Evolution* 61:2693–2700.
- Bonduriansky, R., and S. F. Chenoweth. 2009. Intralocus sexual conflict. *Trends in Ecology and Evolution* 24:280–288.
- Brawley, S. H. 1992. Fertilization in natural populations of the dioecious brown alga *Fucus ceranoides* and the importance of the polyspermy block. *Marine Biology* 113:145–157.
- Brookes, R. H., and L. K. Jesson. 2010. Do pollen and ovule number match the mating environment? an examination of temporal change in a population of *Styloidium armeria*. *Int. J. Plant Sciences* 171:818–827.
- Brunet, J., and D. Charlesworth. 1995. Floral sex allocation in sequentially blooming plants. *Evolution* 49:70–79.
- Bulmer, M. G. 1983. Models for the evolution of protandry in insects. *Theor. Population Biology* 23:314–322.
- Caballero, A., and W. G. Hill. 1992. Effects of partial inbreeding on fixation rates and variation of mutant genes. *Genetics* 131:493–507.
- Chapman, T., et al. 2003. Sexual conflict. *Trends in Ecology and Evolution* 18:41–47.
- Charlesworth, B., and D. Charlesworth. 1978a. A model for the evolution of dioecy and gynodioecy. *The American Naturalist* 112:975–997.
- Charlesworth, B., and D. Charlesworth. 2010. *Elements of evolutionary genetics*. 461–464, 473. Colorado, USA: Roberts / Company.
- Charlesworth, D. 1985. Distribution of dioecy and self-incompatibility in angiosperms. In *Evolution: Essays in honor of John Maynard Smith*, ed. by P. J. Greenwood and M. Slatkin, pp.237–268. Cambridge, U. K.: Cambridge University Press.
- . 2006. Evolution of plant breeding systems. *Current Biology* 16:R726–R735.
- . 2002. Plant sex determination and sex chromosomes. *Heredity* 88:94–101.
- . 1999. Theories of the evolution of dioecy. Chap. 2 in *Gender and sexual dimorphism in flowering plants*, ed. by M. A. Geber, T. E. Dawson, and L. F. Delph, pp.33–60. Heidelberg, Germany: Springer Science / Business Media.
- Charlesworth, D., and B. Charlesworth. 1978b. Population genetics of partial male sterility and the evolution of monoecy and dioecy. *Heredity* 41:137–153.

- Charlesworth, D., and J. Willis. 2009. The genetics of inbreeding depression. *Nature Reviews Genetics* 10:783–796.
- Charlesworth, D., D. W. Schemske, and V. L. Sork. 1987. The evolution of sex and its consequences: sexual versus natural selection. In *The evolution of sex and its consequences*, ed. by S. Stearns, pp.317–336. Boston, MA, USA: Birkhauser.
- Charnov, E. 1982. *The theory of sex allocation*. Princeton, NJ, USA: Princeton University Press.
- Cheng, C., and M. Kirkpatrick. 2016. Sex-specific selection and sex-biased gene expression in humans and flies. *PLoS Genetics* 12 (9): e1006170.
- Chippindale, A. K., J. R. Gibson, and W. R. Rice. 2001. Negative genetic correlation for fitness between sexes reveals ontogenetic conflict in *Drosophila*. *PNAS* 98:1671–1675.
- Christy, J. H. 1978. Adaptive significance of reproductive cycles in the fiddler crab *Uca pugilator*: a hypothesis. *Science* 199:453–455.
- . 2011. Timing of hatching and release of larvae by brachyuran crabs: patterns, adaptive significance, and control. *Integr. Comp. Biol.* 51:62–72.
- Clifton, K. E. 1997. Mass spawning by green algae on coral reefs. *Science* 275:1116–1118.
- Coe, D. 1936. Sexual phases in *Crepidula*. *J. Experimental Zoology* 72:455–477.
- Connallon, T. 2015. The geography of sex-specific selection, local adaptation, and sexual dimorphism. *Evolution* 69:2333–2344.
- Connallon, T., and A. G. Clark. 2012. A general population genetic framework for antagonistic selection that accounts for demography and recurrent mutation. *Genetics* 190:1477–1489.
- . 2014a. Balancing selection in species with separate sexes: insights from Fisher’s geometric model. *Genetics* 197:991–1006.
- . 2014b. Evolutionary inevitability of sexual antagonism. *Proc. Roy. Soc. B* 281:20132123.
- . 2010. Sex linkage, sex-specific selection, and the role of recombination in the evolution of sexually dimorphic gene expression. *Evolution* 64:3417–3442.
- . 2011. The resolution of sexual antagonism by gene duplication. *Genetics* 187:919–937.
- Connallon, T., and C. Y. Jordan. 2016. Accumulation of deleterious mutations near sexually antagonistic genes. *G3* 6:2273–2280.
- Conner, J. 2006. Ecological genetics of floral evolution. Chap. 14 in *Ecology and evolution of flowers*, ed. by L. D. Harder and S. C. H. Barrett, pp.260–277. Oxford, UK: Oxford University Press.
- Cox, R. M., and R. Calsbeek. 2010. Cryptic sex-ratio bias provides indirect genetic benefits despite sexual conflict. *Science* 328:92–94.
- Crow, J., and M. Kimura. 1970. *An introduction to population genetics theory*. New Jersey, USA: The Blackburn Press.
- Cushing, D. H. 1990. Plankton production and year-class strength in fish populations: an update of the match/mismatch hypothesis. *Advances in Marine Biology* 26:249–293.
- . 1969. The regularity of the spawning season of some fishes. *ICES Journal of Marine Science* 33:81–92.

- Darwin, C. 1877. *The different forms of flowers on plants of the same species*. London: John Murray.
- Delcourt, M., M. W. Blows, and H. D. Rundle. 2009. Sexually antagonistic genetic variance for fitness in an ancestral and a novel environment. *Proc. Roy. Soc. B* 276:2009–2014.
- Denny, M. W., and M. F. Shibata. 1989. Consequences of surf-zone turbulence for settlement and external fertilization. *The American Naturalist* 134:859–889.
- Devaux, C., and R. Lande. 2008. Incipient allochronic speciation due to non-selective assortative mating by flowering time, mutation, and genetic drift. *Proc. Roy. Soc. B* 275:2723–2732.
- . 2010. Selection on variance in flowering time within and among individuals. *Evolution* 64:1311–1320.
- Durant, J. M., et al. 2007. Climate and the match or mismatch between predator requirements and resource availability. *Climate Research* 33:271–283.
- Ejsmond, M. J., M. Czarnoleski, and J. Kozłowski. 2010. How to time growth and reproduction during the vegetative season: an evolutionary choice for indeterminate growers in seasonal environments. *The American Naturalist* 175:551–563.
- Elzinga, J. A., et al. 2007. Time after time: flowering phenology and biotic interactions. *Trends in Ecology and Evolution* 22:432–439.
- Fagan, W. F., et al. 2010. Reproductive asynchrony in spatial population models: how mating behaviour can modulate Allee effects arising from isolation in both space and time. *The American Naturalist* 175:362–373.
- Fisher, R. A. 1930. *The Genetical Theory of Natural Selection*. Oxford, UK: Clarendon Press.
- . 1958. *The Genetical Theory of Natural Selection*. New York, NY, USA: Dover.
- Foerster, K. T., et al. 2007. Sexually antagonistic genetic variation for fitness in red deer. *Nature* 447:1107–1109.
- Franke, E. S., R. C. Babcock, and C. A. Styan. 2002. Sexual conflict and polyspermy under sperm-limited conditions: *in situ* evidence from field simulations with the free-spawning echinoid *Evechinus chloroticus*. *The American Naturalist* 160:485–496.
- Friedman, J., and S. C. H. Barrett. 2009. Wind of change: new insights on the ecology and evolution of pollination and mating in wind-pollinated plants. *Annals of Botany* 103:1515–1527.
- Fry, J. D. 2010. The genomic location of sexually antagonistic variation: some cautionary comments. *Evolution* 64:1510–1516.
- Gage, M. J. G., P. Stockley, and G. A. Parker. 1995. Effects of alternative male mating strategies on characteristics of sperm production in Atlantic salmon (*Salmo salar*): theoretical and empirical investigations. *Phil. Trans. Roy. Soc. B* 350:391–399.
- Gelman, A., and D. B. Rubin. 1992. Inference from iterative simulation using multiple sequences. *Statistical Science* 7:457–472.
- Ghiselin, M. 1969. The evolution of hermaphroditism among animals. *Quarterly Review of Biology* 44:189–208.
- Goldberg, E. E., et al. 2017. Macroevolutionary synthesis of flowering plant sexual systems. *Evolution* 71:898–912.

- Gonçalves, C. S., U. P. Souza, and M. V. Volcan. 2005. The opportunistic feeding and reproduction strategies of the annual fish *Cynopoecilus melanotaenia* (Cyprinodontiformes: Rivulidae) inhabiting ephemeral habitats on southern Brazil. *Neotropical Ichthyology* 9:191–200.
- Goodwillie, C. S., S. Kalisz, and C. G. Eckert. 2005. The evolutionary enigma of mixed mating systems in plants: occurrence, theoretical explanations, and empirical evidence. *Ann. Rev. Ecol. Evol. Syst.* 36:47–79.
- Gould, M. C., and J. L. Stephano. 2003. Polyspermy prevention in marine invertebrates. *Microscopy Research Technology* 61:379–388.
- Gregory, P. H. 1973. *Microbiology of the atmosphere, 2nd Ed.* Ayelsbury, UK: Leonard Hill.
- Gross, M. R., and R. Shine. 1981. Parental care and mode of fertilization in ectothermic vertebrates. *Evolution* 35:775–793.
- Haldane, J. B. S. 1926. A mathematical theory of natural and artificial selection III. *Proc. Cambridge Phil. Soc.* 23:363–372.
- Harder, L. D., and S. C. H. Barrett. 2006. *Ecology and evolution of flowers.* Oxford, U.K.: Oxford University Press.
- . 1995. Mating cost of large floral displays in hermaphrodite plants. *Nature* 373:512–515.
- Harder, L. D., S. A. Richards, and M. B. Routely. 2007. Effects of reproductive compensation, gametic discounting, and reproductive assurance on mating-system diversity in hermaphrodites. *Evolution* 62:157–172.
- Harder, L. D., M. A. Aizen, and S. A. Richards. 2016. The population ecology of male gametophytes: the link between pollination and seed production. *Ecology Letters* 19:497–509.
- Harrison, P. L., et al. 1984. Mass spawning in tropical reef corals. *Science* 223:1186–1189.
- Hendry, A. P., and T. Day. 2005. Population structure attributable to reproductive time: isolation by time and adaptation by time. *Molecular Ecology* 14:901–916.
- Holden, L. R. 1979. New properties of the two-locus partial selfing model with selection. *Genetics* 93:217–236.
- Holsinger, K. E. 1991. Mass-action models of plant mating systems: the evolutionary stability of mixed mating systems. *The American Naturalist* 138:606–622.
- Hooten, M. B., and N. T. Hobbs. 2015. A guide to Bayesian model selection for ecologists. *Ecological Monographs* 85:3–28.
- Igic, B., and J. R. Kohn. 2005. The distribution of plant mating systems: study bias against obligately outcrossing species. *Evolution* 60:1098–1103.
- Ims, R. A. 1990. On the adaptive value of reproductive synchrony as a predator-swamping strategy. *The American Naturalist* 136:485–498.
- Ishii, H. S., and L. D. Harder. 2012. Phenological associations of within- and among-plant variation in gender with floral morphology and integration in protandrous *Delphinium glaucum*. *J. Ecology* 100:1029–1038.
- Iwasa, Y. 1991. Asynchronous pupation of univoltine insects as an evolutionary stable phenology. *Res. Population Ecology* 33:213–227.

- Iwasa, Y., and P. Haccou. 1994. ESS emergence pattern of male butterflies in stochastic environments. *Evolutionary Ecology* 8:503–523.
- Iwasa, Y., and S. A. Levin. 1995. The timing of life history events. *J. Theoretical Biology* 172:33–42.
- Iyer, P., and J. Roughgarden. 2008. Gametic conflict versus contact in the evolution of anisogamy. *Theoretical Population Biology* 73:461–472.
- Jarne, P., and J. R. Auld. 2006. Animals mix it up too: the distribution of self-fertilization among hermaphroditic animals. *Evolution* 60:1816–1824.
- Jivoff, P. 1997. The relative roles of predation and sperm competition on the duration of post-copulatory association between the sexes in the blue crab *Callinectes sapidus*. *Behavioural Ecology and Sociobiology* 40:175–185.
- Johnson, S. L., and P. O. Yund. 2009. Effects of fertilization distance on male gain curves in a free-spawning marine invertebrate: a combined empirical and theoretical approach. *Evolution* 63:3114–3123.
- Jordan, C. Y., and D. Charlesworth. 2011. The potential for sexually antagonistic polymorphism in different genome regions. *Evolution* 66:505–516.
- Jordan, C. Y., and T. Connallon. 2014. Sexually antagonistic polymorphism in simultaneous hermaphrodites. *Evolution* 68:3555–3569.
- Jørgensen, C., S. K. Auer, and D. N. Reznick. 2011. A model for optimal offspring size in fish, including live-bearing and parental effects. *The American Naturalist* 177:E119–E135.
- Käfer, J., G. A. B. Marais, and J. R. Pannell. 2017. On the rarity of dioecy in flowering plants. *Molecular Ecology* 26:1225–1241.
- Kenagy, G. J., and S. C. Trombulak. 1986. Size and function of mammalian testes in relation to body size. *J. Mammalogy* 67:1–22.
- Kerr, A. M., A. H. Baird, and T. P. Hughes. 2011. Correlated evolution of sex and reproductive mode in corals (Anthozoa: Scleractinia). *Proc. Roy. Soc. B* 278:75–81.
- Kidwell, J. F., et al. 1977. Regions of stable equilibria for models of selection in the two sexes under random mating. *Genetics* 85:171–183.
- Kim, T. W., et al. 2010. Effect of food addition on the reproductive intensity and timing of both sexes of an intertidal crab. *Marine Ecology Progress Series* 401:183–194.
- Kimura, M., and T. Ohta. 1971. Maintenance of genetic variability in Mendelian populations. Chap. 9 in *Theoretical aspects of population genetics*, pp.141–159. Princeton, New Jersey, U.S.A.: Princeton University Press.
- Kokko, H., and M. J. Jennions. 2008. Parental investment, sexual selection, and sex ratios. *J. Evolutionary Biology* 21:919–948.
- Kudo, G. 2006. Flowering phenologies of animal-pollinated plants: reproductive strategies and agents of selection. Chap. 8 in *Ecology and evolution of flowers*, pp.139–158. Oxford, UK: Oxford University Press.
- Kupriyanova, E. K. 2006. Fertilization success in *Galeolaria caespitosa* (Polychaeta: Serpulidae): gamete characteristics, role of sperm dilution, gamete age, and contact time. *Scientia Marina* 70S3:309–317.

- Kupriyanova, E. K., and J. N. Havenhand. 2013. Effects of temperature on sperm swimming behaviour, respiration, and fertilization success in the serpulid polychaete, *Galeolaria caespitosa* (Annelida: Serpulidae). *Invertebrate Reproduction and Development* 48:7–17.
- Lande, R. 1976. Natural selection and random genetic drift in phenotypic evolution. *Evolution* 30:314–334.
- . 1980. Sexual dimorphism, sexual selection, and adaptation in polygenic characters. *Evolution* 34:292–305.
- Lee, Y. W., et al. 2016. A segregating inversion generates fitness variation in yellow monkeyflower (*Mimulus guttatus*). *Genetics* 202:1473–1484.
- Levitan, D. 1988. Asynchronous spawning and aggregative behavior in the sea urchin *Diadema antillarum* (Phillipi). In *Echinoderm biology*, ed. by R. D. Burke et al., pp.181–186. Rotterdam, N.L.: Balkema.
- . 2002. Density-dependent selection on gamete traits in three congeneric sea urchins. *Ecology* 83:464–479.
- . 2004. Density-dependent sexual selection in external fertilizers: variances in male and female fertilization success along the continuum from sperm limitation to sexual conflict in the sea urchin *Strongylocentrotus franciscanus*. *The American Naturalist* 164:298–309.
- . 1998. Does Bateman's principle apply to broadcast-spawning organisms? egg traits influence *in situ* fertilization rates among congeneric sea urchins. *Evolution* 52:1043–1056.
- . 1991. Influence of body size and population density on fertilization success and reproductive output in a free-spawning invertebrate. *Biological Bulletin* 181:261–268.
- . 2005. Sex-specific spawning behaviour and its consequences in an external fertilizer. *The American Naturalist* 165:682–694.
- . 1993. The importance of sperm limitation to the evolution of egg size in marine invertebrates. *The American Naturalist* 141:517–536.
- Levitan, D., and D. L. Ferrell. 2006. Selection on gamete recognition proteins depends on sex, density, and genotype frequency. *Science* 312:267–269.
- Levitan, D., et al. 2011. Genetic, spatial, and temporal components of precise spawning synchrony in reef building corals of the *Montastraea annularis* species complex. *Evolution* 65:1254–1270.
- Levitan, D., et al. 2004. Mechanisms of reproductive isolation among sympatric broadcast-spawning corals of the *Montastraea annularis* species complex. *Evolution* 58:308–323.
- Lewis, C., et al. 2002. Does seasonal reproduction occur at the optimal time for fertilization in the polychaetes *Arenicola marina* L. and *Nereis virens* Sars? *Invert. Repro. Devel.* 41:61–71.
- Lewis, C., P. J. W. Olive, and M. G. Bentley. 2003. Pre-emptive competition as a selective pressure for early reproduction in the polychaete *Nereis virens*. *Marine Ecology Progress Series* 254:199–211.
- Lewis, D. 1941. Male sterility in natural populations of hermaphrodite plants. *New Phyt.* 40:56–63.
- . 1942. The evolution of sex in flowering plants. *Biol. Rev.* 17:46–67.

- Lloyd, D. G. 1979. Some reproductive factors affecting the selection of self-fertilization in plants. *The American Naturalist* 113:67–79.
- . 1975. The maintenance of gynodioecy and androdioecy in angiosperms. *Genetica* 45:325–339.
- . 1976. The transmission of genes via pollen and ovules in gynodioecious angiosperms. *Theor. Pop. Biol.* 9:299–316.
- Lloyd, D. G., and C. J. Webb. 1986. The avoidance of interference between the presentation of pollen and stigmas in angiosperms I. Dichogamy. *New Zealand J. Botany* 24:135–162.
- Long, T. A. F., A. F. Agrawal, and L. Rowe. 2012. The effect of sexual selection on offspring fitness depends on the nature of genetic variation. *Current Biology* 22:204–208.
- Lotterhos, K. E., and D. Levitan. 2011. Gamete release and spawning behaviour in broadcast spawning marine invertebrates. Chap. 6 in *The evolution of primary sexual characters in animals*, ed. by J. L. Leonard and A. Córdoba-Aguilar, pp.99–120. Oxford, U.K.: Oxford University Press.
- Lowerre-Barbieri, S. K., et al. 2011. Reproductive timing in marine fishes: variability, temporal scales, and methods. *Marine and Coastal Fisheries: Dyn. Man. and Ecosyst. Science* 3:71–91.
- Loya, Y., and K. Sakai. 2008. Bidirectional sex change in mushroom stony corals. *Proc. Roy. Soc. B* 275:2335–2343.
- Manna, F., G. Martin, and T. Lenormand. 2011. Fitness landscapes: an alternative theory for the dominance of mutation. *Genetics* 189:923–937.
- Marshall, D. J. 2002. *In situ* measures of spawning synchrony and fertilization success in an intertidal, free-spawning invertebrate. *Marine Ecology Progress Series* 236:113–119.
- Marshall, D. J., and T. F. Bolton. 2007. Sperm release strategies in marine broadcast spawners: the costs of releasing sperm quickly. *J. Experimental Biology* 210:3720–3727.
- Marshall, D. J., and J. P. Evans. 2005b. Does egg competition occur in marine broadcast spawners? *J. Evolutionary Biology* 18:1244–1252.
- . 2005a. The benefits of polyandry in the free-spawning polychaete *Galeolaria caespitosa*. *J. Evolutionary Biology* 18:735–741.
- Marshall, D. J., and M. K. Keough. 2007. The evolutionary ecology of offspring size in marine invertebrates. *Advances in Marine Biology* 553:1–60.
- Marshall, D. J., D. Semmens, and C. Cook. 2004. Consequences of spawning at low tide: limited gamete dispersal for a rockpool anemone. *Marine Ecology Progress Series* 266:135–142.
- Marshall, D. J., C. A. Styan, and M. K. Keough. 2000. Intraspecific covariation between egg and body size affects fertilization kinetics of free-spawning marine invertebrates. *Marine Ecology Progress Series* 195:305–309.
- Maynard Smith, J. 1982. *Evolution and the theory of games*. Cambridge, U.K.: Cambridge University Press.
- McEuan, F. S. 1988. Spawning behaviors of northeast Pacific sea cucumbers (Holothuroidea: Echinodermata). *Marine Biology* 98:565–585.

- Millar, R. B., and M. J. Anderson. 2003. The kinetics of monospermic and polyspermic fertilization in free-spawning marine invertebrates. *J. Theor. Biol.* 224:79–85.
- Monro, K., and D. J. Marshall. 2015. The biogeography of fertilisation mode in the sea. *Global Ecology and Biogeography* 24:1499–1509.
- Morgan, S. J., and J. H. Christy. 1995. The adaptive significance of the timing of larval release by crabs. *The American Naturalist* 145:457–479.
- Morgan, S. J., et al. 2011. Weak synchrony in the timing of larval release in upwelling regimes. *Marine Ecology Progress Series* 425:103–112.
- Munday, P. L., P. M. Buston, and R. R. Warner. 2006. Diversity and flexibility of sex-change strategies in animals. *Trends in Ecology and Evolution* 21:89–95.
- Nagylaki, T. 1997. The diffusion model for migration and selection in a plant population. *J. Mathematical Biology* 35:409–431.
- Ohta, T., and C. C. Cockerham. 1974. Detrimental genes with partial selfing and effects on a neutral locus. *Genet. Res. Camb.* 23:191–200.
- Olito, C. 2016. Consequences of genetic linkage for the maintenance of sexually antagonistic polymorphism in hermaphrodites. *Evolution* 71:458–464.
- Olito, C., M. Bode, and D. J. Marshall. 2015. Evolutionary consequences of fertilization mode for reproductive phenology and asynchrony. *Marine Ecology Progress Series* 537:23–38.
- Orr, H. A. 2005. Theories of adaptation: what they do and don't say. *Genetica* 123:3–13.
- Otto, S. P., and T. Day. 2007. *A Biologist's Guide to Mathematica Modeling in Ecology and Evolution*. Princeton, NJ, USA: Princeton University Press.
- Owen, A. R. G. 1953. A genetical system admitting of two distinct stable equilibria under natural selection. *Heredity* 7:97–102.
- Panhuis, T. M., N. L. Clark, and W. J. Swanson. 2006. Rapid evolution of reproductive proteins in abalone and *Drosophila*. *Phil. Trans. Roy. Soc. B* 361:2261–268.
- Parker, G. A. 1990a. Sperm competition games: raffles and roles. *Proc. Roy. Soc. B* 242:120–126.
- . 1990b. Sperm competition games: sneaks and extra-pair copulations. *Proc. Roy. Soc. B* 242:127–133.
- . 1982. Why are there so many tiny sperm? *J. Theoretical Biology* 96:281–294.
- Parker, G. A., R. R. Baker, and V. G. F. Smith. 1982. The origin and evolution of gamete dimorphism and the male-female phenomenon. *J. Theoretical Biology* 36:529–553.
- Parker, G. 1979. Sexual selection and sexual conflict. In *Sexual selection and reproductive competition in insects*, ed. by M. S. Blum and N. A. Blum, pp.123–166. Elsevier: Academic Press.
- Patten, M., and D. Haig. 2009. Maintenance or loss of genetic variation under sexual and parental antagonism. *Evolution* 63:2888–2095.
- Patten, M., D. Haig, and F. Úbeda. 2010. Fitness variation due to sexual antagonism and linkage disequilibrium. *Evolution* 64:3638–3642.
- Pearson, G. A., and S. H. Brawley. 1996. Preproductive ecology of *Fucus distichus* (Phaeophyceae): an intertidal alga with successful external fertilization. *Marine Ecology Progress Series* 143:211–223.

- Pemberton, A. J., et al. 2003. Efficient utilization of very dilute aquatic sperm: sperm competition may be more likely than sperm limitation when eggs are retained. *Proc. Roy. Soc. B* 270:S223–S226.
- Pischedda, A., and A. K. Chippindale. 2006. Intralocus sexual conflict diminished the benefits of sexual selection. *PLoS Biology* 4:2099–2103.
- Pollak, E. 1987. On the theory of partially inbreeding finite populations. I. Partial selfing. *Genetics* 117:353–360.
- Porcher, E., and R. Lande. 2005. Reproductive compensation in the evolution of plant mating systems. *New Phytologist* 166:673–684.
- Post, E., et al. 2001. Reproductive asynchrony increases with environmental disturbance. *Evolution* 55:830–834.
- Prout, T. 2000. How well does opposing selection maintain variation? Chap. 9 in *Evolutionary genetics from molecules to morphology*, ed. by R. S. Singh and C. B. Kimbras, pp.157–203. Cambridge, U.K.: Cambridge University Press.
- . 1968. Sufficient conditions for multiple niche polymorphism. *The American Naturalist* 102:493–496.
- Qiu, S., R. Bergero, and D. Charlesworth. 2013. Testing for the footprint of sexually antagonistic polymorphisms in the pseudoautosomal region of a plant sex chromosome pair. *Genetics* 194:663–672.
- Quesne, W. J. F., and S. J. Hawkins. 2006. Direct observations of protandrous sex change in the patellid limpet *Patella vulgata*. *J. Marine Biology Association U.K.* 86:161–162.
- Rabinowitz, D., et al. 1981. Phenological properties of wind- and insect-pollinated prairie plants. *Ecology* 62:49–56.
- Rathcke, B. J., and E. P. Lacey. 1985. Phenological patterns of terrestrial plants. *Ann. Rev. Ecol. Evol. Syst.* 16:179–214.
- Renner, S. 2014. The relative and absolute frequencies of angiosperm sexual systems: dioecy, monoecy, gynodioecy, and an updated online database. *American J. Botany* 101:1588–1596.
- Rice, W. R. 1992. Sexually antagonistic genes: experimental evidence. *Science* 256:1436–1439.
- . 1987. The accumulation of sexually antagonistic genes as a selective agent promoting the evolution of reduced recombination between primitive sex chromosomes. *Evolution* 41 (4): 911–914.
- Rice, W. R., and A. K. Chippindale. 2001. Intersexual ontogenetic conflict. *J. Evolutionary Biology* 14:685–693.
- Robertson, D. R. 1990. Differences in the seasonalities of spawning and recruitment of some small neotropical reef fishes. *J. Experimental Marine Biology* 144:49–62.
- Robertson, D. R., C. W. Petersen, and J. D. Brawn. 1990. Lunar reproductive cycles of benthic-brooding reef fishes: reflections of larval biology or adult biology? *Ecological Monographs* 60:311–329.
- Rondeau, A., and B. Sainte-Marie. 2001. Variable mate-guarding time and sperm allocation by male snow crabs (*Chionoecetes opilio*) in response to sexual competition, and their impact on the mating success of females. *Biological Bulletin* 201:204–217.

- Rothschild, L., and M. M. Swann. 1951. The fertilization reaction in the sea urchin: the probability of a successful sperm-egg collision. *J. Experimental Biology* 28:403–416.
- Roughgarden, J. 1972. Evolution of niche width. *The American Naturalist* 106:683–718.
- Rouse, G., and K. Fitzhugh. 1994. Broadcasting fables: is external fertilization really primitive? Sex, size, and larvae in sabellid polychaetes. *Zoologica Scripta* 23:271–312.
- Sadovy, Y. J. 1996. Reproduction of reef fishery species. Chap. 1 in *Reef Fisheries*, ed. by N. V. C. Polunin and C. M. Roberts, pp.15–59. London, U.K.: Chapman / Hall.
- Sakai, A. K., and S. G. Weller. 1999. Gender and sexual dimorphism in flowering plants. Chap. 1 in *Gender and sexual dimorphism in flowering plants*, ed. by M. A. Geber, T. E. Dawson, and L. F. Delph, pp.1–31. Heidelberg, Germany: Springer Science / Business Media.
- Schemske, D. W., and R. Lande. 1985. The evolution of self-fertilization and inbreeding depression in plants. I. Genetic Models. *Evolution* 39:24–40.
- Sellis, D., et al. 2011. Heterozygote advantage as a natural consequence of adaptation in diploids. *PNAS* 108:20666–20671.
- Sewell, D. 1994. Small size, brooding, and protandry in the Apodid sea cucumber *Leptosynapta clarki*. *Biological Bulletin* 187:112–123.
- Sicard, A., and M. Lenhard. 2011. The selfing syndrome: a model for studying the genetic and evolutionary basis of morphological adaptation in plants. *Annals of Botany* 107:1433–1443.
- Spencer, H. G., and N. K. Priest. 2016. The evolution of sex-specific dominance in response to sexually antagonistic selection. *The American Naturalist* 187:658–666.
- Spielman, M., and R. J. Scott. 2008. Polyspermy barriers in plants: from preventing to promoting fertilization. *Plant Reproduction* 21:53–65.
- Stearns, S. C. 1992. *The evolution of life histories*. Oxford, UK: Oxford University Press.
- Stockley, P., et al. 1997. Sperm competition in fishes: the evolution of testis size and ejaculate characteristics. *The American Naturalist* 249:933–954.
- Strathmann, M. F. 1987. *Reproduction and development of marine invertebrates of the northern Pacific coast. Data and methods for the study of eggs, embryos, and larvae*. Washington, U.S.A.: University of Washington Press.
- Strathmann, R. R. 1985. Feeding and nonfeeding larval development and life-history evolution in marine invertebrates. *Ann. Rev. Ecol. Evol. Syst.* 16:339–361.
- Styan, A. J., C. A. and Butler. 2000. Fitting fertilization kinetics models for free-spawning marine invertebrates. *Marine Biology* 137:943–951.
- . 2003. Scallop size does not predict amount or rate of induced sperm release. *Mar. Fresh. Behav. Phys.* 36:59–65.
- Tazzyman, S. J., and J. K. Abbott. 2015. Self-fertilization and inbreeding limit the scope for sexually antagonistic polymorphism. *J. Evolutionary Biology* 28:723–729.
- Team, R. C. 2015. *R: A Language and Environment for Statistical Computing*. Vienna, Austria: R Foundation for Statistical Computing. <http://www.R-project.org/>.
- . 2016a. *R: A Language and Environment for Statistical Computing*. Vienna, Austria: R Foundation for Statistical Computing. <http://www.R-project.org/>.

- Team, S. D. 2016b. *RStan: the R interface to Stan*. <http://www.mc-stan.org/>.
- Thomson, J. D. 1981. Spatial and temporal components of resource assessment by flower-feeding insects. *J. Animal Ecology* 50:49–59.
- Thorson, G. 1946. Reproduction and larval development of Danish marine bottom invertebrates, with special reference to planktonic larvae in the Sound (Øresund). *Meddelelser Danmark Hav Ser Plankton* 4:1–523.
- . 1950. Reproductive and larval ecology of marine bottom invertebrates. *Biological Reviews* 25:1–45.
- . 1936. The larval development, growth, and metabolism of Arctic marine bottom invertebrates etc. *Meddelelser om Grønland* 100:339–361.
- Tomaiuolo, M., T. F. Hansen, and D. Levitan. 2007. A theoretical investigation of sympatric evolution of temporal reproductive isolation as illustrated by marine broadcast spawners. *Evolution* 61:2584–2595.
- Úbeda, F., D. Haig, and M. Patten. 2010. Stable linkage disequilibrium owing to sexual antagonism. *Proc. Roy. Soc. B* doi:10.1098/rspb.2010.1201:1–8.
- Vance, R. R. 1973. More on reproductive strategies in marine benthic invertebrates. *The American Naturalist* 107:353–361.
- vanDoorn, G. S., and M. Kirkpatrick. 2010. Transitions between male and female heterogamety caused by sex-antagonistic selection. *Genetics* 186:629–645.
- . 2007. Turnover of sex chromosomes induced by sexual conflict. *Nature* 449:909–912.
- Vogel, H. G., et al. 1982. Fertilization kinetics of sea urchin eggs. *Mathematical Biosciences* 58:189–216.
- Warner, R. R. 1988. Sex change and the size advantage model. *Trends in Ecology and Evolution* 3:133–136.
- . 1975. The adaptive significance of sequential hermaphroditism in animals. *The American Naturalist* 109:61–82.
- Webb, C. J., and D. G. Lloyd. 1986. The avoidance of interference between the presentation of pollen and stigmas in angiosperms II. Herkogamy. *New Zealand J. Botany* 24:163–178.
- Wedell, N., M. J. G. Gage, and G. A. Parker. 2002. Sperm competition, male prudence, and sperm-limited females. *Trends in Ecology and Evolution* 17:313–320.
- Weinreich, D. M., and L. Chao. 2005. *Evolution* 59:1175–1182.
- Weis, A. E., E. Nardone, and G. A. Fox. 2014. The strength of assortative mating for flowering date and its basis in individual variation in flowering schedule. *J. Evolutionary Biology* 27:2138–2151.
- Westergaard, M. 1958. The mechanism of sex determination in dioecious flowering plants. *Advances in Genetics* 9:217–281.
- Whitlock, M. C., and A. F. Agrawal. 2009. Purging the genome with sexual selection: reducing mutation load through selection on males. *Evolution* 63:569–582.
- Winemiller, K. O. 1989. Patterns of variation in life history among South American fishes in seasonal environments. *Oecologia* 81:225–241.
- Winemiller, K. O., and K. A. Rose. 1992. Patterns of life-history diversification in North American fishes: implications for population regulation. *Can. J. Fish and Aquatic Science* 49:2196–2218.

- Wolfram. 2014. *Mathematica v.10.1*. Wolfram Research, Champaign, IL, USA.
- Wong, J. L., and G. M. Wessel. 2005. Defending the zygote: search for the ancestral animal block to polyspermy. *Current Topics in Developmental Biology* 72:1–151.
- Wright, S. I., et al. 2008. Genomic consequences of outcrossing and selfing in plants. *Int. J. Plant Sciences* 169:105–118.
- Wright, S. 1931. Evolution in Mendelian populations. *Genetics* 16:97–159.
- Yund, P. O. 2000. How severe is sperm limitation in natural populations of marine free-spawners? *Trends in Ecology and Evolution* 15:10–13.
- Yund, P. O., and S. K. Meidel. 2003. Sea urchin spawning in benthic boundary layers: are eggs fertilized before advecting away from females? *Limnology and Oceanography* 48:795–801.
- Zhang, D. 2006. Evolutionarily stable reproductive investment and sex allocation in plants. Chap. 3 in *Ecology and evolution of flowers*, ed. by L. D. Harder and S. C. H. Barrett, pp.41–60. Oxford, UK: Oxford University Press.